



# Contribution to over-the-air characterization of UHF RFID tags : application to livestock RFID

Hadi El Hajj Chehade

## ► To cite this version:

Hadi El Hajj Chehade. Contribution to over-the-air characterization of UHF RFID tags : application to livestock RFID. Electronics. Université de Rennes, 2023. English. NNT : 2023URENS057 . tel-04400209

**HAL Id: tel-04400209**

**<https://theses.hal.science/tel-04400209>**

Submitted on 17 Jan 2024

**HAL** is a multi-disciplinary open access archive for the deposit and dissemination of scientific research documents, whether they are published or not. The documents may come from teaching and research institutions in France or abroad, or from public or private research centers.

L'archive ouverte pluridisciplinaire **HAL**, est destinée au dépôt et à la diffusion de documents scientifiques de niveau recherche, publiés ou non, émanant des établissements d'enseignement et de recherche français ou étrangers, des laboratoires publics ou privés.

# THÈSE DE DOCTORAT DE

L'UNIVERSITÉ DE RENNES

ÉCOLE DOCTORALE N° 601

*Mathématiques, Télécommunications, Informatique, Signal, Systèmes,  
Électronique*

Spécialité : *Télécommunications*

Par

**Hadi EL HAJJ CHEHADE**

**Contribution to Over-the-air Characterization of UHF RFID tags**

Applications to Livestock RFID

Thèse présentée et soutenue à Université de Rennes, le 1 Décembre 2023

Unité de recherche : IETR - UMR CNRS 6164, Institut d'Electronique et des Technologies du  
numérique, Université de Rennes

## Rapporteurs avant soutenance :

Jean-Marc LAHEURTE	Professeur des Universités, Université Gustave Eiffel
Nicolas BARBOT	Maître de conférences, INP Grenoble

## Composition du Jury :

Président :	Emanuel RADOÏ	Professeur des Universités, Université de Bretagne Occidentale
Examineurs :	Nicolas BARBOT	Maître de conférences, INP Grenoble
	Jean-Marc LAHEURTE	Professeur des universités, Université Gustave Eiffel
	Alice BUFFI	Maître de conférences, Université de Pise
Dir. de thèse :	Bernard UGUEN	Professeur des universités, Université de Rennes
Co-dir. de thèse :	Sylvain COLLARDEY	Maître de conférences, Université de Rennes

## Invités :

Matthieu CORNIC	Coordination de projets R&D, Cooperl
Romain HOTTE	Chef de projets R&D, Cooperl équipements



# ACKNOWLEDGEMENT

---

I would like to express my heartfelt gratitude to several individuals and organizations whose unwavering support has been invaluable throughout my three-year journey in completing this thesis.

First and foremost, I extend my deepest appreciation to my thesis director, Bernard UGUEN. His guidance, mentorship, and unwavering support have been instrumental in shaping the trajectory of my research. Bernard's dedication and expertise have not only enriched my academic experience but also contributed significantly to the successful completion of this work.

I am equally grateful to my co-director, Sylvain Collardey, whose assistance and insights have played a crucial role in the development of this thesis. Sylvain's expertise and willingness to share his knowledge have been indispensable, and I am truly thankful for all the attention and valuable advice he has brought to my work.

I wish to acknowledge the support of the French BPI project, "CAA-Connect," for providing crucial research funding for this project. Their generous contributions have been instrumental in enabling us to conduct this research, and I am deeply appreciative of their commitment to advancing scientific exploration.

To my family, I owe a debt of gratitude that words cannot fully capture. Their precious emotional support and encouragement have been my pillars of strength throughout this challenging journey. Their belief in me and my aspirations has been a constant source of motivation, and I am profoundly thankful for their love and support every day.

Of course, I want to thank all my friends and my beloved Fatma with whom I have shared countless memorable moments. Their companionship and the good times we have enjoyed together have provided essential mental respite during the demanding phases of my research - Reda, Ali, Marc and others.

To each of these individuals and organizations, I offer my sincere thanks. Your contributions have not only shaped this thesis but have also been vital in my personal and academic growth.





# TABLE OF CONTENTS

---

<b>Introduction</b>	<b>17</b>
<b>1 UHF RFID System: Literature Review</b>	<b>31</b>
1.1 Introduction . . . . .	31
1.2 Overview on RFID system . . . . .	32
1.2.1 History of UHF RFID . . . . .	32
1.2.2 RFID system components . . . . .	33
1.2.3 Operation frequencies of RFID . . . . .	35
1.3 UHF RFID system . . . . .	36
1.3.1 Types of UHF RFID tags . . . . .	36
1.3.2 Use cases of UHF RFID . . . . .	38
1.3.3 The Regulations for UHF RFID systems . . . . .	40
1.3.4 EPCglobal Generation 2 . . . . .	41
1.4 Characterization of passive UHF RFID tag . . . . .	42
1.4.1 UHF RFID communication between reader and tag . . . . .	42
1.4.2 Link budget of UHF RFID . . . . .	44
1.4.3 Energy conservation in UHF RFID . . . . .	55
1.4.4 Over-the-air characterization of UHF RFID tag . . . . .	57
1.4.5 Channel modelling in UHF RFID communication . . . . .	60
1.5 Platform description . . . . .	61
1.5.1 Alien 9900+ reader . . . . .	62
1.5.2 Impinj R700 reader . . . . .	63
1.5.3 Reader antenna . . . . .	64
1.6 Conclusion . . . . .	65
<b>2 Theoretical Aspect of UHF RFID</b>	<b>67</b>
2.1 Introduction . . . . .	67
2.2 Intrinsic Characteristics of UHF RFID tag . . . . .	68
2.2.1 Mean power transmission coefficient . . . . .	68

## TABLE OF CONTENTS

---

2.2.2	Modulation Factor . . . . .	71
2.3	RFID transmission channel . . . . .	73
2.3.1	Free space model . . . . .	73
2.3.2	Multipath channel model . . . . .	75
2.4	Activation power profile . . . . .	75
2.4.1	Definition of the transmitted activation profile . . . . .	76
2.4.2	Definition of the received activation profile . . . . .	77
2.5	Expression of modulation factor . . . . .	78
2.6	Definition of the tag receptivity and the tag offset . . . . .	79
2.7	Introduction of the $(\sqrt{M}, \tau)$ chart . . . . .	81
2.7.1	Maximal values of $\tau$ and $M$ for a given $Q$ . . . . .	83
2.7.2	Remarkable points of the chart . . . . .	83
2.7.3	Performance indicators . . . . .	84
2.7.4	Tag efficiency parameter $\gamma$ . . . . .	85
2.7.5	How to place a measured tags in the chart ? . . . . .	85
2.7.6	Free space read range formulation . . . . .	87
2.8	UHF RFID tags evaluation using the proposed chart . . . . .	91
2.8.1	Illustration of chip-antenna combinations performance . . . . .	92
2.8.2	Employing the algorithm to place the tags in the chart . . . . .	92
2.9	Chip validity domain in the $(\sqrt{M}, \tau)$ chart . . . . .	95
2.9.1	Intersection of a constant $Q$ line and $f_{sup}$ . . . . .	96
2.9.2	Maximizing $\tau$ in the chip validity domain . . . . .	96
2.9.3	Optimal matching of a chip . . . . .	97
2.9.4	Optimal matching illustration with the same examples that in [41] . . . .	97
2.10	Conclusion . . . . .	98
<b>3</b>	<b>Experimental characterization of UHF RFID tags</b>	<b>103</b>
3.1	Introduction . . . . .	103
3.2	RSSI acquisition in translation and rotation . . . . .	104
3.2.1	Translation acquisition . . . . .	105
3.2.2	Rotation acquisition . . . . .	106
3.3	RSSI to received power conversion . . . . .	106
3.3.1	Measured power profiles . . . . .	107
3.3.2	RSSI to $dBm$ conversion formula . . . . .	109

3.4	Evaluation and comparison of the performance of a set of tags . . . . .	112
3.4.1	Measured power profiles in $dBm$ . . . . .	113
3.4.2	Comparison of tags using the power-distance profiles . . . . .	116
3.4.3	Distribution of the tag receptivity error . . . . .	118
3.4.4	Placing the 9 tags in the $(\sqrt{M}, \tau)$ chart . . . . .	118
3.4.5	Monza 4 chip validity in the $(\sqrt{M}, \tau)$ chart . . . . .	121
3.4.6	Evaluation of tag performance and read range . . . . .	122
3.4.7	Effect of $P_{inc}$ variation . . . . .	128
3.4.8	Environment propagation scanning using identical UHF RFID tags configuration . . . . .	134
3.5	Conclusion . . . . .	137
<b>4</b>	<b>Experimental characterizations in the context of livestock application</b>	<b>141</b>
4.1	Introduction . . . . .	141
4.2	State of the art on UHF RFID tags mounted on pig ears . . . . .	142
4.2.1	Electrical characteristic of pig tissue . . . . .	143
4.2.2	Effect of pig Ear on UHF RFID tag performance . . . . .	144
4.3	Dielectric characterization of pig ears . . . . .	144
4.3.1	Weight distribution of 25 ears . . . . .	145
4.3.2	Dielectric measurement of Ear 8 . . . . .	146
4.3.3	Evaluation of dielectric property for a sample of 25 ears . . . . .	148
4.3.4	Testing intern vs extern . . . . .	149
4.3.5	Pig ear permittivity model . . . . .	150
4.3.6	Analysis of the correlation between dielectric properties and ear weight	153
4.4	RFID tags on pig ears orientation effect . . . . .	154
4.4.1	Definition of ear orientation . . . . .	154
4.4.2	Tag on ear measurements for different orientations . . . . .	154
4.4.3	Evaluation of the ear and orientation effect using the $(\sqrt{M}, \tau)$ chart . .	159
4.5	Effect of tag response variability for different ears . . . . .	161
4.5.1	Correlation between the read range percentage of the tags and the tangent loss of the ears . . . . .	161
4.5.2	Correlation between the tag efficiency of the tags and the tangent loss of the ears . . . . .	163
4.6	ARDES tags characterisation . . . . .	165

## TABLE OF CONTENTS

---

4.6.1	ARDES tags V2, V3 and V5 comparison . . . . .	166
4.7	RFID tags on pig ears in different planar configurations . . . . .	166
4.7.1	Results analysis of Group of tags aquisition . . . . .	168
4.8	Conclusion . . . . .	171
<b>Conclusion</b>		<b>173</b>
<b>A</b>	<b>Annex A</b>	<b>177</b>
A.1	Variation of $\Delta P_r$ in term of $\Delta$ for 9 different tags . . . . .	177
A.2	Evolution of $\sqrt{M}$ in term of $\Delta$ for 9 different tags . . . . .	178
A.3	Extrapolation of the two activation profiles for 9 different tags . . . . .	178
<b>B</b>	<b>Annex B</b>	<b>180</b>
<b>C</b>	<b>Annex C</b>	<b>185</b>
<b>D</b>	<b>Annex D</b>	<b>189</b>
<b>List of publications</b>		<b>193</b>
	Journal papers . . . . .	193
	International conference papers . . . . .	193
<b>Bibliography</b>		<b>195</b>

# LIST OF FIGURES

---

1	Schéma générale du système RFID UHF . . . . .	24
2	L'abaque $(\sqrt{M}, \tau)$ proposée . . . . .	25
3	Représentation du profil de puissance en translation du transpondeur dogbone/- Monza4 . . . . .	27
4	Comparaison d'un ensemble des transpondeurs dans l'abaque . . . . .	28
1.1	RFID spectrum domain . . . . .	36
1.2	Different families of RFID tags: (a) active tag, (b) Semi-passive tag, (c) passive tag, (d) chipless tag [17] . . . . .	37
1.3	RFID tag on pig ear . . . . .	39
1.4	General schema of UHF RFID system . . . . .	43
1.5	Uniform distribution of an Isotropic Antenna Radiates Power uniformly over the spherical surface[18]. . . . .	45
1.6	Radiation Pattern for a Directional Antenna [18]. . . . .	46
1.7	A block diagram of an RF tag . . . . .	49
1.8	Passive UHF RFID system and its back-scattered signal [37] . . . . .	52
1.9	frequency domain and Energy conservation of RFID tag [38] . . . . .	56
1.10	Friis's radio-propagation model for a passive UHF RFID system [47] . . . . .	58
1.11	5 axes RFID platform (4 translations, 1 rotation) connected to an Alien 9900+ Reader . . . . .	62
1.12	Photo of Alien 9900+ Reader . . . . .	63
1.13	Photo of Impinj R700 Reader . . . . .	63
1.14	Platform's antenna Gaussian pattern $G_{max} = 9 \text{ dB}$ , $HPBW = 65$ . . . . .	65
2.1	General schema of UHF RFID system highlighting the channel reciprocity . . .	69
2.2	The proposed $(\sqrt{M}, \tau)$ chart . . . . .	82
2.3	Evolution of $Q_{optdB}$ with respect to reader and chip sensitivity $S_r$ and $S_c$ , for different transmit power. The $Q_{opt}$ values obtained from the example of [41] are placed in the chart . . . . .	89

2.4	Example on Read Range evaluation ( $S_r = -24dBm$ , $S_c = -80dBm$ , $G_r = 9dB$ , $G_t = 2dB$ ) . . . . .	90
2.5	$(\sqrt{M}, \tau)$ chart representation of Bolomey's data . . . . .	91
2.6	Ordering the combinations of antenna/tag basing on the $\rho_{\frac{1}{2}}$ performance criteria . . . . .	93
2.7	Comparison between the real $(\sqrt{M}, \tau)$ values calculated directly from the impedance, the $(\sqrt{M}, \tau)$ solved by the algorithm for $\tau_{lim} = 0.5$ and the $(\sqrt{M}, \tau)$ solved at $\tau_{lim} = \varphi^{-1}$ . . . . .	94
3.1	Tag translation on the RFID platform represented in plane (X,Z) . . . . .	105
3.2	Variation of RSSI w.r.t distance (m) between tag and antenna . . . . .	105
3.3	Tag rotation on the RFID platform represented in plane (Y,Z) . . . . .	107
3.4	Variation of RSSI w.r.t rotation angle of the tag support . . . . .	108
3.5	Received level after conversion $f(\text{RSSI}(d, P_t))$ upper left corner, cut @ $d = 0.3 m$ (right), max power profile (cut @ $P_t = 30.2 dBm$ ) (bottom) . . . . .	109
3.6	Superposing the two curves $P_t^{th}$ and $P_r^{th}$ under the concept of channel reciprocity . . . . .	110
3.7	Comparison of received power obtained directly (Impinj R700 blue curve) or indirectly using 3.3.2 (Alien 9000+ red curve) . . . . .	111
3.8	Power profile representation in translation of the dogbone/Monza 4 tag . . . . .	114
3.9	Power profile representation in rotation of the dogbone/Monza 4 tag . . . . .	116
3.10	Power profile diagram for 9 different tags : in red $P_r^{max}(d)$ , in black $P_r^{th}(d)$ , in blue $P_t^{th}(d)$ , in green $R$ . . . . .	117
3.11	Distribution of the tag receptivity error resolution $\epsilon_{R^{th}}$ obtained from the 9 measured tag profiles . . . . .	119
3.12	Comparison between $P_t^{th}$ of AD318 tag with $P_t^{th} + offset$ of AD233 tag . . . . .	120
3.13	Proposed chart on a set of tags. On the left: One condition (cond1) applied on the boundary ( $\tau = 1 - M$ ). On the right: Two conditions applied, cond1 and an arbitrary limitation on the value of $\tau$ , here $\tau_{lim} = \varphi^{-1}$ . . . . .	120
3.14	Chart representation of the chip zone validity for the three measured Monza 4 tags . . . . .	121
3.15	Comparison of the performance evaluation criterias ( $\rho_{\varphi^{-1}}$ , $\rho_{\frac{1}{2}}$ and $\rho_{RR}$ ) for a set of tags . . . . .	124
3.16	Theoretical free space read range for different $S_r$ ( $G_t = 2dB$ , $G_r = 9dB$ , $P_t^{max} = 30.5dBm$ ). Cross-hatched: Backward link-limited, No cross-hatched: Forward link-limited . . . . .	124
3.17	Distribution of $\tau$ and $M$ derived under the condition $\tau_{lim} = \varphi^{-1}$ . . . . .	125

3.18	Received power profile at $P_t^{max} = 30dBm$ , for three different impinj's reader sensitivities $S_r = -80, -75, -70 dBm$ . . . . .	127
3.19	Representation of read range in the chart for three different impinj's reader sensitivities $S_r = -80, -75, -70 dBm$ . . . . .	128
3.20	Representation of shifted activation profiles by different $\Delta$ values ranging from 15.7 to 30.6dBm . . . . .	129
3.21	Variation of the offset on the received activation power w.r.t $\Delta$ . . . . .	130
3.22	Variation of the $Q^\Delta$ (in dB) w.r.t $\Delta$ (in dB) . . . . .	131
3.23	Evolution of $\sqrt{M^\Delta}$ (in linear) w.r.t $\Delta$ (in dB) . . . . .	132
3.24	Representation of the power profile with extension . . . . .	133
3.25	Mosaic of an experiments based on 39 tags placed in front of the platform antenna	134
3.26	Photo of the 39 tags placed in a raw in front of the platform antenna surrounded by absorbent panels . . . . .	135
3.27	Received power profiles variation along the rail of 39 RFID tags placed an a raw	136
4.1	Boxplot of the pig ears weight . . . . .	145
4.2	Ordered barplot of ears weight . . . . .	146
4.3	Internal side - Dielectric measurement for ear Number 8 . . . . .	147
4.4	External side - Dielectric measurement for the selected ear (Number 8) . . . . .	147
4.5	Evolution of complex permittivity and conductivity w.r.t frequency - Internal side	149
4.6	Evolution of complex permittivity and conductivity (bottom right) w.r.t frequency - External side . . . . .	150
4.7	Evolution of p-value w.r.t frequency in Two sample t-test testing Intern vs Extern	151
4.8	Evolution of complex permittivity standard deviation w.r.t frequency, Intern and Extern, left (standard deviation), right ( $IQ/1.36$ ) . . . . .	152
4.9	Correlation between ears weights and their permittivities . . . . .	153
4.10	Tag power profiles comparison of the NXP Ucode 8, M730 and Monza4 Tags for 4 different orientations . . . . .	156
4.11	Bar plot of the read range percentage of the NXP Ucode 8, M730 and Monza4 Tags for 4 different orientations . . . . .	157
4.12	Read range comparison of 4x3 NXP Ucode 8, M730 and Monza4 Tags . . . . .	158
4.13	Bar plot of the read range percentage of 4x3 NXP Ucode 8, M730 and Monza4 Tags in H orientation . . . . .	159
4.14	Chart representation of the 12 tags for 4 different orientation in H orientation .	159



4.15	Chart representation for NXP Ucode 8, M730 and M4i tags without ear in H orientation . . . . .	160
4.16	Profiles representation for M730 in Extern Horizontal configuration for 15 different ears . . . . .	162
4.17	Correlation between the read range percentage $\rho_{RR}$ (%) with the loss tangent $\tan\delta$ of the 15 different ears . . . . .	163
4.18	Chart representation of the M730 tag placed on 15 different ears . . . . .	164
4.19	Correlation between the tag efficiency $\gamma$ of the tags and the tangent loss $\tan\delta$ of the ears . . . . .	165
4.20	All Versions of ARDES Tags on ear read range comparison for 4 different orientations . . . . .	167
4.21	Chart representation of ARDES tags . . . . .	168
4.22	Mosaic of Configuration 1 . . . . .	169
4.23	Measured profiles for all configurations with Alien 9900+ reader . . . . .	170
A.1	Variation of $\Delta P_r$ in term of $\Delta$ for a set 9 different tags . . . . .	177
A.2	Representation of the Evolution of $\sqrt{M}$ (in linear) in term of $\Delta$ in dBm scale (or similarly $P_{inc}$ ) for 9 different tags . . . . .	178
A.3	Representation of the extended power profiles for the 9 tags . . . . .	179
C.1	Tag top angular pattern (Antenna 0 top) for $P_r^{max}$ (red) and $P_r^{th}$ (black) . . . . .	186
C.2	Tag angular pattern (Antenna 1 right) for $P_r^{max}$ (red) and $P_r^{th}$ (black) . . . . .	187
C.3	Tag angular pattern (Antenna 2 left) for $P_r^{max}$ (red) and $P_r^{th}$ (black) . . . . .	188
D.1	Mosaic of Configuration 2 . . . . .	189
D.2	Mosaic of Configuration 3 . . . . .	190
D.3	Mosaic of Configuration 4 . . . . .	191
D.4	Mosaic of Configuration 5 . . . . .	191
D.5	Measured profiles for configurations 1, 2, 3 and 4 with Impinj reader . . . . .	192

# LIST OF TABLES

---

1.1	Spectrum allocated to UHF RFID by region [24] . . . . .	40
2.1	$\tau$ , $\sqrt{M}$ and $Q_{dB}$ for a set of known RFID Antennas and IC Chips [29] . . . . .	93
2.2	Chip validity domain in $(\sqrt{M}, \tau)$ chart for: impinj Monza 2 chip, impinj Monza X-8K chip and impinj Monza R6-P chip. . . . .	99
3.1	Characteristics of a collection of commercial tags . . . . .	113
3.2	Data obtained from tag acquisitions . . . . .	123
4.1	Gaussian Model for ear permittivity in [860,960] MHz band . . . . .	152
4.2	The different tags used: their ID, chip type, chip sensitivity and type of antenna . . . . .	155



# LIST OF ABBREVIATIONS AND SYMBOLS

---

## Abbreviations

**RFID** Radio Frequency Identification

**UHF** Ultra High Frequency

**CM** Conjugate Matching

**ERP** Effective Radiated Power

**ETSI** European Telecommunications Standards Institute

**EPC** Electronic Product Code

**IC** Integrated Circuit

**CW** Continuous Wave

**RSSI** Received Signal Strength Indicator

## Symbols

$\tau_1$	power transmission coefficient of state 1 (backscatter state)
$\tau_2$	power transmission coefficient of state 2 (absorbing state)
$\tau$	mean power transmission coefficient
$M$	modulation factor
$\alpha$	transmission channel coefficient
$\alpha_{FS}$	free space channel coefficient
$G_t$	gain of tag antenna
$G_r$	gain of reader antenna
$\Gamma_1$	reflection coefficient of the backscatter state
$\Gamma_2$	reflection coefficient of the absorbing state
$\lambda$	wavelength of the electromagnetic wave
$P_t$	power transmitted by the reader
$P_t^{th}$	minimum transmitted power necessary to activate the tag
$P_{inc}$	incident power to the tag
$P_r$	power received by the reader
$S_c$	chip sensitivity
$S_r$	reader sensitivity
$P_{IC}$	power absorbed by the chip
$\tau^{th}$	mean power transmission coefficient at the threshold power
$M^{th}$	modulation factor at the threshold power
$\Delta$	shift on the activation power profile
$P_t^\Delta$	transmitted activation power shifted with $\Delta$
$P_r^\Delta$	received power at the shifted transmitted activation power
$P_{inc}^\Delta$	incident power at the shifted transmitted activation power
$\tau^\Delta$	mean power transmission coefficient at the shifted incident power
$M^\Delta$	modulation factor at the shifted incident power
$Q$	tag offset
$R_t$	tag receptivity
$\gamma$	tag efficiency
$\rho_{RR}$	read range percentage
$d_{max}^\tau$	forward link read range
$d_{max}^M$	backward link read range
$Q$	tag offset that maximize the read range at condition: $d_{max}^\tau = d_{max}^M$

# INTRODUCTION

---

Automated technologies are becoming increasingly ubiquitous in our daily lives, and RFID is one such technology that has seen significant development over time. This thesis focuses on UHF RFID systems, which have been implemented in a wide range of applications, including retail, animal breeding, e-documents, indoor localization, and motion capture. UHF RFID systems outperform all other RFID technologies in terms of throughput and reading range.

A UHF RFID system typically consists of two essential components: an RFID reader and an RFID tag. The reader emits a radio wave to energize the tag, and once energized, the tag modifies and reflects the received signal by toggling between two input states. The UHF RFID tag is the most crucial component of the system and has been the subject of extensive study and improvement. However, achieving optimal performance of UHF RFID tags remains a challenge due to factors such as tag design, chip sensitivity and reader sensitivity.

Recognizing the significance of RFID tags, this thesis addresses the challenge by characterizing UHF RFID tags in an over-the-air environment and providing a comprehensive evaluation of their performance in various settings. By understanding the intrinsic characteristics of UHF RFID tags and delving into their behavior regarding power absorption and modulation, we aim to evaluate the performance and functionality of these tags in order to improve it.

This thesis is financed by BPI France as part of the collaborative project CAA-Connect, led by Cooperl, a prominent French company offering comprehensive solutions in the pork industry. The project focuses on leveraging RFID technology in the UHF band for livestock monitoring and traceability, given its reliability as an automated device in the livestock sector. Specifically, this thesis aims to investigate the effects of propagation and environmental factors on the RFID system by utilizing the RFID characterization platform at IETR (Institut d'Electronique et des Technologies du numéRique).

In summary, this thesis seeks to improve the functionality and performance of UHF RFID tags, with a specific focus on livestock monitoring and traceability in collaboration with Cooperl. By characterizing UHF RFID tags and evaluating their performance under various environmental conditions, this research aims to enhance the design and operation of these tags, ultimately benefiting the agricultural industry and beyond.

## Problematic of the thesis

The field of UHF RFID passive tags is experiencing continuous growth, with improvements in chip sensitivity and reader sensitivity. However, in the design of passive tags, there exists a trade-off between meeting the requirements for power scavenging and modulation depth, which relates to the load impedances of the tags.

In order to maximize power scavenging, it is typical to achieve antenna conjugate matching (CM) in one modulation state. On the other hand, maximizing the backscattered power implies that short-circuiting the tag antenna in the second modulation state. However, it is essential to strike a balance between these two mechanisms to achieve optimal performance for the passive tag. Note that in reality the modulation input state of the chip is not perfectly a short circuit.

To address this challenge, the concept of the mean power transmission coefficient derived from both chip states, along with the pre-existing modulation factor, is introduced and studied. Consequently the characterisation of UHF RFID tag over-the-air is done in this research to access the mean power transmission coefficient and the modulation factor. This characterization delivers a better understanding on the evaluation and comprehension of tag performance in order to achieve an optimal design for a tag. By representing these parameters in an explicit way, it becomes possible to optimize both the power harvesting and modulation processes for the passive tag. Notably, in the case of semi-passive tags, the optimization of only the modulation process becomes crucial, as power scavenging is no longer the sole concern.

In this thesis, the characterization of UHF RFID tags over-the-air was conducted to determine the mean power transmission coefficient and modulation factor. However, a significant challenge arose due to the reliance of the theoretical formula on unknown parameters such as the gains and polarization of the tag and reader antenna. Moreover, the channel attenuation in complex indoor environments was also unknown. To overcome this challenge, we devised a solution by combining all these unknown variables into a single channel variable referred to as  $\alpha$ . By exploiting the concept of channel reciprocity in UHF RFID link budget, we successfully addressed this issue, allowing us to uncover the intrinsic characteristics of the tag. Importantly, this approach enabled us to perform the characterization of UHF RFID tags over-the-air independently from the specific environmental conditions, as the channel was compensated by averaging the transmitted and received activation profile.

## Organisation and contributions of the thesis

This thesis was initially placed under two constraints. The first was to use the IETR RFID characterization platform to observe the operation of tags placed in a controlled manner in space, and the second was to help to and facilitate the characterization of tags in the application context of a collaborative project on the use of RFID tags on pig farms. It is from these two constraints that the main contribution of this work has emerged, a renewed theoretical framework that exploits quantities well known in the literature, and that enhances the characterization capabilities of the existing device. A conventional RFID reader has been transformed into a rather accurate instrument for comparative tag characterization.

Initially, we focused on comparing the transmitted and received activation profiles. The first profile expresses the lowest transmission power that activate the tag placed at a given distance, which is varied continuously using the main rail. This power profile is natively obtained in dBm. The second profile we can obtain corresponds to the received level. This received level is indicated using an RSSI value, which is not straightforwardly convertible into power in the Alien reader documentation.

The observation that the activation profiles were superposable provided that the RSSI was converted into *dBm* using a formula of the type  $P_r = 20 \log_{10}(RSSI) + constant$ . This result suggests that the proposed measurement is a measurement of the received voltage. Precise determination of the constant was only possible after comparison with a more recent reader, the IMPINJ R700, which provides received levels in *dBm*. There is no method for determining this constant for the conversion formula, which is essential if the reader is to be used as a precise measuring instrument, especially as the reader's sensitivity is not provided by the manufacturer either.

The most surprising result appeared when combining profiles in order to take the arithmetic mean a quasi-perfect constant appeared. This result will be interpreted a posteriori as the manifestation of the reciprocity of the channel when it comes to understand this observation in a more theoretical framework.

The first question that came up was: What is this constant? The first intuition was to think about the sensitivity of the chip because the measured values were very close. But considering the measurements carried out on a large number of tags it could be seen that the difference in the sensitivity of the chip was sometimes positive and sometimes negative of several dB. We decided to name this level the receptivity of the tag and not as it could also have been possible the sensitivity of the tag which was already a concept used in the literature with a different definition.



It appeared that the difference between the receptivity of the tag and the sensitivity of the chip was a quantity directly related to the  $\tau$  and  $M$  characteristics related to the design of the tag, namely the combination of a chip and an antenna. We called this quantity  $Q = \frac{\sqrt{M}}{\tau}$  the tag offset, notice that it is not a tag quality criterion as we thought initially when we introduced the mathematical notation.

The quantities  $M$  and  $\tau$  are both dimensionless. They are convenient because they both take their values between 0 and 1. It was therefore natural to try to understand how a given tag would place in this space of representation. In this diagram  $(\sqrt{M}, \tau)$ , the parameter  $Q^{-1}$  takes the meaning of the slope of a line passing through the origin. Some tags can be designed to give preference to high  $\tau$  values at the expense of the modulation factor  $M$ , other tags on the contrary can be less effective on absorption but present a strong  $M$ . At that point, we have imagined that a "good" tag should seek to find the best compromise between the two criteria. Furthermore, we also define the tag efficiency  $\gamma$  such that a tag is either fully determine at a given frequency by the knowledge of  $(\sqrt{M}, \tau)$  or equivalently by the tag offset and the tag efficiency  $(Q, \gamma)$ .

In this thesis, we seek to access and evaluate the intrinsic characteristics of UHF RFID tag by an over-the-air measurement by examining the reciprocity of the channel, and we develop a methodology for effectively optimizing the tag's design by striking the ideal balance between these pivotal characteristics,  $\tau$  and  $M$  or  $Q$  and  $\gamma$ . This balance depends from various factor, such as the reader sensitivity and chip sensitivity, that will be studied in this thesis.

The manuscript is structured around the objective of characterizing and evaluating of UHF RFID tag. To achieve this, we will firstly present the fundamental parameters of communication in UHF RFID. This study will be divided into two parts: the theoretical aspect will develop the communication theory of passive UHF RFID and the intrinsic characteristics evaluation and dependencies in order to evaluate and improve the performance of UHF RFID tag and investigate the read range and its dependencies in free space condition. It will also explore the variation of these characteristics in term of the incident power on the tag.

The second parts focus on exploiting the experimental aspects based on the theoretical aspects given. The metrics and theory exploited is utilized to evaluate and compare the performance of a set of commercial tags. This evaluation is deeply analysed by a study of intrinsic characteristics of the tags and their variability. We presents in this thesis a methodology to obtain a performance evaluation of a measured tag leading to the optimal design of this tag.

In Chapter 1, we lay the foundation for the subsequent chapters by exploring RFID technology. We provide a clear overview of RFID technology, with a specific focus on passive UHF RFID system. We covers the historical background, evolution, and key components of UHF RFID. We

then explain the link budget of UHF RFID, explore recent advancements in tag-reader interaction and the recent over-the-air method for characterizing UHF RFID tag. Additionally, we introduce the RFID platform used in this research to conduct over-the-air autonomous experimentation. We finally conclude with a summary of our state-of-the-art analysis.

In Chapter 2, we provide a comprehensive study of theoretical aspects of UHF RFID link budget and tag characterization. We focus on two key parameters: the mean power transmission coefficient  $\tau$  which takes into account both input states of the tag, and the modulation factor  $M$ . By deriving the reciprocal channel coefficient and exploiting the activation power profiles, we access a  $Q$  factor relating  $\tau$  and  $M$ . This relation leads to introduce the tag receptivity and to propose a  $(\sqrt{M}, \tau)$  chart for evaluating tag performance. We also define in this chapter the free space read range, considering modulation factor, chip and reader sensitivities and power power transmission coefficients. Furthermore, we bring forth the concept of the validity domain for a chip, determining the optimal matching attainable within this domain. To illustrate this, we analyze three distinct chips and showcase their positioning within the  $(\sqrt{M}, \tau)$  chart. This study enhances our understanding of UHF RFID and aids in future system design and optimization.

In Chapter 3, we focus on the experimental characterization of RFID tags to assess and compare their performance. We firstly analyse power profiles obtained from RSSI measurements, converting them to actual power units. We also extract the defined tag receptivity and  $Q$  values for a set of 9 tags to evaluate efficiency and utilize the  $(\sqrt{M}, \tau)$  chart for visual comparison of the tags placed using the algorithm. Moreover, we study the free space read range limitations visualized in the  $(\sqrt{M}, \tau)$  chart. Additionally, we investigate the impact of varying the incident power on the mean power transmission coefficient and modulation factor of the tag, thus a better comprehension on the non-linear behavior of the UHF RFID tags is explored. Additionally, we investigate and scan the reciprocal propagation channel using a set of identical UHF RFID tags placed in a row configuration.

In Chapter 4, we begin by providing an insightful overview of how UHF RFID technology is employed in livestock management, with a specific focus on its application in tracking and monitoring livestock. Additionally, we delve into a detailed electrical characterization of pig ear tissue, aiming to differentiate between the internal and external surfaces of the ear. This distinction is crucial in understanding how these different surfaces affect the performance of RFID tags attached to pig ears. Moreover, we conduct a comprehensive study to examine the impact of pig ears on RFID tag performance, taking into consideration the differentiation between the internal and external sides of the ear. By analysing this aspect, we gain valuable insights into how the orientation of the ear and the inherent variability in tags can affect RFID

communication in the presence of pig ears. Additionally, we examine the effects of varying the ear on a single tag, exploring the correlation between the electrical characteristics of the ears and tag performance. These investigations aim to deepen our understanding of the complexities and challenges associated with deploying UHF RFID technology for livestock management, particularly in the context of pig ears. By discerning the electrical characteristics of pig ear tissue and evaluating the effects of ear orientation and tag variability, we seek to optimize RFID communication in this specific scenario.

# RÉSUMÉ EN FRANÇAIS

---

## Introduction

Les technologies de l'information deviennent de plus en plus omniprésentes dans notre vie quotidienne, et la technologie RFID en est un exemple qui a connu un développement significatif au cours du temps. Cette thèse se concentre sur les systèmes RFID UHF, qui ont été mis en œuvre dans un large nombre d'applications, notamment l'élevage animal, les documents électroniques, la localisation et la capture de mouvement. Les systèmes RFID UHF surpassent toutes les autres technologies RFID en termes de débit et de portée de lecture.

Un système RFID UHF se compose généralement de deux composants essentiels: un lecteur RFID et un transpondeur RFID. Le lecteur émet une onde radio pour alimenter le transpondeur, et une fois alimenté, le transpondeur modifie et renvoie le signal reçu en basculant entre deux états d'entrée dont l'alternance permet de moduler l'information. L'état 1 est l'état bas, l'état 2 est celui dans lequel se trouve la tag non encore activé et il est destiné à faciliter l'absorption de l'énergie reçu en provenance du lecteur. Le transpondeur RFID UHF est le composant le plus crucial du système et a fait l'objet d'études et d'améliorations approfondies. Cependant, l'atteinte d'une performance optimale des transpondeurs RFID UHF reste un défi en raison de facteurs variés tels que la conception du transpondeur, la sensibilité de la puce et la sensibilité du lecteur.

Conscient de l'importance des transpondeurs RFID, cette thèse aborde le défi en caractérisant les transpondeurs RFID UHF dans un environnement en "over-the-air" et en fournissant une évaluation complète de leur performance dans divers contextes. En comprenant les caractéristiques intrinsèques des transpondeurs RFID UHF et en explorant leur comportement en ce qui concerne l'absorption d'énergie et la modulation, nous visons à évaluer la performance et la fonctionnalité de ces transpondeurs afin d'atteindre la conception optimale des transpondeurs.

En résumé, cette thèse vise à améliorer la fonctionnalité et la performance des transpondeurs RFID UHF, avec un accent particulier mis sur la surveillance et la traçabilité du bétail en collaboration avec Cooperl. En caractérisant les transpondeurs RFID UHF et en évaluant leurs performances dans diverses conditions environnementales, cette recherche vise à améliorer la conception et le fonctionnement de ces transpondeurs, bénéficiant finalement à l'industrie de

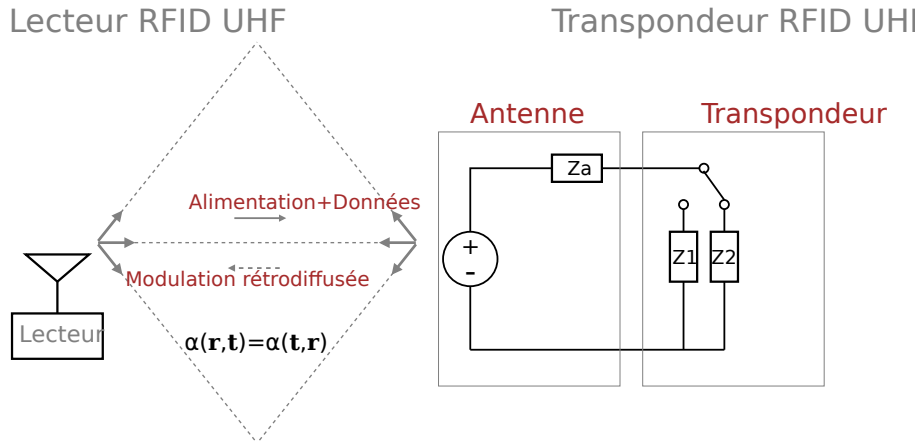


Figure 1 – Schéma générale du système RFID UHF

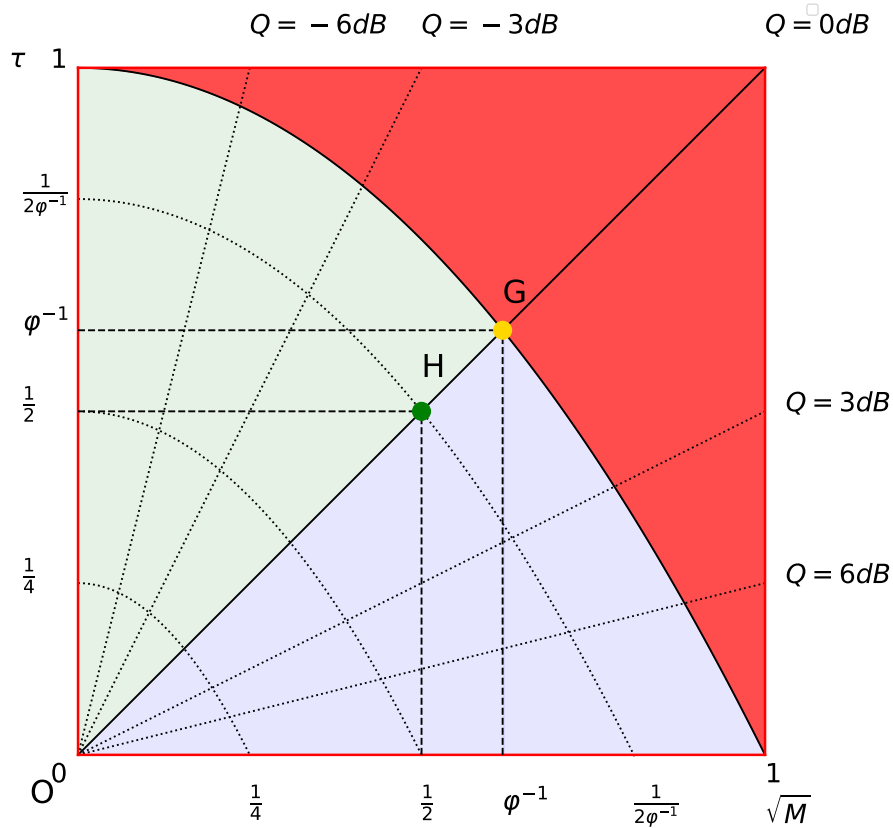
l'élevage et au-delà.

## Aspects théoriques du système RFID

Dans cette thèse, nous proposons une exploration approfondie des aspects théoriques de la technologie RFID UHF. Dans la communication RFID, deux liaisons distinctes sont formées, comme illustré dans la Figure 1 :

- La liaison de transmission: Cette liaison est limitée par la sensibilité de la puce du transpondeur et le coefficient de transmission moyen introduit  $\tau$ . Dans la littérature, l'énergie absorbée par le transpondeur dépend uniquement de l'état d'absorption 2 du transpondeur, c'est-à-dire du coefficient de transmission de puissance  $\tau_2$ . Cependant, en nous basant sur le principe de conservation de l'énergie, nous prenons également en compte l'énergie absorbée par l'état de rétrodiffusion 1. Ainsi, la quantité d'énergie absorbée par la puce est exprimée par le coefficient de transmission moyen de puissance  $\tau$ , qui est la moyenne des deux coefficients de transmission de puissance  $\tau_1$  et  $\tau_2$ .
- La liaison de rétrodiffusion : Cette liaison est limitée par la sensibilité du lecteur et le facteur de modulation  $M$ . Ce dernier est une autre caractéristique intrinsèque du transpondeur qui décrit la quantité d'énergie rétrodiffusée vers le lecteur.

En étudiant ces deux liaisons, nous fournissons deux puissances d'activation : la puissance d'activation transmise, qui est la puissance minimale transmise par le lecteur nécessaire pour activer le transpondeurs, et la puissance d'activation reçue, qui est la puissance reçue par le

Figure 2 – L’abaque  $(\sqrt{M}, \tau)$  proposée

lecteur à la puissance d’activation transmise.

L’observation clé de ce travail est que, en moyennant les deux profils d’activation, nous obtenons une quantité appelée réceptivité du transpondeur  $R^{th}$ , qui est la sensibilité de la puce décalée par le décalage du transpondeur  $Q$ . Cette quantité est une relation des caractéristiques intrinsèques du transpondeur ( $\tau$  et  $M$ ) dans l’environnement aérien. Cela est possible uniquement parce que le canal de transmission de la RFID UHF est réciproque, comme illustré dans la Figure 1.

Après avoir obtenu la réceptivité du transpondeur, nous avons défini un algorithme qui peut extraire le coefficient de transmission moyen de puissance et le facteur de modulation pour un transpondeur. Ensuite, nous introduisons un outil de représentation pour évaluer les performances du transpondeur sous forme d’un abaque  $(\sqrt{M}, \tau)$ , présenté dans la Figure 2. Cet abaque sert d’outil d’analyse précieux pour évaluer les performances des transpondeurs RFID UHF. En utilisant cet abaque, nous pouvons accéder à la correspondance optimale entre la puce

et l'antenne du transpondeur, améliorant ainsi la conception et les performances du transpondeur.

La théorie complète présentée dans ce chapitre pose les bases pour une compréhension plus approfondie en vue de parvenir à une conception optimale du transpondeur dans un scénario spécifique.

## Caractérisation expérimentale de transpondeurs RFID

Dans cette thèse, la plateforme de caractérisation RFID de l'IETR a été initialement exploitée et programmée pour effectuer des expériences sur les transpondeurs RFID UHF. Il s'agit d'un outil automatisé qui nous permet de déplacer le transpondeur sur un rail en translation ou même en rotation. Cette capacité de la plateforme nous permet d'accéder aux profils de puissance définis (y compris la puissance d'activation) en faisant varier la distance entre le transpondeur et l'antenne, tout en faisant varier la puissance transmise par le lecteur à chaque étape. Le lecteur initial utilisé pour les expériences est le lecteur Alien ALR 9900+. La première exploration a commencé par la mesure de ce profil de puissance en RSSI. Ainsi, pour améliorer la précision de la représentation de la puissance du signal reçu, le premier objectif était de convertir le RSSI du lecteur Alien en une quantité de puissance réelle en dBm, car cette conversion n'est pas fournie par le fabricant. Ensuite, nous avons converti les profils d'activation en quantité dBm et les avons présentés dans la Figure 3. Dans cette figure, nous présentons également la réceptivité du transpondeur en vert, qui a été obtenue en moyennant les deux profils d'activation. L'observation étonnante est que cette quantité est quasi constante sur la distance, car elle est indépendante de l'environnement de propagation et uniquement liée aux caractéristiques intrinsèques du transpondeur.

Ensuite, les mêmes acquisitions ont été effectuées pour un ensemble de 9 transpondeurs commerciaux. L'algorithme introduit a ensuite été utilisé pour extraire le coefficient de transmission moyen de puissance  $\tau$  et le facteur de modulation  $M$  pour chaque transpondeur. Nous avons ensuite pu placer ces transpondeurs dans l'abaque  $(\sqrt{M}, \tau)$  défini, présenté dans la Figure 4.

En plaçant ces transpondeurs sur l'abaque, nous avons été en mesure de comparer et d'évaluer les performances de ces transpondeurs. Dans le cas où la sensibilité du lecteur est inconnue, les critères d'évaluation proposés correspondent à l'équilibre maximal entre le coefficient de transmission moyen de puissance et le facteur de modulation présenté par le "point d'or"  $G$  sur le graphique.

De plus, nous avons exploré les dépendances de la portée de lecture, en mettant particulièrement l'accent sur la sensibilité du lecteur ( $S_r$ ) et la sensibilité de la puce ( $S_c$ ). Ensuite, nous nous

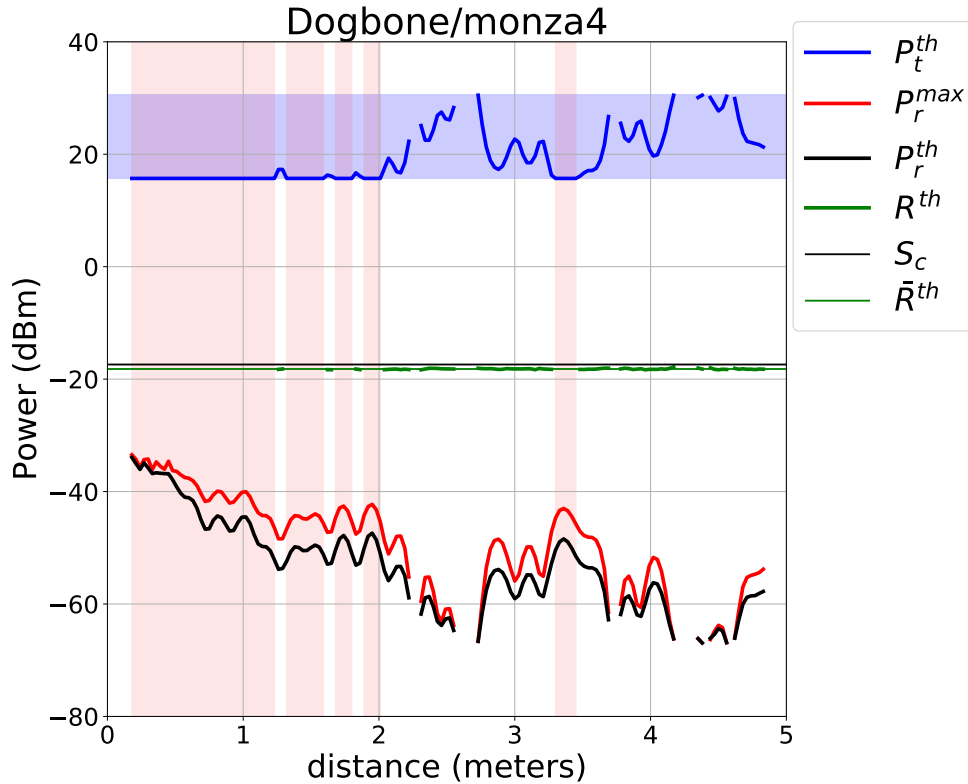


Figure 3 – Représentation du profil de puissance en translation du transpondeur dogbone/Monza4

sommes penchés sur les caractéristiques non linéaires des transpondeurs RFID UHF, illustrant l'impact de la variation de la puissance incidente sur le comportement du transpondeur.

## Caractérisations expérimentales dans le contexte de l'application en élevage

Cette thèse s'inscrit dans un projet collaboratif dirigé par l'entreprise Cooperl, leader en France dans le domaine de l'élevage. Notre rôle dans ce projet était d'étudier les transpondeurs RFID utilisés sur les oreilles des porcs, en prenant en compte les effets de la propagation et de l'environnement. Pour ce faire, nous avons utilisé la plateforme de caractérisation RFID de l'IETR et développé les méthodes de caractérisation présentées précédemment.

Deux grandes campagnes de mesure ont été menées :

- La première campagne de mesure était consacrée à l'étude du comportement d'un transpondeur placé sur l'oreille d'un porc. Nous avons commencé par une exploration complète



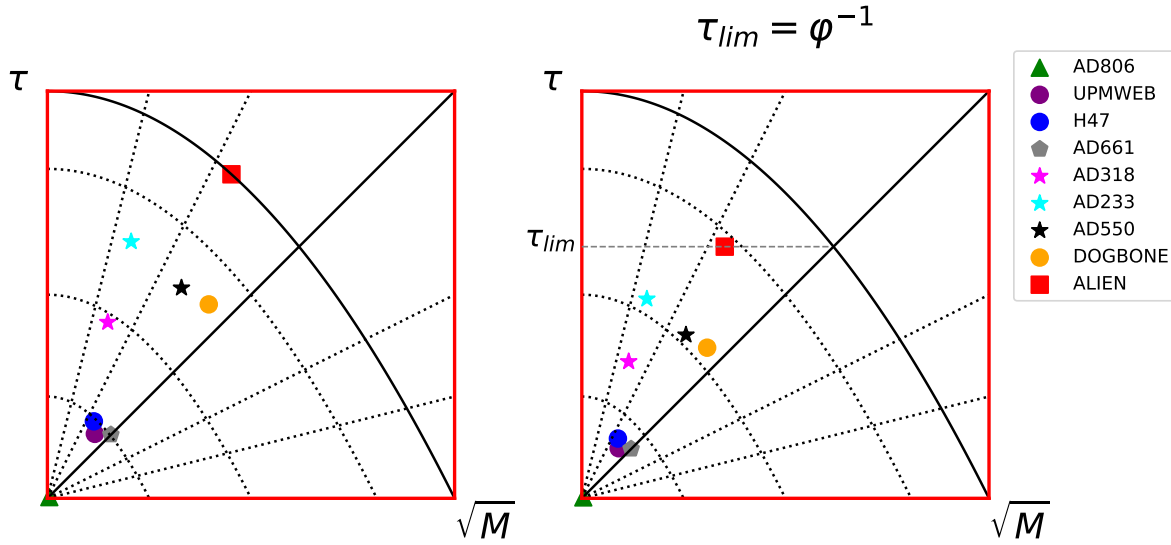


Figure 4 – Comparaison d'un ensemble des transpondeurs dans l'abaque

des caractéristiques diélectriques de 25 oreilles de porc fournies par Cooperl. Les mesures ont révélé des différences perceptibles entre les caractéristiques diélectriques de la face interne et de la face externe de l'oreille. Ces découvertes nous ont fourni des informations essentielles sur les propriétés du matériau de l'oreille de porc, qui peuvent avoir un impact significatif sur les performances des transpondeurs RFID.

De plus, nous avons mesuré les profils de puissance de plusieurs transpondeurs commerciaux avec et sans l'oreille, dans différentes orientations, afin d'évaluer les paramètres les plus influents. Ces expériences ont révélé une différence de performance du transpondeur en fonction de l'orientation, mettant en évidence l'influence de l'emplacement du transpondeur du côté interne ou externe de l'oreille. Cela a également révélé comment l'oreille réduit les performances du transpondeur qui y est fixé, surtout si le transpondeur n'est pas conçu pour fonctionner sur l'oreille de porc. Dans le cadre de cette campagne de mesure, nous avons également étudié la variabilité de la réponse des transpondeurs en fonction des différentes oreilles, montrant que le comportement des transpondeurs commerciaux pouvait varier d'une oreille à l'autre.

- La deuxième série de mesures avait pour objectif d'évaluer les transpondeurs conçus et fabriqués par ARDES, spécifiquement adaptés pour fonctionner sur les oreilles de porc. Nous avons étudié l'effet de l'oreille sur ces transpondeurs adaptés, ainsi que l'impact de

l'orientation de l'oreille sur la portée de lecture. Nous avons comparé différentes versions de ces transpondeurs pour déterminer la plus adaptée à une utilisation sur l'oreille de porc. Notre évaluation nous a permis de conclure que la meilleure version était la plus adaptée. De plus, nous avons étudié comment plusieurs transpondeurs RFID réagissent lorsqu'ils sont utilisés en configuration plane, une information essentielle pour optimiser les performances du système dans des scénarios d'élevage impliquant plusieurs transpondeurs.

## Conclusion

Cette thèse a apporté des contributions significatives au domaine de la technologie RFID UHF, enrichissant à la fois la compréhension théorique et l'application pratique de la RFID UHF.

Nous avons exploré en détail les aspects théoriques de la technologie RFID UHF, plongeant dans les caractéristiques intrinsèques des transpondeurs, telles que le coefficient de transmission moyen de puissance ( $\tau$ ) et le facteur de modulation ( $M$ ). Nous avons profité du concept de "réciprocité de canal" et généralisé le coefficient de canal dans des environnements à trajets multiples, pour accéder à la réceptivité du transpondeur dans l'air. Nous avons également proposé un abaque ( $\sqrt{M}, \tau$ ) pour analyser et évaluer les performances des transpondeurs RFID UHF.

Pour valider notre exploration théorique, nous avons réalisé des expériences à l'aide d'une plateforme de caractérisation de l'IETR pour évaluer les transpondeurs RFID dans l'air. À l'aide de cet outil, nous avons mesuré les profils de puissance en faisant varier la distance entre le lecteur et les transpondeurs, ainsi que la puissance transmise. Ces mesures nous ont permis de calculer les caractéristiques intrinsèques des transpondeurs afin d'évaluer et comparer un ensemble de transpondeurs en les plaçant dans l'abaque de caractérisation ( $\sqrt{M}, \tau$ ). De plus, nous avons analysé la formulation de la portée de lecture en espace libre, en tenant compte des limitations à la fois de la liaison en avant et de la liaison de rétrodiffusion.

Dans le cadre du projet CAA-Connect, notre thèse a présenté des mesures approfondies pour déterminer les propriétés diélectriques des oreilles de porc. Ces mesures ont révélé des différences entre les côtés interne et externe de l'oreille de porc, influençant le comportement des transpondeurs en fonction de l'orientation de l'oreille. Nous avons également exploré comment le comportement des transpondeurs varie lorsqu'ils sont placés sur différentes oreilles et comment la présence de plusieurs transpondeurs dans une configuration

plane influence leurs performances.

En résumé, cette thèse fait progresser la technologie RFID UHF en offrant des éclairages originaux liant l'exploration expérimentale et théorique et trouve des applications pratiques dans l'évaluation comparative des performances des transpondeurs RFID.

# UHF RFID SYSTEM: LITERATURE REVIEW

---

## 1.1 Introduction

This chapter provides an extensive literature review on UHF RFID (Ultra-High Frequency Radio Frequency Identification) systems, which forms the fundamental basis for the subsequent chapters of this thesis. RFID technology is crucial in various domains as it enables automated identification and tracking of objects through wireless communication. The primary focus of this chapter is on passive UHF RFID systems, offering a clear and concise explanation of their principles and functionality. It starts by covering the historical background and evolution of this technology, tracing its path from inception to modern-day innovations. Then it delves into the key components that constitute an RFID system, exploring the roles of RFID tags and readers, as well as the mechanisms by which they interact. The chapter also discusses the advantages, challenges, and regulations associated with UHF RFID. The use cases and the EPCglobal Generation 2 standard are explored. Moreover, the link budget of UHF RFID systems receives significant attention in this chapter. It examines the communication process between RFID readers and tags where it explores the characteristics of passive tag. Additionally, this chapter discusses the energy conservation in the passive tag which is crucial to understand its characteristics. It then investigates method for over-the-air characterization of passive tags, enabling the assessment of tag performance, in order to reach an optimal design of the tag. Then, it presents a multipath channel model for tag-reader communication. Finally, we introduce the characterization IETR platform used to do automated experiments on moved tag as we will see in the followed chapters.

## **1.2 Overview on RFID system**

Radio Frequency Identification (RFID) is basically a technology of capturing digital data by an automatic identification method that uses wireless non-contact radio waves in which data is digitally encoded in RFID tags or smart labels which can be read by a reader through radio waves. In other words, RFID is a wireless system used to detect, control and track objects equipped by an RFID tag which is an intelligent bar-code defined by its own ID. RFID is without doubts a major technology that will be improved and exploited more and more over time.

### **1.2.1 History of UHF RFID**

The ideas and research on RFID came in the wake of the development of radar since RFID is the combination of radio broadcast technology and radar. So the early concept of RFID can be traced back to radar system which has its birth in the early 20th century [1]. In a similar concept of RFID, radar detects and locates an object by the reflection of the radio it transmits, allowing it to determine the position and speed of the detected object. It wasn't until the 1960s and 1970s that RFID technology began to develop for practical use. In the early 1970s the first multi-bit functional passive UHF RFID systems were developed, which were capable of transmitting signals over several meters. These systems did not require a power source and were able to function passively, which means they obtained the energy required for operation from the electromagnetic field generated by the reader. The development of these systems marked a significant breakthrough in radio-frequency identification technology, as they were able to transmit more data and operate over greater distances than earlier RFID systems [2]. Following this, early pioneers in the field include Charles Walton, who in 1973 patented a passive transponder system that is still in use today. The technology continued to evolve through the 1980s [3], with improvements made to increase the efficiency and accuracy of the systems. This led to the development of new applications for RFID technology, such as inventory management and asset tracking in industrial settings. The advancements in RFID technology during this period also paved the way for the development of more sophisticated and complex systems that we see today. Following its growth, in the 1990s the United States installed, in North America, over 3 million RFID tags on rail cars. By the 2000s, RFID technology saw widespread adoption in the retail industry, where it was used to track inventory and prevent theft. Till nowadays, RFID is continuing to improve and grow, it is widely used for applications such as

access control, indoor localization [4], [5], motion capture [6], sensing [7], and industrial automation its playing a central role in many industries, it has been implemented in many fields, like retails, animals breeding, e-documents, etc...

Furthermore, there have been notable advancements in chip sensitivity from 2005 [8] to 2020 [9], with a remarkable reduction of 15 dB. This is partly due to advancements in semiconductor technology, including smaller transistors and lower power consumption. The latest passive chips now exhibit an exceptional sensitivity of  $-24$  dBm [9]. These advancements in chip sensitivity have significantly contributed to the continuous improvement and widespread adoption of RFID technology in various industries.

The reader sensitivity is also an important factor that determines the read range of an RFID system.

In recent years, there have also been significant improvements in the UHF RFID readers. This is due to the development of new antenna designs and signal processing techniques which improved the reader sensitivity and data transfer rate of the RFID reader. As a result of these improvements, the read range of UHF RFID systems has increased significantly. In the early 2000s, the read range of UHF RFID systems was typically limited to a few meters. Today, some UHF RFID systems can read tags from distances of up to 20 meters or more [10]. The combination of improved chip sensitivity and receive sensitivity has made UHF RFID technology even more versatile and powerful.

Overall, RFID technology has evolved over time from its early days to its current state of widespread adoption and use in various industries. An RFID system is typically composed of an RFID tag, an RFID reader and a data management system.

## **1.2.2 RFID system components**

An RFID system is typically composed mainly of an RFID tag and an RFID reader:

### **1.2.2.1 RFID tag**

An RFID tag, is a transponder that exchanges data with a RFID reader by implies of radio-waves. It has information stored inside such as a unique identifier. The communication between the tag and the reader is typically accomplished through electromagnetic fields.

Most of RFID tag is composed of two primary parts:

- An Integrated Circuit (IC) generally made of silicon. The IC contains the unique identification (ID) of the tag and serves multiple functions. It stores and processes

data, allowing the tag to carry information. Additionally, the IC demodulates and modulates the radio frequency (RF) waves it receives from the RFID reader.

- An antenna which is responsible for receiving and reflecting the radio signals. The antenna's size can vary depending on the specific tag and the requirements of the application in which it is used. The design of the antenna is optimized to ensure efficient reception and transmission of RF signals between the tag and the reader.

The combination of the IC and antenna enables the RFID tag to receive power wirelessly from the reader and exchange data with it through radio waves. In general, the IC stores the tag's ID and performs data processing, while the antenna facilitates the reception and transmission of RF signals for communication between the tag and the reader.

#### **1.2.2.2 RFID reader**

RFID readers are devices used to communicate with RFID tags. They come in a variety of form factors, ranging from handheld devices to fixed-position readers for use in warehouses and other industrial settings. They can be connected to computer networks for data processing and analysis, and can provide real-time location tracking for tagged assets or people. RFID readers can operate on different frequency bands, including low frequency (LF), high frequency (HF), ultra-high frequency (UHF), and microwave frequencies. The specific frequency band used depends on the application, the distance between the reader and the tag, and the amount of data that needs to be transmitted.

A UHF RFID reader, also known as an interrogator, is a transceiver that uses communication protocols such as the EPCglobal UHF Class 1 Gen 2 standard to communicate with RFID tags in the UHF band (typically 860-930 MHz). These readers can capture data from RFID tags within range, usually up to several meters. The transmitter part of the reader activates the passive tag by transmitting radio wave signals, which are captured by the tag's antenna. Part of the energy reaches the tag and is absorbed by the IC chip, while the rest is reflected back to the reader. The receiver of the reader captures the reflected signals from the tag for demodulation and processing. The effectiveness of a UHF RFID reader depends on factors such as transmit power, receiver sensitivity, antenna design, operating environment, and the characteristics of the RFID tags used.

### 1.2.3 Operation frequencies of RFID

RFID systems are categorized by their working frequency ranges since radio waves are used for communication between the tag and the reader. Regulatory authorities assign the various frequencies and establish highly detailed guidelines for each frequency's use. Also, these frequencies have been standardized to prevent interference with other devices where each country may have different standards. As illustrated in Fig. 1.1, RFID systems band of frequencies goes from Low Frequency (LF) to extremely high Frequency (SHF):

- Low-frequency (LF) RFID tags: Range of frequencies from 30 kHz to 300 kHz. It allows reading over small distances (less than 10 *cm*). These frequencies are utilized for various applications, including:
  - Automotive: remote keyless entry
  - Security: building access control
  - Science: Animal identification
  - Business: anti-counterfeiting mark
- High-frequency (HF) RFID tags: Range of frequencies from 3 to 30 MHz, commonly operating within the bandwidth of 13.56 MHz. This frequency range is mostly used for applications such as:
  - Contactless cards: payment, public transport, fidelity cards, etc.
  - Transports: postal packet tracking
  - Secured ID: passport, national ID, etc.

HF RFID tags offer a medium reading distance (about one meter) and are more susceptible to surrounding metal or liquid presence.

- Ultra High-Frequency (UHF) RFID tags: Range of frequencies from 300 MHz to 3 GHz, commonly operating within the frequency band of 860 – 960 MHz, with a bandwidth of around 100 MHz. Passive UHF RFID tags offer a range of over 16 *m* [11]. Applications utilizing UHF RFID include:
  - Agriculture: animal tracking [12]
  - Transport: aerial luggage tracking [13]
  - Security: alarm systems, access control [14, 15]
  - Supply chain management [16] portal pallet inventory (Wallmart), store live inventory, etc.



Active tags are typically employed for large items, such as train cars and large reusable containers, that need to be tracked over long distances.

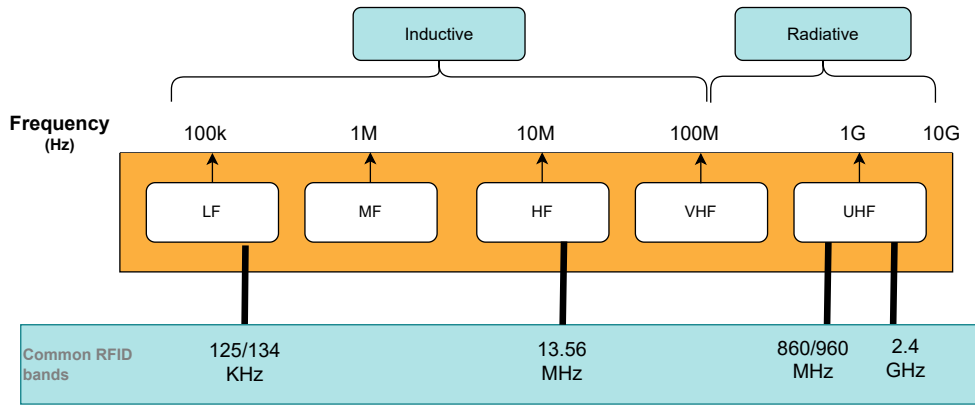


Figure 1.1 – RFID spectrum domain

## 1.3 UHF RFID system

The focus, in this thesis, is on the UHF RFID system. One of the defining features of UHF RFID is its exceptional read range. UHF RFID readers can detect and communicate with tags over long distances, typically ranging until several meters [11]. This extended range facilitates rapid and non-line-of-sight tag identification.

### 1.3.1 Types of UHF RFID tags

The UHF RFID tags can be active, semi-passive, passive and chipless:

- **Active tag:** it has its own power supply which allow a higher read range relatively. It transmits data to reader periodically. These tags are typically utilized in challenging environments. They are, for example, the ideal solution for tracking huge metallic containers that are placed close to each other and have no line of sight from reader to tag. It has a bigger size and higher price than other types, but can achieve the higher read range between them. This tag (up to 900m in outdoor case) where it can produce an output power of 60 mW [18].

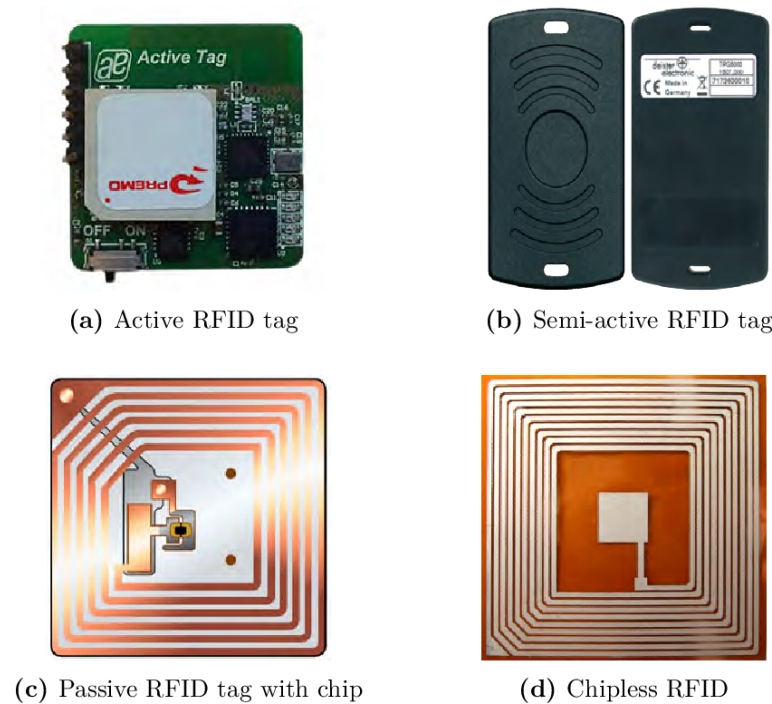


Figure 1.2 – Different families of RFID tags: (a) active tag, (b) Semi-passive tag, (c) passive tag, (d) chipless tag [17]

- **Semi-passive:** Also known as battery-assisted tags. Unlike active RFID tags do not transmit a periodic signal. It contain an embedded power source that is only used to activate the tag once it receives the signal transmitted . The advantages of semi-passive tags are that they allow to keep a rather simple architecture because the response of the transponder is always done via the principle of retro-modulation. Also it has a more read range than passive tags since it has bigger size and higher cost.
- **Passive tag:** does not have a power supply. It rely on harvesting the energy received from the reader in order to activate which allows it to reflect back all the energy from the signal received. In other words, the recovery of the information, its processing and the response signal containing the answer are done only with the help of the energy sent by the reader. Passive tags rely on the reader. The main advantage of passive tags are that they have a simple design, cheap price and small size. Passive tags are the most common and the most cost-effective type of RFID tag. Noting that the focus in this thesis is on passive tags.
- **Chipless tags:** as it's name implies, chipless RFID tags does not have a chip, hence,

it doesn't have a serial number. They use physical characteristics, such as electrical or optical properties, to store and retrieve data. The communication with it is made by taking a snapshot of the reflected waves and uses it as a fingerprint to identify the tag or the tagged object. They are relatively cheaper and have a longer lifespan than traditional RFID tags, however, their readability range is limited and their reliability may not be as high as traditional RFID tags [19].

### 1.3.2 Use cases of UHF RFID

RFID is the most popular solution currently being used to address the challenge of industries which its concern is ensuring the reliability, authenticity, and security of goods purchased, financial transactions, whether it is for access control, banking security, or authentication (UHF Gen2). With the aid of RFID technology, a variety of private data can be uniquely linked to each item. The identifying document for the item can now include the sources, the route, the assurance of quality, and the evidence of authenticity. With the advent of Gen 2 UHF RFID tags, RFID has become a reality. These passive tags don't need their own power source, in contrast to active tags, because the reader supplies the energy to start data transmission. The cost of tags is quite minimal because they don't require any technology. The tags are simply updatable with new data and can be reused. These tags can be used on almost any kind of asset because they can be read from close proximity to up to 30 meters away. For these reasons and more, UHF RFID is investigated widely in many domains; The following is a list of application areas where UHF RFID has proven its value interest:

- **access control:** UHF RFID technology revolutionizes access control in sensitive buildings, offering a highly efficient and secure solution that outperforms traditional magnetic badges. With UHF RFID systems, individuals can authenticate themselves without physical contact, enhancing overall security measures. Unlike radio frequency access badges, which have limited range within a few centimeters, UHF RFID tags go beyond proximity by providing read and write capabilities, enabling the storage of essential information. UHF RFID stands out as a compelling alternative to other sensing technologies due to its distinct advantages, including unique identification, communication capabilities without requiring direct line-of-sight, and rapid reading rates. Consequently, UHF RFID has become the most widely adopted technology in the realm of access control [15].

- **Livestock-Management Industry:** RFID is used in livestock management to identify and track specific animals, such as pigs [20], cows, goats, and more. Each animal has an UHF RFID tag in a robust plastic casing attached to its ear. Numerous tags consist of two discs connected by the animal's ear. By implementing the RFID technology in this field, farmers can identify their animals during inventory quickly and easily, hence, UHF RFID takes this field to another level. This thesis focus later on a study of the UHF RFID tag attached to a pig ear.



Figure 1.3 – RFID tag on pig ear

- **Warehouse and Distribution:** Profitability in the distribution sector is closely correlated with how quickly and precisely inventory enters, passes through, and leaves the warehouse. UHF RFID has been widely used in warehouse inventory [21] [22]. UHF RFID gives warehouse personnel the visibility they need to quickly and precisely process tens of thousands or even hundreds of thousands of goods each day.
- **Motion capture:** Human movement measurement has an interest in many fields, such as biomechanics, rehabilitation engineering, motor control and the gaming and film industries. Passive UHF RFID became widely used for detecting the motion of human [6], also objects, it is due of their unique advantages compared to other sensors, accelerometers, computer vision identify it and even active tags. It has been served in the medical field, for example in [23], passive UHF RFID has been

employed for for shoulder rehabilitation by automatically capturing the motion of the hand using an array of UHF RFID tags.

### 1.3.3 The Regulations for UHF RFID systems

For the RFID field to be commercialized, numerous standards and regulations have been made. It's primary objective aim is to harmonize the RFID sector in order to facilitate access to the market and thus increase market access and consequently increase sales volumes. The regulations must ensure the interoperability of RFID systems and of course, protect the user from the dangers that this technology can cause in terms of health and respect of liberties. Today, two organizations propose standards for RFID systems: the EPCglobal (Electronic Product Code) and the ISO (International Organization for Standardization). As for RFID technology, it can only use the frequency ranges allocated to industrial, scientific or medical applications, called ISM (Industrial Scientific Medical) bands. These bands have the advantage of being free of rights. However, they do not benefit from international harmonization. The regulations governing RFID systems depend on the public authorities. They differ from one country to another, which does not facilitate the implementation of a universal system that is particularly interesting in the current context of globalization. Moreover, RFID frequency bands are used by many other wireless communication technologies.

There is an international consensus on 125 kHz and 13.56 MHz for inductively coupled RFID systems. However, this is not yet the case for UHF frequencies, for which there are 3 regions. In each region different bands and powers are allocated to UHF RFID as shown in Table 1.1. As presented in this table, the power is calculate differently by region,

Region	Frequency band	Power authorities
Europe	869.4 to 869.65 MHz	0.5 W ERP
	865.6 to 867.6 MHz	2 W ERP - ETSI
	916.1 to 918.9 MHz	4 W ERP - EU 2018/1538
America	902 to 928 MHz	4 W EIRP - FHSS
Asia and Oceania	Japan: 916.7 to 920.9 MHz	4 W EIRP - LBT
	Korea: 917 to 920.8 MHz	4 W EIRP - HFSS or LBT
	Australia: 916.1 to 918.9 MHz	4 W EIRP

Table 1.1 – Spectrum allocated to UHF RFID by region [24]

where in Europe the unit is the Watt calculated in ERP (Effective Radiated Power) while

in the other regions, the unit is still the Watt but calculated in EIRP (Equivalent Isotropic Radiated Power). The ratio between the two units is:  $1 \text{ W ERP} = 1.62 \text{ W EIRP}$ .

The regulation in America is defined by FCC regulation 15.247, which allows a maximum transmission power of 1 W with a maximum antenna gain of 6 dBi (corresponding to 4W EIRP). The communication uses Frequency Hopping Spread Spectrum (FHSS) on 80 channels. Whereas the regulations for this technology in Europe are more restrictive as is defined by the 302 208 regulation determined by the ETSI (European Telecommunications Standards Institute). A reader must operate with a maximum power of 2 W ERP on a very narrow frequency band. The LBT (Listen Before Talk) regulation, however, has been adopted in Europe. This regulation states that before an interrogator can transmit a signal, it must first determine whether another signal is present in its transmission sub-band.

In Europe, the responsibility for regulatory matters lies with the European Telecommunications Standards Institute (ETSI).

### **1.3.4 EPCglobal Generation 2**

The EPCglobal Generation 2 UHF RFID system is a widely used and globally recognized standard that improves the reliability and performance of RFID technology through features such as advanced collision prevention, enhanced tag sensitivity, and the ability to read multiple tags simultaneously [25]. It also provides a higher level of data security and accuracy through the use of unique identification numbers for each tag. This standard is implemented in a variety of industries and supported by many RFID hardware manufacturers.

In UHF RFID systems operating in the 860 MHz - 960 MHz frequency range, the EPCglobal Gen2 protocol defines the physical and logical requirements. This protocol specifies the interactions between readers and tags, including the signaling layer, commands, and operating procedures. The reader modulates an RF carrier using different modulation schemes and delivers it to the tags. Tags transmit data by changing the amplitude and/or phase of the RF carrier through backscatter. The reader obtains data by broadcasting an unmodulated RF carrier and listening for the backscattered response.

At the tag identification layer, the reader controls tag populations through select, inventory, and access commands. The select command allows the reader to choose tags based on specific criteria. The inventory commands identify individual tags, and the reader retrieves the tag's Electronic Product Code (EPC). The access commands enable various operations

such as reading, writing, locking, killing, authenticating, or accessing files in the tag's user memory. These commands ensure efficient communication with uniquely identified tags [25]. In essence, RAIN RFID, often synonymous with the EPCglobal Generation 2 UHF RFID system, has achieved widespread adoption across diverse sectors, enhancing data security and accuracy in the process.

## **1.4 Characterization of passive UHF RFID tag**

In this work we focus on passive tags. Indeed, thanks to its low cost, passive UHF RFID technology remains the most deployed one for traceability applications.

The operation of RFID systems and their performance depends mainly on the type of RFID tags used, as there are several of them. The success of a technology is related to its effectiveness and also to its success rate in any configuration to which it is applied. Among the actions that can be carried out to ensure the success of a technology, we can cite the characterization of the system as a main aspect to be taken into account. Hence, characterizing the UHF tags is an valuable and important topic in this field.

### **1.4.1 UHF RFID communication between reader and tag**

In order to characterise the UHF RFID system it is essential to understand how the reader and the passive tag communicate by using electromagnetic waves in any kind of environment.

#### **1.4.1.1 UHF RFID tag operation**

Passive UHF RFID tags do not have batteries and require an external power source to operate. The communication between the RFID reader and the tag begins with the transmission of continuous electromagnetic waves (CW) by the reader to activate the tag. The tag is energized when it reaches a threshold power level, known as the chip sensitivity ( $S_c$ ). Once energized, the tag utilizes a process called backscattering where it modulates and reflects the energy back to the reader. The backscattered signal carries important information such as the tag's unique identification number (UID) and additional data programmed into the tag. The reader captures the backscattered signal and demodulates it to recover the transmitted data. Furthermore, the reader can send commands to the

tag, enabling operations such as reading or writing data stored in the tag's memory and modifying the tag's configuration parameters. The communication between the reader and tag can sometimes be bidirectional which allows data exchange in both directions.

#### 1.4.1.2 Impedance matching and switching in UHF RFID communication

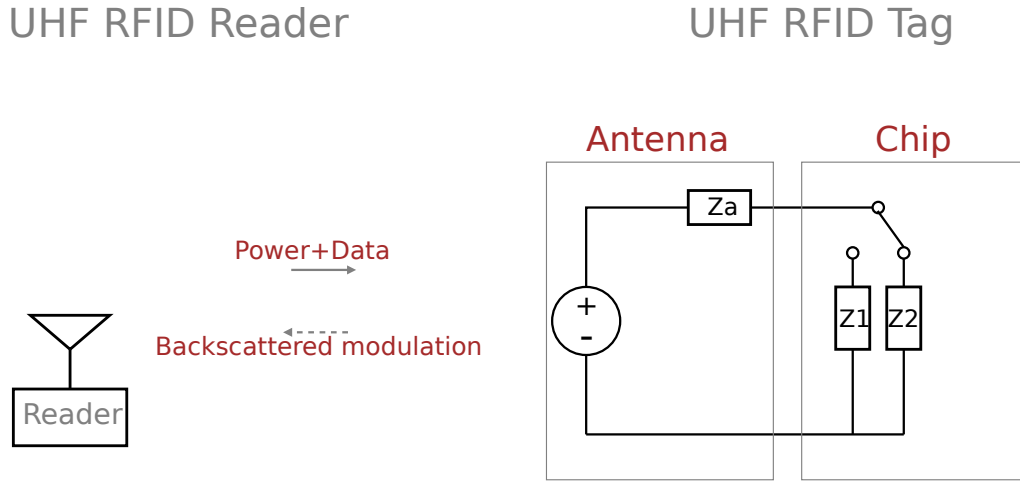


Figure 1.4 – General schema of UHF RFID system

Fig. 1.4 presents the general schema of this communication between the reader and the tag. As shown in this figure, a tag is a combination of an antenna and chip which is an integrated circuit (IC): The antenna can be modelled by a voltage supply and an impedance  $Z_a$ , whereas the chip can varies between two states, thus, it can be modelled by two impedance  $Z_2$  as the absorbing state and  $Z_1$  as the backscattering state. For the communication to work, the tag switches between two states, where it has to absorb the energy firstly with  $Z_2$ , modulates the signal and reflects the energy back to the reader by switching to  $Z_1$ , all while receiving continuously the energy from the reader with a continuous wave (CW) [26].

For optimal power transfer to the integrated circuit (IC) in the tag, impedance matching is important. In the backward link (tag absorbing energy),  $Z_2$  is usually designed to achieve complex conjugate matching with the antenna impedance  $Z_a$ , thus  $Z_2 = Z_a^*$  as shown in [27], [28]. In the forward (tag backscattering energy), a short circuit is the ideal state to reflect the signal, thus  $Z_1 = 0$ . While some literature assumes  $Z_1 = 0$  for simplicity (as in



[29]), practical implementations show that this impedance is not strictly zero and can vary based on the applied power [30], [31]. However, the complex matching condition  $Z_a^* = Z_2$  is enforced by design to maximize power transfer, regardless of the specific value of  $Z_1$  which is not provided in the datasheet.

Furthermore, when an RFID tag absorbs power from a reader signal, its impedance changes in response to the received energy. This change in impedance causes a change in the reflection coefficient which affects the amount of energy that the tag can backscatter. Specifically, when the tag is absorbing power from the reader, its impedance is high at  $Z_2$ , in this case, the reader's signal is no longer being efficiently reflected by the tag's antenna. Instead, some of the absorbed energy is used to power the tag's internal circuitry.

When the tag is not absorbing power from the reader, it is in a low impedance state  $Z_1$ , This allows the tag to backscatter more energy which can be detected by the reader. By switching between low and high impedance states, the tag can modulate the reader's signal to transmit data by affecting both phase and amplitude.

By understanding the principles of impedance matching and switching, as well as the effects of absorption and backscattering, it is possible to design and optimize RFID systems for a wide range of applications. For this purpose, it is important to illustrate the link budget of UHF RFID.

### **1.4.2 Link budget of UHF RFID**

The performance of an UHF RFID system depends on the ability to communicate reliably between the reader and the tag. The distance at which a tag can be read by a reader is influenced by various factors such as the chip sensitivity of the tag, the environment in which the system operates and in some cases by the reader sensitivity. The link budget is a fundamental concept that provides a mean of calculating the maximum distance at which a tag can be read by a reader, taking into account all the variables that affect the signal strength. In this subsection, we will discuss the definition and components of the link budget, including the free space loss, the effect of the antenna gain and polarization, absorption and backscatter. We will also explore the impact of the tag design on the link budget and how the link budget analysis can provide insights into the system's performance and potential issues that may impact the read range. The link budget of UHF RFID system is formed of two distinct links: the transmission link for energizing the passive tag, and the backscatter link of the modulated signal reflected back to the reader receiver. The

differentiation between those two links is necessary to fully understand the mechanism of UHF RFID propagation. Since one of the communicating devices (passive tag) has no power available for communication, the link budget for backscattered signals of passive RFID can be resembled to the radar equation from a far-field reading device. This is where it deviates from the traditional radio link budget.

The read range of RFID tag is an important tag performance characteristic. It represents the maximum distance at which RFID tag is activated and detected by the reader. The read range can be limited by the reader or by the tag.

#### 1.4.2.1 Path loss

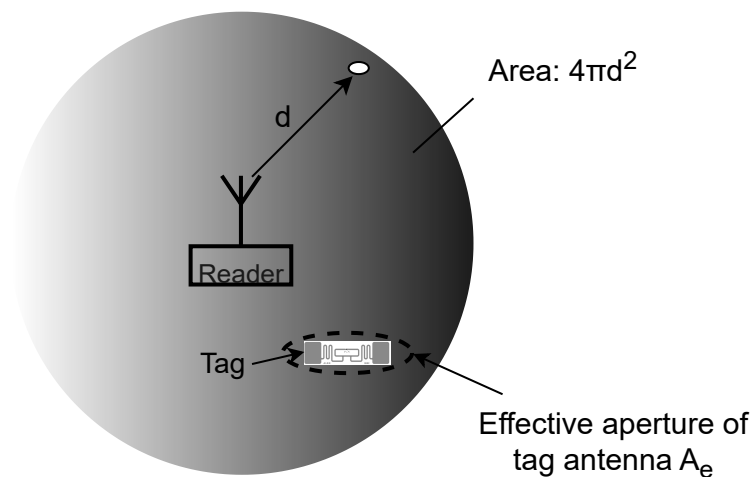


Figure 1.5 – Uniform distribution of an Isotropic Antenna Radiates Power uniformly over the spherical surface[18].

The path loss, which is the difference between the power delivered to the transmitting antenna and the power obtained from the receiving antenna, is an important factor in determining the range of an UHF RFID system. To understand path loss, we need to delve shortly into antenna operations. Let's start with a simplified but not very precise approach: imagining the transmitting antenna as emitting power evenly in all directions, like a light bulb casting light in all directions.

Think of this emitted power as spreading out uniformly over a spherical surface at any given distance from the reader antenna. Some of this radiated power reaches the tag's antenna, as illustrated in Fig. 1.5. The amount of power received depends on the power density hitting the tag. The area of the tag that collects this radiated power is called the effective aperture area, denoted as  $A_e$  and calculated as  $A_e = \frac{\lambda^2}{4\pi}$ , where  $\lambda$  represents the wavelength of the RFID electromagnetic wave (as per [18]). We need this  $A_e$  value to calculate the power received by the tag.

So, for a scenario where the transmitter is isotropic (emitting equally in all directions), the power incident on the tag, labeled as  $P_{inc}$ , can be expressed under the assumption of free space as follows:

$$P_{inc} = P_t \frac{A_e}{4\pi d^2} \quad (1.1)$$

Where  $P_t$  is the transmitted power by the RFID reader and  $d$  is the distance between the reader and the antenna. This RFID configuration using an isotropic antenna is only useful in case the tag can be anywhere around the antenna in the spherical region, but otherwise, in case the tag is to be in a specific directive area, the energy spreading in other directions would go to waste. Here come the role of antenna's directivity.

#### 1.4.2.2 Effect of the antenna gain and polarization

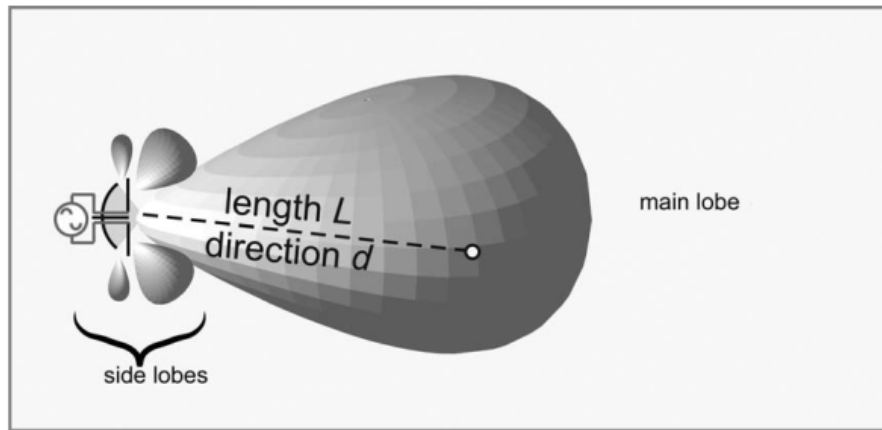


Figure 1.6 – Radiation Pattern for a Directional Antenna [18].

An isotropic antenna can achieve a few meters of read range with 1 Watt of output power in UHF RFID [18]. However, this is not ideal if the tags of interest are located in specific directions relative to the reader. For instance, in livestock-management industry

applications using UHF RFID, tags are attached to specific animal parts that move around in a predefined space. In this case, a directional antenna, as shown in Fig. 1.6, can concentrate its power in the direction of the predefined space, where the tags are most likely to be located. This makes better use of the transmitted power. A directional antenna's radiation pattern depicts the relative power density radiated by the antenna in any direction, and the directive gain is the ratio of radiation intensity in any direction to the intensity averaged over all directions. The directivity of the antenna is the maximum directive gain, and the power gain is the directivity multiplied by the radiation efficiency. In the direction of maximum radiated power density, a directional antenna, specially for readers, can provide  $G$  times more power than an isotropic antenna. Directional antennas are an essential component of the UHF RFID link budget, allowing for efficient use of the transmitted power and maximizing the read range. Adding antenna's gain to the configuration means forcing the antenna to radiate in the directions of the tags presented area. This solve the unnecessary waste of energy caused by radiating the energy all around the reader's antenna. By adding the gain of the antenna, the effective aperture can now be expressed by:

$$A_e = G \frac{\lambda^2}{4\pi} \quad (1.2)$$

where  $G$  is the antenna's gain and  $\lambda$  is the wavelength of the electromagnetic wave. We can establish a comprehensive formula for the power collected by a receiving antenna  $r$  from a transmitting antenna  $t$ , provided that the gains of both antennas and the distance separating them are known. The expected received power by the UHF RFID tag's antenna which is the incident power  $P_{inc}$  at the transmitted power  $P_t$  by the reader's antenna is then expressed by the Friis Formula, in free space, as follows:

$$P_{inc} = P_t G_t \left( \frac{A_e}{4\pi d^2} \right) = P_t G_r G_t \left( \frac{\lambda}{4\pi d} \right)^2 = P_t G_r G_t L_{FS} \quad (1.3)$$

where  $L_{FS}$  is the free space loss factor

$$L_{FS} = \left( \frac{\lambda}{4\pi d} \right)^2 \quad (1.4)$$

Where  $G_r$  and  $G_t$  are respectively the gain of the reader's antenna and tag's antenna.

If we take into account the losses that occur at the tag level and the polarization losses, the total losses can be represented as the backscattered-transmission losses  $L_B$ . The received

power by the reader can then be expressed as:

$$P_r = P_t G_r^2 G_t^2 L_{FS}^2 L_B \quad (1.5)$$

Where  $P_r$  is the received power by the reader from the backscattered power by the tag and  $L$  is the backscattered-transmission losses including the polarization losses [32]. It is important to note that equation (1.5) is valid only for the monostatic antenna configuration [33], where a single antenna serves the purpose of both transmission and reception. The proportionality of the received power with the inverse fourth power of the distance between the reader and the tag is due to the link budget formed by two distincts link reader-to-tag and tag-to-reader, hence, the distance is involved at the power 4 [18].

#### 1.4.2.3 Power reflection coefficient of UHF RFID tag

The power reflection coefficient is a measure of how much power is reflected back from a transmission line or other impedance-matched system. It is a complex number that represents the ratio of the reflected power to the incident power. [34] described the concept of power waves travelling between the source of impedance  $Z_s$  and load of impedance  $Z_l$  and introduced the following definitions for the power wave reflection coefficient :

$$\Gamma = \frac{Z_l - Z_s^*}{Z_l + Z_s} \quad (1.6)$$

As we illustrated, UHF RFID tag has input two states  $Z_1$  and  $Z_2$  therefore it gives us two reflection coefficient  $\Gamma_1$  and  $\Gamma_2$  where  $\Gamma_1$  is the reflection coefficients at the tag's antenna for state 1 and  $\Gamma_2$  is the reflection coefficient at the tag's antenna for state 2. Fig. 1.7 illustrates a block diagram of a single-antenna tag where both impedances are presented and the commuting between each other to modulate the RF signal, which gives :

$$\Gamma_{1,2} = \frac{Z_{1,2} - Z_a^*}{Z_{1,2} + Z_a} \quad (1.7)$$

#### 1.4.2.4 Transmission link budget

The transmission link budget defines the one-way power flow from the reader's transmitter to the tag. As already said, the tag absorbs the power received from the reader by selecting the input state to  $Z_2$  which will maximize the absorption of power by the chip. Once the

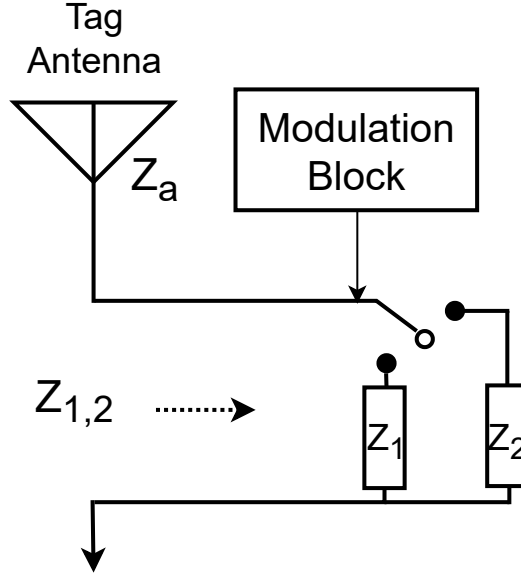


Figure 1.7 – A block diagram of an RF tag

threshold power is obtained, the tag is energized. Typically, a full absorption of the incident power by the chip is based on the assumption that we have an ideal conjugate match between the chip impedance  $Z_2$  and the antenna impedance  $Z_a$ . However, in reality it is not the case, since many factor may cause a power-reducing mismatch. These mismatching effects can be induced by the antenna's radiation impedance changing as a result of coupling with surrounding objects, or by radio-frequency integrated circuit loading of the antenna, which results in extreme or transitory load impedance [27]. In a RFID link budget, the quantity that describes the absorption of the incident power by the chip is more commonly referred as the power transmission coefficient  $\tau_2$  on the state  $Z_2$ , introduced in [27] and [28], and called  $LF$  (load factor) in [29]. This factor is an important characteristic of the tag and must be studied. On the other hand, the power transmission coefficient  $\tau_1$  for state 1 is typically disregarded in literature, as it is assumed that no power is absorbed in this state. Both  $\tau_1$  and, more importantly,  $\tau_2$  are expressed in terms of the antenna impedance  $Z_a = R_a + jX_a$  and the chip impedance for states 1 and 2, denoted as  $Z_{1,2} = R_{1,2} + jX_{1,2}$  [27, 28]:

$$\tau_{1,2} = \frac{4R_a R_{1,2}}{(R_a + R_{1,2})^2 + (X_a + X_{1,2})^2} \quad (1.8)$$

Where  $Z_a$  is the impedance of the tag's antenna and  $Z_2$  is the input impedance of the chip at the absorption state.

Note that  $0 \leq \tau_2 \leq 1$ : We get  $\tau_2 = 1$  in case of an ideal conjugate matching between the antenna and the chip impedance ( $Z_2 = Z_a^*$ ), thus all the energy is transmitted to the chip. whereas  $\tau_2 = 0$  is obtained when the input impedance  $Z_2 = 0$ , thus no energy is transmitted to the chip and all of it is reflected.

The power transmission coefficient is also expressed, in [26] and [29] (defined it as the Load Factor LF), in term of the reflection factor on the absorbing state  $\Gamma_2$  as following:

$$\tau_2 = 1 - |\Gamma_2|^2 \quad (1.9)$$

Where  $\Gamma_2$  is the reflection coefficient at the absorbing state 2. The power transmission coefficient determines the proportion of incident power that is sent to the tag Integrated Circuit (IC) denoted as  $P_{IC}$ . It can be mathematically expressed as:

$$P_{IC} = P_{inc}\tau_2 \quad (1.10)$$

In this equation,  $P_{inc}$  refers to the power received by the tag defined in 1.3, and  $P_{IC}$  refers to the power delivered to the chip. If  $P_{IC}$  is greater than the chip's sensitivity threshold, the tag will activate. Therefore, having a higher  $\tau_2$  value is crucial to improve the tag's ability to transmit incident power to the chip and activate it with less incident power.

In this presented state of the art, the power transmission coefficient  $\tau_2$  is based only on the absorption impedance of the chip and does not take in count the other state  $Z_1$ , and that's by considering this last is equal to zero (as a short circuit) which is only true idealistically. However, in this thesis, the effect of  $Z_1$  on the absorption phase of the tag is not neglected and a new quantity called the mean power transmission coefficient  $\tau$  is introduced.

#### 1.4.2.5 Transmission link read range

The increase of  $\tau_2$  is accompanied by an increase of the power reaching the chip and makes it possible to increase the forward link read range, which corresponds to the maximum distance at which the tag receives enough energy to be activated and thus for its load to be modulated. At the threshold of tag activation, we define the activation power  $P_t^{th}$  as the minimum power transmitted by the reader necessary to supply the RFID chip. At  $P_t^{th}$ , the tag is activated and the power delivered to the chip correspond to the chip sensitivity

threshold  $S_c$  which is an information provided by the chip manufacturer, so in this case:

$$P_{IC}^{th} = S_c$$

By using the Friis equation expressed in (1.3), and based on equation (1.10), the power delivered to the IC at the activation power  $P_t^{th}$  can be expressed as follows:

$$P_{IC}^{th} = S_c = P_{inc}^{th} \tau_2 = P_t^{th} G_r G_t \left( \frac{\lambda}{4\pi d} \right)^2 \tau_2 \quad (1.11)$$

The forward link read range is then expressed, in term of  $P_t$  and other parameters of both tag and reader, as follows:

$$d_{fwd} = \frac{\lambda}{4\pi} \left( \frac{P_t G_t G_r \tau_2}{S_c} \right)^{\frac{1}{2}} \quad (1.12)$$

This expression has been widely employed in RFID literature in order to characterize the RFID tag read range in free space [35], [36], [28], [26]. Some authors assume that the tag is only limited by the forward link thus by the tag, since unlike the tags, the reader are supplied with power so if the tag receives enough power to be activated the reader will be able to collect the information delivered by the tag in general cases. By also assuming the  $\tau_2$  depends only for the absorbing input state  $Z_2$ , so this lastly is the main factor limiting the read range in the forward link design. However, in this thesis we will study both forward and backward read ranges as we will see, in some cases, the read range depends also from the backward link related to the reader part.

#### 1.4.2.6 Backscatter link budget

After the tag's chip is energized the tag switches to the backscattering state using a shunt transistor into the input circuitry of the chip. It then modulates the wave then reflects the power back to the reader which construct the backscatter link. The tag's chip code the 1s and 0s with the two different input states  $Z_1$  and  $Z_2$ , therefore, the power of the digital information scattered toward the reader is also related to the difference in load states. Fig. 1.8 illustrates the backscatter phenomena of a passive UHF RFID tag. The tag sends data during one of the CW periods by switching its input impedance between two states  $Z_1$  and  $Z_2$ , effectively changing its radar cross-section (RCS) between  $RCS_1$  for state 1 and  $RCS_2$  for state 2 and thus modulating the backscattered field. By changing the RCS, an



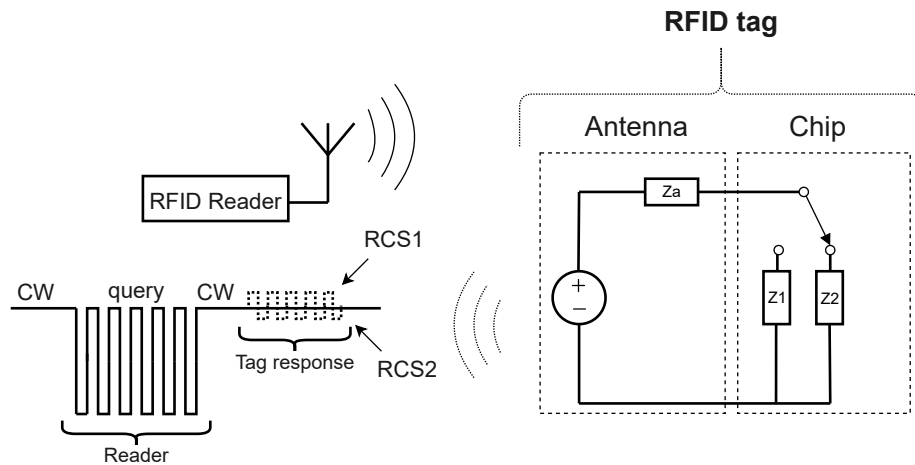


Figure 1.8 – Passive UHF RFID system and its back-scattered signal [37]

important parameter is obtained which is the differential RCS  $\Delta\sigma$ . It has been explicitly studied in [37], [29],[38], and becomes a relevant parameter. The differential RCS  $\Delta\sigma$  in RFID has been introduced in [37] as:

$$\Delta\sigma = \frac{\lambda^2 G_t^2}{4\pi} |\Gamma_1 - \Gamma_2|^2 \quad (1.13)$$

Where  $\lambda$  is the wavelength and  $G_t$  is the gain of the tag antenna. It was then extended in [38] who has distinguish between the static and dynamic term of the backscattered power, and defined the differential RCS corresponding the dynamic part, which satisfy the law of energy conservation, as follows:

$$\sigma_d = \frac{\Delta\sigma}{4} = \frac{\lambda^2 G_t^2}{16\pi} |\Gamma_1 - \Gamma_2|^2 \quad (1.14)$$

The received power by the reader, which can be expressed using the classical radar equation [37], is directly related to the differential RCS:

$$P_r = \frac{P_t G_r^2 \lambda^2 \Delta \sigma}{(4\pi)^3 d^4} \quad (1.15)$$

Where  $P_r$  is the power received by the reader of the modulated signal, at a transmitted power  $P_t$ . The modulated backscattered power depends on the differential of RCS between the two states of the chip  $Z_1$  and  $Z_2$ .

An alternative method for characterizing the power reflected from the RFID tag is the modulation factor  $M$  introduced in [27]. The amount of reflected power will be proportional to the modulation Factor  $M$ . It is an important parameter in the performance evaluation of UHF RFID tags. In [27], it is given in term of the reflection coefficient for the two states as following:

$$M = \frac{1}{4}|\Gamma_1 - \Gamma_2|^2 \quad (1.16)$$

With  $0 \leq M \leq 1$ .

When  $\Gamma_1 = \Gamma_2$ , the value of  $M$  is equal to 0, and in this case there is no energy modulated by the tag. In case where  $\Gamma_2 = 1$  and  $\Gamma_1 = -1$ , we have an ideal open-circuit for energy absorption by  $Z_2$  and an ideal short-circuit load for energy reflection by  $Z_1$ . These extreme reflection coefficients may be quite difficult to achieve in practice, since in a passive RFID tag part of the incident energy is absorbed and part of it is reflected after modulation, hence, the total energy received cannot be all absorbed and back-scattered at the same time. From equations (1.16) and (1.13), we can notice that the  $\Delta\sigma$  is proportional to the modulation factor  $M$ , where:

$$M = \frac{\pi}{\lambda^2 G_t^2} \Delta\sigma \quad (1.17)$$

$M$  is another important characteristic of the tag which describes the capability of the tag to backscatter the modulated wave. This factor will be studied profoundly later in this thesis. The received power by the reader can then be expressed in term of the modulation factor by substituting equations (1.15) and (1.17) it yields :

$$P_r = \frac{P_t G_r^2 G_t^2 \lambda^4 M}{64\pi^4 d^4} \quad (1.18)$$

One limitation on the backscattered signal is the receiver sensitivity of the reader  $S_r$  which corresponds to minimum received signal that can be detected by the reader. By using the radar equation given in 1.15, the round-trip read range can be expressed at  $S_r$  from the modified radar equation as given by [39]:

$$d_{bck} = \sqrt[4]{\frac{P_t G_r^2 \lambda^2 \Delta\sigma}{(4\pi)^3 S_r}} \quad (1.19)$$

The modulation factor is also related to the quality factor  $Q_{ant}$  of the tag's antenna studied in [40]. The  $Q_{ant}$  factor is a measure of the resonance sharpness of the RFID chip's antenna. It represents the ability of the antenna to store and transfer energy efficiently. A high  $Q_{ant}$

factor indicates a narrow resonance frequency bandwidth, which means that the antenna can filter out unwanted signals and maintain a strong resonance at its operating frequency. [40] expresses the read range limiting the backward link, in term of the quality factor  $Q_{ant}$  and for a given minimum received power requirement  $P_{r,min}$  (reader sensitivity), as following:

$$d_{bck} = \frac{\lambda}{4\pi} \left[ \frac{P_t \cdot G_r^2 \cdot G_t^2}{S_r} \right]^{\frac{1}{4}} \left[ \frac{1}{1 + Q_{ant}^2} \right]^{\frac{1}{4}} \quad (1.20)$$

The read range of UHF RFID technology is affected by the two impedance states of the chip. Depending on whether the forward or backward link connection is being used, the two distinct distances  $d_{fwd}$  for the forward link (expressed in (1.12)) and  $d_{bck}$  for the backscatter link (expressed in (1.20)) that characterize the maximum reading range. Although these distances are different from each other, they are both independent. Typically, the read range  $RR$  is determined by the minimum value between the backward and forward link distances:

$$RR = \min(d_{fwd}, d_{bck}) \quad (1.21)$$

A similar approach for the free space read range of the backward link will be presented later in this thesis but in term of the modulation factor  $M$ .

#### 1.4.2.7 Different criteria to determine the antenna impedance

As previously presented, the read range of a passive RFID tag is the minimum value between the forward link range  $d_{fwd}$  calculated using the Friis equation and the backward link range  $d_{bck}$  calculated using the radar equation. Thus, the read range is determined by either the chip sensitivity ( $S_c$ ) and the power transmission coefficient  $\tau$  or the reader sensitivity ( $S_r$ ) and the modulation factor ( $M$ ). It's important to note that the power transmission coefficient and the modulation factor cannot be maximized simultaneously. Manufacturer usually seeks the complex conjugate matching which only results in maximizing the power transmission coefficient  $\tau_2$  on state 2, and thus maximizing the forward link read range:

$$Z_{at} = Z_2^* = R_2 - jX_2 \quad (1.22)$$

Optimizing the forward link read range may not always be the optimal choice, since the limitation can be caused by the backward link in specific scenarios. To maximize the backward link read range, a notable study by the author [42] aims originally to maximize

the power in the side-band of the modulated signal by the tag. Their findings reveal that to achieve maximum power in the backward link, the antenna should not be matched to either of the chip input impedance states. This research led to the derivation of analytical expressions for the antenna impedance  $Z_{ar}$  which maximize  $M$ , denoted as:

$$Z_{ar} = R_{ar} + jX_{ar} \quad (1.23)$$

designed for a specific chip whose the two impedance states have to be known.

$$R_{ar} = \sqrt{R_1 R_2 \frac{(R_1 + R_2)^2 + (X_1 - X_2)^2}{(R_1 + R_2)^2}} \quad (1.24)$$

$$X_{ar} = -\frac{R_2 X_1 + R_1 X_2}{R_1 + R_2} \quad (1.25)$$

The derivation of these expressions is detailed in the Annex B.

Knowing  $Z_{at}$  and  $Z_{ar}$ , the optimal design can be achieved by a trade-off between  $\tau_2$  and  $M$  which allows for the maximization of the read range and achieving an optimal design as studied by author in [41]. The author defines  $Z_{ao}$  as the optimal impedance for a chip, which, in certain cases, lies between  $Z_{at}$  and  $Z_{ar}$ , aimed at maximizing the read range by accounting for both forward and backward links. This optimization process takes into consideration the two-state impedances ( $Z_1$  and  $Z_2$ ). In this thesis, we will delve deeper into this aspect, providing a comprehensive analysis of how to determine the optimal antenna impedance for a given chip in a particular scenario (sec. 2.9).

### 1.4.3 Energy conservation in UHF RFID

As observed, a passive RFID tag operates through energy absorption, modulation, and the subsequent backscattering of the modulated wave. However, it is crucial to emphasize that the power involved in this process must adhere to the law of conservation of energy. This law dictates that the total power received by an RFID tag (assuming an antenna with no energy losses) can only be dissipated within  $Z_i(t)$ , representing the two input states of the tag, namely  $Z_1$  and  $Z_2$ , or backscattered into the environment.

Moreover, it is essential to consider the arbitrary cyclic ratio, denoted as  $\rho$ , which signifies the proportion of time the tag spends in each state. When  $\rho = 0.5$ , it indicates an equal distribution of time between state 1 and state 2.

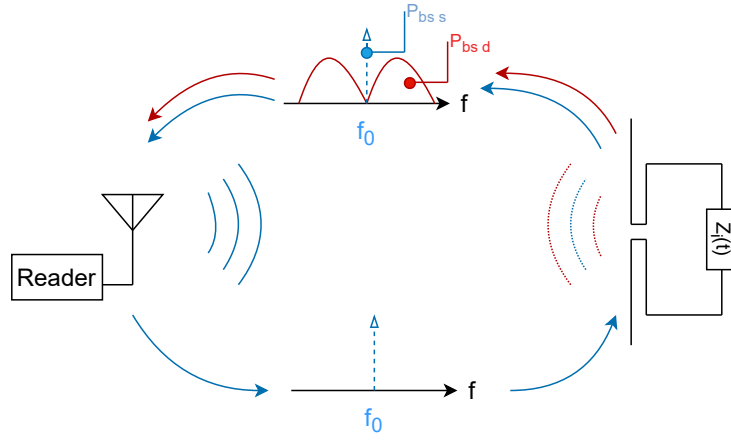


Figure 1.9 – frequency domain and Energy conservation of RFID tag [38]

Authors in [38] describes the energy conservation in the level of the tag. The total power incident to the tag is divided, some of this power is delivered to the chip and is proportional to the aperture of the tag antenna  $A_e$ , noted as  $P_{IC}$ , where  $Z_i$  is equivalent to the chip impedance at the absorption state  $Z_2$ . And the other part of the incident power is modulated and backscattered in the environment, noted as  $P_{bs}$ . As shown in Fig. 1.9, the backscattered power  $P_{bs}$  is of two kind, part of it is static ( $P_{bs_s}$ ) which corresponds to the response of a linear time-invariant system since the power is located at the frequency of the CW received by the tag  $f_0$  whereas the other part is a dynamic power ( $P_{bs_d}$ ) which is not located at  $f_0$  but around it. Hence, the tag cannot be regarded as a linear time-invariant system. For the best performance of the tag, the dynamic power  $P_{bs_d}$  should be maximized, and the carrier power  $P_{bs_s}$  should be minimized. Ideally,  $P_{bs_d} = P_{bs}$  and  $P_{bs_s} = 0$ . It is worth noting that this differential power is easily detectable since it is not positioned at the frequency used by the reader during the emission.

The dynamic power represents the information that the tag is sending back to the reader, while the carrier power represents the continuous wave received by the tag. The dynamic power is the difference between the power scattered by the tag and the power of the continuous wave received by the tag. Maximizing the dynamic power can improve the signal-to-noise ratio, allowing for more reliable communication between the tag and the

reader.

On the other hand, minimizing the carrier power is important to reduce interference and power consumption. The carrier power contributes to the overall power consumption of the tag system and can also interfere with other nearby devices operating at the same frequency. Therefore, reducing the carrier power can not only improve the performance of the tag system but also reduce interference with other devices.

Several techniques can be used to maximize the dynamic power and minimize the carrier power in a tag system. One approach is to optimize the design of the tag antenna to achieve better impedance matching and reduce reflection losses. Additionally, power control algorithms can be implemented to dynamically adjust the power transmitted by the reader based on the received signal strength from the tag, which can further reduce interference and power consumption.

In summary, maximizing the dynamic power and minimizing the carrier power are critical for achieving optimal performance in a tag system. By using advanced modulation techniques and optimizing the design of the tag antenna, tag systems can achieve better signal-to-noise ratios, reduce interference, and improve power efficiency, leading to more reliable and efficient communication between the tag and the reader.

Following the presentation of the UHF RFID system's link budget, we can now delve into an informative discussion on over-the-air characterization of UHF RFID, utilizing the provided information as a foundation.

#### **1.4.4 Over-the-air characterization of UHF RFID tag**

RFID tags are crucial components in wireless communication systems, and it is necessary to carry out thorough characterizations to ensure their proper functioning. One of the most critical aspects of RFID characterization is determining the read range. This measurement is widely used as it is practical and straightforward to obtain. As we have seen, the read range is limited by many factors such as the tag and its sensitivity.

The traditional method of measuring the read range involves the use of the Friis formula, which assumes a free space environment and is obtained indirectly without measuring the tag at the maximum read range distance as we have illustrated.

In some work, a transmission line system is established using a Vector Network Analyzer [30, 43]. This tool is used to calculate the reflection factor, which helps to determine the sensitivity of the chip by identifying the minimum amount of incident power needed to

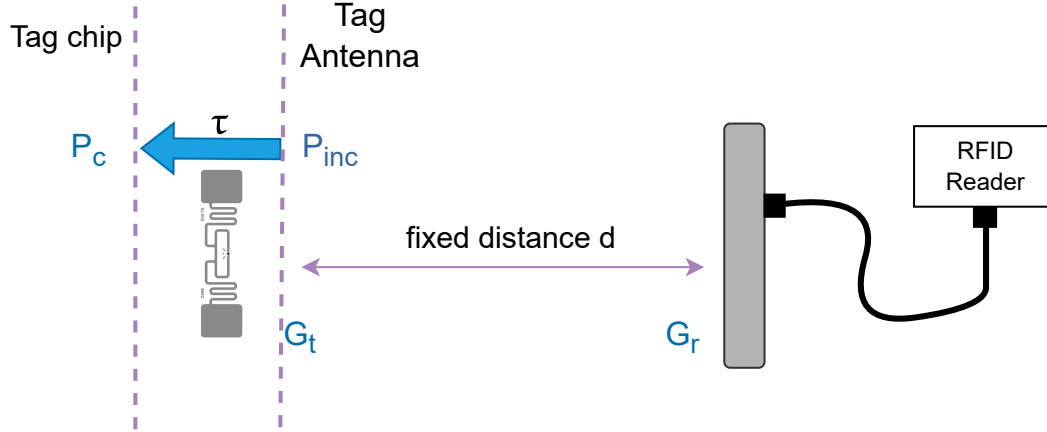


Figure 1.10 – Friis's radio-propagation model for a passive UHF RFID system [47]

activate the tag. Other work, such in [36], use voyantic system which is a toll to characterize and evaluate the tag, and and compare performance between different tag designs. However, the drawback of these methods is that they are a costly methods.

alternatively, more recently various studies have investigated methods for accessing tag sensitivity by exploiting different variations of parameters in an over-the-air environment with low cost. For instance, frequency variation has been explored in [44], angular variation in [45], and distance variation in [46]. The approach of jointly varying distance and transmitted power has been shown to be particularly successful in determining tag sensitivity, as it involves estimating the minimum power required to activate the tag at a fixed and controlled distance [47, 48]. This same approach is adopted in the present study.

#### 1.4.4.1 Over-the-air access of the tag sensitivity by varying the distance

In the literature, all the RFID characterization systems use the Friis formula to calculate the power reaching the RFID chip. And therefore, being able to access the activation power of the chip, which leads us to obtain the chip sensitivity. In the studies presented in [47, 48], an RFID setup was established as depicted in Fig. 1.10. The tag and reader antennas are aligned on a straight horizontal line at a distance  $d$ , which is large enough to meet the

far-field condition. It is imperative to maintain a constant value for  $d$  throughout the testing process. By using the Friis formula, accounting for all losses and the absorption effect on the tag, the power received by the RFID chip is calculated in [47] as follows:

$$P_{IC} = P_t G_r G_t \tau_2 \left( \frac{\lambda}{4\pi d} \right)^2 \eta_{plf} A_{cable} \quad (1.26)$$

In this formula,  $\eta_{plf}$  is the polarization loss factor which varies based on the tag antenna structure,  $A_{cable}$  is the cable loss that occurs from connecting the reader to the antenna, and finally,  $\tau_2$  is the power transmission coefficient defined in 1.8.

Using this expression, the chip sensitivity is then derived by reaching the activation power which is obtained by gradually increase, from zero to the maximum allowed value, the reader transmitted power  $P_t$  and to contextually verify whether or not the tag is energized and, consequently, is able to answer to the reader. The  $S_c$  is then expressed as following:

$$S_c = P_t^{th} G_r G_t \tau_2 \left( \frac{\lambda}{4\pi d} \right)^2 \eta_{plf} A_{cable} \quad (1.27)$$

Where  $P_t^{th}$  is the minimum transmitted power by the reader necessary to activate the tag. Then, the tag sensitivity,  $S_t$ , is calculated based on the chip sensitivity  $S_c$ , by considering all the factors that affect the quality of the tag, such as chip sensitivity, antenna gain, and the conjugate match between the chip and antenna. It is expressed as follows:

$$S_t = \frac{S_c}{\tau_2 G_t} \quad (1.28)$$

The principle of varying jointly distance and transmitted power has been demonstrated to be very fruitful in order to access the sensitivity of the tag. It is based on estimating the minimum power required to energize the tags at a fixed controllable distance [47],[48]. This over-the-air method of varying jointly the distance and transmitted power demonstrated is also the approach chosen in this thesis. However, the method we will present is independent from the channel and doesn't require a previous knowledge on the gains and losses that are occurring in the RFID system since it is not based on the Friis equation, but rather on the channel reciprocity as we will see later.



### 1.4.5 Channel modelling in UHF RFID communication

The real propagation environment is almost never purely free-space for UHF RFID communication. Thus the importance to cover modelling methods for different propagation scenarios. In case of UHF RFID communication, the backscatter modulation is used, so to effectively represents the RFID channel, both forward and backward links must be simultaneously accounted for. The essence of the RFID channel can be likened to a dual fading channel, with each fade occurring twice, once in the forward link and once in the reverse link under the concept of channel reciprocity. Authors in [49] describes a multi ray RFID model for an illustrative scenario of RFID application which involves indoor multipath conditions where line-of-sight communication is present, accompanied by minimal notable reflections. The expression for the deterministic multipath channel's path gain connecting the reader and the tag is given by [49] as follows:

$$G_{path} = \left(\frac{\lambda}{4\pi d^{(0)}}\right)^2 |H|^2$$

Here,  $d^{(0)}$  represents the length of the direct ray path,  $\lambda$  is the wavelength.

The channel response  $H$  considering multipath effects is expressed as:

$$H = 1 + \sum_{i=1}^N g_t^{(i)} g_r^{(i)} \Gamma^{(i)} \frac{d^{(0)}}{d^{(i)}} e^{-jk(d^{(i)} - d^{(0)})}$$

In this equation, the various components are defined as follows:

- $N_r$  is the total number of rays.
- $g_r^{(i)}$  and  $g_t^{(i)}$  are the reader and tag antenna radiation pattern values at  $i$ -th ray direction, respectively.
- $\Gamma^{(i)}$  is the reflection coefficient of the  $i$ -th reflecting surface.
- $d^{(i)}$  denotes the length of the  $i$ -th reflected ray path, namely the distance between the antenna and the virtual tag position.

The power of the tag signal received by the monostatic reader can be formulated as:

$$P_r = P_t G_{path}^2 K$$

$$P_r = P_t \left(\frac{\lambda}{4\pi d^{(0)}}\right)^2 |H|^4 K$$

Where  $K$  is the backscatter gain and it is proportional to the modulation factor  $M$ :

$$K = \eta_{plf} M$$

where  $\eta_{plf}$  is the polarization loss factor,  $G_t$  is the maximum tag antenna gain.

In a more recent paper, Andrea Motroni, Alice Buffi et al [50] take up Nikitin's model ([49]) and give a more precise version:

$$h = g_r^{(0)} g_t^{(0)} \frac{1}{d} e^{-jkd} + \sum_{i=0}^{N_r} g_r^{(i)} g_t^{(i)} \Gamma^{(i)} \frac{1}{d^{(i)}} e^{-jkd^{(i)}} \quad (1.29)$$

Where  $g_r^{(0)}$  and  $g_t^{(0)}$  are the reader and tag antenna radiation pattern values in LOS direction, which might not be the maximum radiation direction, respectively.

The slight difference is that the channel term includes the  $d^{(0)}$  distance dependency, whereas in the initial version of the model this dependency is factorized. Then the received power by the reader can be expressed as following:

$$P_{Rx} = RSSI = P_{Tx} G_r^2 \left(\frac{\lambda}{4\pi}\right)^4 |h|^4 K$$

Understanding the propagation channel as well as evaluating the tag intrinsic characteristics is crucial to characterize the passive tag. Therefore, in this thesis we will explore an automated platform that will serve as our instrument for investigating these facets of characterization.

## 1.5 Platform description

In this thesis, an RFID Platform of the IETR has been used in order to do the experimentation on UHF RFID tags over-the-air. The IETR platform occupies an entire room in the laboratory's basement of volume  $6 \times 4 \times 2.7m^3$ . Within this room, there is an automated mechanical system controlled by a PC. A dedicated Python API has been developed specifically for this system, enabling the control of both the reader and motors. The experimental setup represented in Fig. 1.11 consists of five controllable axes: four for translation and one for rotation. The first translation axis is a 5-meter rail, housing an antenna at its end, positioned at a height of approximately 1.2 meters. The other three translation axes are located on a gantry positioned above the main rail, each with a range

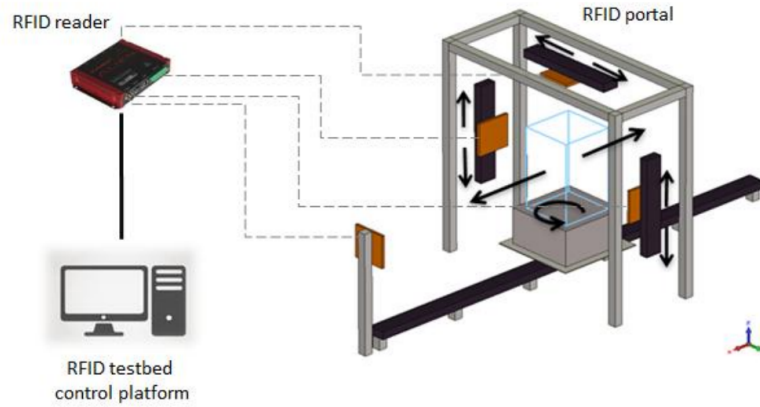


Figure 1.11 – 5 axes RFID platform (4 translations, 1 rotation) connected to an Alien 9900+ Reader

of motion of 1 meter. This arrangement allows for the movement of three antennas, two of which can be vertically positioned on either side of the central rail. The vertical masts of the gantry are spaced approximately 2.4 meters apart. The third antenna is placed on the boom arm at a height of 3 meters. Note that the platform is surrounded by movable absorbing panels to reduce the losses the effect of multipaths on the link budget ,and, if moved, modifying the propagation channel.

In the context of this study, we will use the following naming convention for the antennas: "Antenna 0" refers to the one above, "Antenna 1" refers to the left-side antenna, "Antenna 2" pertains to the right-side antenna, and "Antenna 3" corresponds to the front fixed antenna.

The platform is equipped with two RFID readers: the Alien 9900+, which was available at the beginning of the project, and a more recently acquired reader, the Impinj R700.

### 1.5.1 Alien 9900+ reader

The majority of the experimentation conducted in this thesis utilized the ALR-9900+ alien reader. This reader shown in, photo 1.12, is built compliant with the Global EPC Gen 2 standard and offers an autonomous mode, allowing it to be programmed and controlled through commands [51]. It has numerous features, including a high read rate, excellent sensitivity, and performance. The ALR-9900+ reader has a transmit power range of 15.7 to 30.6 dBm, with a resolution of 0.1 dBm. It adheres to the ETSI regulation and operates within the frequency ranges of 865 – 868 MHz and 915 – 921 MHz.



Figure 1.12 – Photo of Alien 9900+ Reader

However, it's important to note that the alien reader's receiver does not provide the actual power measurement; instead, it outputs the Received Signal Strength Indicator (RSSI). Furthermore, the manufacturer does not provide the specific relationship between RSSI and the actual power in dBm.

Several papers which are using the same Alien 9900+ reader [4, 52, 53], deal with the raw RSSI which is not a power quantity. In Chapter 3, we will address the challenge of converting the integer RSSI value from the reader into an accurate power value in dBm.

### 1.5.2 Impinj R700 reader



Figure 1.13 – Photo of Impinj R700 Reader

In the subsequent stages of experimentation, another reader utilized was the Impinj R700.

This RAIN RFID reader is equipped with four ports and complies with the GS1 UHF Gen2v2 protocol, standardized by ISO/IEC as 18000-63. The Impinj R700, shown in photo 1.13, is specifically designed to cater to the growing requirements of next-generation IoT solutions and enterprise-grade RAIN deployments. It conforms to the ETSI regulation and operates within the frequency ranges of 865 – 868 MHz and 915 – 921 MHz.

The transmit power range of the Impinj R700 reader spans from 10 to 30 dBm, with a transmit power resolution of 0.5 dBm. In this aspect, the alien reader 9900+ holds an advantage with its higher resolution of 0.1 dBm. However, the Impinj R700 reader offers a significant advantage over the alien reader by directly providing the power measurement in dBm, rather than the RSSI. This characteristic is more favorable for our purposes.

Additionally, the Impinj R700 reader boasts a reader sensitivity of -92 dBm, which is likely superior to the Alien reader's sensitivity. Although the manufacturer does not specify the exact sensitivity of the Alien reader, our observations during this research suggest it to be approximately -80 dBm, as no power levels lower than -80 dBm were detected. Note that the Impinj sensitivity can be controlled and modified, which could be helpful to investigate the effect of the sensitivity variation on the RFID link budget. Another advantage of the Impinj R700 reader is its notably faster acquisition speed compared to the alien reader.

To summarize, the Impinj R700 reader offers the advantage of providing power measurements in dBm instead of RSSI, along with a higher sensitivity. However, the alien reader surpasses it in terms of transmit power resolution, with a resolution of 0.1 dBm.

### 1.5.3 Reader antenna

The four reader UHF RFID antennas used in this platform are similar and have a circular polarization. These antennas have a maximum gain in the bore-sight of  $G_{max} = 9dB$  and the half power beam-width is  $HPBW_{deg} = 65 \text{ deg}$ . For determining an angular variation of the antenna pattern we use a Gaussian model:

$$G(\theta) = G_{max} e^{-\frac{\theta^2}{(\frac{HPBW_{rad}}{2})^2 \ln 2}} \quad (1.30)$$

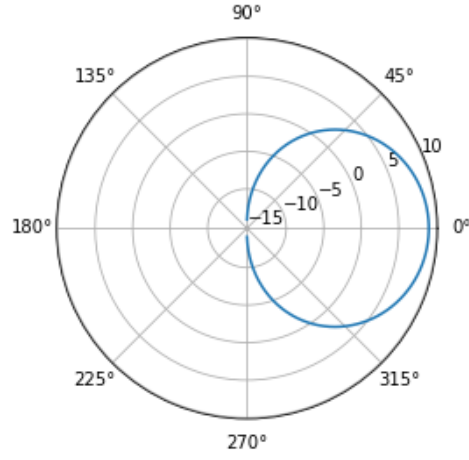


Figure 1.14 – Platform's antenna Gaussian pattern  $G_{max} = 9 \text{ dB}$ ,  $HPBW = 65$

## 1.6 Conclusion

In this chapter, we provided an extensive review of the literature on the UHF RFID system, covering various aspects related to its operation and applications. We began with an introduction to RFID technology, explaining its components, operation frequencies, and highlighting its diverse range of applications. We also discussed the regulatory framework governing RFID systems and explored different types of UHF RFID tags. Additionally, we presented specific use cases of UHF RFID technology and introduced the EPCglobal Generation 2 standard.

Moreover, we delved into the link budget of the UHF RFID system, covering the communication between the reader and tag. We emphasized the importance of characterizing UHF RFID systems by presenting the power transmission coefficient and the modulation factor, and explored energy conservation techniques within this context. We then presented the optimal design of an antenna for a given chip. Additionally, we discussed the over-the-air characterization of UHF RFID tags, providing valuable insights into their behavior in real-world scenarios.

Furthermore, we covered the modelling methods for multipath channel in UHF RFID communication

To conclude this chapter, we provided a detailed description of the RFID platform employed in our research, specifically emphasizing the Alien ALR-9900+ reader and the Impinj R700 reader. This platform enables autonomous experimentation on UHF RFID. It plays a

crucial role in our thesis as it serves as the foundation for conducting all the experiments that will be discussed in the subsequent chapters.

# THEORETICAL ASPECT OF UHF RFID

---

## 2.1 Introduction

This chapter aims to provide a comprehensive study of the theoretical aspects of UHF RFID system. Building upon the state of the art in the field, we explore two key parameters of UHF RFID: the newly defined mean power transmission coefficient  $\tau$  introduced in Sec. 1.4.2.4 and the modulation factor  $M$  discussed in Sec. 1.4.2.6. While these parameters have been mentioned in the literature, we present them in a more detailed and explicit manner, highlighting their significance in characterizing the performance of UHF RFID systems.

To begin, we derive an expression for the channel coefficient, which simplifies the calculation of the power transmission coefficient and modulation factor based on the concept of the reciprocity of the channel. By understanding the channel coefficient, we gain insights into the propagation characteristics and signal strength in UHF RFID systems.

Next, we delve into the concept of activation profiles. The activation profile represents the minimum power transmitted by the reader required to energize the UHF tag. By defining the activation profile, we establish a link between the transmitted power and the tag's sensitivity, an important parameter that directly affects the overall performance of the tag.

In order to provide a more comprehensive evaluation of UHF RFID tags, we introduce the concept of tag receptivity. This measure is derived from the extracted activation profile. The margin between the chip sensitivity and tag receptivity is defined as the tag offset  $Q$ .

To synthesize the performance of UHF RFID tags, we propose a chart that plots the modulation factor against the power transmission coefficient. This chart serves as a valuable tool for visualizing and analyzing the performance of various tags in relation to these key parameters. We also define the tag efficiency  $\gamma$ . The tag can be placed in the chart either by the knowledge of  $(\sqrt{M}, \tau)$  or equivalently by  $(Q, \gamma)$ . Furthermore, we present an algorithm that estimates the power transmission coefficient and modulation factor



of a set of tags based on the  $Q$  quantity and the ratio between the power transmission coefficients. This algorithm aids in the evaluation and comparison of different tags in practical scenarios.

Moreover, we define the read range obtained under the assumption of free space propagation using the theory we propose. This read range is limited by two factors: the backward link, which depends on the modulation factor and reader sensitivity, and the forward link, which depends on the mean power transmission coefficient and chip sensitivity.

Finally, we present in this chapter the validity domain for a chip and illustrate the optimal matching that can be achieved in this domain, by taking three different chips as an example. We will determine the optimal impedances of these chips by using the  $(\sqrt{M}, \tau)$  chart.

By studying the theoretical aspects of UHF RFID in this chapter, we aim to provide a better understanding of the technology and its performance, ultimately leading to improved design and evaluation of UHF RFID tags.

## 2.2 Intrinsic Characteristics of UHF RFID tag

We distinguish two key intrinsic characteristics UHF RFID tag: the mean power transmission coefficient  $\tau$  and the modulation factor  $M$ .

The mean power transmission coefficient  $\tau$  is a newly defined parameter that considers the transmission coefficient in both states, based on the conservation of energy law as seen in Sec. 1.4.3. It quantifies the efficiency of power transfer between the reader and the UHF RFID tag, providing a comprehensive evaluation of power transmission efficiency.

On the other hand, the modulation factor introduced in Sec. 1.4.2.6 is a predefined expression that plays a crucial role in UHF RFID systems. It reflects the tag's modulation capabilities.

### 2.2.1 Mean power transmission coefficient

The operation of an RFID tag involves absorbing and back-scattering the energy it receives from the reader. Let us consider the impedance states of the RFID chip:  $Z_1$ , representing the backscatter impedance state (typically close to a short circuit), and  $Z_2$  representing the absorbing impedance state, as illustrated in Fig. 2.1 and detailed in the reference [18].

To simplify the problem, the author [29] assumes that the backscatter state impedance is a short circuit ( $Z_1 = 0$ ). However, it has been demonstrated in [30, 31] that, in practice, this

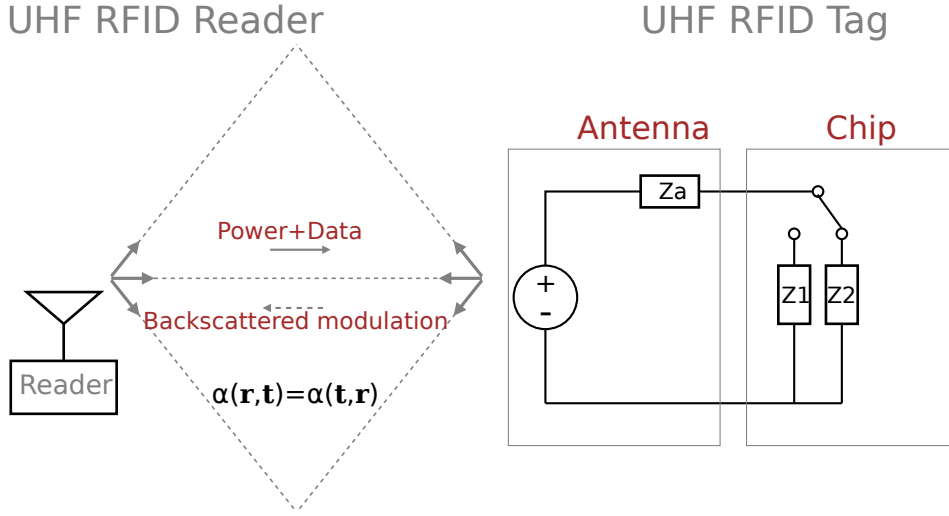


Figure 2.1 – General schema of UHF RFID system highlighting the channel reciprocity

impedance is not strictly zero and may vary depending on the applied power. Generally, the complex conjugate matching condition  $Z_a^* = Z_2$  is designed to maximize power transfer, regardless of the actual value of  $Z_1$  which is often not provided in the chip datasheet. Note that in [27] and [29], the power transmission coefficient ( $\tau_2$ ) depends only on the input state  $Z_2$ . They assume that the two input impedances states of the chip optimally are: the conjugate of the impedance of antenna for  $Z_a^* = Z_2$  for a higher power transfer, and 0 for  $Z_1$  (short circuit) for higher power reflection. However, the definition of  $\tau$  exploited in this work considers the absorption in both states, acknowledging that  $Z_1$  is not ideally zero. Although manufacturers typically do not provide the value of  $Z_1$  it has been demonstrated in [54] that the chip architecture commonly includes a FET transistor in parallel with the rectifier circuitry. As a result,  $Z_1$  can be estimated by considering  $Z_2$  in parallel with the resistance known as  $R_{mod}$  of the transistor:

$$Z_1 = \frac{Z_2 R_{mod}}{Z_2 + R_{mod}} \quad (2.1)$$

Where  $R_{mod}$  is a resistance typically between 10  $\Omega$  and 100  $\Omega$ . We consider this expression of  $Z_1$  to give an analytic expression of the optimum impedance matching  $Z_{ar}$  presented in 1.4.2.7 and detailed in Annex B.

When an incident wave with a power density of  $S$  (measured in  $W/m^2$ ) hits an RFID tag, the tag absorbs a portion of the energy and reflects the rest in all directions. The proportion of the energy that is reflected back towards the RFID reader is referred to as the tag's gain

in the reader's direction explained in Sec. 1.4.2. This gain also determines the amount of energy absorbed by the tag.

The effective surface  $A_e$ , presented in Sec. 1.4.2, allows to express the quantity of power taken from the incident field. But as it is a question of communicating information with the reader, the tag cannot be permanently in the absorption mode, it must also dedicate portions of time with less absorption and more back-scattering. When the load is an open circuit there is neither absorption nor reflection because no electric current is induced on the antenna. The wave continues forward its propagative path unaltered by the tag. On the other hand a short circuit situation induces a maximum of current and therefore a maximum of reflectivity. What matters for the receiver is the power of the fluctuation between these two states 1 and 2, the dynamic power carried by the modulation of the signal. But as this fluctuation is generated by an energy previously captured by the tag, the energy balance necessarily involves a memory effect and must result from an integration over time. On average, the energy received by the tag must be divided equally between the energy used to power the tag and the energy back-scattered statically and dynamically to the environment. Only the energy of the side bands of the spectrum is exploitable in reception for the demodulation. The total electromagnetic power available at the tag is therefore  $P_r = pA_e$  expressed in Watts. This total power is decomposed into a term absorbed by the device and a term backscattered to the environment:

$$\underbrace{pA_e}_{total} = \underbrace{pA_e(1 - |\Gamma_i|^2)}_{absorbed} + \underbrace{pA_e|\Gamma_i|^2}_{reflected} \quad (2.2)$$

$$\underbrace{pA_e}_{total} = \underbrace{pA_e\tau_i}_{absorbed} + \underbrace{pA_e|\Gamma_i|^2}_{reflected} \quad (2.3)$$

$$pA_e = P_{IC} + P_r \quad (2.4)$$

Where the complex reflection coefficient has been introduced in Sec. 1.4.2.

The power transmission coefficient  $\tau_2$  on state 2 parameter was presented in Sec. 1.4.2.4.

Here we introduce the distinction between the power transmission coefficient:

$$\tau_i = 1 - |\Gamma_i|^2 \quad (2.5)$$

and the mean power transmission coefficient over both states with an arbitrary cyclic ratio

$0 < \rho < 1$ , it yields:

$$\tau = \rho\tau_1 + (1 - \rho)\tau_2 = 1 - \rho|\Gamma_1|^2 - (1 - \rho)|\Gamma_2|^2 \quad (2.6)$$

or the most often assuming staying the same time on both state  $\rho = \frac{1}{2}$ :

$$\tau = \frac{\tau_1 + \tau_2}{2} = 1 - \frac{|\Gamma_1|^2 + |\Gamma_2|^2}{2} \quad (2.7)$$

$\tau$  will refer to the mean of the absorption over the two switched impedance unlike in Sec. 1.4.2.4.

Furthermore, let's demonstrate how the modulation factor can be determined and how to partition the energy absorbed by the tag into  $\tau$  and  $M$ .

### 2.2.2 Modulation Factor

The RFID principle consists on switching the termination load, thereby modulating the reflecting coefficient of the tag. Assuming a modulation with a shaping function  $g$ , a symbol duration  $T$  and  $\Gamma_k \in \{\Gamma_1, \Gamma_2\}$  associated to an equiprobable binary train of symbols, we can express the reflecting coefficient as follows:

$$\Gamma(t) = \sum_{k \in \mathbb{Z}^+} \Gamma_{n_k} g(t - kT) \quad (2.8)$$

Assuming that the two commuted states are equally probable, we can obtain the expected value of the reflecting coefficient as:

$$E[\Gamma_k] = \frac{\Gamma_1 + \Gamma_2}{2} \quad (2.9)$$

Sec. 1.4.3 presented this idea of separation between a static and a dynamic contribution, obtained in centering the modulated signal around its mean value. This can be simply written as:

$$\Gamma(t) = \underbrace{E[\Gamma_k]}_{\Gamma_s} + \underbrace{\sum_k (\Gamma_k - E[\Gamma_k]) g(t - kT)}_{\Gamma_d(t)} \quad (2.10)$$

Where a static  $\Gamma_s$  and dynamic  $\Gamma_d(t)$  term have been exhibited. If we now consider the

expectation of the square modulus of this quantity, assuming the ergodicity of the signal, it yields:

$$E(|\Gamma(t)|^2) = |\Gamma_s|^2 + E(|\Gamma_d(t)|^2) \quad (2.11)$$

The second term of the right hand side is the modulation factor  $M$  in illustrated in Sec. 1.4.2.6 and is related to the modulation efficiency  $ME$  in [29].

$$M = E(|\Gamma_d(t)|^2) = \frac{ME}{4} = \frac{|\Gamma_1 - \Gamma_2|^2}{4} \quad (2.12)$$

$0 < M < 1$  while  $0 < ME < 4$ .

Lets impose the static term  $S$ :

$$S = \frac{|\Gamma_1 + \Gamma_2|^2}{4} \quad (2.13)$$

Where  $0 \leq S \leq 1$ .

By introducing (2.9) and (2.12) in (2.11), we obtain:

$$E(|\Gamma(t)|^2) = \frac{|\Gamma_1 + \Gamma_2|^2}{4} + \frac{|\Gamma_1 - \Gamma_2|^2}{4} = \frac{|\Gamma_1|^2 + |\Gamma_2|^2}{2} \quad (2.14)$$

Or equivalently,

$$\underbrace{S}_{static} + \underbrace{M}_{dynamic} = \underbrace{1 - \tau}_{scattered} \quad (2.15)$$

The static term is responsible for the power of the waveform carrier while the dynamic term, which is also the useful term for the tag detection, is responsible for the power in the sidelobes of the modulated spectrum. This relation is simply expressing the energy conservation over time. In RFID technology, we try to obtain a static term  $S = 0$ , which leads to the limiting condition:

$$M = 1 - \tau \quad (2.16)$$

It's essential to understand the characteristics of the tag, but it's also important to demonstrate the RFID transmission channel in order to be able to characterize the tag over the air.

## 2.3 RFID transmission channel

The RFID transmission channel refers to the communication path that encompasses both the transmission from the reader to the tag and subsequently from the tag back to the reader.

Let  $\mathbf{r} = [\vec{p}_r, \theta_r, \phi_r]$  and  $\mathbf{t} = [\vec{p}_t, \theta_t, \phi_t]$  being 5 dimensional vectors gathering position and orientation of reader and tag.

The joint effect of the transmission channel including the tag and reader antenna is expressed in the channel coefficient:

$$\alpha(f, \mathbf{r}, \mathbf{t}) = \alpha(f, \mathbf{t}, \mathbf{r}) = |h(f, \mathbf{r}, \mathbf{t})|^2 \quad (2.17)$$

This is a scalar quantity which account for the channel reciprocity, illustrated in Fig. 2.1 because  $\mathbf{r}$  and  $\mathbf{t}$  are commuting variables meaning this term is the same for the forward and backward link.

In the time domain, we obtain:

$$h(t, \mathbf{r}, \mathbf{t}) = \int_{\Omega_r \times \Omega_t} g_r(t, \Omega_r) C(t, \Omega_r, \Omega_t) g_t(t, \Omega_t) d\Omega_t d\Omega_r \quad (2.18)$$

In the frequency domain, we get :

$$h(f, \mathbf{r}, \mathbf{t}) = \int_{\Omega_r \times \Omega_t} g_r(f, \Omega_r) C(f, \Omega_r, \Omega_t) g_t(f, \Omega_t) d\Omega_t d\Omega_r$$

Where  $C \equiv C(f, \vec{p}_r, \Omega_r, \vec{p}_t, \Omega_t)$  is the power transfer function of the channel, which depends on the position and orientation of both the reader and the tag.

### 2.3.1 Free space model

In case of free space condition (i.e anechoic chamber measurement) we would have the simplification, in time domain:

$$C(t, \vec{p}_r, \Omega_r, \vec{p}_t, \Omega_t) = \frac{\delta(\Omega_r - \omega_r) \delta(t - \frac{|\vec{p}_r - \vec{p}_t|}{c}) \delta(\Omega_t - \omega_t)}{4\pi |\vec{p}_r - \vec{p}_t|^2} \quad (2.19)$$

In frequency domain, the Fourier transform is applied:

$$C(f, \vec{p}_r, \Omega_r, \vec{p}_t, \Omega_t) = \mathcal{F}\{C(t, \vec{p}_r, \Omega_r, \vec{p}_t, \Omega_t)\}$$

$$C(f, \vec{p}_r, \Omega_r, \vec{p}_t, \Omega_t) = \frac{\delta(\Omega_r - \omega_r)\delta(\Omega_t - \omega_t)}{4\pi|\vec{p}_r - \vec{p}_t|^2} e^{-jk|\vec{p}_r - \vec{p}_t|}$$

where  $\omega_r = (\theta_r, \phi_r)$ ,  $\omega_t = (\theta_t, \phi_t)$  and  $d = |\vec{p}_r - \vec{p}_t|$  such that:

$$h_{FS}(f, \mathbf{r}, \mathbf{t}) = \frac{g_r(f, \omega_r)g_t(f, \omega_t)}{\sqrt{4\pi}} \frac{e^{-jkd}}{d}$$

The alpha term is real and corresponds to the square modulus of the channel as introduced in the papers by Nikitin [49] and Motroni [50].

$$\alpha_{FS}(f, \mathbf{r}, \mathbf{t}) = |h_{FS}|^2 = \frac{G_r(f, \omega_r)G_t(f, \omega_t)}{4\pi d^2} \quad (2.20)$$

We define  $P_{inc}(P_t, \mathbf{r}, \mathbf{t})$  as the incident power on the tag at a configuration  $\mathbf{t}$  from the reader at configuration  $\mathbf{r}$ :

$$P_{inc}(P_t, f, \mathbf{r}, \mathbf{t}) = P_t \alpha(f, \mathbf{r}, \mathbf{t}) \frac{\lambda^2}{4\pi} \quad (2.21)$$

The multi-path fading and the polarization factor  $\eta_{plf}$  are assumed to be all included in the  $\alpha$  term which is a deterministic non linear function of positions, antennas orientation and frequency  $f$ . In the basic free space situation we recover the well known Friis expression 1.3:

$$P_{inc}(P_t, f, d) = P_t G_r G_t \left( \frac{\lambda}{4\pi d} \right)^2 = P_t G_r G_t L_{FS} \quad (2.22)$$

by equating (2.21) and (2.22), it yields:

$$\frac{\lambda^2 \alpha_{FS}}{4\pi G_t G_r L_{FS}} = 1 \quad (2.23)$$

In the case of a channel which is not free space, we define a dimensional coefficient which is a good index of the position of the measured channel w.r.t free space:

$$\mu = \frac{\lambda^2 \alpha}{4\pi G_t G_r L_{FS}} \quad (2.24)$$

In case where  $\mu > 1$ , the channel decreases slower than free space. Where if  $\mu < 1$ , the channel decreases faster than free space. This index will be studied in Subsec. 3.4.8.

### 2.3.2 Multipath channel model

In case of a multi path channel model the indoor channel modelling defined in eq. (1.29) by [50] can be used:

$$C(\vec{p}_r, \Omega_r, \vec{p}_t, \Omega_t, f) = \frac{\delta(\Omega_r - \omega_r^{(0)})\delta(\Omega_t - \omega_t^{(0)})}{\sqrt{4\pi}|\vec{p}_r - \vec{p}_t|} e^{-jk|\vec{p}_r - \vec{p}_t|} + \sum_{i=1}^{N_r} \frac{\delta(\Omega_r - \omega_r^{(i)})\Gamma^i\delta(\Omega_t - \omega_t^{(i)})}{\sqrt{4\pi}(|\vec{p}_r - \vec{p}^{(i)}| + |\vec{p}_t - \vec{p}^{(i)}|)} e^{-jk|\vec{p}_r - \vec{p}_t|} \quad (2.25)$$

Which leads to:

$$h(\vec{p}_r, \Omega_r, \vec{p}_t, \Omega_t, f) = \frac{g_r(\Omega_r - \omega_r^{(0)})g_t(\Omega_t - \omega_t^{(0)})}{\sqrt{4\pi}|\vec{p}_r - \vec{p}_t|} e^{-jk|\vec{p}_r - \vec{p}_t|} + \sum_{i=1}^{N_r} \frac{g_r(\Omega_r - \omega_r^{(i)})\Gamma^i g_t(\Omega_t - \omega_t^{(i)})}{\sqrt{4\pi}(|\vec{p}_r - \vec{p}^{(i)}| + |\vec{p}_t - \vec{p}^{(i)}|)} e^{-jk|\vec{p}_r - \vec{p}_t|} \quad (2.26)$$

Where  $g_r$  and  $g_t$  are the reader and tag antenna radiation pattern values at  $i$ -th ray direction, respectively.  $\Gamma^i$  is the reflection coefficient of the  $i$ -th reflecting surface, and  $N_r$  is the number of rays.

The reciprocal transmission channel  $\alpha$  will be used to introduce the activation power profile, and we will see later that  $\alpha$  will be compensated to access the intrinsic characteristics of the tag independently from the environment.

## 2.4 Activation power profile

The activation process of a tag involves the transmission of a specific power level by the reader, which is then absorbed by the tag's integrated circuit (IC). This absorbed power is responsible for activating the tag and initiating its response. In this context, the transmitted activation profile refers to the minimum transmitted power, by the reader, necessary to activate the tag as function of distance or angle. Consequently, we introduce the received activation profile as the received power by the reader at this transmission activation power as a function of distance or angle.



### 2.4.1 Definition of the transmitted activation profile

A portion of the incident power to the tag, denoted as  $P_{IC}$ , is absorbed by the tag's integrated circuit (IC) when it is in either of its commutated states. The absorbed power is determined in average on the two commutated states, when neglecting the losses, by the incident power  $P_{inc}$  and the mean power transmission coefficient  $\tau$  as follows:

$$P_{IC}(P_t, f, \mathbf{r}, \mathbf{t}) = P_{inc}(P_t, f, \mathbf{r}, \mathbf{t})\tau(P_t, f, \mathbf{r}, \mathbf{t}) \quad (2.27)$$

Where  $\tau(P_t, \mathbf{r}, \mathbf{t})$  is the mean power transmission coefficient defined in (2.7). Note that this function is entering in contradiction with eq. (1.10) as we consider the power absorbed by the tag and reaching the chip comes from both chip states. Let  $S_c$  be the reading power sensitivity threshold of the chip which is an information provided by the chip manufacturer. The activation power  $P_t^{th}(\mathbf{r}, \mathbf{t})$  corresponds to the transmit power required to reach the IC chip sensitivity:

$$P_{IC}^{th}(P_t^{th}, f, \mathbf{r}, \mathbf{t}) = S_c \quad (2.28)$$

This equality determines the transmitted activation profile  $P_t^{th}(f, \mathbf{r}, \mathbf{t})$  which corresponds to the transmit power required to activate the tag at a given position. By using the simplified expression:

$$\tau^{th} = \tau(P_t^{th}, f, \mathbf{r}, \mathbf{t}) \quad (2.29)$$

and by replacing  $P_{inc}$  with its expression (??), it yields:

$$P_t^{th}(f, \mathbf{r}, \mathbf{t}) = \frac{4\pi S_c}{\lambda^2 \alpha(f, \mathbf{r}, \mathbf{t}) \tau^{th}} \quad (2.30)$$

This simply means that the tag activates when the impinging power reaches the IC threshold  $S_c$ . This profile can be easily characterized by sweeping the transmission power of the reader for each position of the tag.

This relation allows to express the mean power transmission coefficient as:

$$\tau^{th}(P_t^{th}, f, \mathbf{r}, \mathbf{t}) = \frac{4\pi S_c}{P_t^{th}(f, \mathbf{r}, \mathbf{t}) \alpha(f, \mathbf{r}, \mathbf{t}) \lambda^2} \quad (2.31)$$

The  $P_t^{th}$  profile is defined by ensuring that the IC chip receives exactly the minimum power represented by the chip sensitivity  $S_c$ . This implies that the incident power  $P_{inc}$  remains

constant and unchanged at  $P_t^{th}$ . Consequently, if we shift the activation profile by a value of  $\Delta$  in the dBm scale, it will cause a corresponding shift in the incident power by the same  $\Delta$  value while still maintaining it constant. We define the new shifted activation profile as follows:

$$P_t^{\Delta}{}_{dBm}(f, \mathbf{r}, \mathbf{t}) = P_t^{th}(f, \mathbf{r}, \mathbf{t}) + \Delta \quad (2.32)$$

In linear:

$$P_t^{\Delta}(f, \mathbf{r}, \mathbf{t}) = 10^{\frac{\Delta}{10}} P_t^{th}(f, \mathbf{r}, \mathbf{t}) \quad (2.33)$$

Noting that  $\Delta$  is a positive shifting value in dB scale, where for  $\Delta = 0$ :

$$P_t^0 = P_t^{th} \quad (2.34)$$

Varying the incident power causes a variation in the mean power transmission coefficient  $\tau$ , which can be expressed as following:

$$\tau^{\Delta}(P_t^{\Delta}, f, \mathbf{r}, \mathbf{t}) = \frac{4\pi P_{IC}(P_t^{\Delta}, f, \mathbf{r}, \mathbf{t})}{P_t^{\Delta}(f, \mathbf{r}, \mathbf{t})\alpha(f, \mathbf{r}, \mathbf{t})\lambda^2} \quad (2.35)$$

## 2.4.2 Definition of the received activation profile

The received power profile, denoted as  $P_r(P_t, f, \mathbf{r}, \mathbf{t})$ , corresponds to the power received by the reader in the RFID system at the transmitted power  $P_t$  for a given position  $(\mathbf{r}, \mathbf{t})$ . The expression of the received power follows the same principle as the radar equation, as it takes into account both forward and backward propagation, thus involves twice the reciprocal propagation channel. The equation for the received power profile is as follows:

$$P_r(P_t, f, \mathbf{r}, \mathbf{t}) = P_{inc} M(P_t, f, \mathbf{r}, \mathbf{t}) \alpha(f, \mathbf{r}, \mathbf{t}) \frac{\lambda^2}{4\pi} \quad (2.36)$$

By replacing  $P_{inc}$  with its expression ??, it yields:

$$P_r(P_t, f, \mathbf{r}, \mathbf{t}) = \frac{P_t \lambda^4}{(4\pi)^2} \alpha^2(f, \mathbf{r}, \mathbf{t}) M(P_t, f, \mathbf{r}, \mathbf{t}) \quad (2.37)$$

By considering  $P_t = P_t^{th}(f, \mathbf{r}, \mathbf{t})$ , we obtain the received power at the activation transmitted power which is denoted as the received power activation profile:

$$P_r^{th}(f, \mathbf{r}, \mathbf{t}) = \frac{P_t^{th}(f, \mathbf{r}, \mathbf{t}) \lambda^4}{(4\pi)^2} \alpha^2(f, \mathbf{r}, \mathbf{t}) M^{th} \quad (2.38)$$

Where  $M^{th} = M(P_t^{th}, f, \mathbf{r}, \mathbf{t})$ . This expression of the received power profile is convenient in any kind of environment as it is expressed in term of  $\alpha$  defined in Sec. 2.3, unlike the received power in free space assumption given in Sec. 1.4.2.6.

Additionally, we define the received power profile at the shifted activation profile:

$$P_r^\Delta(f, \mathbf{r}, \mathbf{t}) = P_r(P_t^\Delta, f, \mathbf{r}, \mathbf{t})$$

It can be expressed by considering  $P_t = P_t^{th}(f, \mathbf{r}, \mathbf{t})$  in equation (2.37):

$$P_r^\Delta(P_t^\Delta, f, \mathbf{r}, \mathbf{t}) = \frac{P_t^\Delta \lambda^4}{(4\pi)^2} \alpha^2(f, \mathbf{r}, \mathbf{t}) M^\Delta \quad (2.39)$$

Where

$$M^\Delta = M(P_t^\Delta, f, \mathbf{r}, \mathbf{t})$$

is the modulation factor obtained from the  $\Delta$  shifted activation profile.

## 2.5 Expression of modulation factor

The modulation factor  $M$ , defined in Sec. 1.4.2.6, plays a significant role in understanding and evaluating the RFID system. It quantifies the modulation properties of the system based on the received power and the transmitted power. In particular, we can express the modulation factor  $M$  in terms of the received power  $P_r$  at a specific transmitted power  $P_t$  based on equation (2.37), as follows:

$$M(P_t, f, \mathbf{r}, \mathbf{t}) = \frac{P_r(P_t, f, \mathbf{r}, \mathbf{t})(4\pi)^2}{P_t \alpha^2(f, \mathbf{t}, \mathbf{r}) \lambda^4} \quad (2.40)$$

In particular, if we consider the received activation power  $P_r^\Delta$ , we obtain the modulation factor  $M^\Delta$  expressed as follows:

$$M^\Delta = M(P_t^\Delta, f, \mathbf{r}, \mathbf{t}) = \frac{P_r^\Delta(f, \mathbf{r}, \mathbf{t})(4\pi)^2}{P_t^\Delta \alpha^2(f, \mathbf{t}, \mathbf{r}) \lambda^4} \quad (2.41)$$

$M^\Delta$  is a key quantity for this work as we will see later it is possible to access this intrinsic criteria of the tag by measuring the shifted activation profiles and the variation of this quantity in term of the incident power variation will be discussed. In particular, if we

consider  $\Delta = 0$  we obtain  $M^0 = M^{th}$  in term of the activation profiles as follows:

$$M^{th} = M(P_t^{th}, f, \mathbf{r}, \mathbf{t}) = \frac{P_r^{th}(f, \mathbf{r}, \mathbf{t})(4\pi)^2}{P_t^{th}\alpha^2(f, \mathbf{t}, \mathbf{r})\lambda^4} \quad (2.42)$$

Hereafter for concision, the explicit parameter dependencies are omitted.

## 2.6 Definition of the tag receptivity and the tag offset

Let's consider the channel coefficient included in equation (2.35). This equation allows us to derive a simplified expression for the channel coefficient  $\alpha(f, \mathbf{r}, \mathbf{t})$  in terms of the  $P_t^\Delta(f, \mathbf{r}, \mathbf{t})$  and the power delivered to the IC ( $P_{IC}$ ):

$$\alpha = \frac{4\pi P_{IC}^\Delta}{P_t^\Delta \tau^\Delta \lambda^2} \quad (2.43)$$

Let's consider in addition, a variation  $\Delta_c$  in dBm on the power delivered to the IC for a  $\Delta$  variation on the transmitted activation power. This leads to:

$$P_{IC}^\Delta = S_c + \Delta_c \quad (2.44)$$

Then  $\alpha$  can be expressed in term of  $S_c$  and  $\Delta_c$  as follows:

$$\alpha = \frac{4\pi(S_c + \Delta_c)}{P_t^\Delta \tau^\Delta \lambda^2} \quad (2.45)$$

Now for the particular case  $\Delta = 0dB$  which implies  $\Delta_c = 0dB$ , thus,  $S_c = P_{IC}^0$ , then  $\alpha$  can be expressed as follows:

$$\alpha = \frac{4\pi S_c}{P_t^{th} \tau^{th} \lambda^2} \quad (2.46)$$

Note that the channel coefficient  $\alpha$  is only related to transmission channel and is invariant with respect to the transmitted power variation.

In introducing this expression in (2.37), it simplifies into a relation independent of the propagation channel which relates measurable or known quantities to  $M$  and  $\tau^{th}$ . We then obtain this equality:

$$P_r P_t^{th2} = P_t S_c^2 \frac{M}{\tau^{th2}} \quad (2.47)$$

or equivalently in defining for the first time the tag receptivity  $R$  :

$$R = \frac{\sqrt{M}}{\tau^{th}} S_c = \sqrt{\frac{P_r P_t^{th^2}}{P_t}} \quad (2.48)$$

If we consider the shifted transmitted activation power  $P_t = P_t^\Delta$ , we obtain  $R^\Delta$  as function of  $M^\Delta$  defined in (2.41) and  $P_t^\Delta$  defined in (2.32):

$$R^\Delta = \frac{\sqrt{M^\Delta(P_t^\Delta)}}{\tau^{th}} S_c = \sqrt{\frac{P_r^\Delta P_t^{th^2}}{P_t^\Delta}} \quad (2.49)$$

$$R^\Delta = \frac{\sqrt{M^\Delta}}{\tau^{th}} S_c = \frac{1}{10^{\frac{\Delta}{10}}} \sqrt{P_r^\Delta P_t^\Delta} \quad (2.50)$$

We define  $Q^\Delta$ , a quantity which relates the  $\Delta$  modulation factor to the threshold mean power transmission coefficient:

$$Q^\Delta = 10^{\frac{\Delta}{10}} \frac{\sqrt{M^\Delta}}{\tau^{th}} \quad (2.51)$$

We then obtain:

$$R^\Delta = Q^\Delta S_c = 10^{\frac{\Delta}{10}} \sqrt{P_r^\Delta P_t^\Delta} \quad (2.52)$$

Furthermore, if we particularize this expression at the transmitted activation power  $P_t = P_t^{th}$ , we obtain the tag receptivity:

$$R^{th} = Q^{th} S_c = \sqrt{P_r^{th} P_t^{th}} \quad (2.53)$$

$R^{th}$  is the chip sensitivity multiplied by the design dependent factor  $Q^{th}$  (called tag offset).

The Tag receptivity is a metric that we have introduced to encompass the intrinsic characteristic of the tag. It plays a vital role in assessing the tag's performance and understanding its behavior in the RFID system as it is related to the chip sensitivity by the tag offset  $Q$ . By examining the activation profiles and analyzing the resulting receptivity, we gain valuable insights into the capabilities and limitations of the tags under investigation. This term serves as a useful metric for evaluating how well the tag responds to activation signals and helps us understand its overall functionality within the RFID system in term of absorption

and backscattering.

$$Q^{th} = \frac{\sqrt{M^{th}}}{\tau^{th}} \quad (2.54)$$

If we express (2.53) in dB scale, we get a dB offset which is a combination of the 3 main intrinsic properties of the tag:  $S_{cdB}$ ,  $\tau^{th}$  and  $M^{th}$ . The typical chip sensitivity  $S_c$  can be obtained from the tag IC datasheet. Thus, by combining eq. (2.54) and eq. (2.53), we express the tag receptivity in dBm scale as follows:

$$R_{dB}^{th} = 5 \log_{10} M^{th} - 10 \log_{10} \tau^{th} + S_{cdB} \quad (2.55)$$

A practical relation is obtained from the right hand side of (2.49) which gives access to the tag receptivity simply in averaging the transmitted activation profile and the associated received activation profile.

$$R_{dB}^{th} = \frac{P_r^{th} + P_t^{th}}{2} \quad (2.56)$$

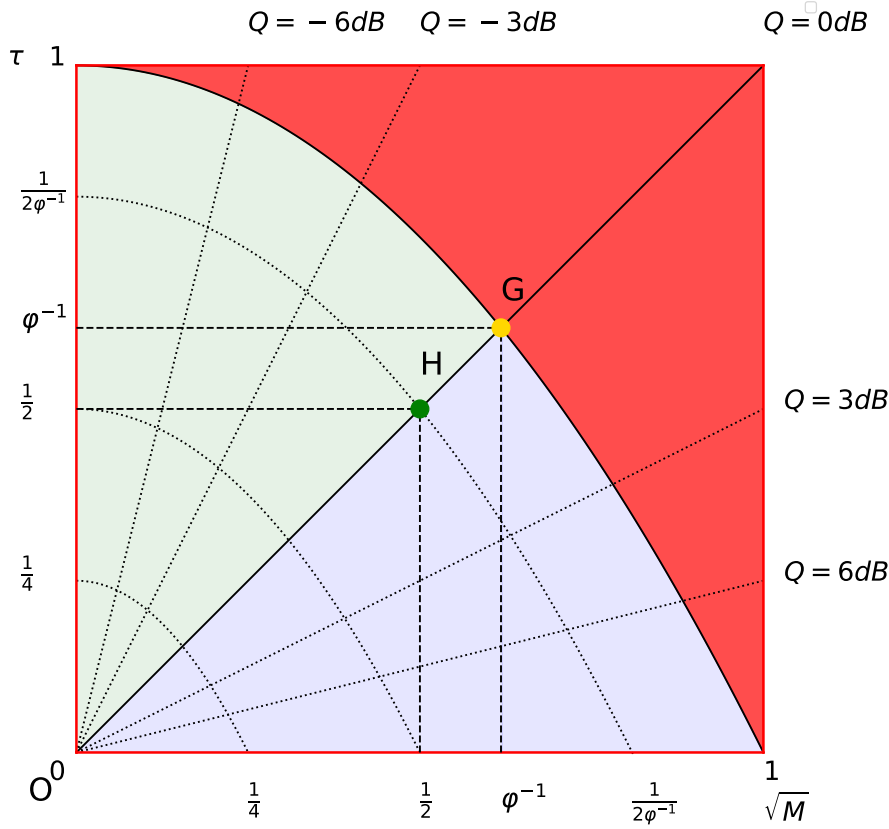
$Q_{dB}^{th}$  is obtained experimentally from the dB offset between the typical chip sensitivity and the above measured tag receptivity as:

$$Q_{dB}^{th} = \bar{R}_{dB}^{th} - S_{cdB} \quad (2.57)$$

Where  $\bar{R}^{th}$  is the mean value of  $R^{th}$  value. It is observed experimentally that this quantity has a very small variance as shown in Sec. 3.4.3.

## 2.7 Introduction of the $(\sqrt{M}, \tau)$ chart

As we have seen  $\tau$  accounts for the mean absorption of the tag and  $M$  for its reflectivity or the contrast that is presented to the reader on the return path. An RFID tag is as good as it provides the proper balance between energy harvesting and high receiving contrast simultaneously. The goal is often to maximize both of these quantities which is usually not possible. Given that  $\tau$  and  $M$  are quantities that range from 0 to 1, it is natural to try to find an appropriate representation that can synthesize the performance of an RFID tag for a given frequency and incident power on the tag. Instead of representing  $\tau$  w.r.t  $M$  as it could be envisaged, we propose representing  $\tau$  w.r.t  $\sqrt{M}$ . This has the advantage of


 Figure 2.2 – The proposed  $(\sqrt{M}, \tau)$  chart

facilitating the interpretation of the values of constant  $Q$  which are manifested by straight lines of slope  $Q^{-1}$  originating from the origin. The upper parabolic boundary corresponds to the limit situation where  $M = 1 - \tau$ , which corresponds, if we return to formula (2.15), to the situation where the tag does not backscatter any power on the carrier frequency, resulting in maximum power in the sidebands and thus maximizing the contrast  $M$  for a given power transmission coefficient  $\tau$ .

Fig. 2.2 presents the proposed chart. A tag at a given frequency is a point on this chart at coordinates  $(\sqrt{M}, \tau)$ . We have distinguished 3 regions based on the values of  $\sqrt{M}$  and  $\tau$ .

- The red region represents the impossible region for a tag's design. This region is bounded between two lines and one curve:
- The horizontal line which corresponds for a  $\tau = 1$  is not possible since the backscattering cannot happen if all the incident energy in both states 1 and 2 is

absorbed by the tag, in other words,  $\sqrt{M}$  is constrained to be 0 in this case.

- The vertical line corresponds to the values of  $\sqrt{M} = 1$ , hence, all the incident energy would be backscattered, therefore no is absorbed and  $\tau$  is strictly 0, and the tag is unable to wake up.
- The parabolic curve from point (0,1) to (1,0) draws the boundary of the non physical where physical laws of conservation would be violated.
- The light blue region corresponds to the region where  $Q_{dB}^{th} > 0$ , therefore  $\sqrt{M} > \tau$ . In this region tag receptivity is smaller than chip sensitivity  $S_c$ .
- The light green region corresponds for the region where  $Q_{dB}^{th} < 0$ , therefore  $\sqrt{M} < \tau$ . In this region tag receptivity is greater than chip sensitivity  $S_c$ .

The upper frontier (parabolic curve) corresponds also to the condition where the static term  $S = 0$  (see 2.13), meaning:

$$|\Gamma_1 + \Gamma_2|^2 = 0 \quad (2.58)$$

i.e the two complex reflecting coefficient symmetrically spaced w.r.t origin.

### 2.7.1 Maximal values of $\tau$ and $M$ for a given $Q$

For a given value of  $Q$  we get limitations on the possible values of  $\tau$  and  $\sqrt{M}$  as the intersection between the line of slope  $Q^{-1}$  (expressed in (2.54)) and the parabolic boundary  $M = 1 - \tau$ . The resulting limitations are as follows:

$$\tau_{max}(Q) = \frac{\sqrt{1 + 4Q^2} - 1}{2Q^2} \quad (2.59)$$

$$\sqrt{M_{max}}(Q) = \frac{\sqrt{1 + 4Q^2} - 1}{2Q} \quad (2.60)$$

For a given tag offset  $Q$ , let define the point  $K = (\sqrt{M_{max}}, \tau_{max})$ , lying on the upper limit parabola.

### 2.7.2 Remarkable points of the chart

If we impose additionally that  $\frac{\sqrt{M}}{\tau} = 1$ , we obtain  $\sqrt{M_{max}} = \varphi^{-1}$  and  $\tau_{max} = \varphi^{-1}$  which maximizes simultaneously mean absorption and contrast with the golden ratio  $\varphi = \frac{1+\sqrt{5}}{2}$ ,



$\varphi^{-1} \approx 0.618$ . A remarkable point in the chart is then  $G = (\varphi^{-1}, \varphi^{-1})$ . Notice that if  $Z_1 = 0$ , then  $|\Gamma_1| = 1$  and the best achievable point is  $H = (\frac{1}{2}, \frac{1}{2})$ , where  $\tau_{max} = \frac{1}{2}$ .

In the chart, a constant  $Q$  corresponds to a line that starts from the origin and has a slope of  $Q^{-1}$  since  $\tau = Q^{-1}\sqrt{M}$ .

### 2.7.3 Performance indicators

Furthermore, we define two heuristic criteria to evaluate the tag performance: one is obtained by calculating the Euclidean distance between the point presenting the tag in the chart  $T = (\sqrt{M}, \tau)$  and the point  $G$  (defined by  $\rho_{\varphi^{-1}}$ ), and the other is obtained by calculating the Euclidean distance between  $T$  and  $H$  which represents a perfect conjugate matching (defined by  $\rho_{\frac{1}{2}}$ ).

The following equations express the two proposed criteria:

$$\rho_{\varphi^{-1}} = \left(1 - \frac{\|\vec{TG}\|}{\|\vec{OG}\|}\right) \times 100\% \quad (2.61)$$

$$\rho_{\frac{1}{2}} = \left(1 - \frac{\|\vec{TH}\|}{\|\vec{OH}\|}\right) \times 100\% \quad (2.62)$$

While considering these criteria, it's important to note that they may not necessarily represent the optimal tag design. This last depends on external variables such as the reader sensitivity  $S_r$  as we will see later. However, the reader sensitivity is not always known, and the tag manufacturer would sometime seek a design that work efficiently in any kind of application despite the reader sensitivity. In such case, we can make an implicit assumption that the closer the tag is to either  $G$  or  $H$ , the better the design as it describes a balance between the mean power transmission coefficient and the modulation factor. The idea is to compromise between  $\tau$  and  $M$ . Consequently, higher values of either  $\rho_{\varphi^{-1}}$  or  $\rho_{\frac{1}{2}}$  indicate better tag performance in general.

### 2.7.4 Tag efficiency parameter $\gamma$

With eq (2.59) and eq. (2.60), for a given tag point  $P(\sqrt{M}, \tau)$  in the chart, we can also define a new parameter :

$$\gamma = \frac{\|\vec{OT}\|}{\|\vec{OK}\|} = \frac{\sqrt{\tau^2 + M}}{\sqrt{\tau_{max}^2 + M_{max}}} \quad (2.63)$$

This  $\gamma$  parameter is a tag efficiency indicator (unlike  $Q$ ), we call it the tag efficiency.

The iso- $\gamma$  curve are parabolas starting at point  $(0, \gamma)$  and ending at point  $(\gamma, 0)$ . The equation of those iso  $\gamma$  curves is simply :

$$\tau = \gamma - \frac{M}{\gamma} \quad (2.64)$$

Notice that those curves would be parallel lines in a  $(\sqrt{M}, \tau)$  chart. The iso- $\gamma$  line passing through the center point  $H$  is  $\gamma_H = \frac{1}{2\varphi-1} = 0.809$ , suggesting that a tag with perfect conjugate impedance matching in one state and a perfect short circuit on the other would be only 80.9% efficient.

Since the chart reflects the bijection between  $(\sqrt{M}, \tau)$  and  $(Q, \gamma)$  tag representation, we have also the following reciprocal relation which gives  $M$  and  $\tau$  when  $Q$  and  $\gamma$  are known.

$$M = \gamma M_{max}(Q) = \gamma \frac{\sqrt{1 + 4Q^2} - 1}{2Q} \quad (2.65)$$

$$\tau = \frac{\sqrt{M}}{Q} \quad (2.66)$$

### 2.7.5 How to place a measured tags in the chart ?

The exploitation of the activation profiles is necessary to access the intrinsic characteristics of the tag, thus placing the tag in the chart, however, it's not sufficient. To accurately position a tag on the evaluation chart, values for  $\tau$  and  $M$  need to be obtained. However, these two quantities are interconnected by  $Q$  factor, which can only be determined from the acquisitions. Consequently, separating  $\tau$  and  $M$  becomes challenging. Therefore, further investigation of additional information is necessary to achieve greater precision in placing the tag on the chart. For this reason, we will present an algorithm to place the tags in the chart.

### 2.7.5.1 Power transmission coefficient ratio between tags

If we consider two different RFID tags  $T_{(i)}$  and  $T_{(j)}$  placed at the same position in the same channel (important condition) we have the relation :

$$\frac{P_t^{th_i}(\mathbf{r}, \mathbf{t})}{P_t^{th_j}(\mathbf{r}, \mathbf{t})} = \frac{S_c^{(i)} \tau_j^{th}}{S_c^{(j)} \tau_i^{th}} = \frac{S_c^{(i)}}{S_c^{(j)}} \tau_{i,j} \quad (2.67)$$

Where  $\tau_{i,j}$  is the ratio between two values of mean power transmission coefficient  $\tau_{(i)}$  and  $\tau_{(j)}$  as:

$$\tau_{i,j} = \frac{\tau_{(j)}}{\tau_{(i)}} \quad (2.68)$$

it is obtained from the offset between activation profiles of two tags and the ratio of their respective chip sensitivity as:

$$\tau_{i,j} = \frac{P_t^{th_i}(\mathbf{r}, \mathbf{t}) S_c^{(j)}}{P_t^{th_j}(\mathbf{r}, \mathbf{t}) S_c^{(i)}} \quad (2.69)$$

This measured ratio will be exploited in the next subsection in the attempt of best placing tags on the chart based on the knowledge of their  $Q^{th}$  and several  $\tau_{i,j}$  ratios.

### 2.7.5.2 Interval halving algorithm to place tags in the chart

In practice, a single tag cannot be placed in the chart from the only knowledge of its  $Q^{th}$  factor. Hopefully, if several tags activation profiles are measured and their  $\tau_{i,j}$  ratio (offset in dB scale) are evaluated, the task becomes partly achievable. Let assume a set of  $N$  tags, placed at the same position, measured in the same channel, and whose profiles are measured under as similar conditions as possible. Let then define the sequence of  $Q$ :

$$\mathbf{Q} = [Q_1, \dots, Q_N] \quad (2.70)$$

and the corresponding sequence of ratio (2.68) between consecutive values of  $\tau$ :

$$\mathbf{t} = [\tau_{1,2}, \dots, \tau_{N-1,N}] \quad (2.71)$$

These two vectors are provided as inputs of the interval halving algorithm (Algorithm 1) which guesses for each tag  $n$  its  $\tau_n$  and  $\sqrt{M_n}$  values.

The general principle of the algorithm is the following:

- Each tag should be placed on the line corresponding to its  $Q$  value.
- All the ratios involving a tag should be respected. This is obtained iteratively by an interval halving procedure, which adjust the  $\tau$  value of the first tag until all the tags have their  $\tau$  less or equal than  $\tau_{max}$ . This is achieved through `cond1`.
- The highest value of  $\tau$  can be optionally limited in a reasonable range defined as  $\tau_{lim}$ . This is achieved through `cond2`.

---

**Algorithm 1** Determine  $\sqrt{M_n}$  and  $\tau_n$  by interval halving

---

**Require:**  $\mathbf{Q}, \mathbf{t}, \tau_{lim}, \epsilon$

**Output :**  $\sqrt{M_n}$  and  $\tau_n$

$\tau_{max} = f(\mathbf{Q})$  using eq (2.59)

$x_0 = \tau_{max}[0]$

$x_1 = \tau_{max}[0] + 2\epsilon$

$k=2$

$i=1$

**while**  $|x_{i-1} - x_i| > \epsilon$  **do**

$\mathbf{v} = [x_{i-1}, \mathbf{t}]$

$\mathbf{pv}[n] = \prod_{i=1}^n \mathbf{v}[i] \quad \forall n \in \{1, \dots, N\}$

$\text{cond1} = \exists(\mathbf{pv}[n] > \tau_{max}[n]) \quad \forall n \in \{1, \dots, N\}$

$\text{cond2} = \exists(\mathbf{pv}[n] > \tau_{lim}) \quad \forall n \in \{1, \dots, N\}$

**if**  $\text{cond1}|\text{cond2}$  **then**

$x_i = x_{i-1} - \frac{x_{i-1}}{k}$

**else**

$x_i = x_{i-1} + \frac{x_{i-1}}{k}$

$k \leftarrow 2k$

**end if**

$i \leftarrow i + 1$

**end while**

$\tau_n = \mathbf{pv}[n] \quad \forall n \in \{1, \dots, N\}$

$\sqrt{M_n} = \tau_n \mathbf{Q}[n] \quad \forall n \in \{1, \dots, N\}$

---

## 2.7.6 Free space read range formulation

If we assume a free space propagation situation the read range can be constrained either by the forward or the backward link. In the one hand, the read range is a function of  $\tau$  when limited by the tag activation. Then it can be obtained by replacing  $\alpha_{FS}$  (2.20) in the  $P_t^{th}$  expression (2.30):

$$d_{max}^{(\tau)} = \frac{\lambda}{4\pi} \left( \frac{P_t G_t G_r \tau}{S_c} \right)^{1/2} \quad (2.72)$$

Unlike the forward read range expression (1.12) which is a function of  $\tau_2$ .

On the other hand, in defining the reader sensitivity as  $S_r$ , the read range is a function of  $M$  when limited by the backward link. It can be obtained by replacing  $\alpha_{FS}$  (2.20) in the  $P_r^{th}$  expression (2.38), where  $P_r^{th} = S_r$  at the backward link limit:

$$d_{max}^{(M)} = \frac{\lambda}{4\pi} \left( \frac{P_t G_t^2 G_r^2 M}{S_r} \right)^{1/4} \quad (2.73)$$

Similarly to the expression (1.19). The resulting read range is defined as

$$d_{max}^{(\tau, M)} = \min(d_{max}^{(\tau)}, d_{max}^{(M)}) \quad (2.74)$$

The condition  $d_{max}^{(\tau)} = d_{max}^{(M)}$  yields the condition on the tag offset  $Q_{opt}$  necessary to achieve the maximum read range.

$$Q_{opt} = \frac{\sqrt{S_r P_t}}{S_c} \quad (2.75)$$

The Fig. 2.3 illustrates the evolution of the  $Q_{opt}$  with respect to its 3 dependent parameters  $S_r$ ,  $S_c$  and  $P_t$ .

Moreover, by taking into account the condition  $d_{max}^{(\tau)} = d_{max}^{(M)}$  and by considering the maximum values of  $\tau$  and  $M$  (derived from equations (2.59) and (2.60)) at the calculated  $Q_{opt}$ , we determine the maximum free space read range that an ideal tag can achieve with chip sensitivity  $S_c$  and a reader with read sensitivity  $S_r$ . We express it as follows:

$$\max_{\tau, M} d_{max}^{(\tau, M)} = \frac{\lambda}{4\pi} \sqrt{G_t G_r \frac{S_c}{2S_r} \left( \sqrt{1 + \frac{4S_r P_t}{S_c^2}} - 1 \right)} \quad (2.76)$$

This formula will be examined in the following in order to evaluate the maximum read range and its dependencies by visually presenting it in the proposed chart.

### 2.7.6.1 Example on free space read range examination

The UHF RFID tag's free space read range can be altered by adjusting the reader sensitivity and chip sensitivity, as shown in eq. (2.76). Two types of links were analyzed: the forward link read range, presented in eq. (2.72), is primarily influenced by the mean power transmission coefficient  $\tau$  and the chip sensitivity  $S_c$ , while the backward link read range, presented in eq. (2.73), is determined by the modulation factor  $M$  and the reader

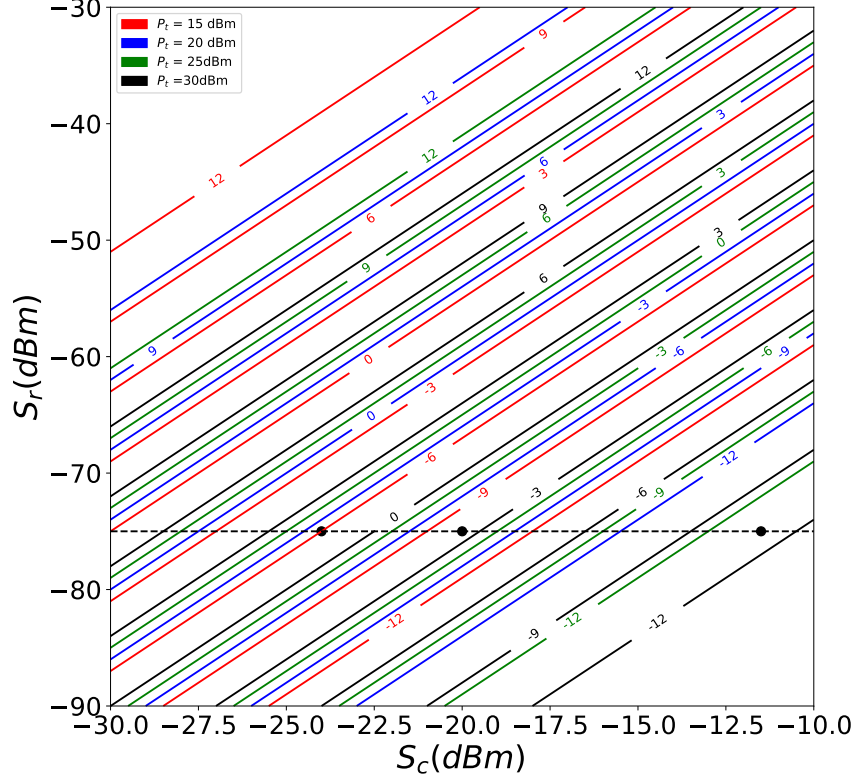


Figure 2.3 – Evolution of  $Q_{optdB}$  with respect to reader and chip sensitivity  $S_r$  and  $S_c$ , for different transmit power. The  $Q_{opt}$  values obtained from the example of [41] are placed in the chart

sensitivity  $S_r$ . An equilibrium is established when the modulation factor and mean power transmission coefficient are balanced, as indicated by eq. (2.75). An example of the read range examination is illustrated in the  $(\sqrt{M}, \tau)$  chart in Fig. 2.4, where  $S_c = -24 \text{ dBm}$ ,  $S_r = -80 \text{ dBm}$  and  $P_t = 25 \text{ dBm}$  are assumed. In this example, the equilibrium is determined and expressed by the tag offset  $Q_{opt}$ . The gains of the reader and tag are chosen logically to be  $G_r = 9 \text{ dB}$  (as per the platform antenna, see 1.5.3) and  $G_t = 2 \text{ dB}$ . To examine the maximum read range that can be obtained in a free space condition, we use eq. (2.76), which yields a maximum read range of  $\max_{\tau, M} d_{max}^{(\tau, M)} = 25.4 \text{ m}$ . This means that an optimally designed tag with a chip sensitivity of  $-24 \text{ dBm}$  can be interrogated by a reader with a sensitivity of  $-80 \text{ dBm}$  at a maximum distance of  $25.4 \text{ m}$ . Fig. 2.4 shows the read range distribution for this scenario, where no conditions other than the parabolic

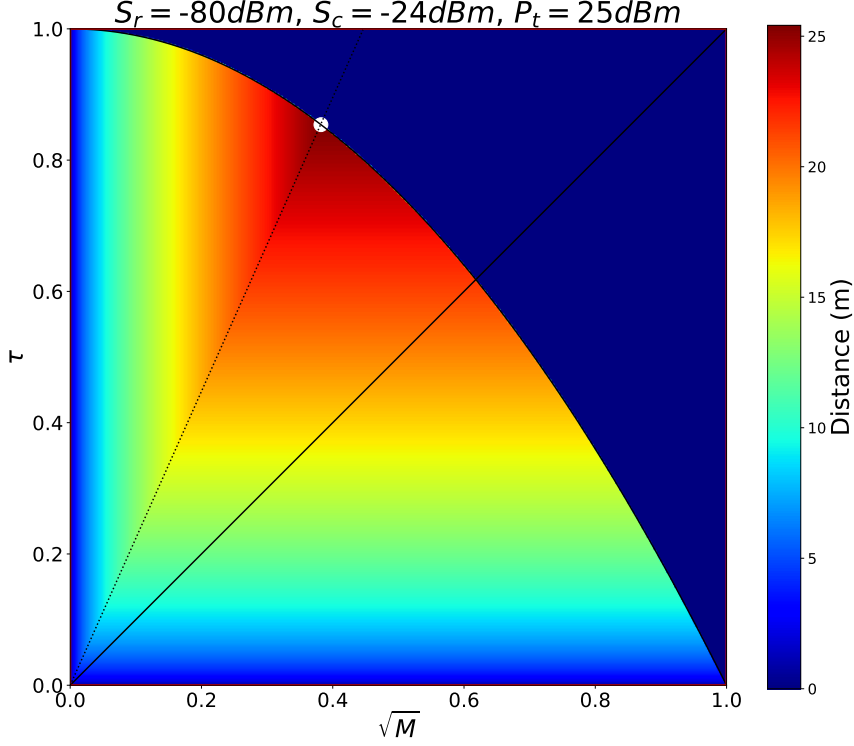


Figure 2.4 – Example on Read Range evaluation ( $S_r = -24dBm$ ,  $S_c = -80dBm$ ,  $G_r = 9dB$ ,  $G_t = 2dB$ )

boundary are applied. The white dot on the graph represents the point with the maximum read range, which is the intersection of the  $Q$  line of  $Q_{opt}$  value obtained from eq. (2.75) with the parabolic boundary.

The read range dependency can be divided into three regions:

- The right side of the  $Q_{opt}$  line corresponds to the region where  $d_{max}^{(\tau)} < d_{max}^{(M)}$ , and in this case,  $d_{max}^{(\tau, M)} = d_{max}^{(\tau)}$ . Here, the read range is affected by the  $\tau$  value, and the higher the  $\tau$  value, the better the read range. This results in a vertical colored variation in the figure.

- On the left side of the  $Q_{opt}$  line, the opposite is true, and the read range is affected by the  $M$  value. Here, the higher the  $M$  value, the better the read range, resulting in a horizontal colored variation in the figure.
- Finally, the  $Q_{opt}$  line corresponds to the  $\tau$  and  $M$  values that give  $d_{max}^{(\tau)} = d_{max}^{(M)}$ . At the white dot, we have an ideal point which give the maximum read range defined in eq. (2.76).

## 2.8 UHF RFID tags evaluation using the proposed chart

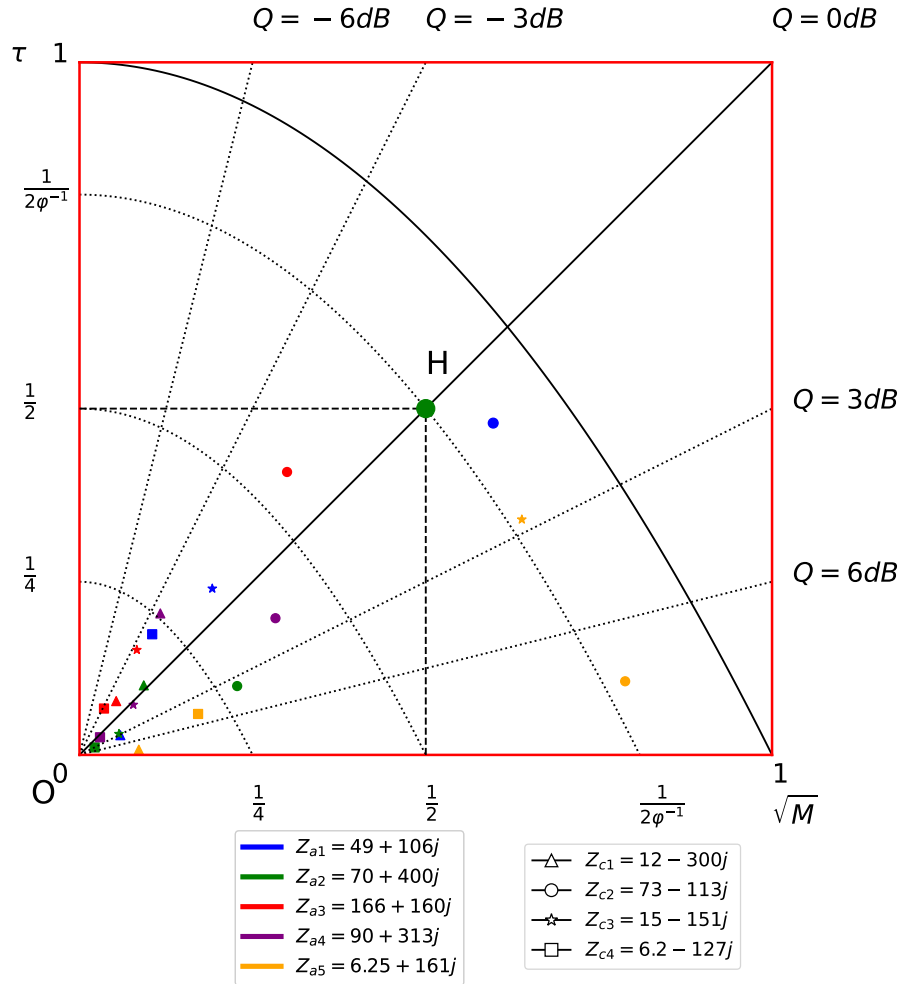


Figure 2.5 –  $(\sqrt{M}, \tau)$  chart representation of Bolomey's data

In order to illustrate how the proposed chart can be used, we take the chip and antenna



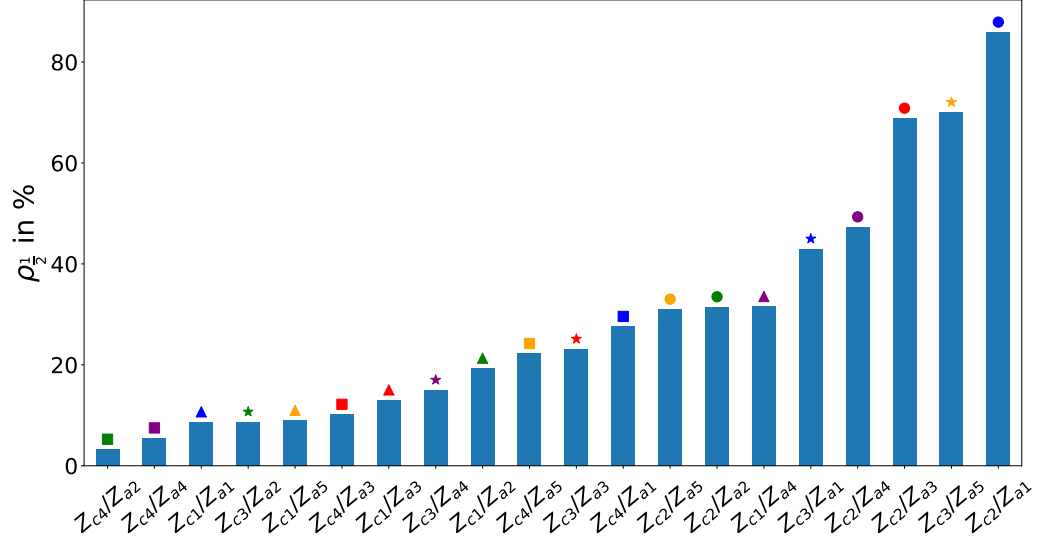
pairs presented in the Bolomey's paper [29]. Since the impedances of these chips and antennas are given, the  $\tau$  and  $\sqrt{M}$  can be calculated using (2.7) and (2.12). Table 2.1 contains the calculated values of  $\tau$  (using eq. (2.7)) and  $\sqrt{M}$  (using eq. (2.12)) for all combinations of known chips and antennas, as well as the  $Q$  values derived from these two quantities.

### 2.8.1 Illustration of chip-antenna combinations performance

The values of this table are presented in Fig. 2.5 by a colored dot with different shapes. Each color refers to a specific antenna (5 in total) while each shape refers to one specific chip (4 in total). By combining each chip with each antenna, a total of 20 combinations are obtained and presented in the chart. Since this data are based on the assumption that  $Z_1 = 0$ , the way to evaluate the performance of the design is assumed to be the distance from the point H which represents a perfect conjugate matching as explained in 2.7. Therefore, the criteria to be used for this evaluation is  $\rho_{\frac{1}{2}}$  defined in (2.62). Fig. 2.6 represents the values of  $\rho_{\frac{1}{2}}$  for each combination in an ascending order. As it appears, the combination of chip  $Z_{c2} = 73 - 113j\Omega$  and antenna  $Z_{a1} = 49 + 106j\Omega$  represented by a blue circle has the highest  $\rho_{\frac{1}{2}}$  value among the tags. This combination is the closest to the center (large green circle) with  $\tau = 0.479$  and  $\sqrt{M} = 0.597$ , making it the best design among the tags which balance power absorption and power backscattering. This outcome was expected, as the combination of the two impedances is almost conjugate-matched. On the other hand, it is noticeable that not any combination are effective. In this association procedure many combinations result in very low  $\tau$  and  $\sqrt{M}$  value, thus a very low  $\rho_{\frac{1}{2}}$  values such i.e  $Z_{c4}/Z_{a2}$  and  $Z_{c4}/Z_{a4}$ . The chart can be helpful to select the appropriate chip-antenna combination for a UHF RFID tag. For instance, if we consider the antenna  $Z_{a2}$ , combining it with  $Z_{c1}$  would yield the same  $\tau$  as combining it with  $Z_{c2}$ . However, the second combination has a higher  $\sqrt{M}$  value compared to the first one. Consequently, the combination  $Z_{c2}/Z_{a2}$  has a higher  $\rho_{\frac{1}{2}}$  value than  $Z_{c1}/Z_{a2}$ . This can be observed in Fig. 2.6, where the green triangle and green circle correspond to  $Z_{c1}/Z_{a2}$  and  $Z_{c2}/Z_{a2}$  respectively.

### 2.8.2 Employing the algorithm to place the tags in the chart

After obtaining the mean power transmission coefficient ( $\tau$ ) and the  $Q$  factor for each tag of the chip-antenna pair, the tag's position in the  $(\sqrt{M}, \tau)$  chart can be indirectly determined using the algorithm described in Sec. 2.7.5.2. This algorithm takes an input

Figure 2.6 – Ordering the combinations of antenna/tag basing on the  $\rho_{\frac{1}{2}}$  performance criteria

$Z_a$	$Z_c$											
	12-300j			73-113j			15-151j			6.2-127j		
	$\tau$	$\sqrt{M}$	$Q_{dB}$	$\tau$	$\sqrt{M}$	$Q_{dB}$	$\tau$	$\sqrt{M}$	$Q_{dB}$	$\tau$	$\sqrt{M}$	$Q_{dB}$
49+106j	0.028	0.059	3.17	<b>0.479</b>	<b>0.597</b>	0.955	0.240	0.191	-0.979	0.174	0.105	-2.204
70+400j	0.100	0.092	-0.347	0.099	0.227	3.598	0.030	0.057	2.739	0.010	0.022	3.062
166+160j	0.077	0.052	-1.662	0.408	0.299	-1.348	0.151	0.082	-2.636	0.066	0.035	-2.773
90+313j	0.204	0.116	-2.433	0.197	0.282	1.562	0.072	0.077	0.301	0.025	0.029	0.655
6.25+161j	0.007	0.085	10.497	0.106	0.787	8.699	0.339	0.638	2.736	0.059	0.171	4.617

Table 2.1 –  $\tau$ ,  $\sqrt{M}$  and  $Q_{dB}$  for a set of known RFID Antennas and IC Chips [29]

array of  $Q$  values and an array of  $\tau$  ratios. The algorithm's results are presented in Fig. 2.7 for two conditions:  $\tau_{lim} = \varphi^{-1}$  in blue and  $\tau_{lim} = 0.5$  in orange. In addition, the figure shows, in red, the real values obtained analytically from the impedances (presented in Table 2.1), with the reminder that  $Z_1 = 0$ .

As anticipated, the values produced by the algorithm for  $\tau_{lim} = \varphi^{-1}$  exhibit a more significant deviation from the actual values compared to those for  $\tau_{lim} = 0.5$ . This divergence is expected since  $\tau$  cannot exceed 0.5 (such as  $\varphi^{-1}$ ) when  $Z_1 = 0$ . It is worth noting that

the closer the constraint  $\tau_{lim}$  is to the maximum  $\tau$  value among the combinations (which is 0.401 according to Table 2.1), the more accurate the algorithm's results become. Thus, careful consideration should be given when imposing constraints on  $\tau_{lim}$  for improved algorithm accuracy. For example, when  $Z_1$  is non-zero, selecting  $\tau_{lim} = \varphi^{-1}$  can be a suitable choice.

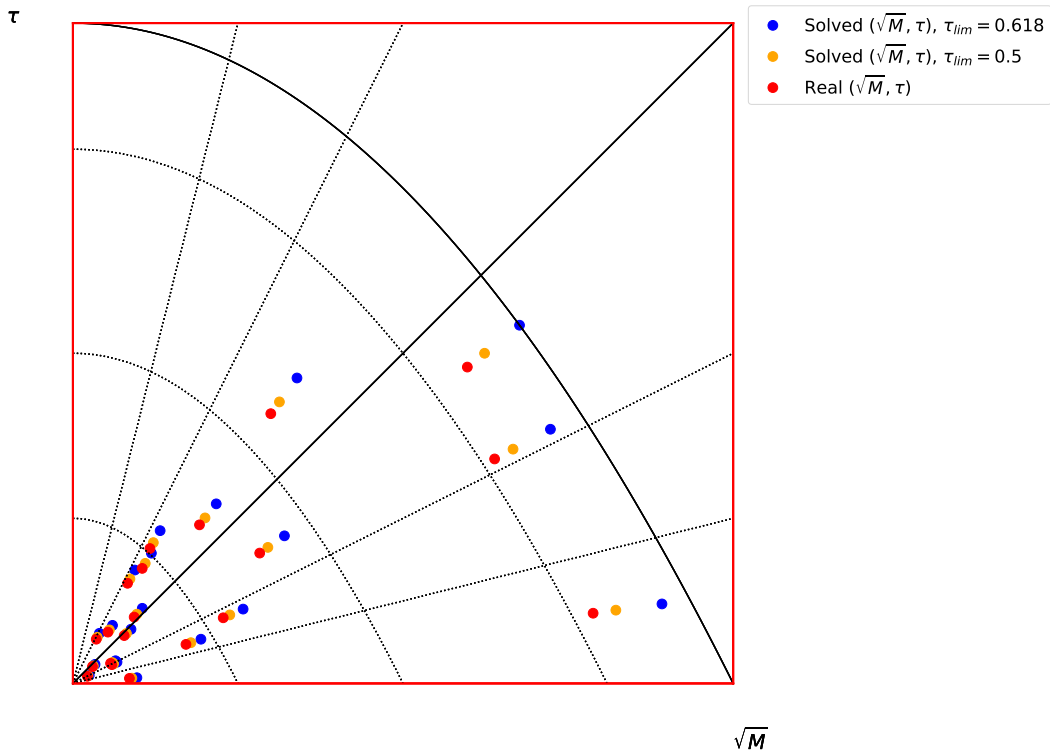


Figure 2.7 – Comparison between the real  $(\sqrt{M}, \tau)$  values calculated directly from the impedance, the  $(\sqrt{M}, \tau)$  solved by the algorithm for  $\tau_{lim} = 0.5$  and the  $(\sqrt{M}, \tau)$  solved at  $\tau_{lim} = \varphi^{-1}$

These findings illustrate that by appropriately limiting  $\tau$ , the algorithm can more accurately position the tags on the chart. Nevertheless, by imposing suitable limitations, the chart remains a valuable tool for evaluating and comparing tags, as the algorithm's conditions do not affect the relative ratios between the factors.

## 2.9 Chip validity domain in the $(\sqrt{M}, \tau)$ chart

The proposed chart can also be used to represent what we call the chip validity domain, i.e all the points in the chart that can be reached with a given antenna design for a given chip. We assume that the chip impedance  $Z_2$  and  $Z_1$  are known. For  $Z_2$  the information is available in the chip datasheet.  $Z_1$  can be inferred from assumption on the  $R_{mod}$  value and eq. (2.1). With  $Z_1$  and  $Z_2$ , we determine the region that can be reached in the  $(\sqrt{M}, \tau)$  space for this chip by means of the choice of antenna and its input impedance  $Z_a$ . For a given chip we define the two points  $R = (\sqrt{M_r}, \tau_r)$  and  $T = (\sqrt{M_t}, \tau_t)$  respectively obtained with the antenna impedances  $Z_{ar}$  (1.23) and  $Z_{at}$  (1.22).

The point  $T$  is always placed on the upper boundary  $M_r = 1 - \tau_r$ , whereas the point  $R$  lies always on the upper limit. The diagonal from the origin to this point  $R$  yields to the lower limit  $f_{inf}(\sqrt{M})$  of the chip validity domain  $\mathcal{D}_{chip}$ . This limit corresponds to a straight line whose slope corresponds the inverse of the tag offset  $1/Q_r$ . with:

$$Q_r = \frac{\sqrt{M_r}}{1 - M_r} \quad (2.77)$$

$$f_{inf}(\sqrt{M}) = \frac{\tau_r}{\sqrt{M_r}} \sqrt{M} \quad (2.78)$$

The upper limit  $f_{sup}$  is a parabola through which 3 points pass : the origin  $O$ ,  $R$  and  $T$ .

$$f_{sup}(\sqrt{M}) = AM + B\sqrt{M} \quad (2.79)$$

with the 2 defined constants:

$$A = \frac{\tau_r - B\sqrt{M_r}}{M_r} \quad (2.80)$$

$$B = \frac{\tau_t - \tau_r \frac{M_t}{M_r}}{\sqrt{M_t} - \frac{M_t}{\sqrt{M_r}}} \quad (2.81)$$

The validity domain of a chip is then defined as :

$$\mathcal{D}_{chip} = \{(\sqrt{M}, \tau) | \tau \leq f_{sup}(\sqrt{M}) \text{ and } \tau \geq f_{inf}(\sqrt{M})\} \quad (2.82)$$

The tag offset which gives the maximum read range lies on the diagonal defined by  $Q_{opt}$  in eq. (2.75).

Notice that under the interpretation of  $d_{fwd}$  (1.12) in [41] which differs from (2.72) in the fact that it uses  $\tau_2$  instead of  $\tau$ :

$$Q_{opt}^{(2)} = Q_{opt} \left( 2 - \frac{\tau_2}{\tau} \right) \quad (2.83)$$

We will present later some illustrated examples on the chip validity domain (sec. 2.9.4).

### 2.9.1 Intersection of a constant $Q$ line and $f_{sup}$

When both impedance  $Z_1$  and  $Z_2$  of a tag are known, a point of intersection of  $Q$  and  $f_{sup}$  is  $K = (\sqrt{M_{max}}, \tau_{max})$ , where:

$$M_{max} = \frac{Q^{-1} - B}{A} \quad (2.84)$$

$$\tau_{max} = \frac{\sqrt{M_{max}}}{Q} \quad (2.85)$$

While this formula is true for any  $Q$  value, it gains particular significance when  $Q = Q_{opt}$ , defined in eq. (2.75). This specific value helps to identify the optimal point  $K$  in the validity domain in this case.

### 2.9.2 Maximizing $\tau$ in the chip validity domain

Maximizing the modulation factor, thus, the backward link budget is represented by the point  $R$  in the chart. Conversely, to maximize the mean power transmission coefficient  $\tau$ , we null the derivative of  $f_{sup}$  with respect to  $\sqrt{M}$ :

$$\frac{\partial f_{sup}}{\partial \sqrt{M}} = 0 \quad (2.86)$$

$$2A\sqrt{M} + B = 0 \quad (2.87)$$

This gives us:

$$\sqrt{M'_t} = \frac{-B}{2A} \quad (2.88)$$

$$\tau'_t = \frac{-B^2}{4A} \quad (2.89)$$

When  $\sqrt{M'_t} < \sqrt{M_r}$ , we define the point  $T' = (\frac{-B}{2A}, \frac{-B^2}{4A})$  which gives  $Z'_{at}$  that maximizes  $\tau$ . This point represents the intersection of the straight line with a slope of  $\frac{1}{Q'_t}$  with  $f_{sup}$ , where:

$$Q'_t = \frac{2}{B} \quad (2.90)$$

In cases where  $\sqrt{M'_t} \geq \sqrt{M_r}$ , we get  $T' = R = (\sqrt{M_r}, \tau_r)$  which offers the highest  $\tau$  value within the validity domain. Here,  $Q'_t = Q_r$ .

It's worth noting that, unlike  $T$ , the point  $T'$  doesn't correspond to the conjugate matching, as it is based on the mean power transmission coefficient  $\tau$  rather than the power transmission coefficient  $\tau_2$  of state 2 only.

### 2.9.3 Optimal matching of a chip

There are three cases that we should consider to decide the optimal matching of a chip by considering its validity domain by knowing  $Q_{opt}$  (2.75),  $Q_r$  (2.77) and  $Q'_t$  (2.90):

- If  $\frac{1}{Q_{opt}} > \frac{1}{Q'_t}$ : the optimal antenna impedance should maximize the forward link read range, thus maximizing  $\tau$ . In this scenario, the optimal design corresponds to  $Z'_{at}$  and is represented by the point  $T'$ .
- If  $\frac{1}{Q_{opt}} < \frac{1}{Q_r}$ : the optimal impedance is the one maximizing the backward link read range, thus, maximizing  $M$ . The ideal design in this case is  $Z_{ar}$ , represented by the point  $R$ .
- If  $\frac{\sqrt{M_r}}{\tau_r} < Q_{opt} \leq \frac{\sqrt{M'_t}}{\tau'_t}$ : the optimal design falls in between  $Z_{ar}$  and  $Z'_{at}$  and is represented by the point  $K$  (see eq. (2.85)). In this scenario, the read range is maximized at a value between the two extremes.

### 2.9.4 Optimal matching illustration with the same examples that in [41]

Table 2.2 presents an extension of the study conducted by [41] regarding the optimal matching by taking three types of chips as an example: impinj Monza 2 chip, impinj Monza X-8K chip, and impinj Monza R6-P chip. For each chip, the table presents its chip validity in the  $(\sqrt{M}, \tau)$  chart, highlighting the two points  $T$  and  $R$  representing the antenna impedances  $Z_{at}$  and  $Z_{ar}$  respectively.

Authors in [41] derived the optimal impedance based on the power transmission coefficient  $\tau_2$  in absorption state 2, which gives the blue  $Q_{opt}^{(2)}$  lines in the  $(\sqrt{M}, \tau)$  charts of table 2.2. However, we interpret the results based on the mean power transmission coefficient  $\tau$ , which gives the  $Q_{opt}$  red lines in the charts.

To note that the optimal impedance in both cases is dependent on the assumed reader sensitivity, which is set at  $S_r = -75$  dBm. Additionally, we consider  $R_{mod} = 50 \Omega$  and the transmitted power  $P_t = 30$  dBm.

In the case of Monza 2 chip, both  $\frac{1}{Q_{opt}}$  (slope of the red line) and  $\frac{1}{Q_{opt}^{(2)}}$  (slope of the blue line), are greater than  $\frac{1}{Q'_t}$  and  $\frac{1}{Q_t}$  respectively. In this case,  $Z'_{at}$  at point  $T'$ , which maximize  $\tau$ , is the optimal impedance, whereas  $Z_{at}$  is considered the optimal design in [41] and which maximize  $\tau_2$ .

As for the Monza X-8k chip,  $Q_{opt}$  and  $Q_{opt}^{(2)}$  lines fall within the zone and give nearly identical optimal impedance that, in this instance, is neither  $Z'_{at}$  nor  $Z_{ar}$  but a value in between (very close to  $Z_{ar}$  in this case).

Lastly, for the Monza R6 chip,  $\frac{1}{Q_{opt}} > \frac{1}{Q'_t}$ , while  $\frac{1}{Q_{opt}^{(2)}} > \frac{1}{Q_t}$ , leading to  $Z'_{at}$  when considering  $\tau$  and an intermediate value between  $Z_{ar}$  and  $Z_{at}$  when considering  $\tau_2$ .

In conclusion, we demonstrated the impact of considering the mean power transmission coefficient  $\tau$  when determining the optimal matching for a specific chip.

In summary, we highlighted the impact of considering the mean power transmission coefficient  $\tau$  in determining the optimal matching for a specific chip.

## 2.10 Conclusion

In this chapter we delved into the theoretical aspects of UHF RFID technology. We explored the intrinsic characteristics of UHF RFID tags, such as the mean power transmission coefficient and modulation factor. The chapter highlights the channel reciprocity in UHF RFID, which is the main key to access the intrinsic characteristics of the tag over-the-air. After defining the transmission channel  $\alpha$ , we presented the transmitted and received activation power. These two important powers led to a new quantity, the tag receptivity, which has been introduced. This quantity is independent from the distance where it is only related to the tag's characteristics: the mean power transmission coefficient and the modulation factor. Then, the  $(\sqrt{M}, \tau)$  chart has been presented, which is formed from these two characteristics. The chart reveals a visual representation for evaluating the

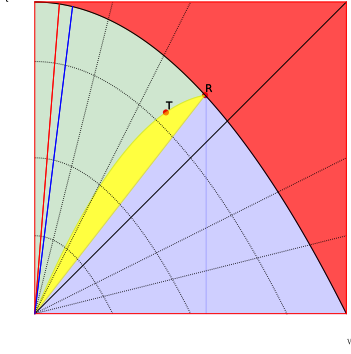
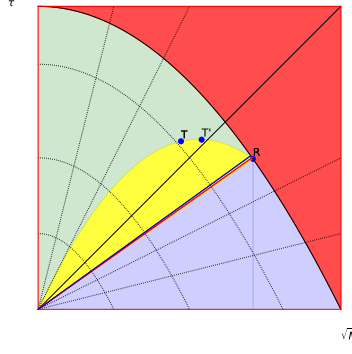
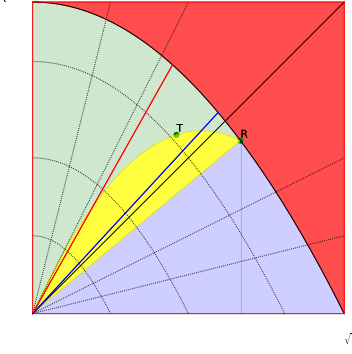
	Monza 2	Monza X-8K	Monza R6-P
$Z_{at}$	$52 + j158$	$17.8 + j172$	$16.4 + j139.5$
$Z_{ar}$	$87.0 + j777.5$	$78.2 + j125$	$61.8 + j105$
$S_{cdBm}$	-11.5	-24	-20
$T$	(0.42, 0.66)	(0.47, 0.55)	(0.46, 0.57)
$R$	(0.54, 0.7)	(0.7, 0.5)	(0.67, 0.55)
$T'$	(0.42, 0.66)	(0.53, 0.56)	(0.54, 0.58)
Chart			

Table 2.2 – Chip validity domain in  $(\sqrt{M}, \tau)$  chart for: impinj Monza 2 chip, impinj Monza X-8K chip and impinj Monza R6-P chip.

performance of UHF RFID tag. Then, an interval halving algorithm has been presented to place tags in the chart by using the mean power transmission coefficient ratio of the tags and their  $Q$  values.

Additionally, We explored the formulation of the free space read range based on the previous theory, which takes into account the limitations imposed by the forward link read range and backscatter link limitations. The forward link limitation, estimated by the Friis equation, depends on the mean power transmission coefficient and chip sensitivity. Conversely, the backscatter link limitation, estimated by the radar equation, is influenced by the modulation factor  $M$  and reader's reader sensitivity  $S_r$ . The proposed chart is then utilized to evaluate UHF RFID tags, where a known chip and antennas are combined to find the best match. We also determine, using this chart, the validity domain for a chip with the knowledge of the two states impedance  $Z_1$  and  $Z_2$  of the chip, and determined the optimal matching for a given chip in its validity domain by taking three chips as an example.

Overall, this chapter has provided a comprehensive theoretical foundation for understanding UHF RFID link budget and tag characterization, highlighting the importance of power profiles and channel reciprocity to access the intrinsic characteristics of the tag. This



chart can be used as a tool to evaluate tag performance using the proposed chart and determine the optimal impedance for a chip.

## Summary

- **Theory Development:** This chapter established a comprehensive theory regarding the link budget of UHF RFID and offered insights into tag characterization.
- **Channel Reciprocity:** The chapter highlighted the importance of channel reciprocity in UHF RFID and delved into specific details of channel coefficient characterization in free space. This reciprocity concept is a key to access the mean power transmission coefficient  $\tau$  and modulation factor  $M$ .
- **Activation Power Analysis:** It explored the transmitted activation power  $P_t^{th}$ , representing the minimum power required to activate the RFID tag, and the received activation power  $P_r^{th}$ , which measures the power received at the transmitted activation power level. These two profiles are the key to access the intrinsic characteristics of the tag.
- **Tag Receptivity:** This chapter also introduced the concept of tag receptivity, a factor closely linked to the intrinsic characteristics of the tag denoted by  $\tau$  and  $M$ . It is obtained by compensation of channel by averaging the transmitted and received activation profiles in dBm scale:

$$R_{dB}^{th} = \frac{P_t^{th}{}_{dB} + P_r^{th}{}_{dB}}{2}$$

The tag receptivity is related to the chip sensitivity  $S_c$  by quantity called the  $Q^{th}$  factor:

$$R_{dB}^{th} = S_{c,dB} + Q^{th}$$

- **$(\sqrt{M}, \tau)$  Chart:** The chapter introduced the  $(\sqrt{M}, \tau)$  chart, a valuable tool for characterizing UHF RFID tags. It is formed from the mean power coefficient and the modulation factor, thus a tag can be evaluated based on these two characteristics and the equilibrium between them. This chart is associated with an algorithm, introduced in this chapter, to place the tags in the chart. Hence, this chart aids in the evaluation and comparison of various UHF RFID tags, offering a way for optimizing the tag design.

- **Chip validity domain and optimal matching:** This chapter focuses on utilizing the chart to determine the chip's validity domain. Essentially, this domain ensures that the tag, regardless of the chosen antenna impedance, remains within this validity domain. The boundaries of this zone are defined by the two-state impedance of the chip. This validity domain has been used to determine the optimal matching of the considered chip.



# EXPERIMENTAL CHARACTERIZATION OF UHF RFID TAGS

---

## 3.1 Introduction

In this thesis the IETR RFID characterization platform was initially exploited and programmed to do experimentation on UHF RFID tags. Initially, the primary objective of these experiments was to explore various measurement scenarios based on the need of CAA-Connect project. This exploration started with the measurement of the RSSI of a moving tag along a rail in translation, and in rotation. To enhance the accuracy of the received signal's power representation, the first objective was to convert the RSSI of Alien reader to a real power quantity in dBm since this conversion is not provided by the manufacturer.

As the experiments progressed, they harmoniously evolved alongside the refinement of the theoretical framework discussed in the preceding chapter. This evolution was instrumental in the gradual acquisition of a well-defined power profiles for a tag. Initially, we recorded three distinct power profiles that we converted to *dBm*: the activation profile, the received profile at maximum transmitted power, and the received profile at the activation power. The revelation of the activation profiles appeared to be a crucial step, offering insight into the intrinsic characteristics of the tag itself. The intrinsic characteristics, denoted as the mean power transmission coefficient  $\tau$  and the modulation factor  $M$ , as introduced in chapter 2, were empirically derived through a multi-step experimental process. Initially, this involved compensating for the reciprocal transmission channel, represented by  $\alpha$ , which in turn yielded to a constant value: the tag receptivity  $R$  which appears to be the chip sensitivity shifted by the tag offset value  $Q$ . This factor is related to the  $\sqrt{M}$  and  $\tau$  as we have seen in Sec. 2.6. Subsequently, based on the exploitation of the activation profiles and the tag offset, we applied the algorithm to extract the characteristics  $\tau$  and  $M$ . The empirical

acquisition of these characteristics, explained in the previous chapter, can then be used to present a tag in the characterization chart  $(\sqrt{M}, \tau)$ . This chart will be used as a valuable comparative characteristics tool.

The chapter begins by discussing the acquisition of RSSI data, considering both translation and rotation scenarios. We then explore the process of converting RSSI to received power units (dBm), which is crucial for accurately representing the power profiles of the tags.

Next, we proceed with the evaluation and comparison of the performance of a set of 9 commercial tags by extracting their power profiles and interpreting them.

Furthermore, we examine the distribution of the tag receptivity error, which allows us to assess the consistency and reliability of the performance evaluation. By understanding the variations in tag receptivity, we can better comprehend their performance characteristics.

To effectively present and compare the performance of the tags, we employ the algorithm presented in Sec. 2.7.5.2 to position nine measured tags in the  $(\sqrt{M}, \tau)$  chart. This chart provides a visual representation of the tag's performance and read range, facilitating a comprehensive understanding of their performances.

We then investigate the impact of varying the incident power ( $P_{inc}$ ) on the mean power transmission coefficient  $\tau$  and the modulation factor.

Finally, we present an experimental setup that utilizes a collection of 39 UHF RFID tags to scan the propagation channel environment. Through an analysis of the power profiles of these 39 tags, which are strategically positioned in a linear array and moved along a rail, this study demonstrates the ability to characterize the propagation channel.

Through this experimental characterization of RFID tags, we aim to provide valuable insights into their performances. By comparing different type of tags and studying their intrinsic characteristics, we contribute to a better understanding of the UHF RFID tag behavior.

## **3.2 RSSI acquisition in translation and rotation**

To begin, the IETR platform introduced in Sec. 1.5 is programmed and used to deliver an autonomous experiments in both translation and rotation scenarios. In this section, the platform's degree of freedom in translation and rotation will be presented. The initial reader utilized to conduct the experiments is the alien reader 9900+ presented in Sec. 1.5.1.

### 3.2.1 Translation acquisition

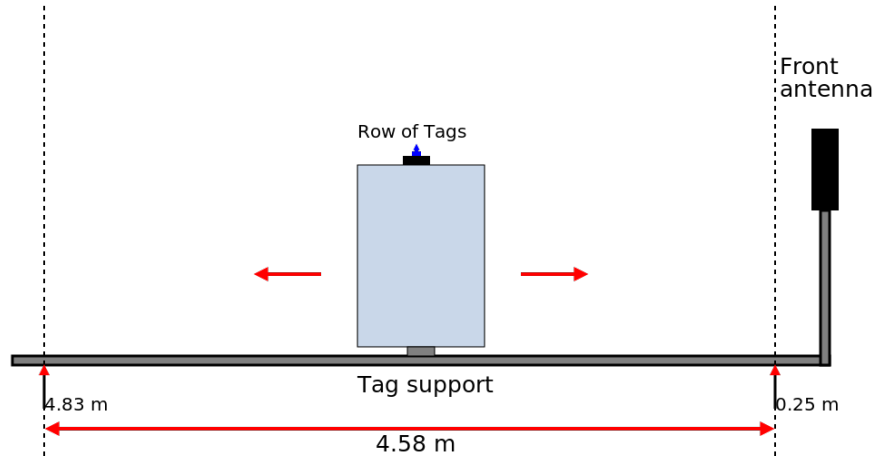


Figure 3.1 – Tag translation on the RFID platform represented in plane (X,Z)

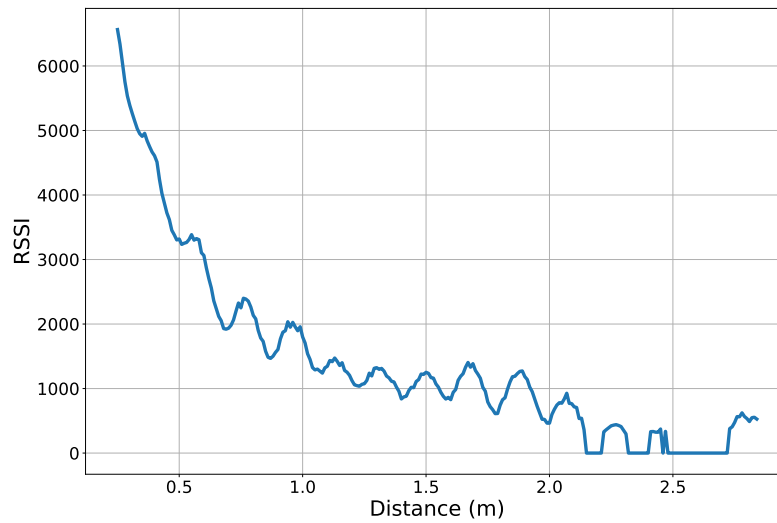


Figure 3.2 – Variation of RSSI w.r.t distance (m) between tag and antenna

The initial experiment on the platform involved tracking the translation of an NXP Ucode8 tag. We positioned the tag in front of the fixed antenna, as illustrated in Fig. 3.1 in Sec. 1.5, and systematically moved it away from the antenna in  $50\text{mm}$  increments, covering distances from  $0.25\text{m}$  to  $2.86\text{m}$ . The resulting RSSI (Received Signal Strength Indicator)

values, obtained from the alien reader, are presented in Fig. 3.2. These RSSI measurements were taken while maintaining a constant transmitted power of  $P_t = 30.2dBm$ . As expected, the RSSI gradually decreased with increasing distance, indicating a weakening signal strength. However, it's essential to note occasional unexpected drops in RSSI, attributed to environmental factors such as multipath and reverberation effects, which introduce interference and affect received power. It's worth highlighting that all RSSI values are positive, where a value of 0 signifies a no-detection scenario. This variation will be further investigated in the upcoming section to quantify the RSSI in terms of received power.

### 3.2.2 Rotation acquisition

The second experiment is the rotation acquisition on a dogbone tag [55] based on monza 4 chip [56]. This tag was used for rotation acquisition as it has a bidirectional antenna. We placed the tag in the middle of the platform under the portal, and the acquisition was made by the left antenna (we can similarly choose the right antenna), as shown in Fig. 3.3 in planes (Y,Z). The tag is then rotated in  $5^\circ$  increments, covering a full  $360^\circ$  rotation. At each angle, the RSSI value is measured, capturing the fluctuation of RSSI as the angle between the tag and the antenna changes. These results are presented in Fig. 3.4. The experiment utilizes a transmitted power of  $P_t = 30.6dBm$ . We can see that the dogbone Monza 4 tag, described in [55], has a directional antenna. The maximum RSSI value is achieved around  $180^\circ$ , while the minimum RSSI values are observed between  $90^\circ$  and  $270^\circ$ . These findings suggest that the tag's antenna is oriented in a specific direction, resulting in varying signal strengths based on the angle of rotation.

## 3.3 RSSI to received power conversion

The purpose of this section is to present an use case of an experimental RFID platform which can be applied to address the problem of converting the reader integer RSSI value to an actual power value we propose in this section to exploit 2 different distance profiles : the activation profile and the received profile at maximum transmitted power. The proposed expression is consistent with the multi-tags characterization using two different readers (including Alien 9900+) presented in [4] and has been adjusted by enforcing the channel reciprocity (exactly the same channel for the forward and backward link).

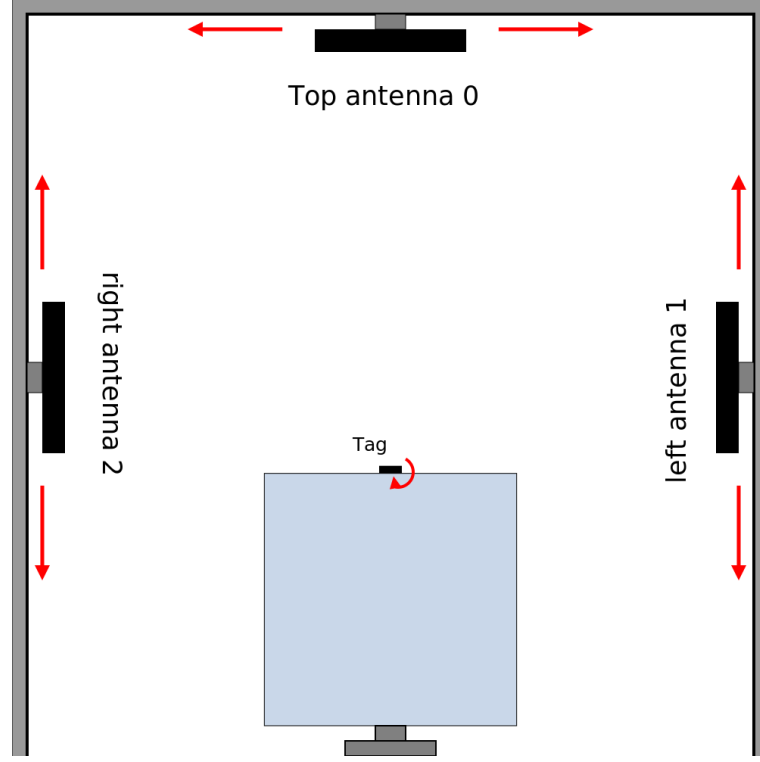


Figure 3.3 – Tag rotation on the RFID platform represented in plane (Y,Z)

### 3.3.1 Measured power profiles

Our experimental scenario involves jointly varying the power and distance in order to access the power profiles that are illustrated in the theory presented in chapter 2. The used UHF tag for converting the Alien RSSI quantity is based on a Monza R6 IC [57] which has a chip read sensitivity of  $S_c = -22 \text{ dBm}$ . To carry this out, for each tag position along the rail, the transmitted power has been swept over the defined range from  $15.7 \text{ dBm}$  to  $30.6 \text{ dBm}$ . This gives us  $\text{RSSI}(P_t, d)$ , the Alien RSSI for each distance  $d$  and each transmitted power  $P_t$ .

We obtain 3 power profiles presented in Fig 3.5:

- The transmitted activation profile is noted  $P_{tdB}^{th}(d)$  obtained in  $\text{dBm}$ , it corresponds to the minimum transmitted power required to observe a tag response. This profile is an increasing function of distance. It can be obtained from the measurement matrix  $\text{RSSI}(P_t, d)$  by extracting the boundary (green line) between the responding and non-responding tag regions (dark blue region).
- The RSSI max profile is defined as the RSSI obtained at maximum transmitted power



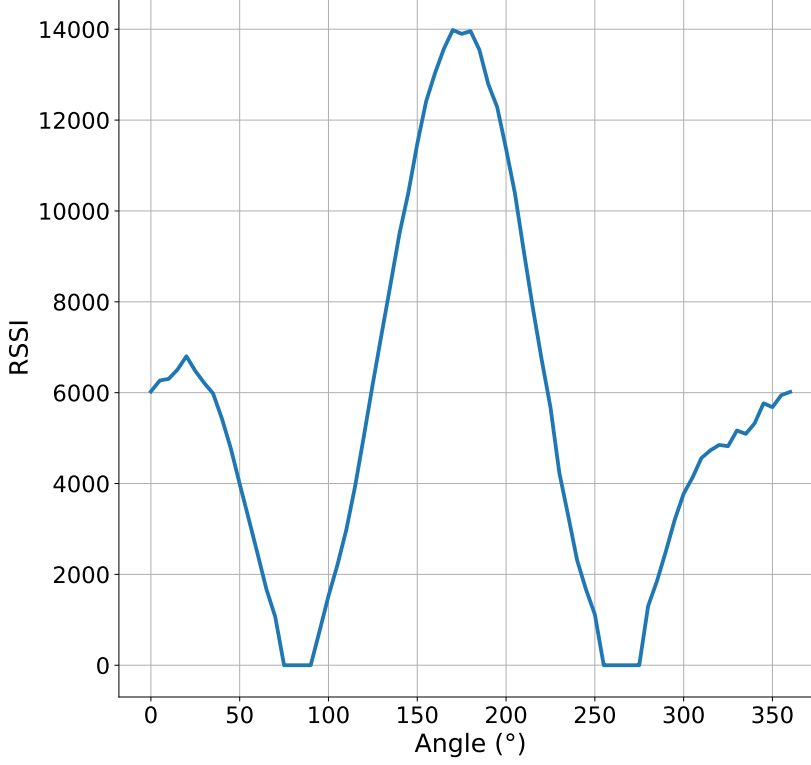


Figure 3.4 – Variation of RSSI w.r.t rotation angle of the tag support

$$P_t^{max} = 30.2dBm.$$

$$RSSI^{max}(d) = \mathbf{RSSI}(P_t = P_t^{max}, d) \quad (3.1)$$

This profile is a decreasing function of distance. After converting the RSSI into dBm using the conversion formula detailed in Subsec. 3.3.2, this profile transforms into  $P_{rdB}^{max}(P_t = P_t^{max}, d)$ .

- The RSSI threshold profile is defined as the RSSI obtained at the transmitted activation power.

$$RSSI^{th}(d) = \mathbf{RSSI}(P_t = P_t^{th}, d) \quad (3.2)$$

This profile is a decreasing function of distance. After power conversion this profile becomes  $P_r^{th}(d)$ . Generally,  $RSSI^{th}(d) \leq RSSI^{max}(d)$  or equivalently  $P_r^{th}(d) \leq$

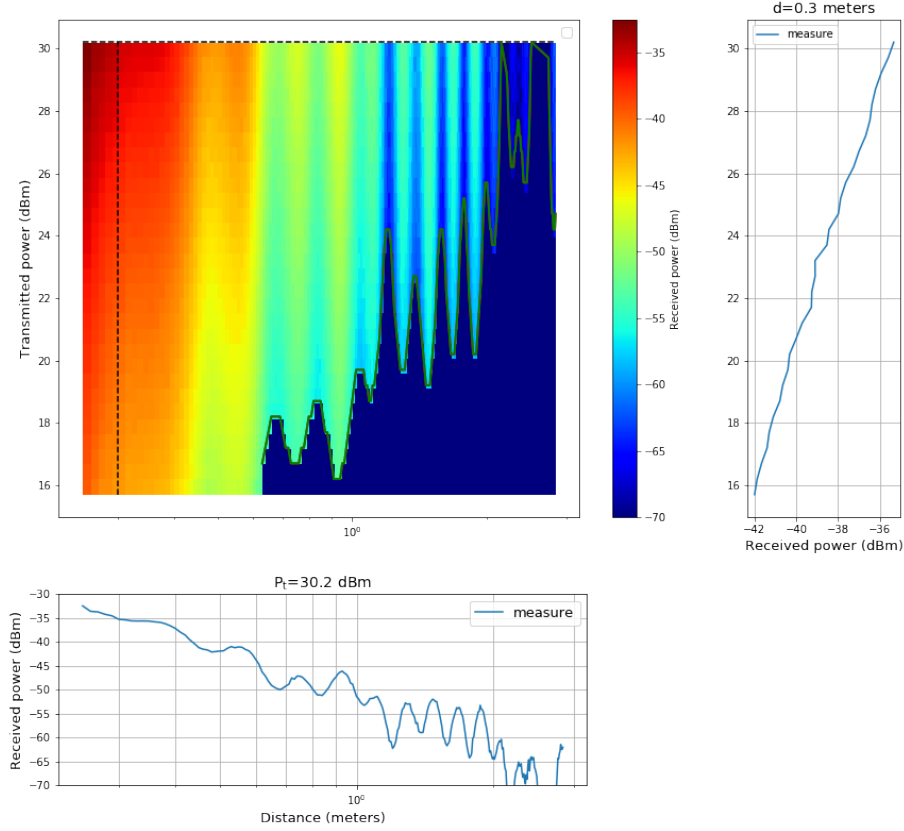


Figure 3.5 – Received level after conversion  $f(\text{RSSI}(d, P_t))$  upper left corner, cut @  $d = 0.3 \text{ m}$  (right), max power profile (cut @  $P_t = 30.2 \text{ dBm}$ ) (bottom)

$P_{r_{dB}}^{max}(d)$ , but it is not always the case, as we will see in the experiments results later.

### 3.3.2 RSSI to $\text{dBm}$ conversion formula

In this study, our primary objective is to establish a reliable conversion formula for RSSI (Received Signal Strength Indicator) for the alien reader 9900+. The RSSI provides crucial information about the received signal strength, and a conversion formula allows us to relate RSSI values to the received power in  $\text{dBm}$ .

To achieve this, we conducted an extensive analysis of the RSSI variation function. For this purpose, we collected multi-tags characterization data using two different RFID readers, including the Alien 9900+ model, as presented in the study by Chawla et al. [4]. By relying on this study and the power profiles that we obtained experimentally, the variation function is then found to be of logarithmic nature. The conversion expression we propose is as

follows:

$$P_r \text{ dBm} = f(RSSI) = a \log_{10}(RSSI) + b \quad (3.3)$$

### 3.3.2.1 Determination of $a$

The critical parameter  $a$  needs to be accurately determined for the formula. We made use of the concept of channel reciprocity in RFID tag-reader communication. By knowing the profile of transmitted power ( $P_t^{th}$ ) in dBm, we expected a corresponding variation for the received power ( $P_r^{th} = f(RSSI^{th})$ ) but with an opposite sign. To obtain the correct value of  $a$ , compensating for the channel characteristics, we searched for the value that would result in a constant sum of  $P_t^{th}$  and  $P_r^{th}$  over varying distances. After careful analysis,

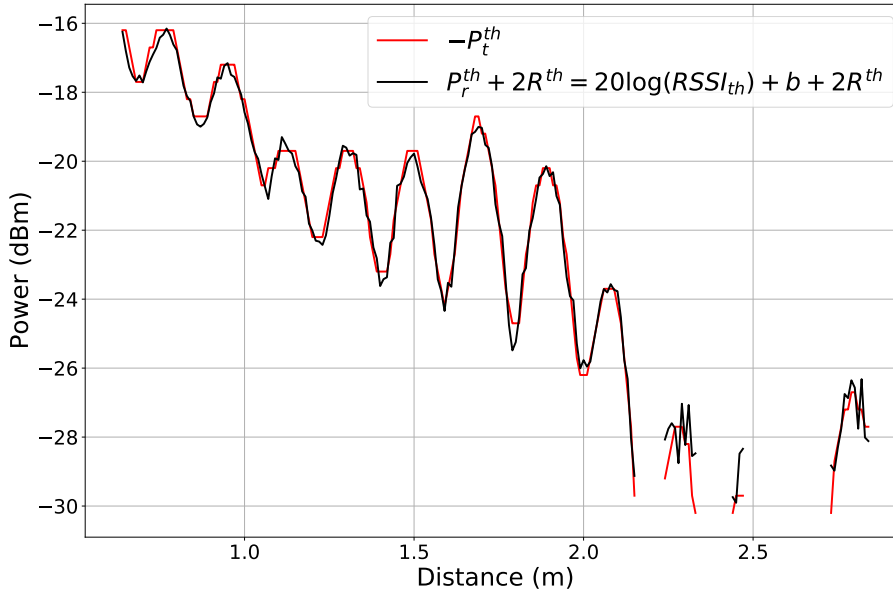


Figure 3.6 – Superposing the two curves  $P_t^{th}$  and  $P_r^{th}$  under the concept of channel reciprocity

we found that  $a = 20$  achieved the desired compensation, as visually represented in Fig. 3.6 where  $-P_t^{th}$  and  $P_r^{th} + 2R^{th}$  overlapped at this value. This observation is a posteriori obvious and simply means that the RSSI of the reader is a quantity proportional to the

received voltage. This observation increases strongly the confidence in this part of the conversion formula. And the only remaining value to determine to transform the Alien reader into a reliable powermeter is to determine the remaining offset  $b$ . Noting that  $R^{th}$  is the tag receptivity defined in eq. (2.56). The offset  $b$  is composed of the reader offset and the reader receptivity.

### 3.3.2.2 Determination of $b$

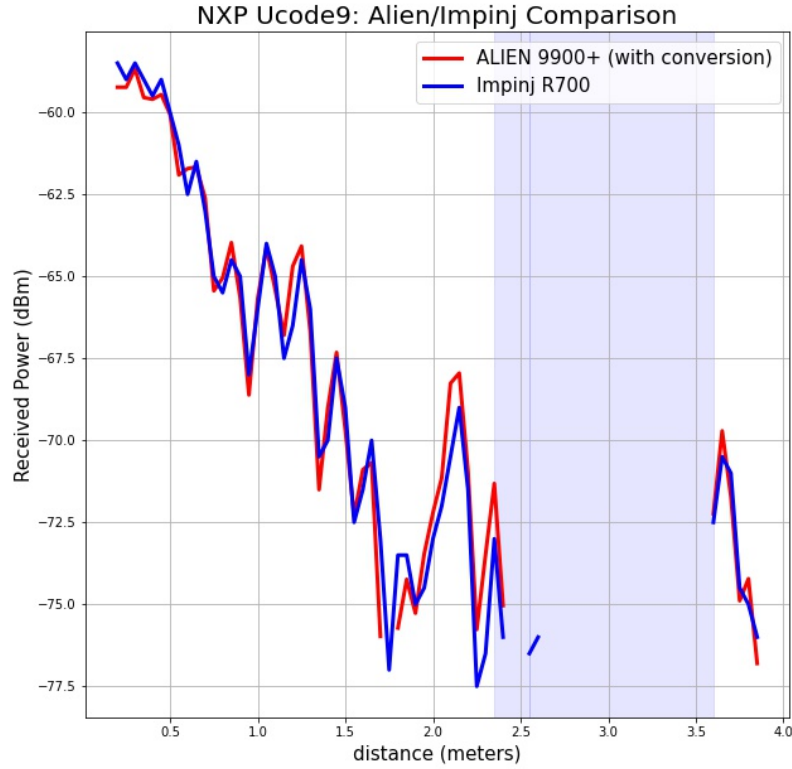


Figure 3.7 – Comparison of received power obtained directly (Impinj R700 blue curve) or indirectly using 3.3.2 (Alien 9000+ red curve)

To determine  $b$  of the conversion formula derived for the Alien 9900+ reader, an additional experiment was conducted using the impinj R700 reader, a more recent model that provides actual received power in  $dBm$ . Both experiments involved acquiring tag range under identical conditions using the same tag based on NXP-Ucode9 chip [58]. The results of

the experiments are presented in Fig. 3.7, where the red curve denotes the received power obtained indirectly by applying the conversion of the received signal strength indicator (RSSI) delivered by the Alien reader. The value  $b$  is obtained by fitting this curve to the blue curve which represents the received power obtained directly in  $dBm$  by the impinj R700. The results demonstrate a remarkable level of consistency between the two readers, thereby confirming the proposed conversion formula's validity at  $b = -128$ . The proposed formula is then presented as follows:

$$P_{rdBm} = f(RSSI) = 20 \log_{10}(RSSI) - 128 \quad (3.4)$$

Thanks to the proposed conversion expression above, raw RSSI translates to the measured received power matrix:

$$\mathbf{P}_{rdBm}(P_t, d) = f(\mathbf{RSSI}(P_t, d)) \quad (3.5)$$

To conclude, we have introduced a conversion formula that translates the Alien reader RSSI into a  $dBm$  measurement. This formula will be consistently applied to all subsequent data acquisitions to derive the received profiles in  $dBm$ .

### 3.4 Evaluation and comparison of the performance of a set of tags

After converting the RSSI to  $dBm$ , a set of commercial tags have been selected in order to compare their performances as per the previously explained theory in chapter 2, by firstly measuring their power profiles by a power-distance variation measurements, and then placing the tags in the  $(\sqrt{M}, \tau)$  chart using the information extracted from the experimental acquisitions.

Table 3.1 displays the features of the selected tags, including their size in  $mm^2$ , chip type, typical sensitivity  $S_c$ , and calculated tag receptivity  $R^{th}$ . Some of the tags have the same IC chip but different antennas. The tag receptivity was calculated, while the typical IC sensitivity was obtained from the chip datasheets. The process of determining  $R^{th}$  from power profiles will be covered later.










Geometry	Tag Name	Size ( $mm^2$ )	Chip Name	$S_{cdBm}$	$R^{th}_{dBm}$
	Dogbone	86 x 24	Monza 4 [56]	-17.4	-18.2
	H47	44 x 44	Monza 4	-17.4	-19.59
	UPMWEB	30 x 49	Monza 4	-17.4	-18.73
	AD550	41 x 79	Monza 5 [59]	-17.8	-19.76
	AD318	41.4 x 16	Monza 5	-17.8	-22.45
	AD233	70 x 14.5	Monza 5	-17.8	-22.66
	Alien	94.8 x 8.1	Higgs 3 [60]	-18	-20.46
	AD661	90 x 19	Monza R6 [57]	-22.1	-24.21
	AD806	16 x 16	NXP Ucode7 [61]	-21	-22.98

Table 3.1 – Characteristics of a collection of commercial tags

### 3.4.1 Measured power profiles in $dBm$

In this subsection we present the power profiles in  $dBm$  by following similar steps as in 3.3.1. Firstly, the tag is translated on the central rail from a distance between tag and antenna of  $0.25\text{ m}$  to  $4.83\text{ m}$  over a full range of  $L_{max} = 4.58\text{ m}$ . The selected channel is centred on  $866.3\text{ MHz}$ . For each position of the tag along the rail, we systematically vary the transmitted power from  $15.7\text{ dBm}$  to  $30.5\text{ dBm}$ , incrementing it in steps of  $0.1\text{ dBm}$ , similarly to the previous experimentation. This process yields the  $P_{rdB}(P_t, d)$  profile. This profile has been obtained by converting the Alien RSSI, at each distance  $d$  and for each transmitted power  $P_t$ , into a real power quantity in  $dBm$  using the conversion formula (3.4) that we proposed.

Three power profiles have been illustrated:

- The received power at maximum transmitted power  $P_{rdB}(P_t = P_t^{max}, d)$ . This profile is a decreasing function of distance.
- The activation profile  $P_{tdB}^{th}(d)$  defined in (2.30) and presented in subSec. 3.3.1.
- The received activation profile  $P_{rdB}^{th}$  as defined in equation (2.38) and presented in subSec. It typically represents the minimum level of received power that can be achieved.

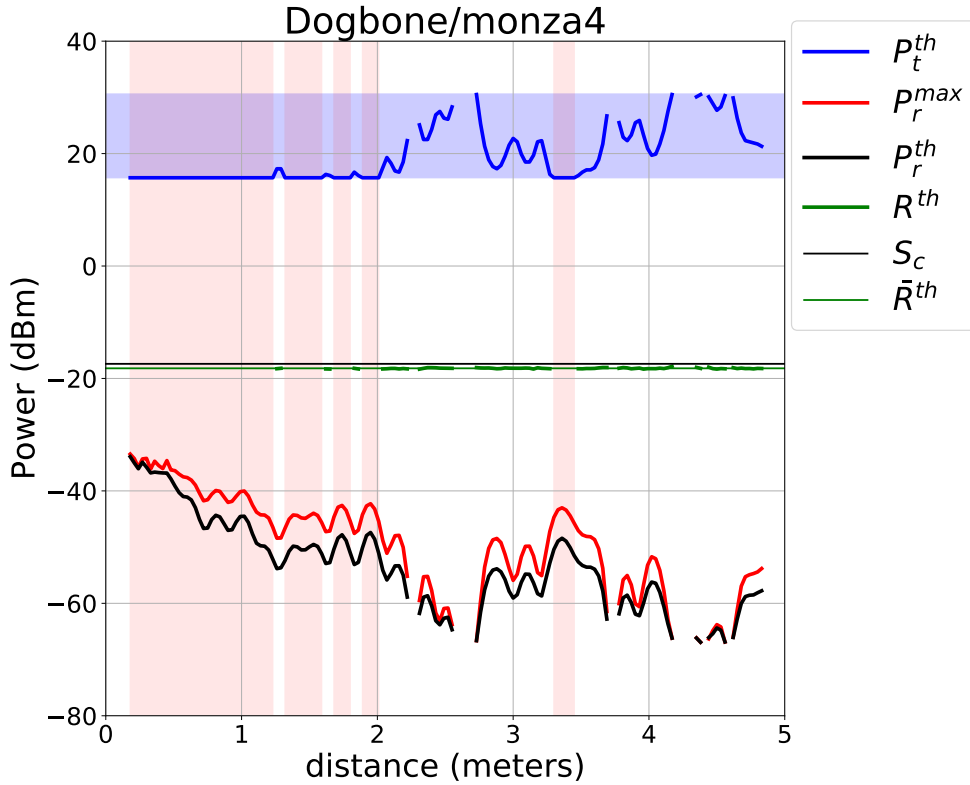


Figure 3.8 – Power profile representation in translation of the dogbone/Monza 4 tag

Fig. 3.8 presents the acquisition of these power profiles for the Monza 4 Dogbone tag, the first tag listed in Table 3.1. The Dogbone’s chip sensitivity,  $S_c = -17.4dBm$ , is represented by an horizontal thin black line. The blue line corresponds to the activation profile and is lying in the shaded blue region between the minimum ( $P_t^{min} = 15.7dBm$ ) and maximum ( $P_t^{max} = 30.5dBm$ ) transmitted power from the Alien 9900+ reader. The red line corresponds to the received power profile at the maximum transmitted power ( $P_t^{max} = 30.5dBm$ ). The black thick line represents the received activation profile, obtained from the tag responding at the threshold power. It appears to exhibit a mirroring

variation with the transmitted activation profile, due to the reciprocity of the channel. Hence, the tag receptivity  $R^{th}$  represented by a thick green line, is derived from these two activation profiles, and calculated at each distance using the equation (2.56). A nearly perfect horizontal line is obtained using this formula, as the effect of the fading channel has been nearly compensated by combining the two profiles. This compensation is grounded in the principle of channel reciprocity, leading to an evaluation of the tag sensitivity, which is independent from the distance and which depends solely on the tag's design. As a result, the mean of tag receptivity ( $\bar{R}^{th}$ ) can be calculated and is represented by an horizontal thin green line. The shift between the mean tag receptivity and the chip sensitivity is given by  $Q^{th}$ .

The red region represents the zone where the transmitted and received activation profiles cannot be obtained since it is not possible for the Alien reader to go below the minimum transmission power of  $P_t^{min} = 15.7dBm$ . It is important to note that, in this region, the received power activation profile in black is also obtained from the transmission power of  $P_t^{min} = 15.7dBm$ , and not from the actual activation power of the tag (which is lower than  $15.7dBm$ ). Thus, the blue plot in this region is constant at  $P_t^{min}$  and the black plot corresponds to the received power at  $P_t^{min}$ . For that reason, the tag receptivity is only evaluated in the complementary region, where the actual activation power is available.

We observe an interruption of the tag response at specific range values, particularly between 2 and 3 meters. This is because even with the maximum transmitted power  $P_t^{max}$ , the tag fails to activate, which results from the strong fading in this area, specifically, in the gantry area.

The angular measure of the Dogbone Monza 4 tag was determined in an experiment where the tag was placed at the center of a platform and the left antenna (see Fig. 3.3) was used for acquisition. The tag was rotated from 0 to 360° with a 5° step and the transmitted power was swept over a range from 15.7 dBm to 30.5 dBm with a 0.1 dBm step. This allowed for the acquisition of the activation power profiles and the maximum received power in an angular form, presented in Fig. 3.9. The results show a dipole antenna symmetry with a gap in communication at 90° and 270°. The red zone represents the region where the tag was activated at the minimum power of  $15.7dBm$ , thus the activation profiles cannot be obtained. In addition, the blue zone represents the angular positions where the tag has not been detected. Whereas outside of these two zones, the activation profiles are presented, therefore, the tag receptivity  $R^{th}$  was obtained and represented in green. The  $R^{th}$  value was found to be almost constant close to the chip sensitivity  $S_c$  and of value  $-18.9 dBm$



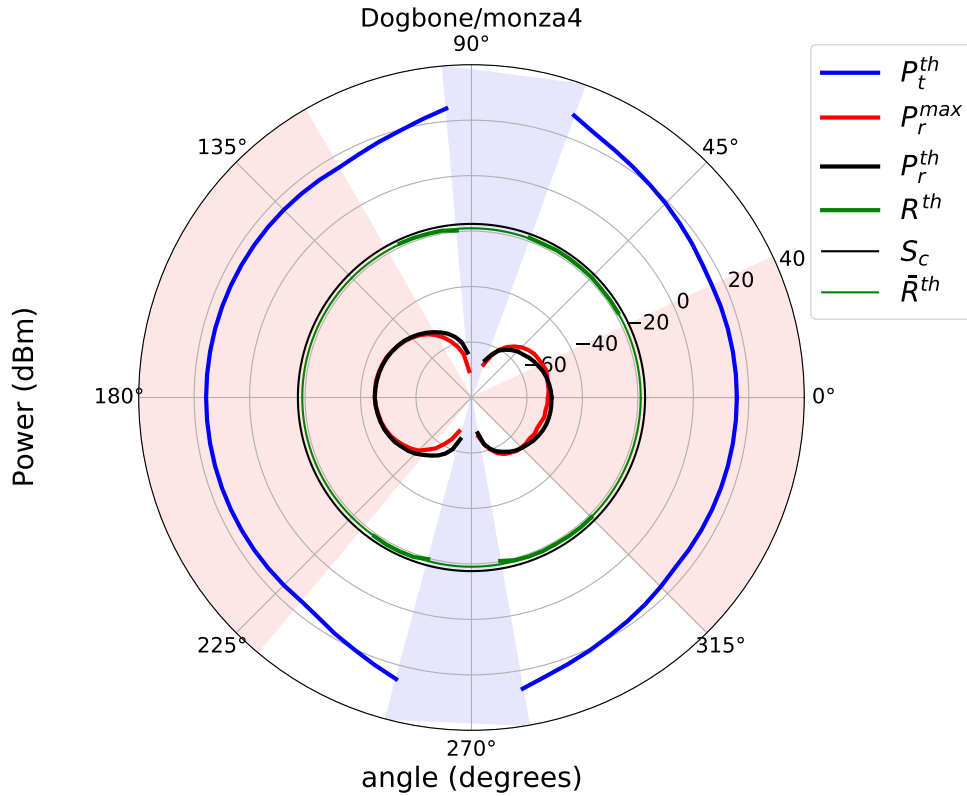


Figure 3.9 – Power profile representation in rotation of the dogbone/Monza 4 tag

quasi-equal to the value obtained from translation. To conclude, whether it is a translation or rotation, a specific characteristic of the tag can be obtained by acquiring the activation profiles, which is the tag receptivity  $R^{th}$ .

### 3.4.2 Comparison of tags using the power-distance profiles

The same experiments were conducted on all 9 tags described in table 3.1 under identical conditions to ensure that the resulting profiles could be compared.

Fig. 3.10 illustrates the profiles acquired for these tags, with the data arranged in the following manner:

- The first row displays three Monza 4 tags with different antennas.
- The second row displays three Monza 5 tags with different antennas.
- The third row displays tags with different chips and different antennas.

For each tag, a subplot presents the 3 profiles, the chip sensitivity and the tag receptivity (given in table 3.1) presented with the same color conventions.

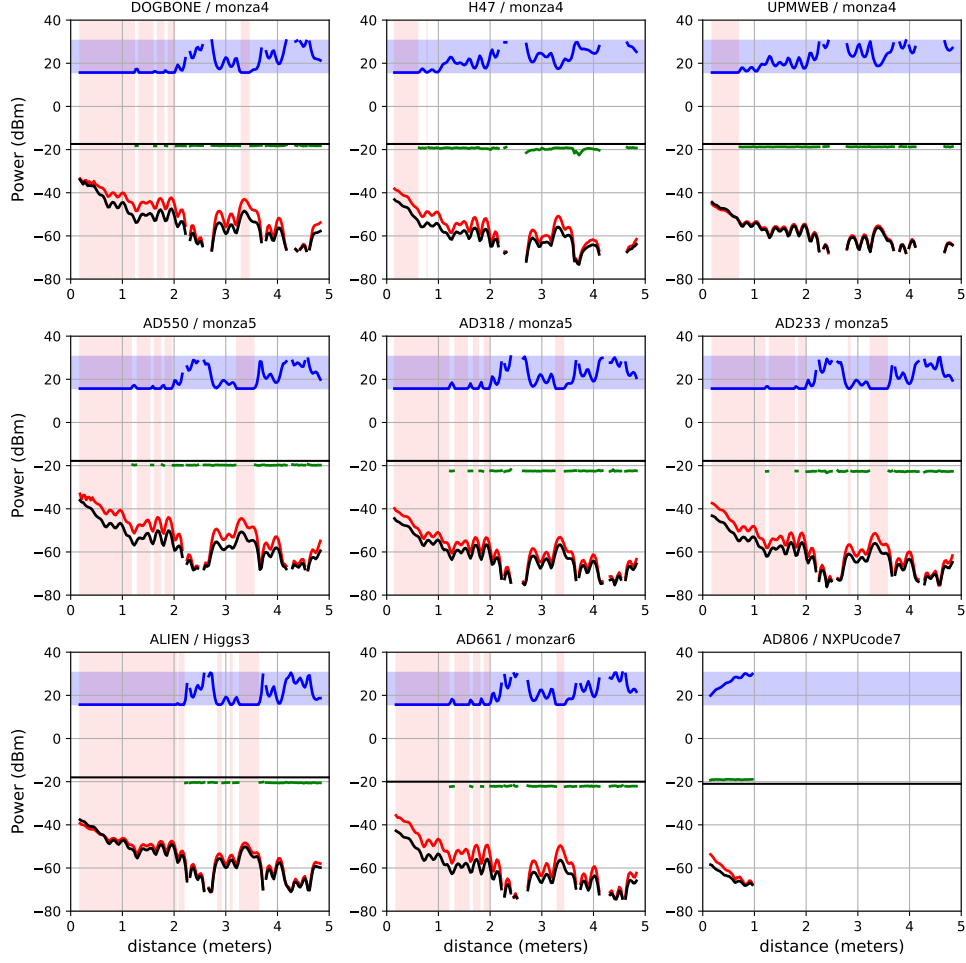


Figure 3.10 – Power profile diagram for 9 different tags : in red  $P_r^{max}(d)$ , in black  $P_r^{th}(d)$ , in blue  $P_t^{th}(d)$ , in green  $R$

Across all measured tags, we consistently observe a nearly flat and stable behavior denoted in green, signifying a high level of reliability in the reported  $Q_{dB}^{th}$  values listed in Table 3.1. A closer examination of the six graphs reveals that the disparity between chip sensitivities and tag receptivities varies significantly from one tag to another, primarily due to differences in their designs, even when the chips are identical (i.e. Monza 4 with the 3 observed values of  $Q^{th}$  :  $-0.8\text{ dB}$ ,  $-2.19\text{ dB}$ ,  $-1.33\text{ dB}$ ).

When looking at the last row of the figure from left to right comes first the Alien tag which seems to be the best since it has the fewest non-detection gaps, then the AD661 which has an almost equal value for chip sensitivity and tag receptivity ( $Q^{th} = -0.01\text{ dB}$ ),

then comes the tag with the clearly worst performance the AD806 with chip NXP Ucode 7 (right bottom). Its read range is 1 meter only, despite having a good chip sensitivity ( $S_c = -21 \text{ dBm}$ ) compared to the other tags. This behavior is attributed to the tag's small antenna size (as shown in table 3.1), since the antenna size has a great impact on performance as shown in [62]. In addition, it is designed to work on a dielectric surface (such as liquid-filled glass) and not in the air [63].

### 3.4.3 Distribution of the tag receptivity error

In the following we focus on the estimation error that may appear on the values of  $Q_{dB}^{th}$  in equation (2.57). This is mostly due to the variability of the measured values of  $R^{th}$ . Fig. 3.11 shows the distribution of the error

$$\epsilon_{R^{th}} = R^{th} - \bar{R}^{th} \quad (3.6)$$

obtained by aggregating the data from the 9 measured tags (973 points). The data gathered from each tag made of the  $R$  calculated at every step outside of the red zone where the activation profile is not provided.

The distribution of errors exhibits a generally symmetric shape, with the interquartile range measuring  $0.156 \text{ dBm}$ . Notably, the majority of error values are concentrated between the first quartile,  $Q_1 = -0.08 \text{ dB}$ , and the third quartile,  $Q_3 = -0.071 \text{ dB}$ . It's important to mention that the presence of outliers in the data does not exert a significant influence on the overall estimation of  $R^{th}$ , which is primarily determined by its mean value, denoted as  $\bar{R}^{th}$ .

This analysis underscores the high accuracy of our proposed method, a characteristic that can be largely attributed to its exploitation of channel reciprocity.

### 3.4.4 Placing the 9 tags in the $(\sqrt{M}, \tau)$ chart

The proposed chart introduced in 2.2 is then exploited to study the performance of the 9 measured tags. By positioning the tags in the chart the algorithm (1), their relative performances can be compared.

The  $Q^{th}$  values are obtained for the 9 tags using equation (2.57) and gathered in vector  $Q$ . Additionally, the sequence of ratios  $t$ , defined in (2.71), is obtained by calculating the shift between the activation profiles of each sequential pair of tags as explained in 2.7.5.1.

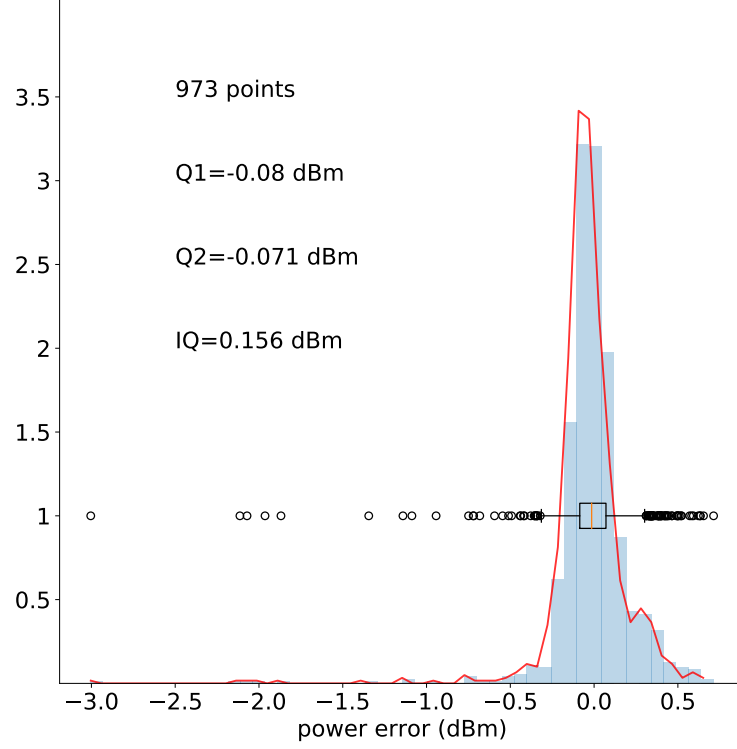


Figure 3.11 – Distribution of the tag receptivity error resolution  $\epsilon_{R^{th}}$  obtained from the 9 measured tag profiles

This is legitimate because the tags were measured in the same position and channel (see 2.7.5.1).

Fig. 3.12 illustrates two profiles: the transmitted activation profile of the AD318 tag and the transmitted activation profile of the AD233 tag, with an offset eq. (2.67) related to the ratio of  $\tau$ . In the case of these two tags the offset is the ratio of  $\tau$  itself as they have both the same sensitivity (see eq. (2.68)), we obtain an offset of 1.63 dB or 1.456 in linear. As we can see, the two profiles are superposed, confirming that the channel remains consistent for both tags and, thus, the ratio  $t$  is a reliable quantity that describes the  $\tau$  ratio between the tags.

Using  $Q$  and  $t$ , the algorithm (1) described in Sec. 2.7.5.2 is used to obtain the values of  $\tau$   $M$ , thus place the tags on the chart and their relative performances can be compared.

The results in Fig. 3.13 presents two charts obtained with two different constraints.

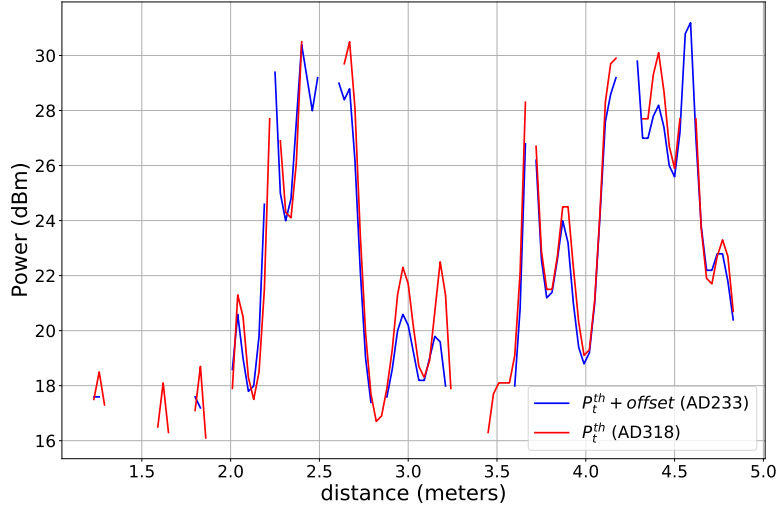


Figure 3.12 – Comparison between  $P_t^{th}$  of AD318 tag with  $P_t^{th} + offset$  of AD233 tag

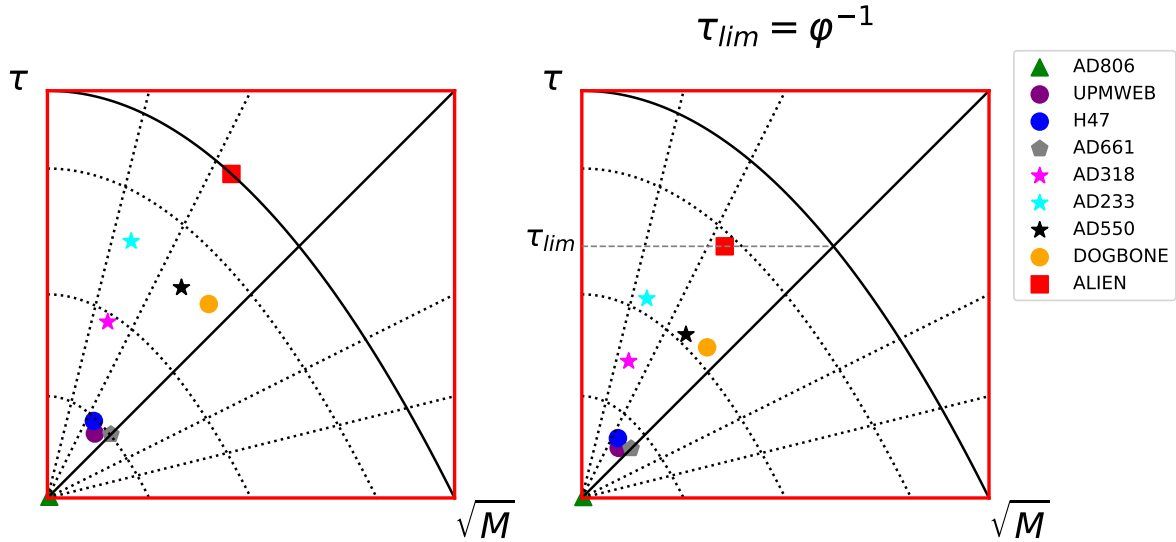


Figure 3.13 – Proposed chart on a set of tags. On the left: One condition (cond1) applied on the boundary ( $\tau = 1 - M$ ). On the right: Two conditions applied, cond1 and an arbitrary limitation on the value of  $\tau$ , here  $\tau_{lim} = \varphi^{-1}$

The first chart on the left enforces that the tag cannot be placed in the impossible zone (only cond1 is applied in algorithm 1).

The second chart on the right assumes, in addition, that  $\tau$  cannot go over  $\tau_{lim}$  (cond1 and cond2 are applied in algorithm 1). In this case,  $\tau_{lim} = \varphi^{-1}$ . This limitation is chosen heuristically as it may be unrealistic to assume a design with a higher  $\tau$  value, as it is the case for the Alien tag (red square) in the first chart (left). It is unclear, what is the best possible choice for  $\tau_{lim}$  in order to access to the more realistic value of  $\tau$  and  $M$ . The ordering of the tags in terms of both  $\tau$  and  $M$  remains unchanged in both charts, however, the placement of the tags has shifted downwards when adding the limitation on  $\tau$  in the second chart, while maintaining the same  $Q$  and  $t$ .

### 3.4.5 Monza 4 chip validity in the $(\sqrt{M}, \tau)$ chart

After placing the tags in the chart, our objective is to assess the placement accuracy of these tags within the chip's validity explained in Sec. 2.9. We have chose the Monza 4 chip, for which we have measured three distinct tags: the Dogbone, UPMWEB, and H47 tags.

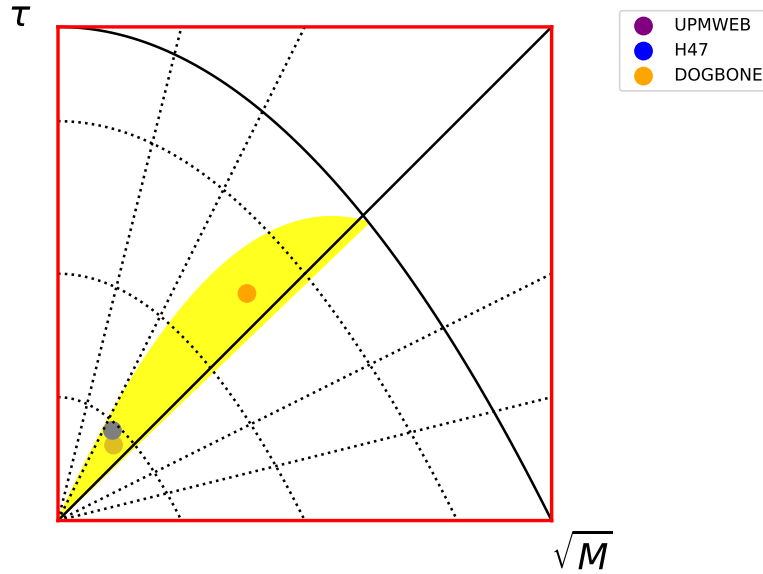


Figure 3.14 – Chart representation of the chip zone validity for the three measured Monza 4 tags

To illustrate the validity of the Monza 4 chip, we have supposed a nominal value of  $R_{mod} = 90 \Omega$  (defined in eq. 2.1). This value has been chosen heuristically as for the tag to be inside the validity zone. Consequently, the valid zone is defined by the curve  $f_{sup}$  (2.79) and the line  $f_{inf}$  (2.78), which are visually represented in Fig. 3.14.

Upon examination of the figure, it becomes evident that all three Monza 4 tags fall within this validity zone when choosing  $R_{mod} = 90 \Omega$ . Notably, the Dogbone tag stands out as the closest to achieving the optimal antenna impedance  $Z_{ar}$  (presented in Sec. 1.4.2.7), showcasing superior performance in this regard.

### 3.4.6 Evaluation of tag performance and read range

The objective in this subsection is firstly to evaluate performance, using indicators we'll define on the one hand, and using the characterization chart on the other. Secondly, to evaluate the read range and investigate its dependency from the chip sensitivity and the reader sensitivity.

#### 3.4.6.1 Definition of the observed performance indicators

Based on the measurement of power profiles of the 9 tags with our specific platform, we define the following three performance metrics:

- $r_{min}$  as the minimum range where the tag is not responding. The higher the value of  $r_{min}$  the better the tag's is responding in the high fading region.
- $r_{max}$  as the maximum (observed) range where the tag is responding.
- $L$  as the length (in meters) of the union of tag-responding intervals (i.e the range regions along the rail where the tag is responding). We have  $L \leq L_{max}$  (see 3.4.1), the higher the value of  $L$ , the better the tag's performance.

Therefore, we define the read range percentage as

$$\rho_{RR} = \left( \frac{L}{L_{max}} \right) \times 100\% \quad (3.7)$$

Where the measure of the responding region is divided by the full available range of  $L_{max} = 4.83m$  out of  $5m$  rail length.

#### 3.4.6.2 Comparison between the performance metrics

Table 3.2 presents the results obtained from the 9 tags. These results include two categories of parameters. The first set of parameters:  $r_{min}$ ,  $r_{max}$ , and  $\rho_{RR}$ , was directly extracted from the profiles showcased in Fig. 3.10. The second set of parameters:  $\tau$ ,  $\sqrt{M}$ ,  $\rho_{\varphi^{-1}}$ , and  $\rho_{\frac{1}{2}}$ ,

name	$\sqrt{M}$	$\tau$	$\rho_{\varphi^{-1}}$	$\rho_{\frac{1}{2}}$	$\gamma$	$\rho_{RR}$	$r_{min}$	$r_{max}$
AD806	0.004	0.002	0.48	0.59	0.004	19.9	0.96	0.96
UPMWEB	0.09	0.123	17.22	21.27	0.15	75.2	2.25	4.83
H47	0.089	0.147	18.91	23.32	0.17	78.3	2.16	4.83
AD661	0.121	0.121	19.61	24.24	0.22	85.7	2.22	4.83
AD318	0.115	0.336	34.02	40.82	0.33	87.6	2.22	4.83
AD233	0.16	0.49	45.55	51.86	0.48	92.5	2.19	4.83
AD550	0.256	0.401	51.7	62.74	0.46	91.9	2.16	4.83
DOGBONE	0.308	0.37	54.55	67.18	0.47	86.3	2.22	4.83
ALIEN	0.351	0.618	69.45	73.12	0.68	95.7	2.25	4.83

Table 3.2 – Data obtained from tag acquisitions

was derived from the chart depicted in Fig. 3.13. Note that the calculations for  $\tau$  and  $\sqrt{M}$  were performed under the condition  $\tau_{lim} = \varphi^{-1}$ . The two heuristical criteria  $\rho_{\varphi^{-1}}$ , and  $\rho_{\frac{1}{2}}$  were defined in Sec. 2.7 which describe a good design as one who give an equilibrium between  $\tau$  and  $M$ . However it is not necessary the optimal design of the tag.

Tags in table 3.2 were sorted in ascending order by the values of  $\rho_{\varphi^{-1}}$  calculated using (2.61). Comparing the tags based exclusively on their  $\rho_{RR}$ ,  $r_{min}$ , and  $r_{max}$  values poses challenges, primarily because, with the exception of AD806, all tags have reached the maximum attainable read range of  $r_{max} = 4.83m$ . Consequently, the maximum detection distance for these tags remains unknown. Additionally, the  $\rho_{RR}$  values for these tags are closely clustered, making direct comparisons arduous. Consequently,  $\rho_{RR}$ ,  $r_{min}$ , and  $r_{max}$  are not suitable metrics for tag comparison.

To address these limitations, Fig. 3.15 presents the values of  $\rho_{\varphi^{-1}}$ ,  $\rho_{\frac{1}{2}}$ , and  $\rho_{RR}$  for the tags, arranged in ascending order based on  $\rho_{\varphi^{-1}}$  and  $\rho_{\frac{1}{2}}$ . Both of these metrics yield identical performance rankings for the tags. It's worth noting that the  $\rho_{RR}$  values, highlighted in green, exhibit only marginal variations between different tags. In contrast,  $\rho_{\varphi^{-1}}$  and  $\rho_{\frac{1}{2}}$  exhibit more substantial variations, providing a more sensitive performance ranking. Consequently, the tags are ordered from the poorest to the best performance using  $\rho_{\varphi^{-1}}$  (or equivalently,  $\rho_{\frac{1}{2}}$  in this case).

### 3.4.6.3 Read range evaluation in free space condition

Fig. 3.16 presents the theoretical read range for each tag assuming free space, based on their  $M$  and  $\tau$  values and calculated using formula (2.74), under the condition  $\tau_{lim} = \varphi^{-1}$ . The read range is calculated by supposing three different reader sensitivities  $S_r$ :  $-80dBm$ ,  $-70dBm$  and  $-60dBm$ , where  $S_r = -80dBm$  is the reader sensitivity employed in the



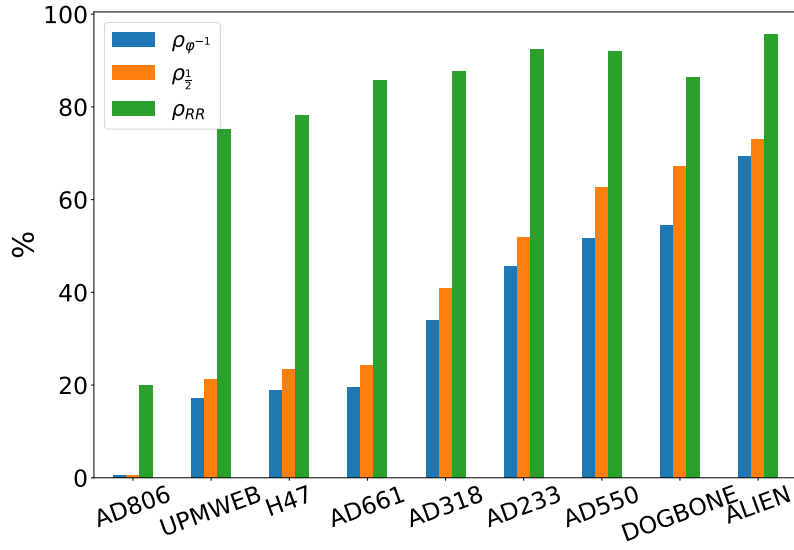


Figure 3.15 – Comparison of the performance evaluation criterias ( $\rho_{\varphi^{-1}}$ ,  $\rho_{\frac{1}{2}}$  and  $\rho_{RR}$ ) for a set of tags

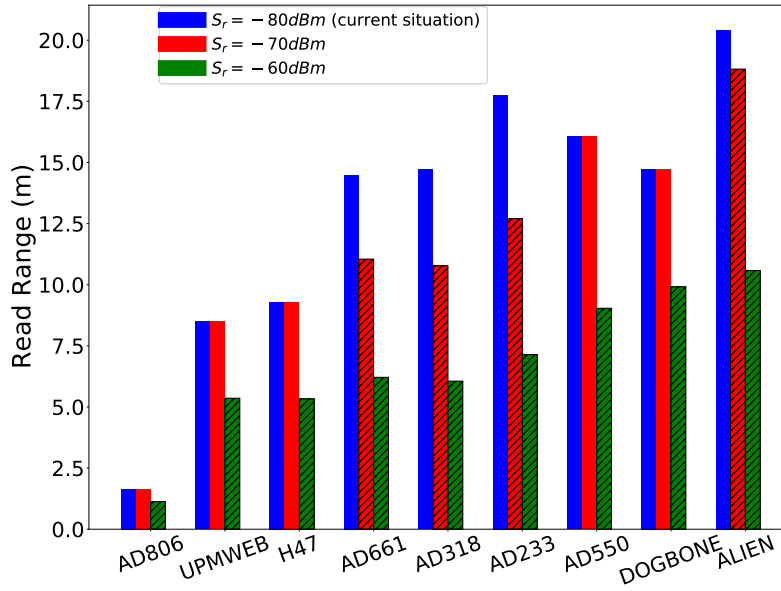


Figure 3.16 – Theoretical free space read range for different  $S_r$  ( $G_t = 2dB$ ,  $G_r = 9dB$ ,  $P_t^{max} = 30.5dBm$ ). Cross-hatched: Backward link-limited, No cross-hatched: Forward link-limited

current measurements. The figure distinguishes two read ranges: one is constrained by the forward link ( $d_{max}^{(\tau,M)} = d_{max}^{(\tau)}$ , represented by no cross-hatched bars), and the other is constrained by the backward link ( $d_{max}^{(\tau,M)} = d_{max}^{(M)}$ , represented by cross-hatched bars). At  $S_r = -80dBm$  the read ranges (in blue) for all the tags are only determined by  $d_{max}^{(\tau)}$ . This means that the backward link does not have any impact on the read range of these tags at this relatively low reader sensitivity, and the limitation is only due to the forward link. Additionally, the arrangement of the tags based on the calculated read range is the same as the arrangement based on the read range ratio  $\rho_{RR}$  obtained from the acquisitions (depicted in blue in Fig. 3.16). This demonstrates an agreement between the experimental acquisitions and the calculated read ranges.

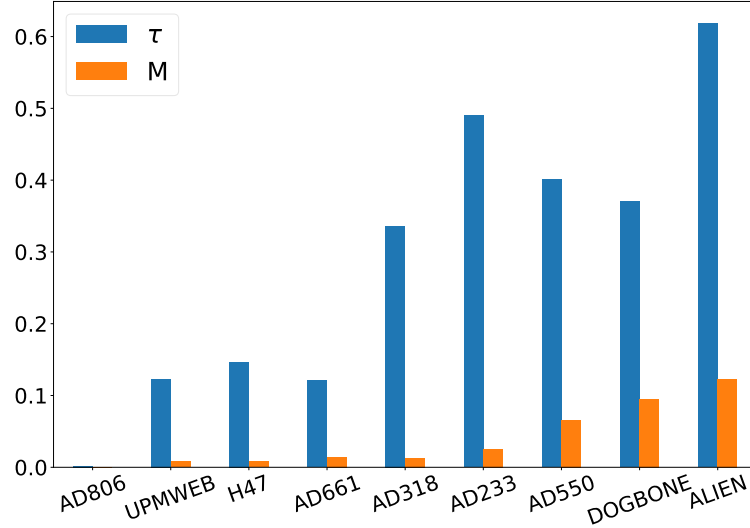


Figure 3.17 – Distribution of  $\tau$  and  $M$  derived under the condition  $\tau_{lim} = \varphi^{-1}$

Moreover, we present in Fig. 3.17 the distribution of  $\tau$  and  $M$  values (given in table 3.2) for the tags by remaining the same order. We notice that the arrangement of the tags based on  $\tau$  is similar to the arrangement based on the read range ratio  $\rho_{RR}$  and the maximum read range  $d_{max}$  (except for AD661 which has the best chip sensitivity), validating that the performances of the tags are manifested by their absorption capability in this particular experiment.

However, when a higher  $S_r$  value is imposed, a limitation may arise in the backward link. At  $S_r = -70dBm$  (indicated in red), some tags (AD806, UPMWEB, H47, AD550, and Dogbone) continue to experience read range limitations primarily imposed by the forward

link, thus remaining unaffected. On the contrary, for other tags (AD661, AD318, AD233, and ALIEN), the backward link becomes the constraining factor, leading to a reduction in their respective read ranges. Consequently, this shift in limitations alters the ranking of the tags based on their read ranges.

At  $S_r = -60\text{dBm}$  (in green), all tags have their read ranges limited by the backward link ( $d_{max}^{(M)}$ ). This results in yet another adjustment in the order of tags based on their read ranges.

As a result, the arrangement of tags concerning their performance is not definitive, as it depends on various factors such as the chip sensitivity  $S_c$ , and the reader sensitivity  $S_r$  which is not always known. To address this unknown variability, the criteria  $\rho_{\varphi^{-1}}$  and  $\rho_{\frac{1}{2}}$  have been proposed as compromise measures for evaluating tag design. These criteria strike a balance between  $\tau$  and  $M$ , aiming to achieve a design that consistently performs well across diverse scenarios and applications. Nevertheless, further analysis is required to determine the optimal approach for assessing tag performance using this methodology.

#### **3.4.6.4 Investigation on the effect of the reader sensitivity on the tag's optimal design**

We have theoretically explored the effect of the reader sensitivity on the read range hierarchy among tags in free space. Now, delving deeper into our investigation, let's explore how manipulating  $S_r$  can alter the optimal tag design in this context.

Firstly, let's investigate the influence of reader sensitivity ( $S_r$ ) on the experimental read range of a single tag. To conduct our experiments, we utilized the Impinj reader R700 and the NXP Ucode 8 tag ( $S_c = -23\text{ dBm}$ ). We specifically chose the Impinj reader due to its capability to precisely control and adjust reader sensitivity, as elaborated in Subsec. 1.5.2. Our experiments involved configuring the Impinj reader to its maximum transmitted power ( $P_t^{max} = 30\text{ dBm}$ ) while varying the reader sensitivity at three distinct levels:  $S_r = -80\text{ dBm}$ ,  $S_r = -75\text{ dBm}$ , and  $S_r = -70\text{ dBm}$ . These experiments produced the received power profiles illustrated in Fig. 3.18. It's worth noting that all measurements were conducted under identical conditions, ensuring consistency in the tag's position and antenna orientation.

The results revealed a clear correlation between reduced reader sensitivity and a decrease in the read range. With  $S_r$  set at  $S_r = -80\text{ dBm}$ , we successfully detected the tag across the entire rail, covering a distance of over 5 meters. This indicates that at  $S_r = -80\text{ dBm}$ ,

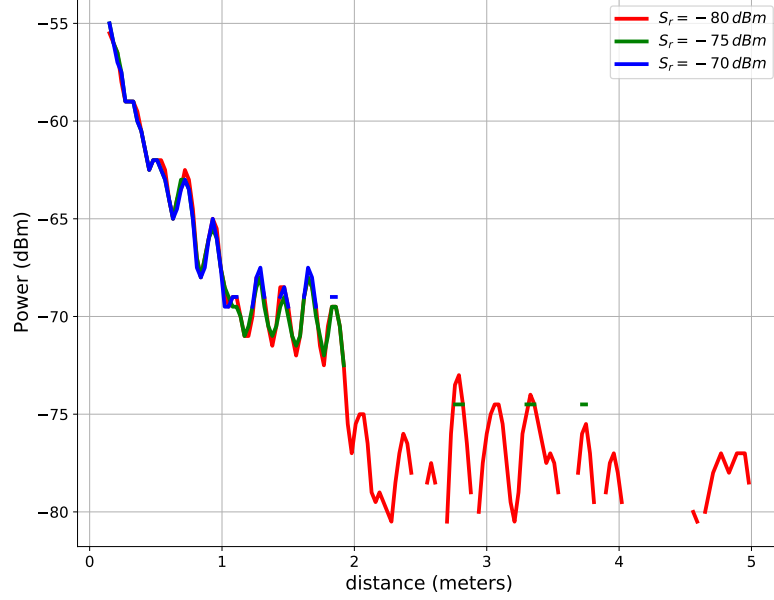


Figure 3.18 – Received power profile at  $P_t^{max} = 30\text{dBm}$ , for three different impinj’s reader sensitivities  $S_r = -80, -75, -70\text{ dBm}$

there were no limitation caused by the reader on the reading range. However, decreasing the reader sensitivity of 5 dBm to  $S_r = -75\text{ dBm}$  reduced the read range to approximately 2 meters. Further reduction to  $S_r = -70\text{ dBm}$  yielded a read range of around 1.7 meters. These results underscore that, for  $S_r = -70\text{ dBm}$  and  $S_r = -75\text{ dBm}$  scenarios, the limitation in read range is primarily driven by the backward link, emphasizing the significant role of the modulation factor in these particular reader sensitivity settings, since having a higher modulation factor will produce a higher backscattered power.

Additionally, we examined the read range under free-space conditions for the three reader sensitivities, as depicted in Fig. 3.19, on a  $(\sqrt{M}, \tau)$  chart. The blue dashed line represents the Q value obtained for the NXP Ucode 8 tag, which is around  $-2.24\text{ dBm}$ , while the black dashed line corresponds to  $Q_{opt}$  (2.75), optimizing the read range and establishing the boundaries of read range dependency. For  $S_r = -80\text{ dBm}$ , the blue and black lines closely align, signifying equilibrium between  $\tau$  and  $M$ . However, for  $S_r = -75\text{ dBm}$  and  $S_r = -70\text{ dBm}$ , the black line resides below the blue line, indicating that the read range is constrained by  $\sqrt{M}$ , i.e., the backward link. This aligns with our earlier observations

where the tag did not achieve a 5-meter detection range under these two scenarios. Therefore, this method provides a valuable information on the read range limitation, effectively highlighting the impact of reader sensitivity on read range within the UHF RFID system, also highlighting the importance of the having a balance between  $\tau$  and  $M$ .

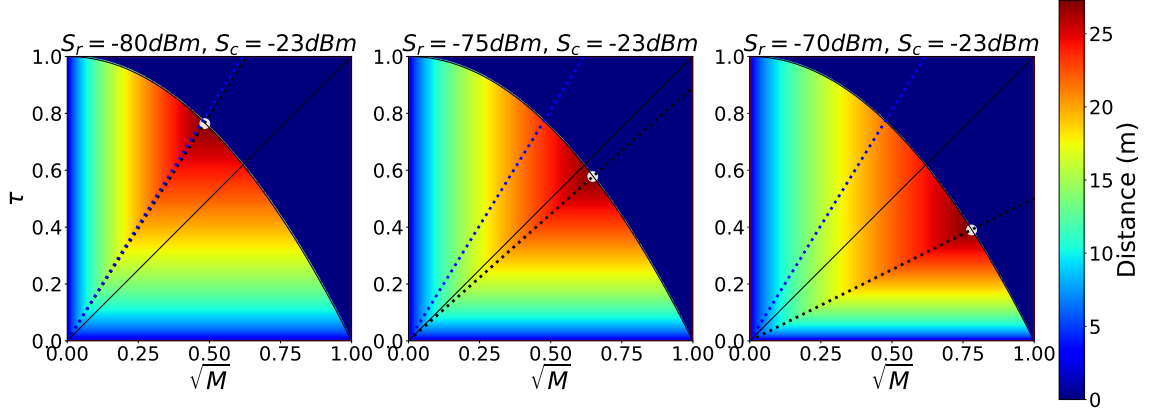


Figure 3.19 – Representation of read range in the chart for three different impinj's reader sensitivities  $S_r = -80, -75, -70$  dBm

### 3.4.7 Effect of $P_{inc}$ variation

This section examines the impact of varying the tag's incident power on its behavior. Specifically, we investigate the indirect effects of changing the incident power ( $P_{inc}$ ) on the received power and the modulation factor. The transmitted power of the alien reader can range from 15.7 dBm to 30.5 dBm, allowing us to determine the activation profiles by sweeping the power from  $P_{min}$  to  $P_{max}$ .

Since we cannot directly measure  $P_{inc}$  in our experiments due to it occurring over the air, we rely on the fact that  $P_{inc}$  remains constant when the tag is activated (according to eq. (??)).

#### 3.4.7.1 Investigation on the relation between $P_r^\Delta$ and $\Delta$

To explore the effects of altering the transmitted activation profile, we conducted measurements on the NXP Ucode 8 chip-based tag across the entire range of possible transmitted

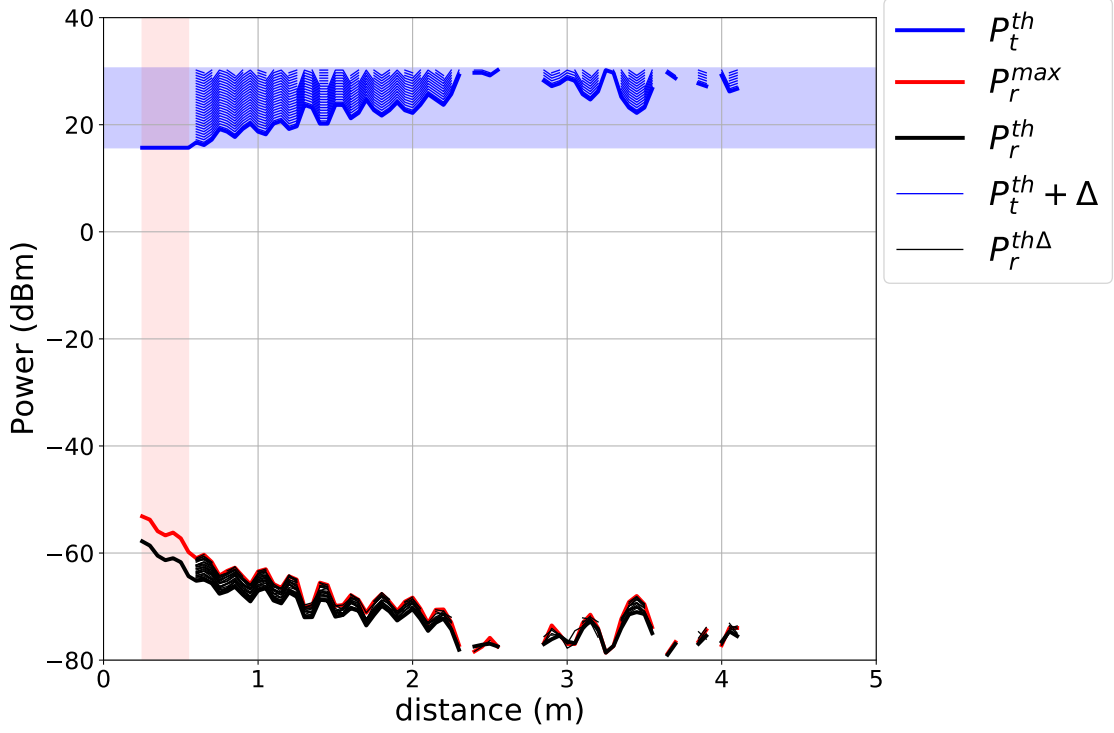


Figure 3.20 – Representation of shifted activation profiles by different  $\Delta$  values ranging from 15.7 to 30.6 dBm

power. In this section, our investigation extended beyond the acquisition of the activation profile, we also systematically shifted the transmitted activation profile by a parameter  $\Delta$ , as defined in Sec. 2.4.1. This shift effectively modified the incident power reaching the tag by an amount  $\Delta$  as explained in Subsec. 2.4.1. As a result, by continuously shifting the transmitted activation profile with different values of  $\Delta$  ranging from 0 to 14 dB with step of 0.5 dB, we obtained a set of shifted transmitted activation profiles ( $P_t^\Delta = P_t^{th} + \Delta$ ) introduced in eq. (2.32). This also leads to a corresponding shifted constant ( $P_{inc}^\Delta = P_{inc}^{th} + \Delta$ ) and a shifted received activation profile  $P_r^\Delta$  defined in eq. (2.39).

Fig. 3.20 illustrates the results of all the shifted activation profiles of this experiment. It is important to note that in some cases, when shifting the activation profile with a high  $\Delta$  value, the transmitted power exceeds the maximum possible transmitted power ( $P_{max} = 30.6 \text{ dBm}$ ). In such cases, the received power data is not available, limiting the information obtained, whereas no information was available for  $\Delta$  higher than 14 dB. However, the available acquisitions are already sufficient to access the shifted tag receptivity  $R^\Delta$ , defined in eq. (2.52), since it is not distance-dependent.

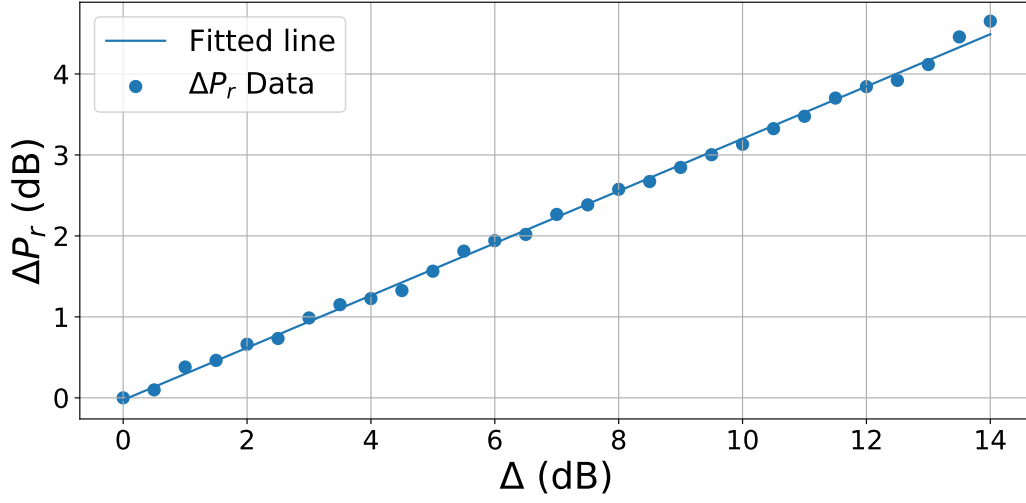


Figure 3.21 – Variation of the offset on the received activation power w.r.t  $\Delta$

Fig. 3.20 demonstrates that shifting the transmitted activation profile by  $\Delta$  does not result in an equal shifting on the received power side. This can be clearly observed by comparing the margins of the shifted transmitted profiles and the shifted received profiles in the figure. The evolution of the shift on the received activation power ( $\Delta P_r$ ) w.r.t the shift on the transmitted activation power ( $\Delta$ ) is represented in Fig. 3.21, where  $\Delta$  varies from 0 to 14 dB with a steps of 0.5 dB. Notably, the variation  $\Delta P_r$  exhibits a linear relationship with  $\Delta$ . Moreover, at  $\Delta = 14$  dB for example, we observe a shift  $\Delta P_r = 4.7$  dB, indicating that variations in transmitted power do not cause an equivalent variation in reception due to the non-linearity of the tag. This linear relationship has been observed for all previous measured 9 tags as shown in Annex A, however the slope differs from tag to another and it is likely related to intrinsic characteristics of the tag and needs thorough investigations.

#### 3.4.7.2 Evolution of $Q$ and $M$ by $P_{inc}$ variation

Consequently, we calculated the  $Q$  values for each shifted activation profiles by first determining the shifted tag receptivity using formula (2.52), followed by applying formula (2.57). The variation of  $Q$  with the offset  $\Delta$  is presented in Fig. 3.22, revealing a linear relationship.  $Q^\Delta$  ranges from  $Q^{th}$  at  $\Delta = 0$  dB (corresponding to the activation profiles) to  $Q^\Delta = 8$  at  $\Delta = 14$  dB. Thus, varying  $P_{inc}$  on the tag induces a linear variation in  $R$  and  $Q$  values, which in turn affects the  $\tau$  and  $M$  characteristics. After revealing the  $Q^\Delta$  variation, we can now determine  $M^\Delta$  by using eq. (2.51) under the assumption of

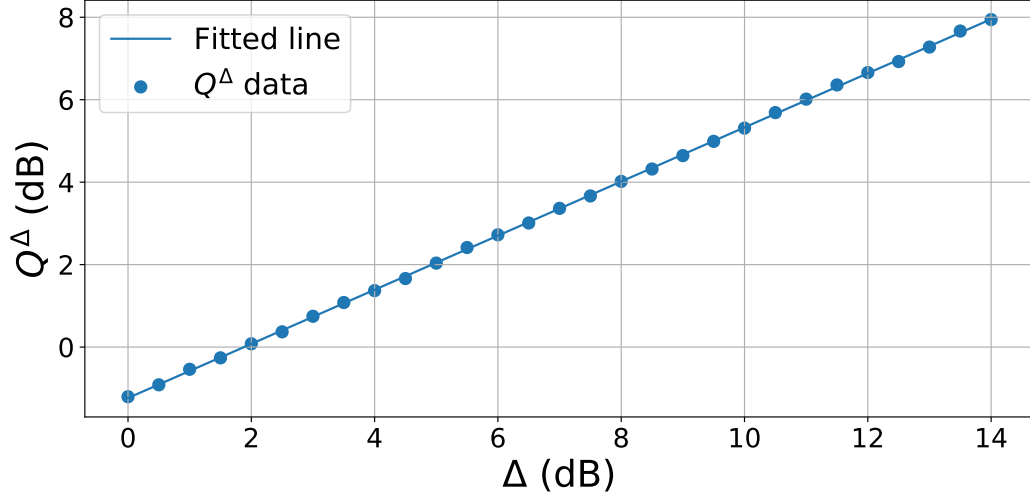


Figure 3.22 – Variation of the  $Q^\Delta$  (in dB) w.r.t  $\Delta$  (in dB)

$\tau^{th}$  is known experimentally for the NXP Ucode 8. The variation of  $\sqrt{M^\Delta}$  w.r.t  $\Delta$  is observed in Fig. 3.23. As we can see,  $\sqrt{M^\Delta}$  decreases linearly with the variation of the incident power from around 0.39 to 0.12 for the NXP Ucode 8 tag measured (also seen in [64]). Remarkably, the highest values of  $\sqrt{M^\Delta}$  are attained when the tag operates under conditions of minimal reception power. This outcome aligns perfectly with the designer's goal of achieving optimal performance even in the most challenging reception scenarios, thereby maximizing the communication range between the reader and the tag. We explored the variation of  $\sqrt{M^\Delta}$  for all the 9 tags experimented in 3.4.2 and presented the results in A. We observed different linear variation of  $M$  where it differs from tag to another even for the tags of same chip.

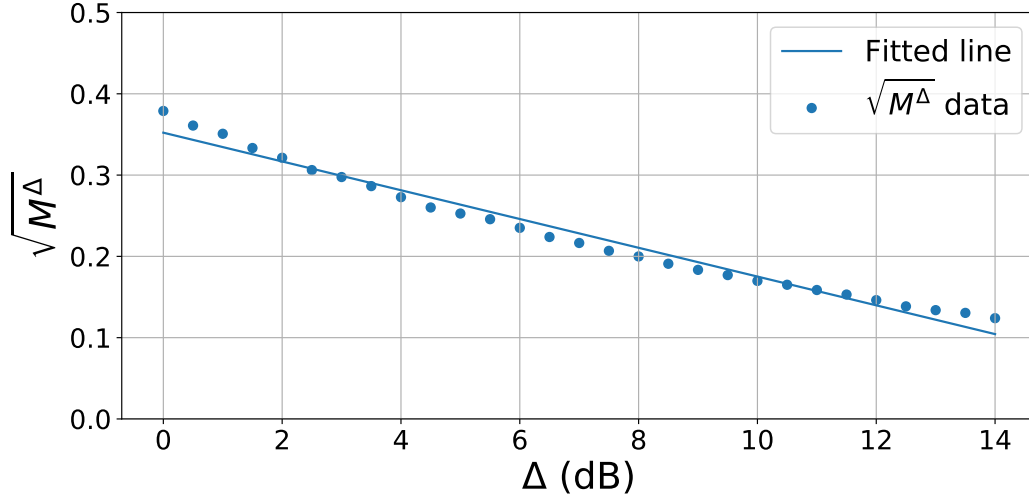
### 3.4.7.3 An estimated extension of the two Activation profiles

To account for the lack of activation power information in the red region for both transmission and reception as previously presented in 3.8, an estimated extension of the two activation profiles can be created using the knowledge of tag receptivity and the maximum received power in this region.

As we have seen from Fig. 3.21, the shift on the received power  $\Delta P_r$  varies linearly with the shift on the transmitted power  $\Delta$ , which gives us this relation:

$$\Delta P_r = a\Delta + b \quad (3.8)$$




 Figure 3.23 – Evolution of  $\sqrt{M^\Delta}$  (in linear) w.r.t  $\Delta$  (in dB)

$$P_r^{(2)} - P_r^{(1)} = a(P_t^{(2)} - P_t^{(1)}) + b \quad (3.9)$$

Where  $a$  and  $b$  are the slope and the y-intercept respectively of the line representing the linear variation of  $\Delta P_r$  in term of  $\Delta$ .

If we consider  $P_t^{(1)} = P_t^{th}$  which gives  $P_r^{(1)} = P_r^{th}$ , and  $P_t^{(2)} = P_t$ , it yields:

$$P_r = aP_t - aP_t^{th} + P_r^{th} + b \quad (3.10)$$

and by replacing  $P_r^{th} = 2R - P_t^{th}$  (from eq. (2.56)), we obtain the relation between  $P_r$  at  $P_t = \text{constant}$  and  $P_t^{th}$ , knowing the mean tag receptivity  $\bar{R}^{th}$  (defined in 3.4.3) as follows:

$$P_r = -(a + 1)P_t^{th} + aP_t + b + 2\bar{R}^{th}$$

$$P_t^{th} = \frac{-P_r + aP_t + 2\bar{R}^{th} + b}{a + 1}$$

The extension of  $P_t^{th}$  in the blue region can be then obtained using the maximum received power  $P_r^{max}$  at  $P_t^{max}$ :

$$P_t^{th} = \frac{-P_r^{max} + aP_t^{max} + 2\bar{R}^{th} + b}{a + 1} \quad (3.11)$$

And thus, the transmitted activation profile can be extended using this expression which is of the same accuracy as of  $\bar{R}^{th}$  illustrated in 3.4.3.

Thereafter, the received activation profile  $P_r^{th}$  can also be extended by applying eq. (2.56), knowing the extracted quasi-constant value  $R^{th}$ . Fig. 3.24 shows the extended activation

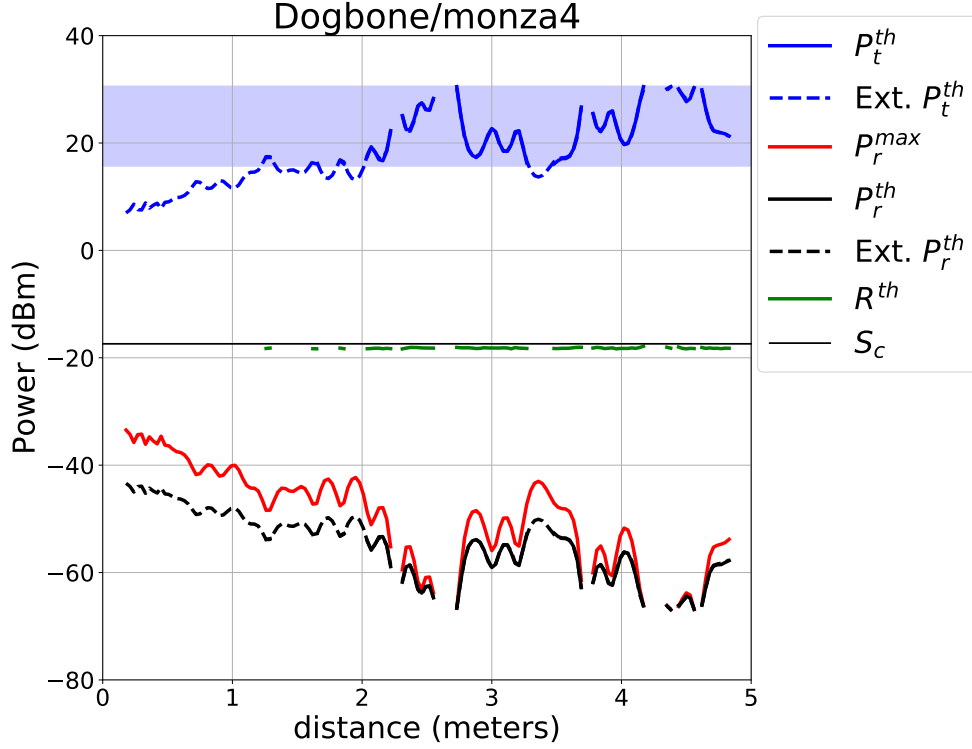


Figure 3.24 – Representation of the power profile with extension

power profiles of the Dogbone tag already presented in Fig. 3.8 . We can see two different linestyle for the plotted activation profile (in blue) and the received profile at the activation power (in black). The continuous plotting refers for the real acquisitions of these two profiles, whereas the dashed plotting (mostly on small distances) is an estimation of these two profiles obtained by applying eq. (3.11) by considering  $P_t^{max} = 30.5 \text{ dBm}$ . The accuracy of this estimation was shown to be high, closely matching the real activation power profiles. It is worth noting that this estimation exhibits high accuracy, closely resembling the real activation power profiles. This methodology has been applied to all nine measured tags, as detailed in the Annex A. Furthermore, this extension approach can also be applied to angular measurements. In summary, we have introduced a method to extend the activation profiles by leveraging knowledge of the received power at a constant transmit power.

### 3.4.8 Environment propagation scanning using identical UHF RFID tags configuration

Gaining a comprehensive understanding of how radio waves propagate in a given environment is a crucial aspect when implementing UHF RFID technology. Various factors such as obstacles, reflections, and interference can significantly impact the behavior of radio waves, resulting in signal attenuation or fading [65].

This section introduces a methodology for examining channel propagation fading using UHF RFID. A work in [66] characterizes the forward propagation channel only between the reader and a tag antenna by using a VNA tool. However, the proposed approach involves setting up a linear configuration of 39 identical RFID tags and gradually moving them away from the antenna at different distances. At each distance, the tags are detected, and measurements of signal strength and fading are recorded.

By analyzing the data collected from the RFID tags, valuable insights into the propagation characteristics of radio waves in the environment can be obtained.

#### 3.4.8.1 Experimental setup

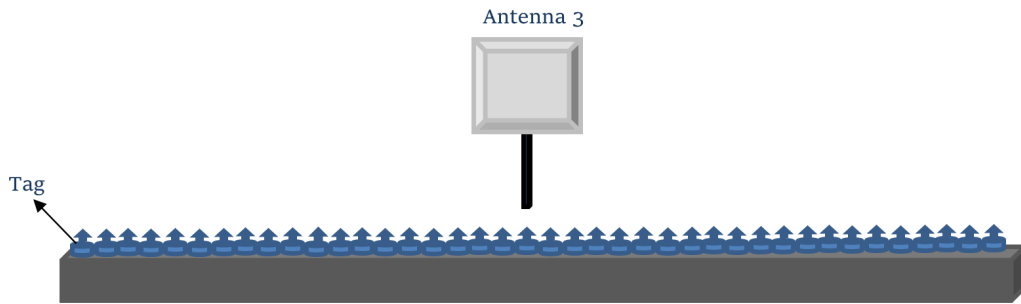


Figure 3.25 – Mosaic of an experiments based on 39 tags placed in front of the platform antenna

For the experimental setup, an NXP Ucode 8 chip-based UHF tag with a typical sensitivity of  $S_c = -23, dBm$  was utilized [58]. A total of 39 tags, each equipped with an NXP Ucode 8 chip, were arranged in a linear formation facing the stationary antenna of the platform, as shown in Fig. 3.25. The experimental setup, illustrated in Fig. 3.26, also incorporated absorbent panels in the surrounding area to minimize external interference and improve measurement accuracy, although complete elimination of interference was not achieved.



Figure 3.26 – Photo of the 39 tags placed in a row in front of the platform antenna surrounded by absorbent panels

During the experiment, the setup was moved along a rail, capturing data for each tag at every step and extracting power profiles, similar to the methodology described in Sec. 3.4.1 for an individual tag. The distance between the center of the tag row and the antenna ranged from  $d_{min} = 0.18\text{ m}$  to  $d_{max} = 4.98\text{ m}$ , with a distance increment of  $48\text{ mm}$ . This distance granularity facilitated highly accurate measurements, benefiting from the capabilities of the platform. The transmitted power range considered spanned from  $15.7\text{ dBm}$  to  $30.2\text{ dBm}$ , with a step size of  $0.3\text{ dBm}$ . The experiment employed the Alien reader 9900+, which efficiently reads multiple tags simultaneously, enabling this power range to be achieved with small resolution for all the tags.

#### 3.4.8.2 Fading results analysis

The tags are arranged and positioned based on their ID, with tag 1 located at  $-0.5\text{ m}$  and tag 39 positioned at  $0.5\text{ m}$ . The results are represented in Fig. 3.27 which illustrates in five subplots:

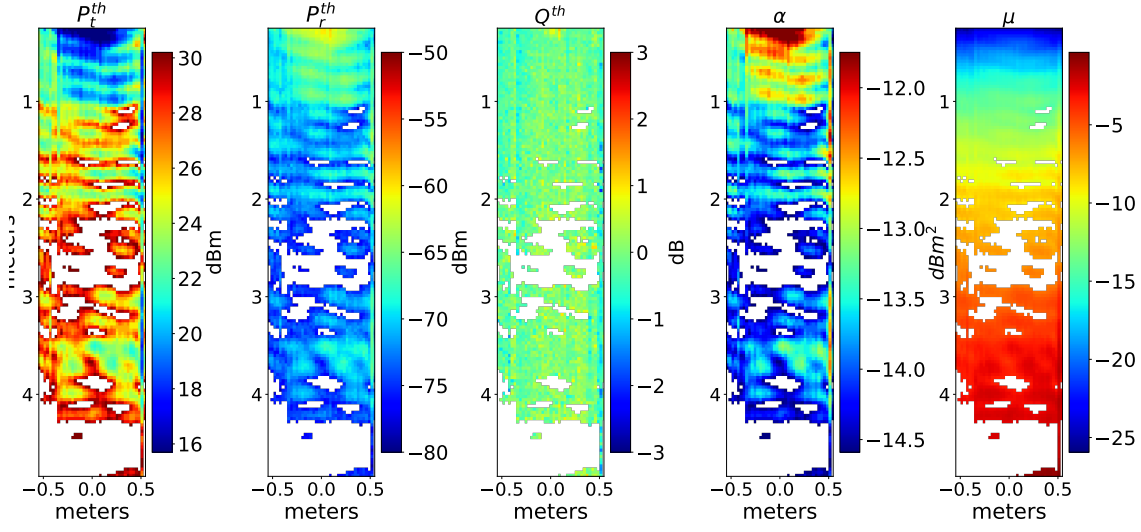


Figure 3.27 – Received power profiles variation along the rail of 39 RFID tags placed on a row

- The evolution of the transmitted activation power profiles  $P_t^{th}$  for all 39 tags: it exhibits an increasing variation with distance.
- The evolution of the received activation power profiles  $P_r^{th}$ : we can notice a similar evolution as of the transmitted activation profiles but in decreasing manner.
- The tag offset  $Q^{th}$ : it remains relatively constant across different distances and for all tags, with values approaching zero. This consistency was expected since similar tags should exhibit nearly identical intrinsic characteristics.
- The transmitted channel coefficient  $\alpha$ : It is obtained by applying eq. (2.46) with the assumption that  $\tau^{th} = 0.5$ . The variation of  $\alpha$  profiles vividly demonstrate the presence of fading phenomenon in this multi-path channel, with the exception of tag 38, which exhibits exceptional performance and differs from the other tags by achieving a read range of  $4.8\text{ m}$ . This exceptional performance can be attributed to its superior characteristics compared to the other tags.
- The dimensional coefficient  $\mu$ , introduced in eq. (2.24): in this specific scenario, the value of  $\mu$  is less than 0 in a linear scale, signifying a more rapid decline in the channel compared to a free space channel. Notably, as we examine the relationship with distance, we see that  $\mu$  exhibits an increasing trend. This observation underscores the dynamic nature of channel fading within the environment compared to the a free space channel. The dimensional coefficient  $\mu$  thus emerges as a valuable indicator,

offering insights into characterizing the channel and comprehending its impact on the response of the tags.

Additionally, a distinct detection gap is observed around  $2\text{ m}$  and  $2.75\text{ m}$ , indicating a region of high fading within the channel. This gap is particularly prominent for the tags positioned in the middle, as they display a diminished response. Despite efforts to increase the transmitted power, the existence of this gap remains largely unaffected, making it challenging to detect tags within this specific region. While similar observations were made in the measurements discussed in Sec. 3.4.1 for individual tags, the absence of detection in this region is more pronounced in the presented array configuration. This finding emphasizes the presence of signal reception variations and underscores the need for further investigation and potential mitigation strategies to address this fading phenomenon.

### 3.5 Conclusion

This chapter focused on the experimental characterization of RFID tags, providing valuable insights into their performance and comparing different commercial UHF RFID tags. We started by exploring the theory we developed on the UHF RFID system and then proceeded with practical experiments to validate our findings.

The acquisition of RSSI data in both translation and rotation scenarios allowed us to capture the behavior of the tags under different conditions. The representation of RSSI directly provided by the alien reader ALR-9900+ enabled us to analyze the evolution of RSSI and its conversion to received power units in dBm. This conversion was necessary since the manufacturer did not provide a direct relationship between RSSI and dBm.

By exploiting the measured power profiles in dBm, we were able to evaluate and compare the performance of a set of nine UHF RFID commercial tags. The power profiles served as a basis for assessing the characteristics of the tag  $\tau$  and  $M$  by extracting the tag receptivity. This last is found to be quasi-constant and invariant by the distance.

Traditionally, the algorithm presented in chapter 2 was employed to place a set of 9 measured tags in the  $(\sqrt{M}, \tau)$  chart. This chart facilitated a deeper understanding of the intrinsic characteristics of the tags and provided a visual representation of their performance. Thus, we evaluated and compared these tags using two criteria  $\rho_{\varphi^{-1}}$  and  $\rho_{\frac{1}{2}}$  which seeks an equilibrium between  $\tau$  and  $M$ .

We then explored the evaluation of tag performance and read range under the assumption of free space and for different reader sensitivity  $S_r$ . By comparing the measured performance

evaluation with the expected read range and reader sensitivity, we gained insights into the limitation on read range for a UHF RFID tag in real world scenario. We investigated the optimal design that maximize the read range which depends from the reader sensitivity. Moreover, in this chapter we investigated the impact of varying the tag's incident power, on the performance of the tag, more specifically on the modulated power. By doing that we have analysed the non-linearity of a passive tag.

Finally we conducted an experiment on a configuration of 39 similar tags placed in a row in order to scan the propagation environment, revealing the multipath channel and non-detection areas.

Through this experimental characterization, we have contributed to the field of RFID technology by providing practical insights into the performance variations and capabilities of UHF RFID tags. Our findings assist in the selection and optimization of RFID systems, ensuring optimal performance and reliable operation.

Future research can build upon these experimental results to further enhance the performance and efficiency of RFID tags, leading to advancements in various industries and applications reliant on RFID technology.

## Summary

- **Conversion Formula for Alien Reader's RSSI:** In this chapter, we proposed a conversion formula to transform the alien ALR 9900 reader's RSSI into a real power quantity dBm, an important finding since this information is not given by the manufacturer:

$$P_{rdBm} = f(RSSI) = 20 \log_{10}(RSSI) - 128$$

- **Exploitation of the Power Profiles and tag receptivity:** By systematically varying both distance and transmitted power, we have exploited the power profiles in transmission and reception. These profiles have allowed us to extract the tag receptivity, introduced in Chapter 2. The tag receptivity serves as a key parameter associated with the intrinsic characteristics of the tag  $\tau$  and  $M$ . Thereby, the tag can be evaluated in the chart using these two characteristics.
- **Performance Evaluation with  $(\sqrt{M}, \tau)$  Chart:** We have utilized the  $(\sqrt{M}, \tau)$  chart to evaluate and compare the performance of different commercial RFID

tags. The evaluation criteria proposed correspond to the maximum equilibrium between the mean power transmission coefficient and the modulation factor.

- **Read Range Dependencies Investigation:** We also have explored read range dependencies, particularly focusing on reader sensitivity ( $S_r$ ) and chip sensitivity ( $S_c$ ). Specifically, we varied the impinj reader sensitivity to study its impact on the read range.
- **Non-linear Tag Characteristics:** We have delved into the non-linear characteristics of UHF RFID tags, illustrating the impact of varying incident power on tag behavior. This analysis revealed a linear variation, in  $dBm$  scale, of the received power, the tag offset and the modulation factor, with the variation of the transmitted power.
- **Reciprocal Transmission Channel Scanning:** Finally, we introduced a novel approach wherein a linear configuration of similar UHF RFID tags is employed to scan the reciprocal transmission channel. This observation offers a better comprehension of the multipath propagation channel and the non-detection areas present in it.





# EXPERIMENTAL CHARACTERIZATIONS

## IN THE CONTEXT OF LIVESTOCK

### APPLICATION

---

#### 4.1 Introduction

This thesis is part of a collaborative project led by the Cooperl company. Cooperl is the leading French company which offer a global solution in the livestock farming. It combines a variety of technology and services for customers looking to invest in the pig industry. The project aims to propose an innovative solution for the follow-up of livestock using RFID technology in UHF band.

Our role in this project was to characterize the RFID tag working on pig ear, and taking better into account the effects of propagation and the environment. To achieve this goal, we used the RFID characterization platform at the IETR, and we develop the characterization methods presented in the previous chapters. We have experimented and evaluated RFID tags manufactured by ARDES, one of the partner of the project, in charge of the tag design. Two major measurement campaigns were carried out:

- The first measurement campaign was devoted to studying the behavior of a tag placed on a pig ear. There were 3 different steps. The first step was to characterize the dielectric properties of pig ears, which could have a significant influence on the performance of the tag. The second step was to measure the power profiles of several commercial tags with and without ear, for different orientations, in order to evaluate the most influential parameters. The third step was to appreciate tag response variability for different ears on the behavior of the commercial tags.
- The second measurement campaign was devoted to evaluate tags designed and manufactured by ARDES which are specifically adapted to work on pig ears. The

aim of the measurements was to study the effect of the ear on this adapted tags, and the effect of the orientation of the ear on the read range. These tags of different versions were also compared between each other to see the most suitable to work on pig ear.

In Sec. 4.2, we first present a literature review on the UHF RFID for applications involving pig ears. Then we present an extensive measurements of the dielectric properties of pig ears.

Following that, we investigate the impact of pig ears on the performance of commercial tags, while also examining the orientation effect of these tags on the ears. Moving forward, we scrutinize the tag response variability on 15 different ears. Then, we present in this chapter an evaluation of specialized tags provided by our project partner ARDES, designed specifically for pig ears. Utilizing the chart introduced in Chapter 2, we assess the performance of these tags across different versions when fixed to the ear. Finally, we conduct experimentation with ARDES tags placed in various Planar configurations to assess their performance when responding simultaneously.

## **4.2 State of the art on UHF RFID tags mounted on pig ears**

Over the past two to three years, there has been extensive discussion surrounding the digitalization of livestock farming processes. This term encompasses various advancements in automation, data collection and services, as well as the integration of different stakeholders within agricultural supply chains.

Passive ultra-high frequency radio frequency identification (UHF RFID) is a promising technology for precision livestock farming applications, enabling electronic identification of animals and facilitating automated data collection. In particular, UHF RFID tags attached to pig ears have been widely used in animal breeding projects to monitor individual animal health and performance, as well as to track their movements and behavior. However, the performance of UHF RFID tags in this context is affected by various factors, including the size, shape, and composition of the pig ear, as well as the orientation and distance of the tag from the reader. These factors can influence the tag's antenna characteristics, signal propagation, and electromagnetic coupling with the surrounding tissue, resulting in variations in the tag's read range, sensitivity, and reliability. Therefore, it is essential to

characterize the tag's performance on pig ears and to develop appropriate measurement techniques and models to assess and optimize its performance in real-world conditions. In this section, we will review the state of the art in UHF RFID technology for pig ear applications, including the challenges and opportunities of UHF RFID in precision livestock farming, the existing approaches and techniques for measuring and optimizing tags on pig ear, and the future directions and research needs in this field.

#### 4.2.1 Electrical characteristic of pig tissue

The electrical characteristics of pig ears play a crucial role in understanding the behavior and performance of UHF RFID tags specifically designed for ear applications. These characteristics, including conductivity and permittivity, exert a significant influence on the overall effectiveness of RFID systems operating within the UHF frequency range.

Conductivity, which measures a material's ability to conduct electric current, directly affects the efficiency of energy transfer between the RFID tag and the reader. A study conducted by [67] focused on measuring the dielectric properties of porcine skin tissue in the frequency range of 300 MHz to 3 GHz. The findings revealed that the conductivity of pig ear tissue exhibited an increasing trend from 0.4 S/m to 2.1 S/m as the frequency increased within this range. Notably, in the UHF RFID frequency range (860/960 MHz), the conductivity was observed to be approximately 0.67 S/m.

Another critical electrical characteristic is the permittivity, which expresses a material's ability to store electrical energy. In the context of pig ears, permittivity affects the propagation of electromagnetic waves and the efficiency of signal coupling between the RFID tag and the reader. The same study by [67] reported that the permittivity of pig ear tissue decreases with increasing frequency within the range of 300 MHz to 3 GHz. Specifically, within the UHF RFID frequency range, the relative permittivity of pig skin was approximately reported being  $|\epsilon_r| = 42$ .

Understanding the variations in pig ear electrical characteristics and their relationship with frequency holds big importance in the design optimization of UHF RFID systems tailored for animal tracking, identification, and monitoring applications. By taking into account the inherent electrical properties of pig ears and their impact on the antenna impedance of the tag, researchers and practitioners can customize RFID tag designs to better adapt and operate optimally on pig ears. This approach aims to enhance reliability, and to extend read range in realistic scenarios involving RFID applications involving pig ears.

### **4.2.2 Effect of pig Ear on UHF RFID tag performance**

UHF-RFID technology has proven to be a suitable option for monitoring livestock activities. However, a study conducted by authors in [68] compared data collected from RFID tags attached to pigs ears with reference data obtained through video observation. The findings of the study highlighted the vulnerability of UHF-RFID transponder ear tags to interference from the surrounding tissue, leading to the occurrence of both false positive and false negative readings. This underscores the significance of adapting the RFID tag to the animal's ear to counteract the impact of tissue-induced changes in resonance frequency.

Furthermore, several studies have investigated this effect of pig ear on UHF RFID tag performance. A study by [20] demonstrated that the read range and the performance of UHF RFID tags is significantly affected when placed on pig ears, it decreases due to the absorption and reflection of the electromagnetic energy by the ear.

The results in [20] showed that there were clear differences in measurements between the front and back of the ear, with higher variances and less repeatability at the front of the ear. Therefore, it is crucial to consider the positioning of the UHF RFID tag on the pig's ear when conducting measurements for precision livestock farming applications. By understanding the effects of positioning and using appropriate transponder types, more accurate and reliable UHF-RFID technology can be developed to support precision livestock farming practices.

This chapter also addresses the question of positioning the UHF RFID tag on the pig's ear, by examining the impact of placing the tag in both the internal and external side of the ear.

## **4.3 Dielectric characterization of pig ears**

Because of its two keys practical advantages of being entirely passive and wireless, UHF RFID tags have proved quite helpful in the livestock industry. However, deploying them in real-world circumstances and scenarios is challenging since their behavior can be very sensitive to the properties of the ear. Thus, the use of UHF tags on animal ear is currently hampered by the substantial impact that body tissue in the proximity of the transponders has on the performance. A dielectric characterization of pig ear in this case is necessary to understand the surrounding of the tag and achieve a better design of the tag on the pig ear. For our measurement campaign, we obtained 25 pig ears coming from Cooperl for experimental purpose. We focused first on measuring their dielectric properties. This study

provides insightful data on the properties of the ears and their variability. For this purpose, we used a SPEAG measurement system with a DAK-12 probe (4MHz-3GHz) [69] on the 25 pig ears. The selected frequency range goes from 700 MHz to 2GHz. These measurements were performed on both sides of the ear (internal and external side) in order to see if the side matters in placing the tag on the ear as it has been observed in 4.2.2.

### 4.3.1 Weight distribution of 25 ears

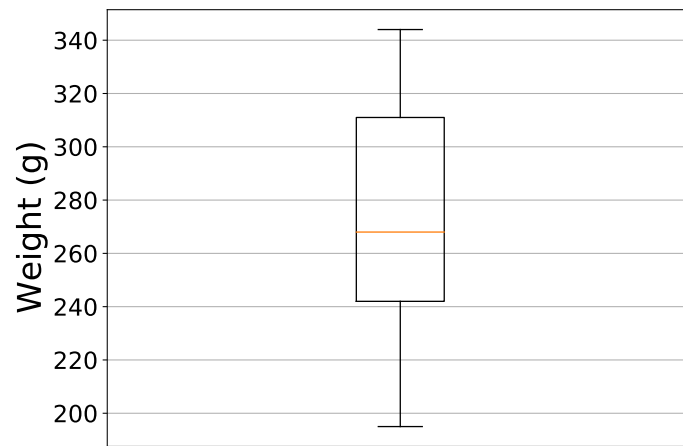


Figure 4.1 – Boxplot of the pig ears weight

Before measuring dielectric properties, we have measured the weight of the 25 ears that knowing that pigs may differ in size and weight which could have an effect on the efficiency of the RFID tag on ear and which may affect the dielectric characteristics of the ear.

Fig. 4.1 shows the boxplot of the weight of the 25 ears obtained, and more detailed, Fig. 4.2 shows a sorted vertical bar plot which indicates the weight of each ear. As it appears, there is significant difference in weights between the ears. Where it varies between 195 g (ear 25) and 344 g (ear 19). This information could have been used further to check if there is any significant relation between tag reading performance and its constitutive parameter.

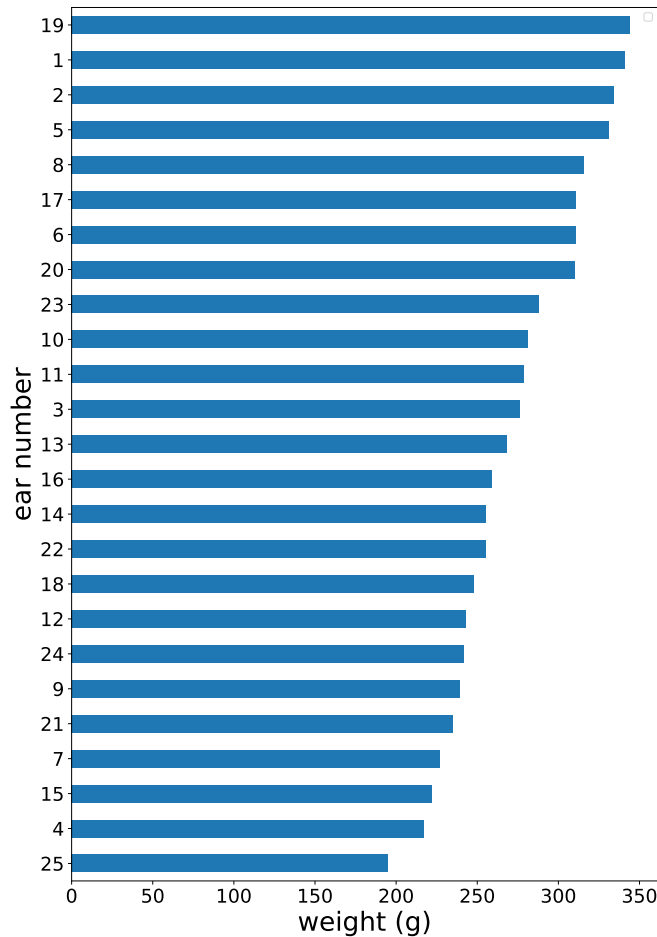


Figure 4.2 – Ordered barplot of ears weight

### 4.3.2 Dielectric measurement of Ear 8

After measuring the weight of the ears, we proceeded in the dielectric measurement for each ear. Using the SPEAG measurement system, the dielectric properties were repetitively measured for each side of each ear. Fig. 4.3 and 4.4 illustrate the results obtained from measuring the ear 8 dielectric properties of the internal and external sides respectively. Notice that the choice of this ear for the upcoming measurements is partially due to the fact that it was an ear with a pre-existing tag hole.

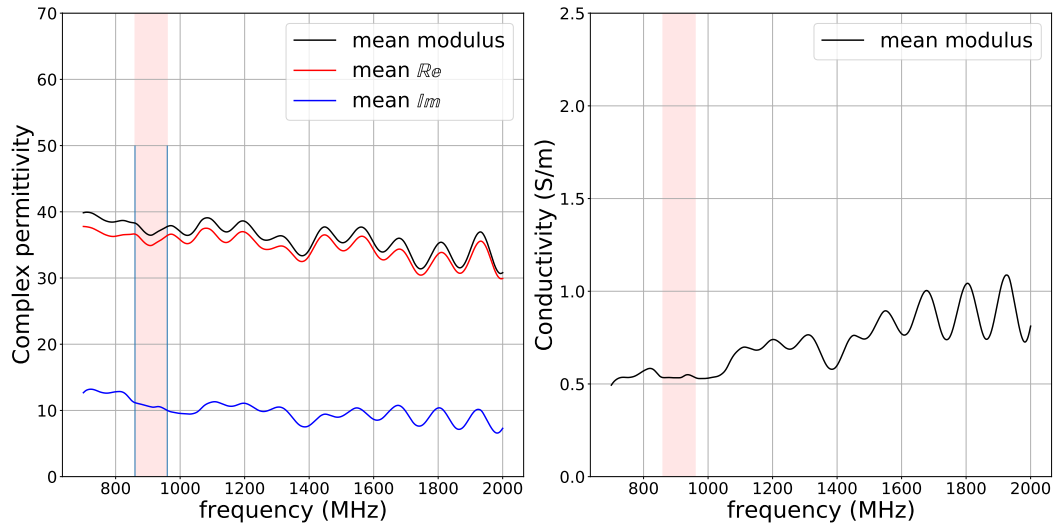


Figure 4.3 – Internal side - Dielectric measurement for ear Number 8

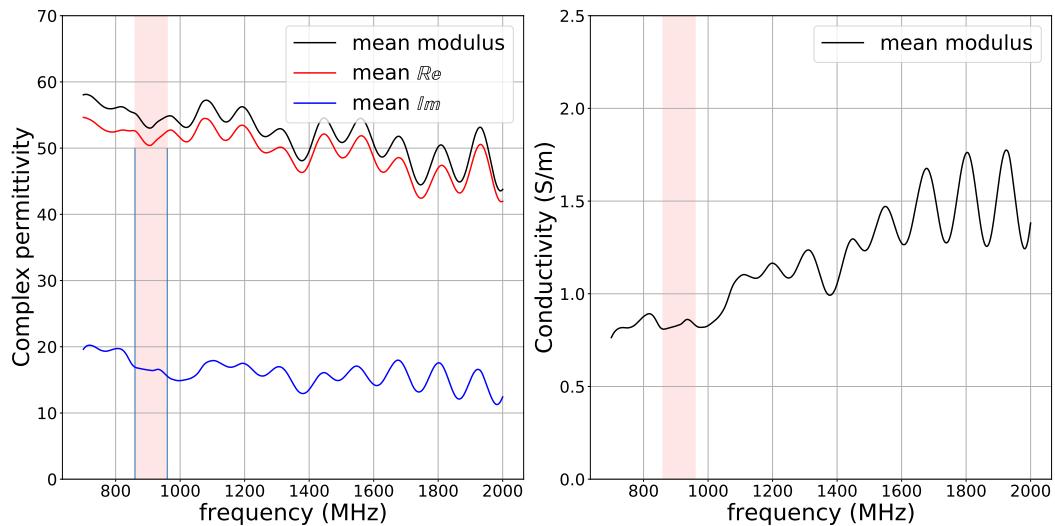


Figure 4.4 – External side - Dielectric measurement for the selected ear (Number 8)

In these two figures, the upper left corner axes correspond to the real (in red) and imaginary (in blue) parts of permittivity for internal (Fig. 4.3) and external (Fig. 4.4) sides of the ear. The upper right corner axes is the measured conductivity while the lower left corner is the loss tangent.

Each side (internal and external) were measured several times, and no significant variation on the permittivity and conductivity have been observed, which mean that the results are accurate and reproducible as we can see in the figures.



One can tell that the permittivity is decreasing w.r.t frequency whereas the conductivity is increasing w.r.t the frequency. Noting that the same observation can be found in [67].

The red zone in these figures corresponds to the frequency domain of UHF RFID around  $860\text{ MHz}$  and  $960\text{ MHz}$ . In this domain, for the internal side, we observe a permittivity  $\varepsilon_{int} \approx 36$  and the conductivity  $\sigma_{int} \approx 0.55\text{ S/m}$ , whereas, for the external side, the values are significantly higher where  $\varepsilon_{ext} \approx 52$  and  $\sigma_{ext} \approx 0.65\text{ S/m}$ . Which mean that the ear 8 does not have the same dielectric properties from both side, hence, it is a variation that should be taken into account when placing the tag on the ear. This will be further studied by placing the tag on each side of the ear 8 to see if there is any difference in the performance of the tag as the dielectric properties differs for each side.

### 4.3.3 Evaluation of dielectric property for a sample of 25 ears

Dielectric property measurements were conducted on all 25 pig ears, considering both the internal and external sides of each ear. The results indicated that the pig ears exhibit similar dielectric characteristics with significant variances. There are notable differences between the internal and external sides as observed for ear 8. The acquisition was carried out between  $700\text{ MHz}$  and  $2\text{ MHz}$  well beyond the frequency window used by RFID (represented by the pink vertical band).

Fig. 4.5 displays the evolution of complex permittivity and conductivity obtained from measurements on the internal side for all the 25 ears. The mean permittivity value, represented in blue, decreases from around 40 at  $200\text{ MHz}$  to 32 at  $2\text{ GHz}$ . In the UHF RFID frequency range (indicated in light red vertical region), the measured mean permittivity is around  $\bar{\varepsilon}_{int} \approx 37$ . As for the conductivity, it goes from  $0.5\text{ S/m}$  at  $f = 200\text{ MHz}$  to  $0.8\text{ S/m}$  at  $f = 2\text{ GHz}$ . In the frequency range of UHF RFID, the mean conductivity of the internal side is:  $\bar{\sigma}_{int} \approx 0.53\text{ S/m}$ . The median and mean are very close suggesting a symmetric underlying distribution.

Fig. 4.6 illustrates the average values of complex permittivity and conductivity obtained from measurements on the external side. The mean permittivity value, represented in blue (on the left), decreases from approximately 50 at  $200\text{ MHz}$  to 38 at  $2\text{ GHz}$ . In the frequency range relevant to UHF RFID (the red zone), the measured permittivity is approximately  $\bar{\varepsilon}_{ext} \approx 46$  around the value obtained in [67] as seen in subsec. 4.2.1. As for the conductivity in the right subplot, it is an increasing function of frequency. It goes from  $0.65\text{ S/m}$  at  $f=200\text{ MHz}$  to  $1\text{ S/m}$  at  $f=2\text{ GHz}$ . In the frequency range of UHF RFID,

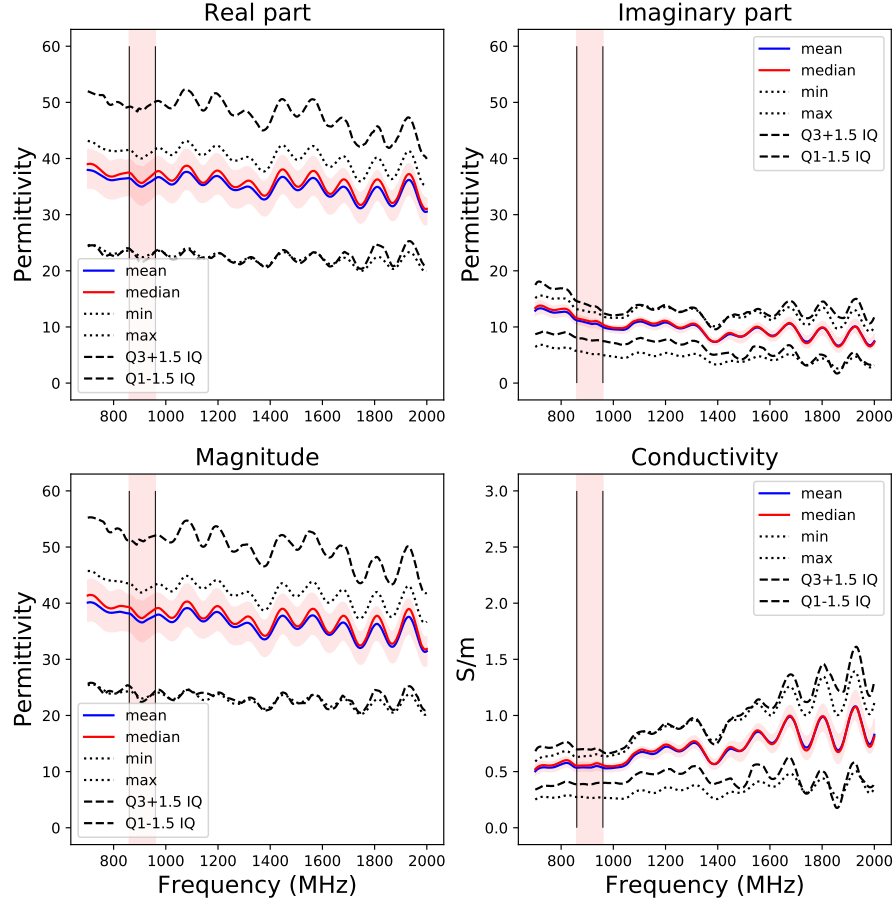


Figure 4.5 – Evolution of complex permittivity and conductivity w.r.t frequency - Internal side

the conductivity of the external side is:  $\bar{\sigma}_{ext} \approx 0.7 \text{ S/m}$  (around the value given in subsec. 4.2.1).

#### 4.3.4 Testing intern vs extern

In order to appreciate whether the difference observed between intern and extern side of the ear is statistically significant, we have performed a Welsh two sample t test for all frequency point testing the null hypothesis that intern and extern face of the ear are equivalent. The evolution of the p-value of this test with frequency shown in Fig 4.7 illustrates that we can firmly reject the null hypothesis for real part of the permittivity at

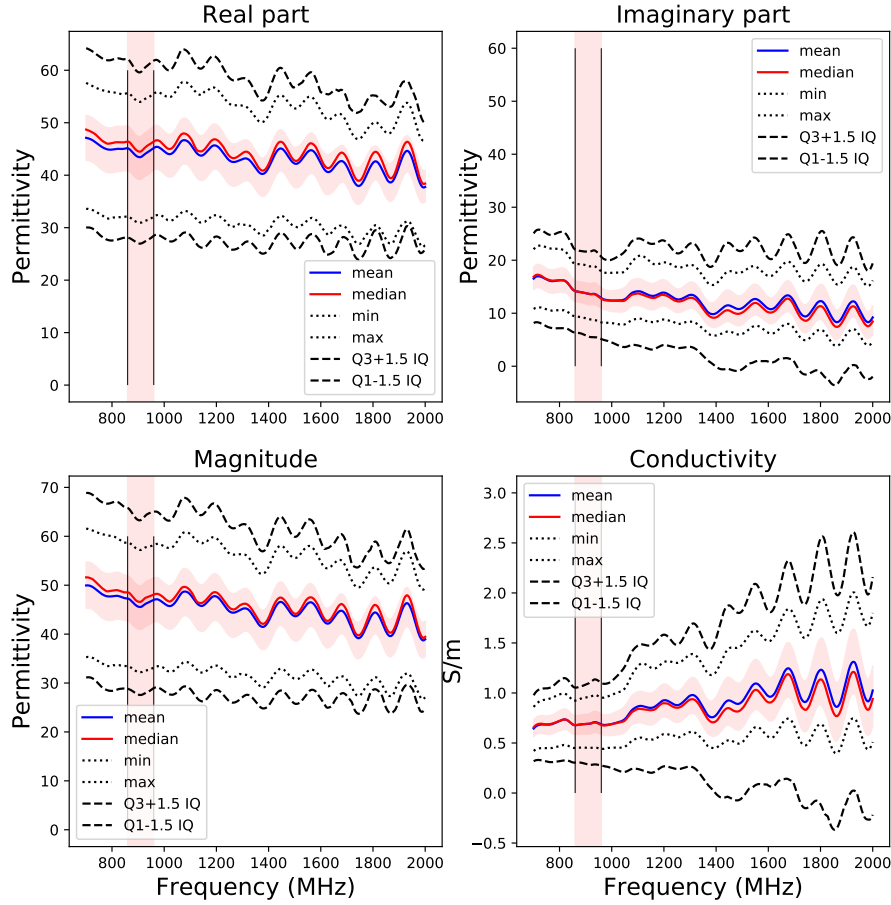


Figure 4.6 – Evolution of complex permittivity and conductivity (bottom right) w.r.t frequency - External side

very large confidence and larger than 95% (red horizontal line), even if the strength of the decision is getting weaker as the frequency increases for imaginary part. Notice that the p-value for conductivity and imaginary part of the permittivity are the same. This is simply because these two quantities are not independent and are deduced one from another.

### 4.3.5 Pig ear permittivity model

We assume from the observation that the distribution of the dielectric properties of the ears follow reasonably a Gaussian distribution. We will propose a Gaussian model for real

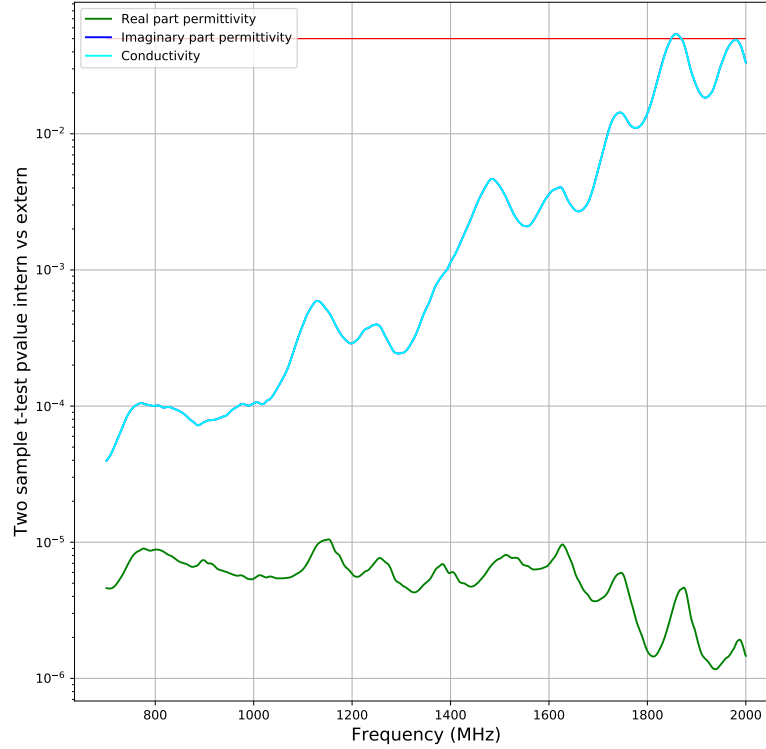


Figure 4.7 – Evolution of p-value w.r.t frequency in Two sample t-test testing Intern vs Extern

and imaginary part and for intern and extern side of the ear. In Fig. 4.8 the evolution of standard deviation is illustrated on the left side of the figure whereas on the right side is illustrated a conversion of the Inter Quartile into standard deviation under the assumption of a normal distribution. For a normal distribution the inter-quartile value is  $IQ \approx 1.36\sigma$ . This later information is less sensitive to possible outliers and potentially more robust as an estimator of the actual standard deviation. The different means and standard deviations proposed for the pig ear permittivity model are summarized in table 4.1.

Remarkably, there exists a discernible shift of approximately 10 units in  $\epsilon_r$  (permittivity) and about 0.2 units in  $\sigma$  (conductivity) between the inner and outer sides of the ear. This effect is reproducible and has been observed for all ears.

We can confirm that the measured values for the inner side are lower than those for the outer side due to variations in the types of porcine biological tissue presented on each

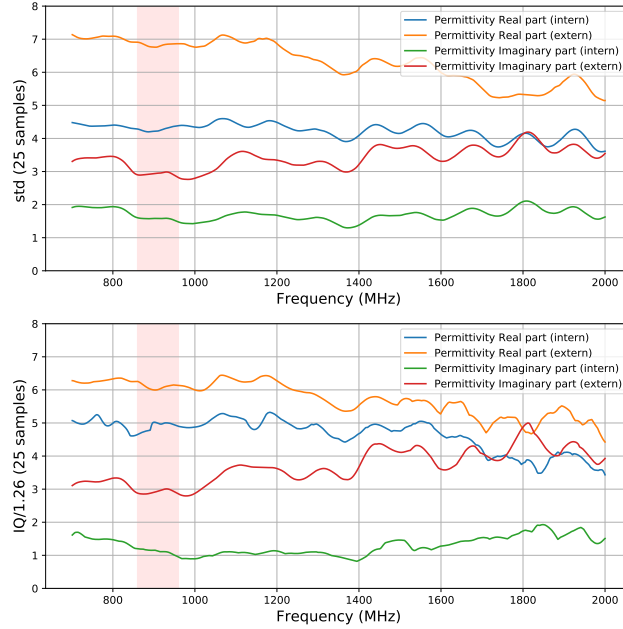


Figure 4.8 – Evolution of complex permittivity standard deviation w.r.t frequency, Intern and Extern, left (standard deviation), right ( $IQ/1.36$ )

	Mean	std
$\Re(\epsilon_r)$ intern	36	5
$\Im(\epsilon_r)$ intern	12	1.5
$\Re(\epsilon_r)$ extern	45	6
$\Im(\epsilon_r)$ extern	15	3

Table 4.1 – Gaussian Model for ear permittivity in [860,960] MHz band

side of the ear. This finding may lead to a difference in tag's performance when placed in internal and external side of the ear. Note that in practice, the tag is placed on the external face of the ear.

In conclusion, we observe a significant variability in permittivity values. Nevertheless, these measurements can help to design next RFID tags for pig ears. Our measurement could be used for designing new tag with realistic hypothesis on the ear properties and could be also used for designing specific phantom. Those results will be used later in the following sections in order to appreciate if there is any observable correlation between the dielectric nature of the ears and the read range performance of several tags (Sec. 4.4).

### 4.3.6 Analysis of the correlation between dielectric properties and ear weight

We do not observe any correlation between the dielectric properties and the ear weight.

A scatter plot illustrating this absence of correlation between ear weight and dielectric constant @868MHz is presented in Fig. 4.9. This result makes sense a posteriori.

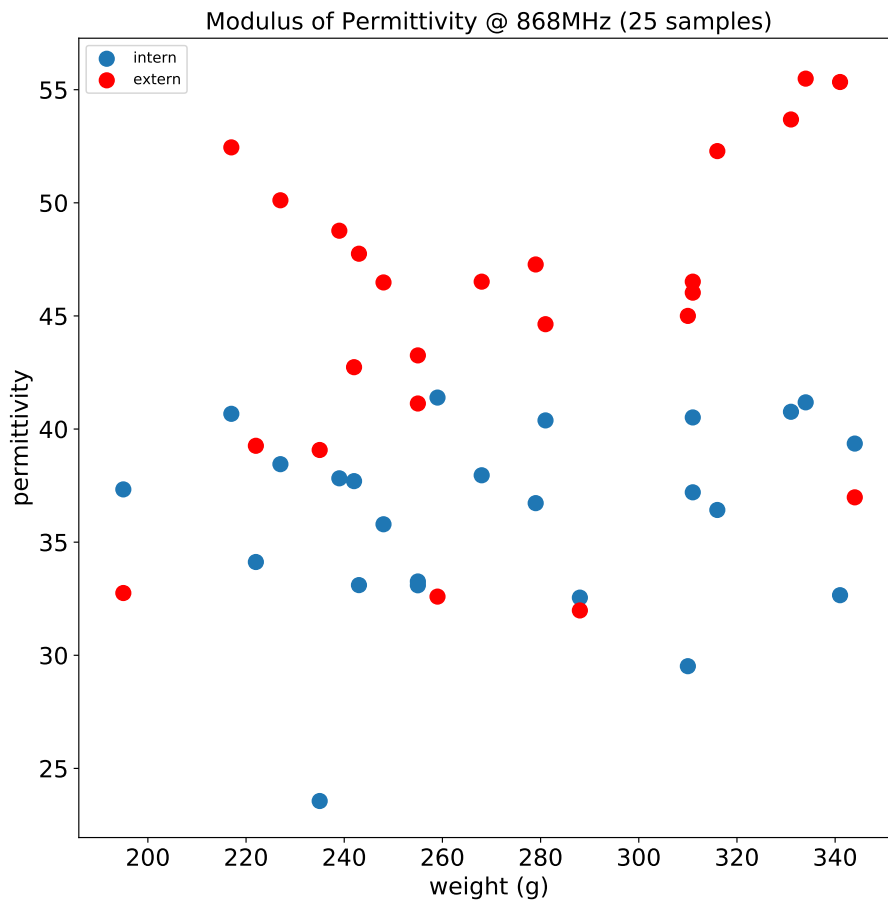


Figure 4.9 – Correlation between ears weights and their permittivities

## **4.4 RFID tags on pig ears orientation effect**

We have seen that the dielectric characteristics differs for the intern and extern side of the ear. In this section, we will investigate the effect of pig ear's orientation on the performance of the RFID tags essentially for the project needs, in order to find the best way to place the tag on the ear. Firstly, we will exploit the power profiles for the tags on ears with different orientation all by keeping the same environmental conditions to have an accurate comparison. Then the chart introduced in Chapter 3 will be utilized to evaluate and compare the performance of the tags for different orientation. The first experiments conducted for this project were involving different commercial tags based on different chips and different antennas. We also used the same ear 8 (characterised in subsec. 4.3.2) in this experiments in order to avoid getting performance's variation due to the ear's variability.

### **4.4.1 Definition of ear orientation**

In these measurements, the tag was fixed on the ear and was measured in 4 different orientations. for each measurement, we obtained the three defined power profiles.

We consider 6 tags, 2 of the same kind and for each of them we apply the measurement protocol : 1 translation (similarly as in sec. 3.8) and 1 rotation below the portal, for 4 different orientations. Note that the ear can be placed horizontally (H) or vertically (V) in front of the antenna. In addition, the visible part (from the antenna) of the ear can be the extern (E) or the intern (I) face.

So in summary we get the following orientations:

- Extern Horizontal (tag facing the ceil)
- Intern Horizontal (tag facing the floor)
- Extern Vertical (tag in the shadow of the ear)
- Intern Vertical (tag facing the front antenna 3)

### **4.4.2 Tag on ear measurements for different orientations**

The IETR platform was used to do the experimentation on the tags placed on ear in different orientations, firstly in a translation configuration (in front of front antenna 3 as shown in Fig. 3.1) and secondly in a rotation configurations (using antenna 0, 1 and 2 as shown in Fig. 3.3).

ID	Chip Type	$S_{cdBm}$	Type of Antenna
6A9 6A8	Impinj M730 [70]	-24	long meandering dipole
1000 2000	Monza 4i [56]	-17.4	bipolar
7816 C16	NXP Ucode 8 [58]	-22.9	Short meandering dipole

Table 4.2 – The different tags used: their ID, chip type, chip sensitivity and type of antenna

We used 6 tags with 3 different chips for these acquisitions. Table 4.2 shows more details about the tags used: their ID, chip type, chip sensitivity  $S_c$  and antenna type.

#### 4.4.2.1 Measurement of the tags on ear for different orientations

To obtain the power profiles in translation, we followed the same steps presented in the measurement setup in sec. 3.4.1 by varying the distance between the tag on ear and the fixed antenna from 0.15 m to 4.98 m, and by varying the transmitted power of the alien reader from 15.7 dBm to 30.6 dBm.

Fig. 4.10 illustrates the acquisition of the power profiles, in translation, for the 6 tags for 3 different types of chip when placed on ear for 4 different orientations. The transmitted and received activation activation profiles has been presented as well as the received power at the maximum transmitted power of  $P_t^{max} = 30.6 \text{ dBm}$ . The tag receptivity was also presented for each configuration, and thus, the tag could be compared and evaluated by extracting their intrinsic characteristics.

Moreover, Fig. 4.11 presents the values of the read range percentage  $\rho_{RR}$  defined in eq. 3.7.

We can notice two kind of effects on the read range results obtained:

— **Effect of the orientation:**

Regarding the impact of orientation, when the tag is situated internally, it is concealed by the ear. However, the ear's influence on the results appears to be relatively minor. Notably, there is not a significant difference between configurations like External Horizontal and Internal Horizontal, or External Vertical and Internal Vertical for example.

— **Effect of the type of tag:**



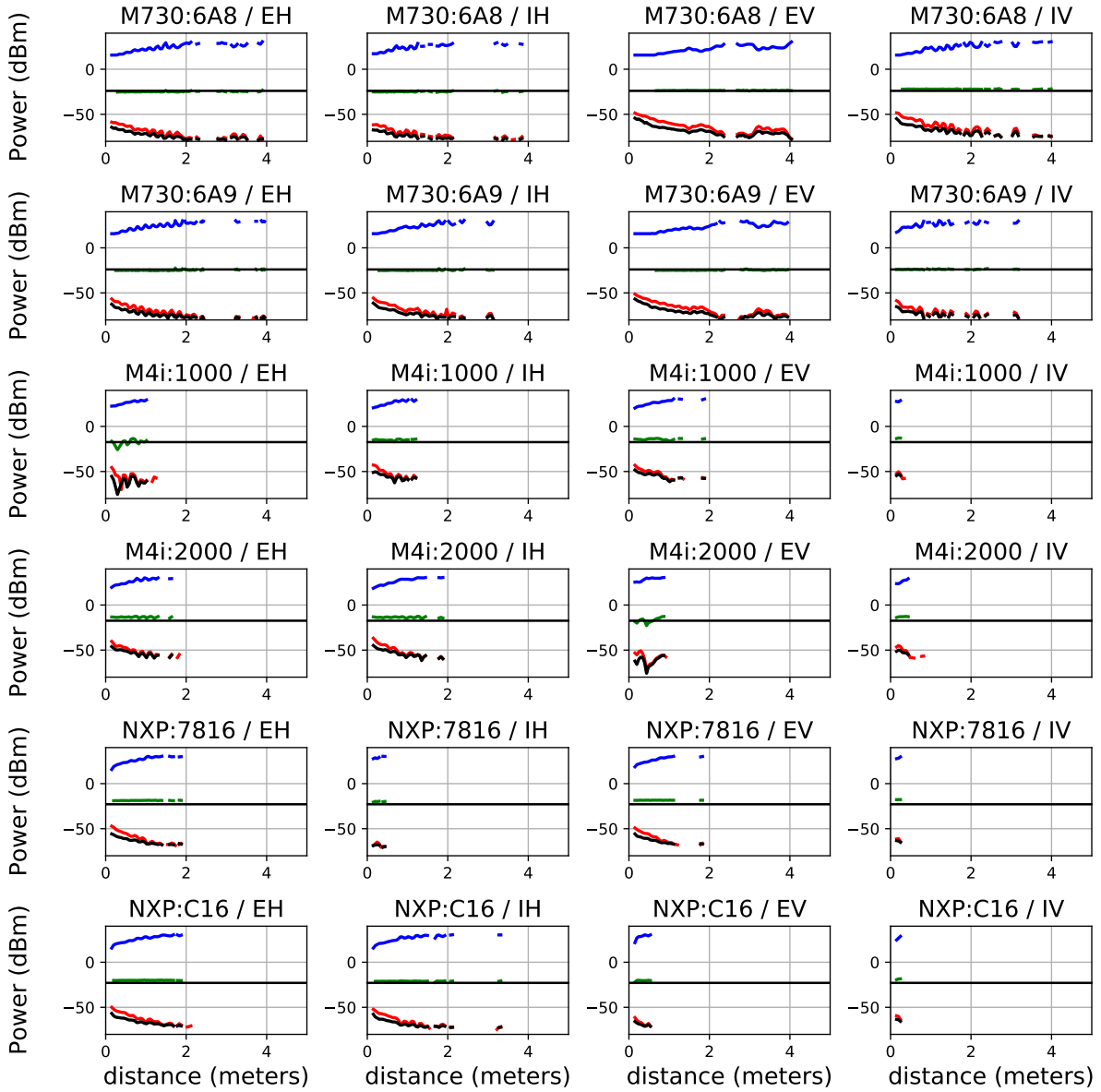


Figure 4.10 – Tag power profiles comparison of the NXP Ucode 8, M730 and Monza4 Tags for 4 different orientations

The tag of family M730 has much better performances than the two others : Monza 4i and NXP Ucode 8, where we can see in Fig. 4.11 that the tags with the highest  $\rho_{RR}$  are the M730 tags for all orientations, especially in EV where it reaches  $\rho_{RR} = 76.6\%$ . Whereas the worst performance is that of the tag NXP in IV orientation with a  $\rho_{RR} = 5.1\%$ .

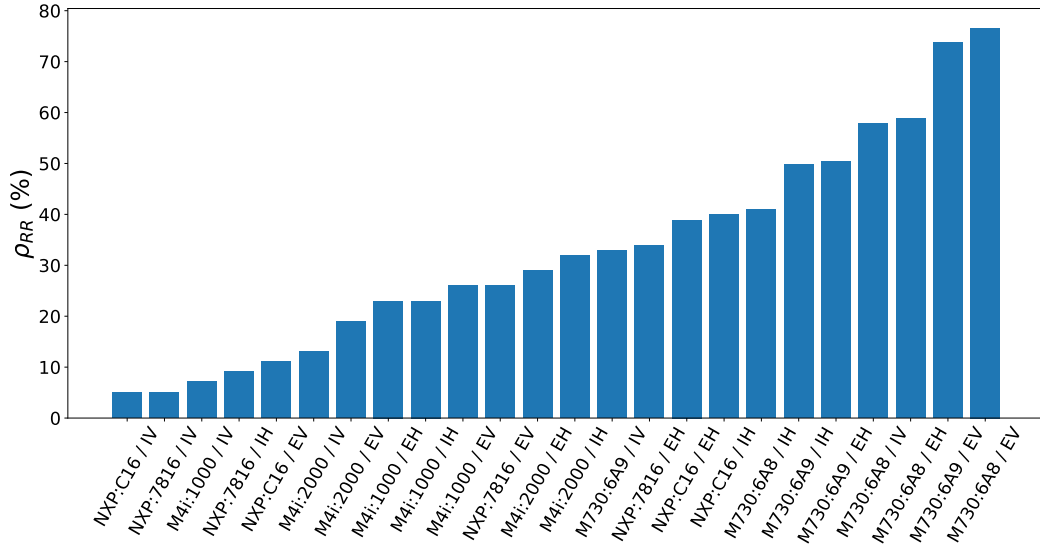


Figure 4.11 – Bar plot of the read range percentage of the NXP Ucode 8, M730 and Monza4 Tags for 4 different orientations

In addition, we measured the tags on ear with different orientation in a rotation configuration using the antenna 0, 1 and 2 of the platform (see sec. 1.5). The results are shown in Annexe C.

#### 4.4.2.2 Measurement of the tags without ear in horizontal orientation

Furthermore, we also measured the tags without ear to appreciate its effect on their performance. Fig. 4.12 illustrates the acquisition translation profiles for 2 different orientations (Horizontal and Vertical) and for 12 tags from 3 different kind (the tags used in the tag-on-ear acquisition (Fig. 4.10) is included) in free space situation (without ear).

In addition, we show in Fig. 4.13 the read range percentage  $\rho_{RR}$  obtained from the acquisitions. We can clearly see that the tag with the highest performance is the M730, followed by the M4i tag and lastly the NXP Ucode8 tag. These results show clearly that the tags without ears exhibit a significantly extended read range. Notably, the presence of ears had a significant impact on the performance of certain tags, particularly the Monza4 and NXP Ucode 8, which were barely detectable on the ear but achieved a high  $\rho_{RR}$  (between 60% and 80%) without the presence of an ear. In contrast, the M730 tags was the least impacted by the ear and maintained robust performance across different orientations in the presence of the ear. Therefore, we can conclude that the M730 tag is the most suitable

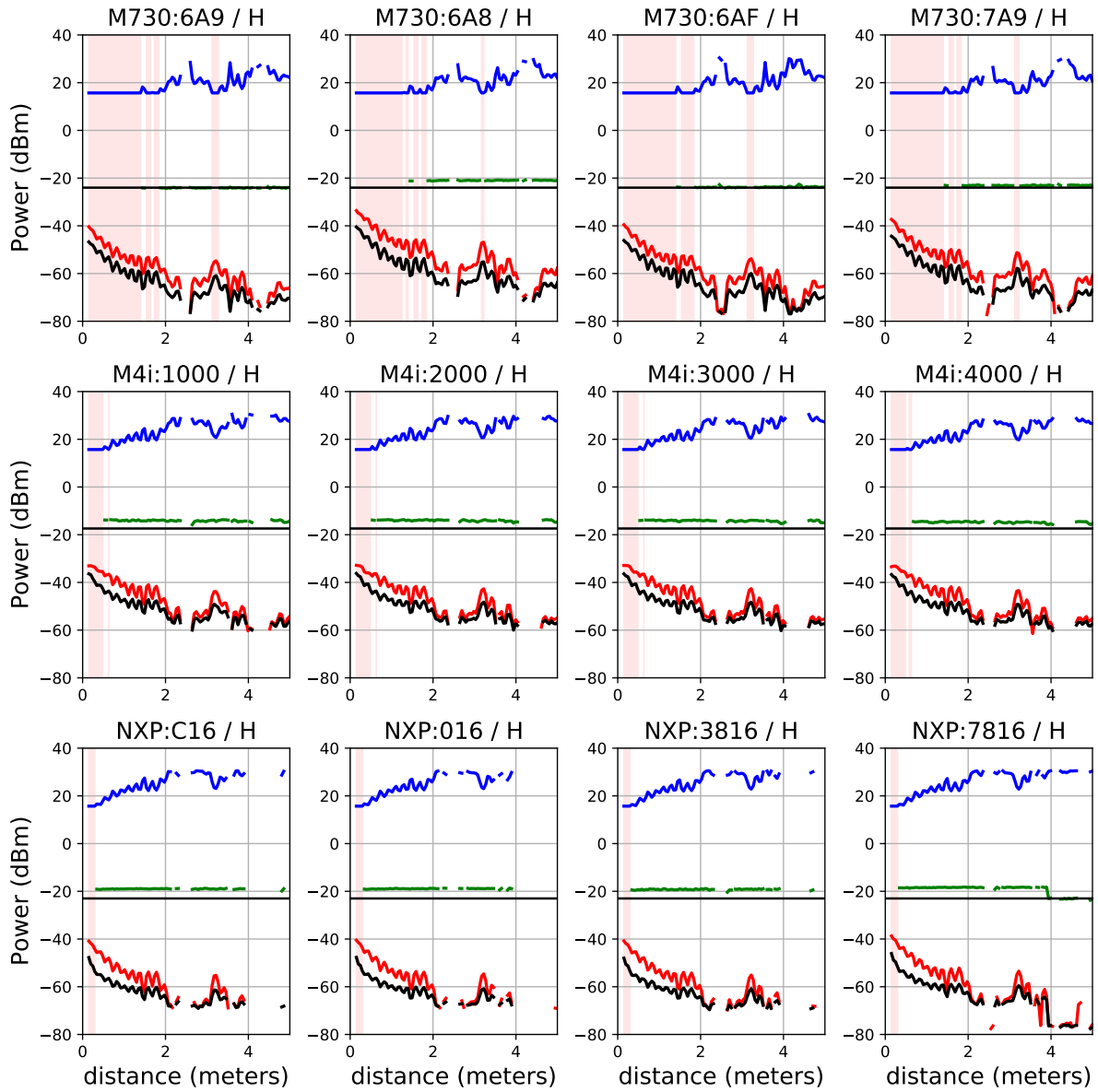


Figure 4.12 – Read range comparison of 4x3 NXP Ucode 8, M730 and Monza4 Tags

choice for ear-based applications compared to the other tags.

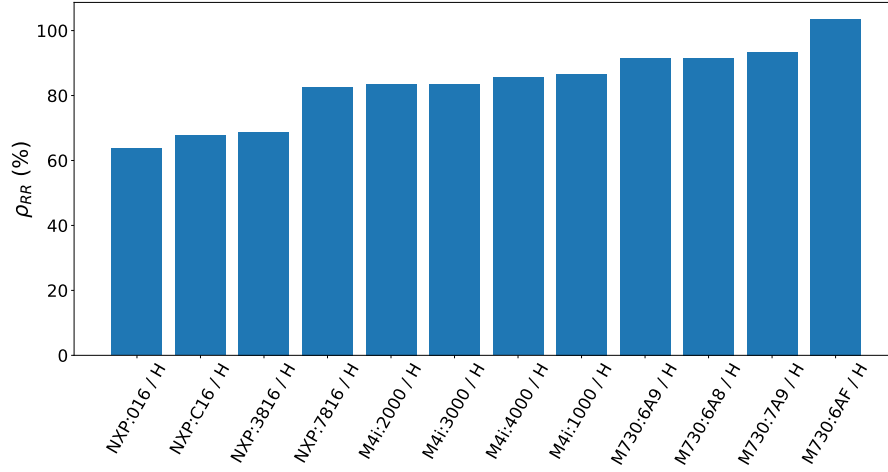


Figure 4.13 – Bar plot of the read range percentage of 4x3 NXP Ucode 8, M730 and Monza4 Tags in H orientation

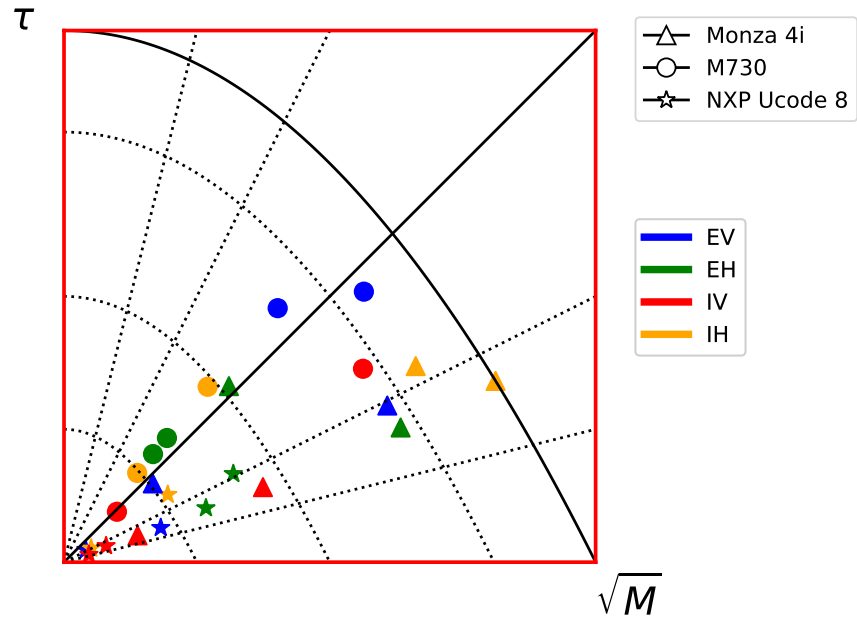


Figure 4.14 – Chart representation of the 12 tags for 4 different orientation in H orientation

#### 4.4.3 Evaluation of the ear and orientation effect using the $(\sqrt{M}, \tau)$ chart

After the activation profiles has been acquired, we can now compare and evaluate the tags in the chart. This task is possible since we have all the requirements to use the algorithm

(1): The  $Q$  values are obtained for all the configurations, in addition, since these tags on ear were measured under the same condition, the  $\tau$  ratio defined as  $t$  is also obtained. The chart representation of the tags on ears (for all orientations) is shown in Fig. 4.14 where no limitation on  $\tau$  has been applied in the algorithm.

It's evident from the chart that the tag characteristics, including  $\tau$  and  $\sqrt{M}$ , are influenced by the orientation and exhibit variations even among tags of the same type. Notably, the orientation that yields the least favorable tag performance is IV (in red), located closest to the chart's origin. However, as for the other orientations, it's challenging to discern a clear superiority among them.

Moreover, in terms of tag type diversity, the M730 tags, represented by circles, demonstrate superior performance, particularly in the EV orientation (depicted in blue).

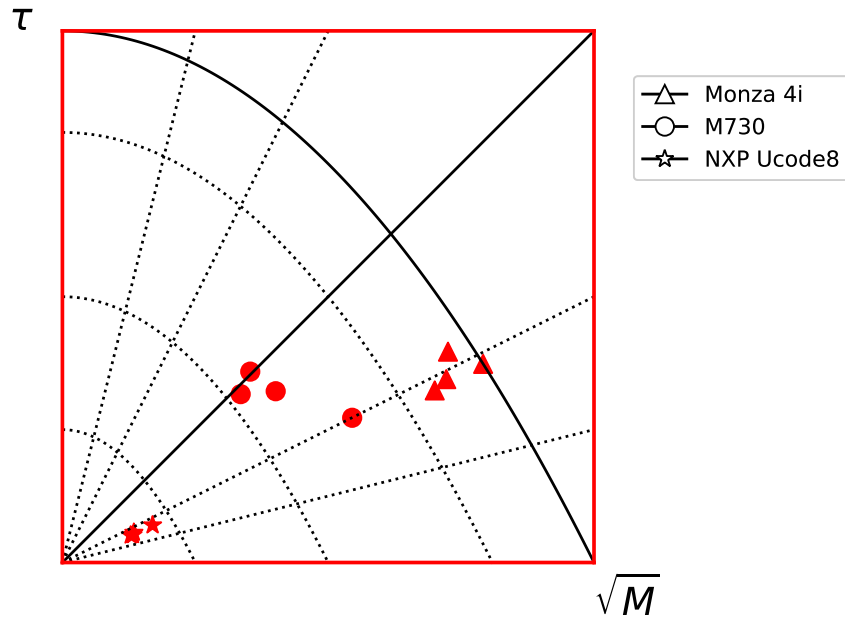


Figure 4.15 – Chart representation for NXP Ucode 8, M730 and M4i tags without ear in H orientation

Additionally, we utilized the  $(\sqrt{M}, \tau)$  chart to also evaluate these tags without ear. The resulting chart, depicted in Fig. 4.15, reveals three distinct clusters: one for the M730 tags (represented by circles), another for the NXP tags (stars), and a third for the Monza 4i tags (triangles). This clustering suggests that tags of the same type exhibit similar performance when not placed on the ear, in contrast to the variations observed when tags interact with the ear, as seen in Fig. 4.14. These findings underscore the substantial influence of the ear

on tag performance.

We can conclude that the characteristics of the tag can be affected by the ear and its orientation as it's affected by the electrical properties of the object attached to. The difference in dielectric properties between the inner and outer sides of the ear result in variations in the tag's performance when placed to either side.

## 4.5 Effect of tag response variability for different ears

In this section we study the effect of changing the ear on the performance of a single tag M730. This tag is chosen as being the one with the best performance as we have seen in the previous experiments. This same tag will be fixed on 15 different ears and the same experimental set-up is applied each time.

The overall runs along the 5 meters translation rail are summarized in Fig. 4.16 where all the power profiles are presented.

We clearly observe a difference in performance from ear to another. For instance, the best performance is observed for ear  $n^\circ 15$  ( $\rho_{RR} = 84.8\%$ ) while the worst is observed for ear  $n^\circ 5$  ( $\rho_{RR} = 23.2\%$ ). Upon noticing that, we would like to see if this variation in performance is correlated with the electrical characteristics that we measured for these 15 ears.

### 4.5.1 Correlation between the read range percentage of the tags and the tangent loss of the ears

Fig. 4.17 illustrates the read range percentage ( $\rho_{RR}$ ) obtained from the measurements presented in Fig. 4.16, alongside the loss tangent ( $\tan \delta$ ) for each of the 15 ears, derived from the studied dielectric properties detailed in Sec. 4.3. A discernible correlation between  $\rho_{RR}$  and  $\tan \delta$  is observable, with some exceptions (highlighted in red) potentially attributable to minor variations in tag placement on the ear. Notably, the regression reveals a decrease in the tag's read range percentage with respect to the loss tangent of the ear it is positioned on. The strong correlation coefficient  $R^2 = 0.88$ , excluding the four ears depicted in red, underscores this observation, while the overall set of ears yields a coefficient of  $R^2 = 0.43$ . Thus, we can infer that the tag's performance is indeed influenced by the variance in dielectric properties across different ears. A higher tangent loss of the ear directly corresponds to poorer tag performance.

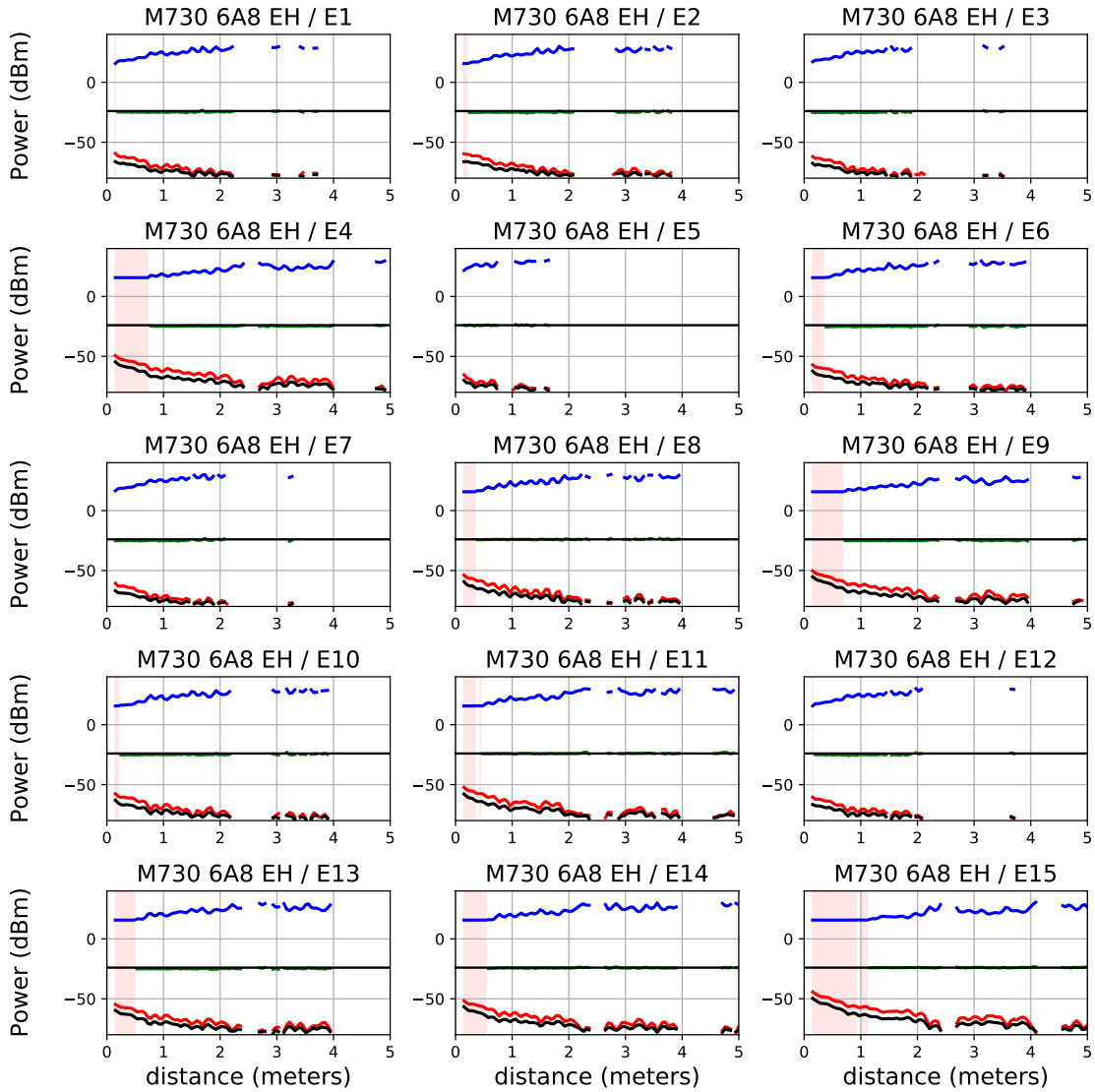


Figure 4.16 – Profiles representation for M730 in Extern Horizontal configuration for 15 different ears

It is worth noting that, in hindsight, the apparently arbitrary selection of ear 8 has proven to be a good choice in terms of performance, as it falls within the midrange of the distribution.

Efforts also were made to establish a relationship between these findings and the ear weights discussed in Subsec. 4.3.1; however, no significant association was observed between the performance order and these variables in this specific experiment.

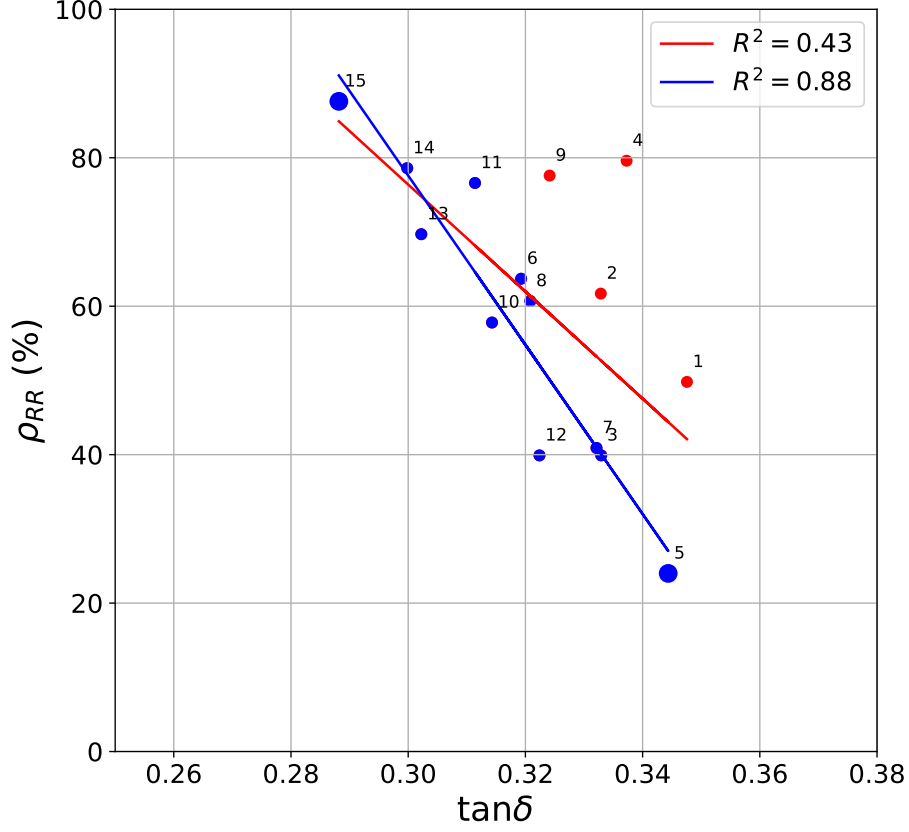


Figure 4.17 – Correlation between the read range percentage  $\rho_{RR}$  (%) with the loss tangent  $\tan \delta$  of the 15 different ears

#### 4.5.2 Correlation between the tag efficiency of the tags and the tangent loss of the ears

The other striking observation is that the reconstructed tag receptivity  $R^{th}$  appears to be a good invariant from ear to ear and very close to the chip sensitivity  $S_c = -24 \text{ dBm}$ , which gives us a Q values quasi-equal to 0. This information is graphically represented in the  $(\sqrt{M}, \tau)$  chart in Fig. 4.18, where the tag positions align closely with the diagonal Q line for all ears. It's worth noting that no constraints were applied to  $\tau_{lim}$  in the algorithm. For instance, in the case of ear n°15, the value of  $\tau_{max}$  is  $\varphi^{-1}$ , which, as we have seen, corresponds to the ear that gives the highest observed read range. Conversely, for ear n°5, the tag is positioned closest to the origin, reflecting the poorest performance.



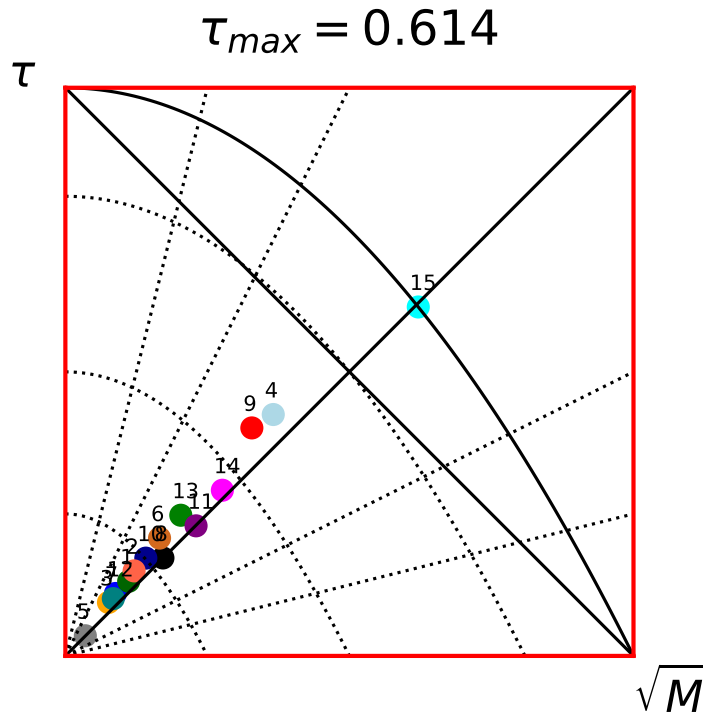


Figure 4.18 – Chart representation of the M730 tag placed on 15 different ears

Furthermore, to assess the relationship between the tag's performance and the tangent loss of the tag ( $\tan \delta$ ), we computed the tag efficiency of the tag ( $\gamma$ ) for all 15 points, as defined in eq. 2.63. The results of the  $\gamma$  values in terms of  $\tan \delta$  are depicted in Fig. 4.19. This figure includes two regression lines: the red regression line is derived from all 15 ears, whereas the blue regression line excludes ear 15, known for its superior performance, along with the three abnormal cases (ear numbers 4 and 9, as previously discussed). Notably, a significant correlation is observable between the tag efficiency  $\gamma$  of the tag and the tangent loss  $\tan \delta$ , evidenced by an  $R^2$  value of 0.86 for the data excluding abnormalities and 0.38 for the complete dataset. We can see clearly that the tag efficiency  $\gamma$  decreases as the tangent loss  $\tan \delta$  increases.

In conclusion, our evaluation methodology has successfully demonstrated a clear correlation between the dielectric properties of the ear and the performance of the tag.

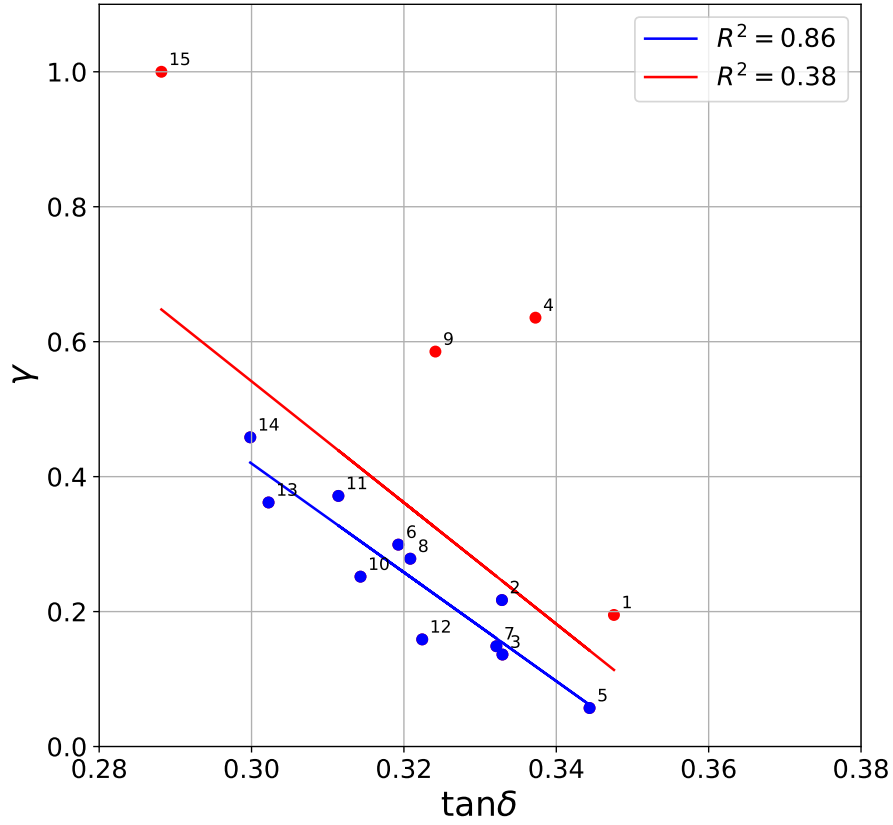


Figure 4.19 – Correlation between the tag efficiency  $\gamma$  of the tags and the tangent loss  $\tan \delta$  of the ears

## 4.6 ARDES tags characterisation

As part of the CAA-CONNECT project, our primary objective was to thoroughly characterize the tags designed and developed by our partner, ARDES. These tags were specifically designed to work efficiently on pig ears. This is where the significance of the dielectric analysis we conducted becomes evident, as it can play a crucial role in designing an antenna that would be well-suited for the unique dielectric properties of pig ears.

In the course of this project, we initially received the ARDES tags Version 2 (V2) from our partner. Subsequently, we conducted the first measurement campaign to evaluate the performance of these tags when placed on pig ears. Later on, we received both ARDES

tags V3 and V5 and evaluated them in the second measurement campaign. All of these assessments were conducted using our established methodology. It's worth noting that these tags were based on the NXP Ucode 9 chip, which boasts a chip sensitivity of  $S_c = -24dBm$ .

In this section, we present the results of our evaluation of the ARDES tags for the 3 versions V2, V3 and V5.

#### **4.6.1 ARDES tags V2, V3 and V5 comparison**

We made the same experiments on all the ARDES tags to exploit their power profiles. We gathered the results obtained on one tag V2, one tag V3 and one tag V5, in order to compare all these versions. Fig. 4.20 represents a comparison between these tags. Noting that the tag A/version 3 and tag A/version 5 were measured in the same day and on the same ear (second measurement campaign), whereas the tag A/version 2 was measured in a different day and different ear (first measurement campaign), so it may have an impact on the comparison, however, by looking at the Fig. 4.20, we don't notice significant difference between V2, V3 and V5 tags. In term of read range its almost the same for all of three tags compared on the same orientation.

Furthermore, we present the tag in the  $(\sqrt{M}, \tau)$  chart displayed in Fig. 4.21 where no limitations are imposed on  $\tau$ . This chart provide us with a better evaluation of the tags that is hard to exploit by only looking at the profiles representation. The V3 tag particularly exhibits slightly superior performance compared to the others especially in IH orientation where it achieved the highest  $\tau$  value of 0.37 at this orientation. Followed by the V5 tag, which ranks second in terms of performance. Lastly, the V2 tag is closest to the origin and demonstrates comparatively lower performance.

We can conclude from this results that the ARDES tag V3 is the one most adapted to work on pig ear.

### **4.7 RFID tags on pig ears in different planar configurations**

The objective of this section is to investigate the impact of tag on ear response when it is placed in proximity to other tags that are fixed to the ears. This experiment is inspired

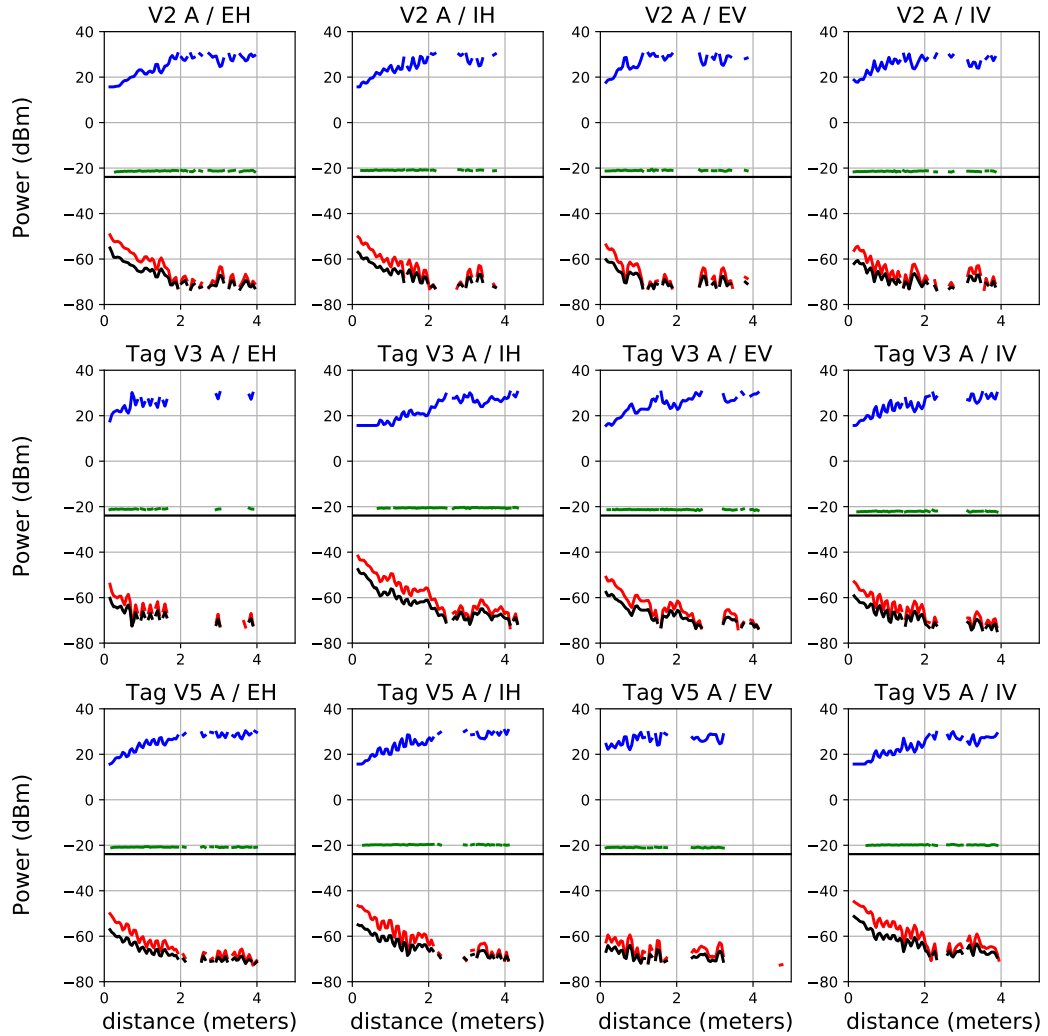


Figure 4.20 – All Versions of ARDES Tags on ear read range comparison for 4 different orientations

by a prior study [71], which delved into the effects of mutual coupling on the intrinsic characteristics of antennas. This study explored scenarios where a large number of RFID tags were densely concentrated within a confined space. In our work, we aim to analyze this impact by situating a number of ear-tagged RFID tags in close proximity to each other within a small volume.

To examine this phenomenon, we conducted various group experiments involving the placement of multiple RFID tags on a single plate. The plate was then translated to assess the performance of these tags when they respond simultaneously. Notably, we employed two different RFID readers to estimate differences in reading accuracy. The results from the

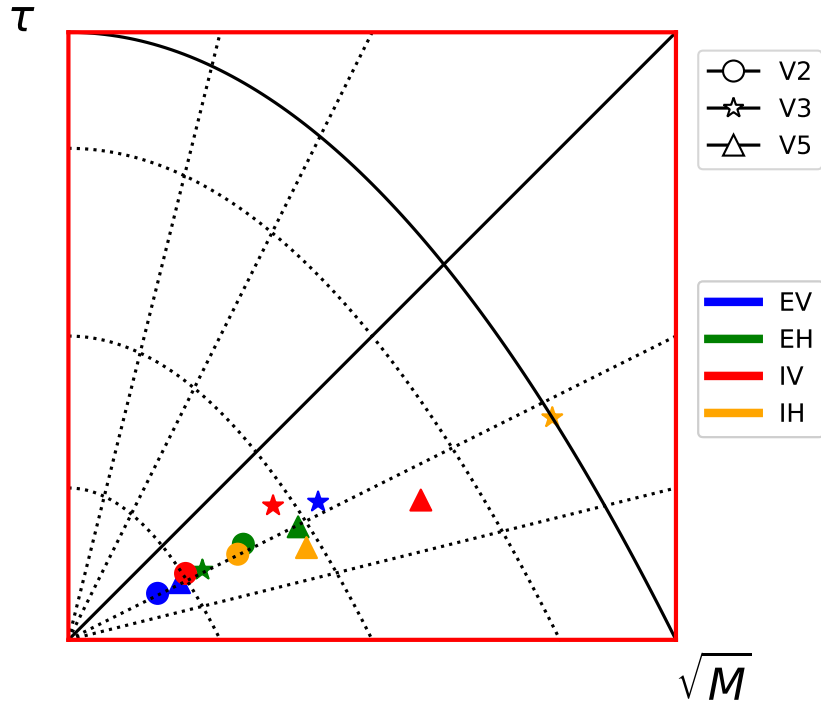


Figure 4.21 – Chart representation of ARDES tags

alien reader 9900+ acquisitions are graphically presented in Fig. 4.23, while the outcomes from the impinj R700 reader are depicted in Fig. D.5 of the Annex D.

#### 4.7.1 Results analysis of Group of tags aquisition

Fig. 4.23 illustrates all the measures on a set of 6 tags (two V2 tags + two V3 + two V5) for the 6 configurations which has been tested. The objectives of this work is to distinguish the influence of the tag from its position in the group of 6 tags by comparing different configurations with different spacing between the tags and different positioning. The measurement on every configuration (except configuration 5) has been made using two reader (Alien reader and Impinj reader), so another objective is to compare the measurement of the two readers. In order to do so, five configuration has been setted up:

- Configuration 1 (Fig. 4.22): this configuration is made with a spacing between tags of 30 cm. Noting that the wavelength is 34.56 cm at 868MHz. The step of displacement is 48 mm on a 5 m rail.

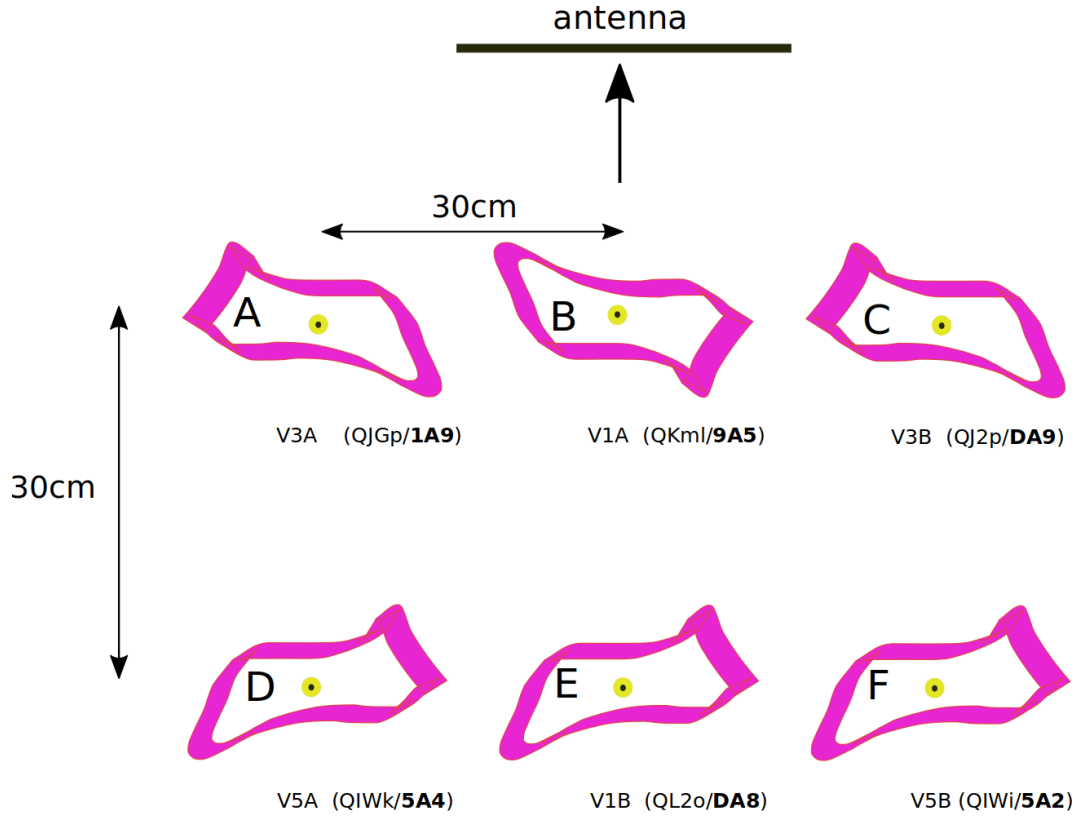


Figure 4.22 – Mosaic of Configuration 1

- Configuration 2 (Fig. D.1): similar to configuration 1 but with a rotation of 90 degree.
- Configuration 3 (Fig. D.2): similar to configuration 2 but with increase of the distance between the ears which corresponds to the wavelength of 34.6cm in this configuration.
- Configuration 4 (Fig. D.3): similar to configuration 3 but with a rotation of 90 degree (back to the group positioning of config 1 ).
- Configuration 5 (Fig. D.4): adjusting the configuration 4 by a rotation of 180 degree.

The results presented in Fig. 4.23 contains the power profiles for every tag in every configuration, each row represents a configuration from configuration 1 (C1) in the first row to the configuration 5 (C5) in the fifth row, whereas each column represents a specific tag. We can notice by looking at the results that the performance of the tag in group reading are degraded w.r.t tag alone configuration. Furthermore, the response from a given tag presents strong similarities from one configuration from another. For example, the tag V2A has a very good performances compared to the other tags in a group. In the other hand, we don't notice a significant improvement from V1 to V3 and V5. Regarding the effect

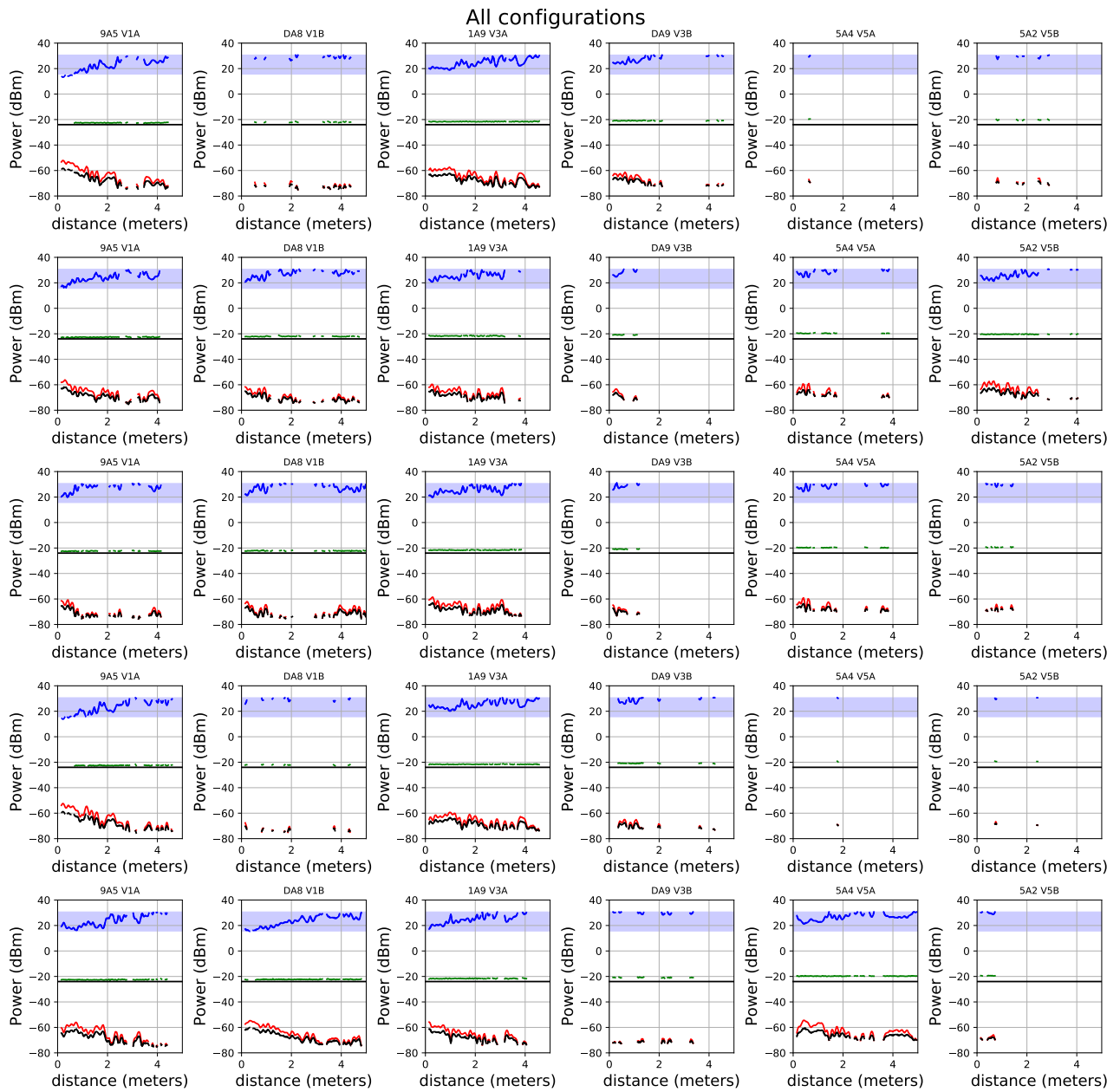


Figure 4.23 – Measured profiles for all configurations with Alien 9900+ reader

of changing the position of a tag and the spacing between the tags, we can compare the Horizontal configurations (C1,C4,C5) versus the vertical configurations (C2,C3), so as we can see there is not big difference between C1 C4 whereas C5 shows a better performances for all the tags. As for the vertical configurations, C2 shows a better performance than C3

where the spacing is higher.

We repeated the experiments by using the Impinj reader instead of using the Alien reader. The results are represented in the Fig. D.5.

This experiment is helpful for the CAA-Connect project as it show how the tag on pig ear would behave in a real world scenario where it will be surrounded by a group of other tags.

## 4.8 Conclusion

In this chapter, we delved into a comprehensive exploration of RFID technology in the context of livestock management, with a specific focus on pig ears. The research conducted as part of CAA-CONNECT, a collaborative project with Cooperl and ARDES aimed to enhance the functionality of RFID systems in farm environments by considering environmental factors such as the impact of pig ear on the performance of the UHF RFID tag.

We also discussed the state of the art of using UHF RFID technology for tracking and managing livestock, especially pigs. This technology has the potential to bring automation and data collection to farming, but it's not without its challenges. We presented in the state of the art the dielectric properties of the porcine skin, which is important when designing the tag to work properly on pig ear. This state of the art also showed the impact of the position of the tag on the ear on its performance.

Thereafter, we presented our work, which started by studying the characterization of pig ears dielectric properties, where we noticed a difference in these properties from intern and extern side of the ear. After that, we illustrated the two measurement campaigns that we did: in the first, we looked at how different kind of tags placed on pig ears behaved, considering things like the orientation of the ear and how it influenced the tag's reach. We also studied the effect of tag variability on the read range, using a single ear. In the second campaign, we tested different versions of ARDES tags, which are designed to work better on pig ears, in various setups. We then presented measurements of a set of ARDES tags on pig ears, placed in different Planar Configuration in order to observe if the tag response will be influenced by the its surrounding.

This chapter's findings are of significant importance for the project specially for our partner ARDES for whom we evaluated and compared different tag design versions.



## Summary

- **Dielectric characteristics of pig ear exploration:** In this chapter, we initiated a comprehensive exploration of the dielectric characteristics of pig ears, highlighting the discernible differences between the inner and outer sides of the ear. These findings provided us with essential insights into the material properties of the pig ear, which can significantly impact RFID tag performance. We have proposed a pig ear permittivity model for intern and extern side of the ear.
- **Orientation effect study:** We conducted a thorough investigation into the effect of ear orientation on tag performance. We examined variations in performance between the inner and outer sides of the ear, as well as between horizontal and vertical ear orientations. This analysis sheds light on how the positioning of the ear can influence RFID tag behavior.
- **Tag response variability analysis for different ears:** In this chapter, we analysed the impact of ear variability on the performance of a single RFID tag. By understanding how tag performance varies across different ears, we gain valuable information for practical applications involving diverse ear shapes and sizes.
- **Performance evaluation of ARDES tag:** We assessed the performance of the ARDES tag, our project partner's RFID tag, when placed on the ear. This evaluation was conducted using the methodologies we explained in previous chapters.
- **Multi-Tag response in planar configuration:** This chapter also examined the effects of multiple RFID tags responding within a planar configuration. Understanding how multiple tags interact in this setup is vital for optimizing system performance in livestock scenarios where multiple tags may be present.

# CONCLUSIONS AND PERSPECTIVES

---

## Conclusion

This PhD thesis has made significant and comprehensive contributions to the field of UHF RFID technology. The research has not only deepened the theoretical understanding of UHF RFID but has also bridged the gap between theory and practice through extensive experimental characterizations and evaluations of passive tags over-the-air. The following key contributions and findings have emerged from this thesis:

- **Theoretical Contribution:** In our thesis, we have provided a thorough exploration of the theoretical aspects of UHF RFID technology. This exploration delved into the intrinsic characteristics of UHF RFID tags, including the mean power transmission coefficient  $\tau$  and modulation factor  $M$ . We've highlighted the concept of **channel reciprocity** and the generalization of the channel coefficient in multipath environment, which has been the key to access the **tag receptivity**, a relation of the intrinsic characteristics of the tag over-the-air. Additionally, we've presented and analysed the formulation of the free space read range, considering the limitations imposed by the forward link and backscatter link. This comprehensive analysis has laid the foundation for a deeper understanding to achieve the optimum design of the tag in a specific scenario

Furthermore, within the context of our thesis, we've proposed a  $(\sqrt{M}, \tau)$  chart. This chart serves as a valuable visual representation tool for analysing and evaluating UHF RFID tag performance. By using this chart, we can access the optimum matching between the chip and the antenna of the tag, thereby improving tag design and performance.

- **Experimental Characterizations:** We conducted extensive practical experiments to characterize and evaluate UHF RFID tags based on the theoretical methodologies we presented. Initially, we proposed a formula for converting the RSSI of the alien 9900+ reader into real received power units in dBm, as this formula was not provided by the manufacturer. This conversion was an important step in our evaluation process.

---

Using the measured power profiles in dBm, we then proceeded to evaluate and compare a set of commercial UHF RFID tags. We accomplished this using the proposed  $(\sqrt{M}, \tau)$  chart, which allowed us to visually assess and compare their performance based on a balance between the mean power transmission coefficient and the modulation factor. This balance is chosen implicitly when the reader sensitivity is not known.

Additionally, we delved into the analysis of the read range in a free-space condition and its correlation with the intrinsic characteristics of the tag, the chip sensitivity and the reader sensitivity. This investigation provided valuable insights into the factors which influence tag performance. This work brings the possibility of obtaining an optimal design of the tag when the reader sensitivity is known.

Moreover, we conducted experiments to investigate the non-linear behavior of the tag. Specifically, we demonstrated experimentally how varying the tag's incident power affected its modulated power. Furthermore, as part of our research, we presented a scanning of the reciprocal channel. This was achieved by using a linear configuration of similar tags, which allowed us to gain a deeper understanding of the tag-to-reader communication multipath propagation. This knowledge of the multi-path channel is useful for phase-based localization in future work.

- **Collaborative Project and Application:** Our collaboration with the Cooperl company, a prominent figure in the pork industry, has enabled us to assess UHF RFID technology in a practical agricultural setting. The RFID tags, which were produced by our project partner, ARDES, underwent comprehensive experimental testing and evaluation on pig ears by using our developed methodologies.

Throughout the course of our research, my thesis has presented the results of extensive measurements conducted to determine the dielectric properties of pig ears. These measurements have yielded to differentiate between the dielectric characteristics of the inner and outer side of the pig ear. We explored the influence of this finding on the behavior of the tag for different orientation of the ear. In addition we conducted measurement of one tag on different ears to appreciate the variability of the tag behavior when placed in different ears and found a correlation between the dielectric properties of the ear and the performance of the tag placed on it. Moreover, we explored the influence of the tag on ear by its surrounding tags by conducting measurements of a set of Ardes tags in a Planar configuration responding simultaneously.

The insights gained from our research have played a pivotal role in reporting func-

---

tional performance evaluation for different tag versions of our partner ARDES . This proposal takes into account various factors related to signal propagation and the unique environmental conditions encountered in agricultural settings. With these findings, we aim to advance the comprehension of RFID tag on ear behavior in practical farming applications for the project CAA-CONNECT.

In conclusion, this PhD thesis has significantly advanced the characterization of UHF RFID tags. Through a comprehensive exploration of theoretical foundations, extensive experimental characterizations, and the evaluation of RFID systems in real-world scenarios, this research has contributed to the improvement and optimization of UHF RFID technology across diverse industries and applications. The findings and insights gained from this thesis provide a valuable basis for future research and development in the field of RFID technology, specifically in seeking an optimal design for a tag that can reach a better read range.

## Perspectives

The research conducted in this thesis introduces valuable methodologies for analyzing the attributes of RFID tags in an over-the-air context.

RFID tags play a crucial role in RFID systems, and researchers are continuously working to improve their design. Our experiments and evaluations provide useful information that could significantly boost RFID technology, especially in terms of creating better passive tags.

Looking ahead, the methodologies outlined in this study serve as a robust foundation for future investigations aiming to fine-tune tag design. A particularly promising avenue involves manufacturing an optimal tag using the optimal antenna, impedance considering the both chip states 1 and 2. This strategic approach aims to harness the maximum absorption and backscatter capabilities of the tag, thus pushing the boundaries of RFID performance.

Another perspective of this work is the possibility to create a model for the pig ear using the dielectric characteristics that we discovered and which differ the inner side from external side of the ear. By using the unique characteristics we've identified, this model could be useful for customizing tags specifically for pig ears. It could also help distinguish between the inner and outer sides of the ear, which is crucial for effective RFID use in animal

---

tracking and management.

By shedding light on these important avenues, our work not only contributes to understanding RFID technology but also its potential applications in various fields, including animal breeding.

# ANNEX A

In this annex, we provide additional details and figures on the effect of varying  $P_{inc}$  on the intrinsic characteristics of a set of 9 measured tags:

## A.1 Variation of $\Delta P_r$ in term of $\Delta$ for 9 different tags

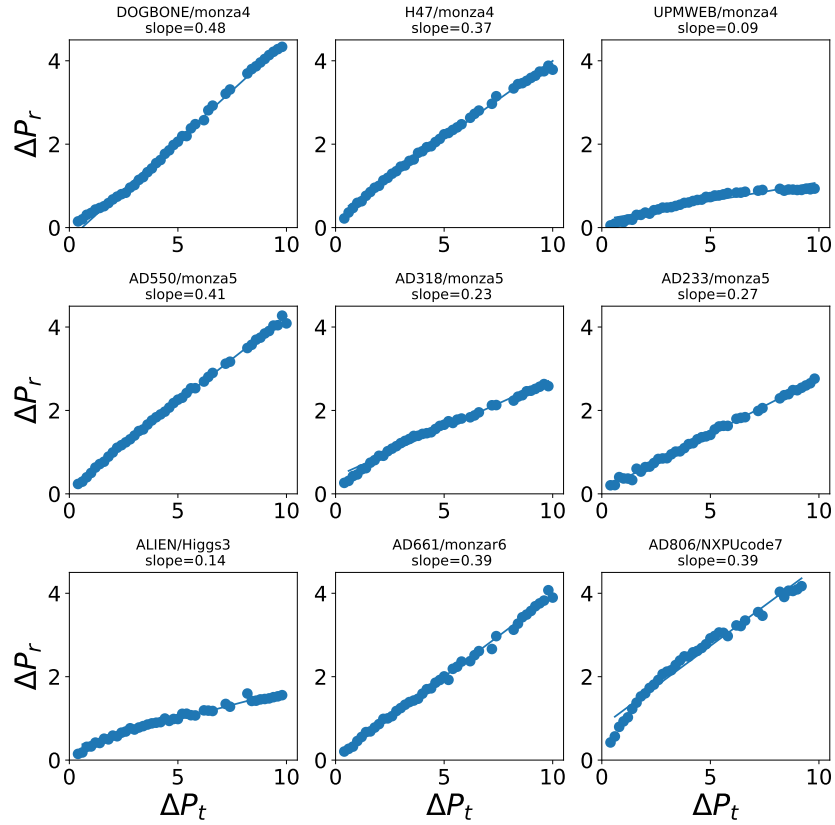


Figure A.1 – Variation of  $\Delta P_r$  in term of  $\Delta$  for a set 9 different tags

## A.2 Evolution of $\sqrt{M}$ in term of $\Delta$ for 9 different tags

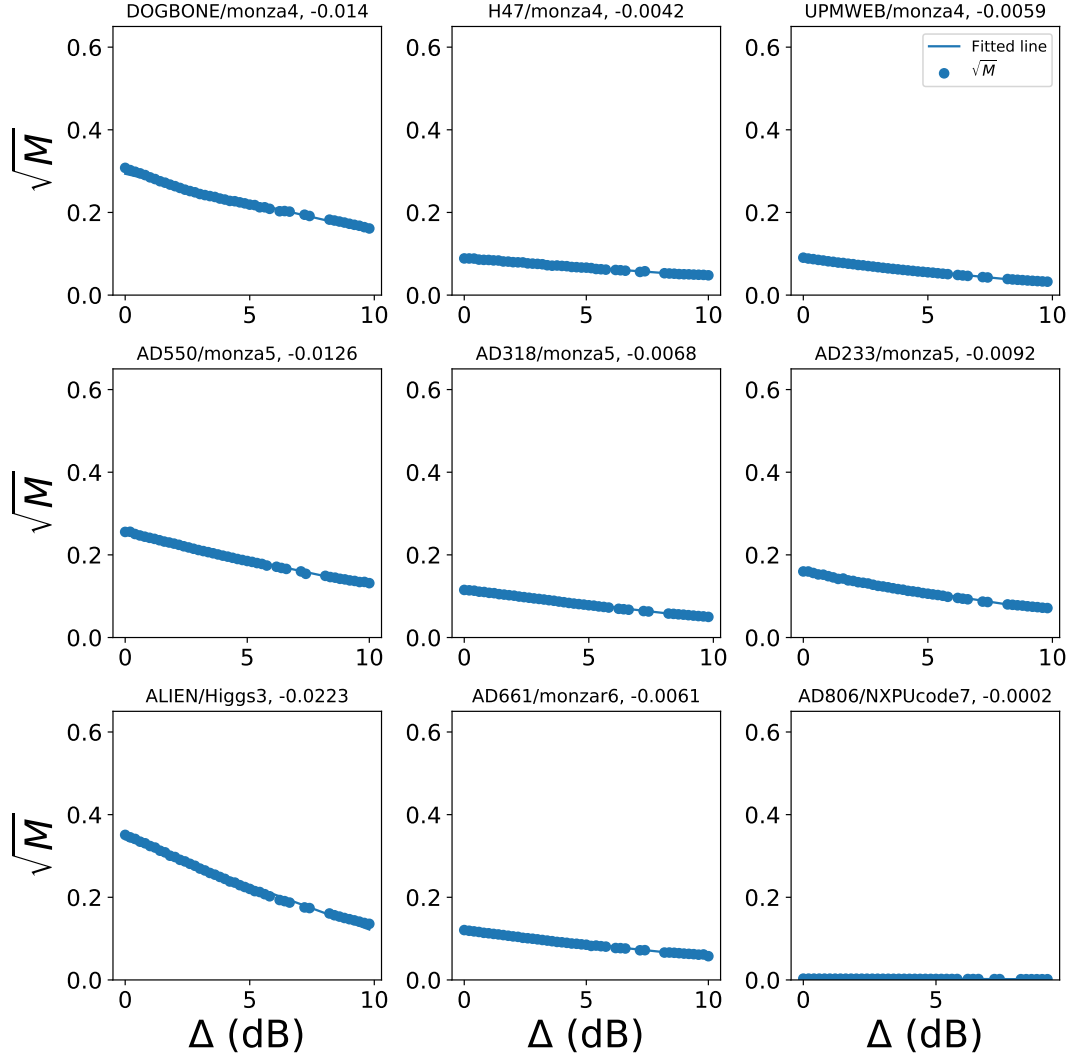


Figure A.2 – Representation of the Evolution of  $\sqrt{M}$  (in linear) in term of  $\Delta$  in dBm scale (or similarly  $P_{inc}$ ) for 9 different tags

## A.3 Extrapolation of the two activation profiles for 9 different tags

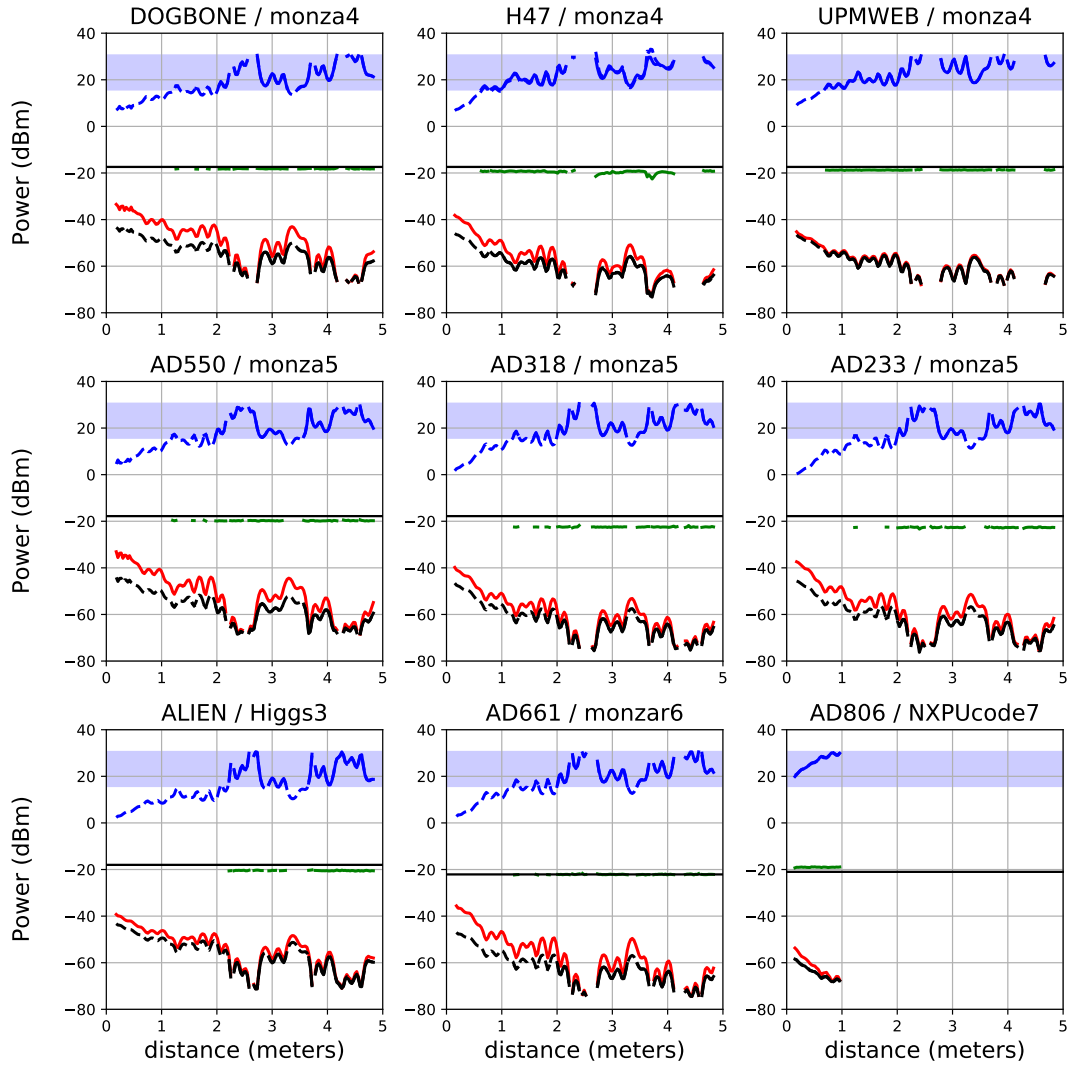


Figure A.3 – Representation of the extended power profiles for the 9 tags



# ANNEX B

---

This annex presents a sequence of calculation which explains the expression 1.24 and 1.25 presented in [66].

We define the 3 following impedances:

$$Z_1 = R_1 + jX_1$$

$$Z_2 = R_2 + jX_2$$

$$Z_a = R_a + jX_a$$

Respectively, the 2 state impedances of the chip and the impedance of the antenna.

The two reflexion coefficients are respectively:

$$\Gamma_1 = \frac{Z_1 - Z_a^*}{Z_1 + Z_a} \quad (\text{B.1})$$

and,

$$\Gamma_2 = \frac{Z_2 - Z_a^*}{Z_2 + Z_a} \quad (\text{B.2})$$

The modulation factor is then given by:

$$M = \frac{|\Gamma_1 - \Gamma_2|^2}{4} \quad (\text{B.3})$$

The aim is to maximize M by adjusting the antenna impedance value.

If we develop M as a function of its 6 dependent parameters, it yields

$$M = \frac{N}{D}$$

$$N = R_a^2 (R_1^2 - 2R_1R_2 + R_2^2 + X_1^2 - 2X_1X_2 + X_2^2)$$

---

Where the denominator  $D$  is the sum of 35 terms of order 4

$$D = T_1 + T_2 + T_3 + T_4$$

$$T_1 = R_a^4 + X_a^4$$

$$\begin{aligned} T_2 = & R_1^2 R_2^2 + X_1^2 X_2^2 + 2R_a^2 X_a^2 \\ & + R_1^2 (R_a^2 + X_a^2 + X_2^2) \\ & + R_2^2 (R_a^2 + X_a^2 + X_1^2) \\ & + (X_1^2 + X_2^2) (R_a^2 + X_a^2) \\ & + 2R_a^3 (R_1 + R_2) + 2X_a^3 (X_1 + X_2) \end{aligned}$$

$$\begin{aligned} T_3 = & 2R_1^2 (R_2 R_a + X_2 X_a) + 2R_2^2 (R_1 R_a + X_1 X_a) \\ & + 2X_1^2 (X_2 X_a + R_2 R_a) + 2X_2^2 (X_1 X_a + R_1 R_a) \\ & + 2R_a^2 (X_1 X_a + X_2 X_a) + 2X_a^2 (R_1 R_a + R_2 R_a) \\ & + 4X_1 X_2 X_a^2 + 4R_1 R_2 R_a^2 \end{aligned}$$

$$T_4 = 4R_a X_a (R_1 X_2 + R_2 X_1)$$

We then null the partial derivative of  $M$  with respect to  $R_a$  and  $X_a$

$$\frac{\partial M}{\partial R_a} = 0$$

$$\frac{\partial M}{\partial X_a} = 0$$

Those two conditions are equivalent to the two equalities below:

$$F_1(\underbrace{R_a, X_a}_{\text{antenna}} \underbrace{(R_1, X_1, R_2, X_2)}_{\text{chip}}) = R_a^4 + A_1 R_a^3 + B_1 R_a + C_1 = 0 \quad (\text{B.4})$$

---


$$F_2(R_a, X_a, (R_1, X_1, R_2, X_2)) = A_2 X_a^3 + B_2 X_a^2 + C_2 X_a + D_2 = 0 \quad (\text{B.5})$$

with

$$\begin{aligned} A_1 &= R_1 + R_2 \\ B_1 &= -R_1 (R_2^2 + (X_2 + X_a)^2) - R_2 (R_1^2 + (X_1 + X_a)^2) \\ C_1 &= (-R_1^2 - (X_1 + X_a)^2) (R_2^2 + (X_2 + X_a)^2) \end{aligned}$$

and,

$$\begin{aligned} A_2 &= 2 \\ B_2 &= 3(X_1 + X_2) \\ C_2 &= ((R_1 + R_a)^2 + (R_2 + R_a)^2 + X_1^2 + X_2^2 + 4X_1 X_2) \\ D_2 &= X_1^2 X_2 + X_1 X_2^2 + X_1 (R_2 + R_a)^2 + X_2 (R_1 + R_a)^2 \end{aligned}$$

In order to null simultaneously the two conditions, we define the composite function

$$F(R_a, X_a, R_1, X_1, R_2, X_2) = F_1^2 + F_2^2$$

The gradient with respect to the two free variable  $R_a$  and  $X_a$  is expressed as :

$$\nabla F = \begin{bmatrix} \frac{\partial F}{\partial R_a} \\ \frac{\partial F}{\partial X_a} \end{bmatrix} \quad (\text{B.6})$$

With the two components

$$\frac{\partial F}{\partial R_a} = 2 \frac{\partial F_1}{\partial R_a} F_1 + 2 \frac{\partial F_2}{\partial R_a} F_2 \quad (\text{B.7})$$

$$\frac{\partial F}{\partial X_a} = 2 \frac{\partial F_1}{\partial X_a} F_1 + 2 \frac{\partial F_2}{\partial X_a} F_2 \quad (\text{B.8})$$

Considering the term which depends on  $F_1$  it comes :

$$\frac{\partial F_1}{\partial R_a} = 4R_a^3 + 3A_1 R_a^2 + B_1 \quad (\text{B.9})$$

---


$$\frac{\partial F_1}{\partial X_a} = R_a \frac{\partial B_1}{\partial X_a} + \frac{\partial C_1}{\partial X_a} \quad (\text{B.10})$$

with

$$\frac{\partial B_1}{\partial X_a} = -2R_1X_a - 2X_aR_2 - 2X_1R_2 - 2X_2R_1 \quad (\text{B.11})$$

and

$$\frac{\partial C_1}{\partial X_a} = -2 \left( R_1^2 + (X_1 + X_a)^2 \right) (X_2 + X_a) - 2 \left( R_2^2 + (X_2 + X_a)^2 \right) (X_1 + X_a) \quad (\text{B.12})$$

Considering the terms which depends on  $F_2$  it comes :

$$\frac{\partial F_2}{\partial R_a} = X_a \frac{\partial C_2}{\partial R_a} + \frac{\partial D_2}{\partial R_a} \quad (\text{B.13})$$

with

$$\frac{\partial C_2}{\partial R_a} = 2(R_1 + R_2 + 2R_a) \quad (\text{B.14})$$

and

$$\frac{\partial D_2}{\partial R_a} = 2X_1(R_2 + R_a) + 2X_2(R_1 + R_a) \quad (\text{B.15})$$

$$\frac{\partial F_2}{\partial X_a} = 3A_2X_a^2 + 2B_2X_a + C_2 \quad (\text{B.16})$$

At this point we have a closed form expression for  $F = F_1 + F_2$  and of its gradient w.r.t  $R_a$  and  $X_a$ . This information can be exploited to determine very precisely through an optimization method the value of  $Z_{ar}$ .

The close form expression provided by Lukas Mayer in [42] gives

$$X_{ar} = -\frac{R_2X_1 + R_1X_2}{R_1 + R_2} \quad (\text{B.17})$$

We can observe that this optimal reactance can be obtained if we impose the decoupling condition:

$$\frac{\partial B_1}{\partial X_a} = 0 \quad (\text{B.18})$$

The mathematical justification of this necessary condition remains unclear for the author.

---

Once  $X_{ar}$  has been guessed with the condition B.18, one can inject this value in B.5. It comes a basic quadratic equation in  $R_a$ , whose the order 1 term is zero :

$$AR_a^2 + C = 0 \quad (\text{B.19})$$

whose the positive solution is :

$$R_a = -\frac{C}{A} \quad (\text{B.20})$$

With

$$A = X_1 + X_2 - \frac{2R_1X_2 + 2R_2X_1}{R_1 + R_2} \quad (\text{B.21})$$

and

$$C = C_0 + C_1 + C_2 + C_3 \quad (\text{B.22})$$

$$C_0 = R_2^2X_1 + X_1^2X_2 + X_1X_2^2 + R_1^2X_2 \quad (\text{B.23})$$

$$C_1 = -\frac{(R_1X_2 + R_2X_1)(R_1^2 + R_2^2 + X_1^2 + 4X_1X_2 + X_2^2)}{R_1 + R_2} \quad (\text{B.24})$$

$$C_2 = \frac{(3X_1 + 3X_2)(R_1X_2 + R_2X_1)^2}{(R_1 + R_2)^2} \quad (\text{B.25})$$

$$C_3 = -\frac{2(R_1X_2 + R_2X_1)^3}{(R_1 + R_2)^3} \quad (\text{B.26})$$

One can verify after some algebra that

$$R_{ar} = -\frac{C}{A} = \sqrt{R_1R_2 \frac{(R_1 + R_2)^2 + (X_1 - X_2)^2}{(R_1 + R_2)^2}} \quad (\text{B.27})$$

which is consistent with 1.24.

# ANNEX C

---

This annex presents the tags on ear with different orientation measured in a rotation configuration. The angular measurements were done by placing the ear in the center of the platform (as shown in Fig. 3.3) and the acquisition was done by the antennas 0,1 and 2 alternatively at each angle. The ear was rotated from  $0^\circ$  to  $360^\circ$  to form a full rotation with a step of  $5^\circ$ , and at each step the power was varied as usually done. Thus, the received profiles were obtained for each tag with each rotation by the antenna 0 on the top as shown in Fig. C.1, by the antenna 1 on the right as shown in Fig. C.2, and lastly by the antenna 2 on the left of C.3. We can obviously see that the received profiles acquired by the left antenna is the mirror of those acquired by the right antenna.

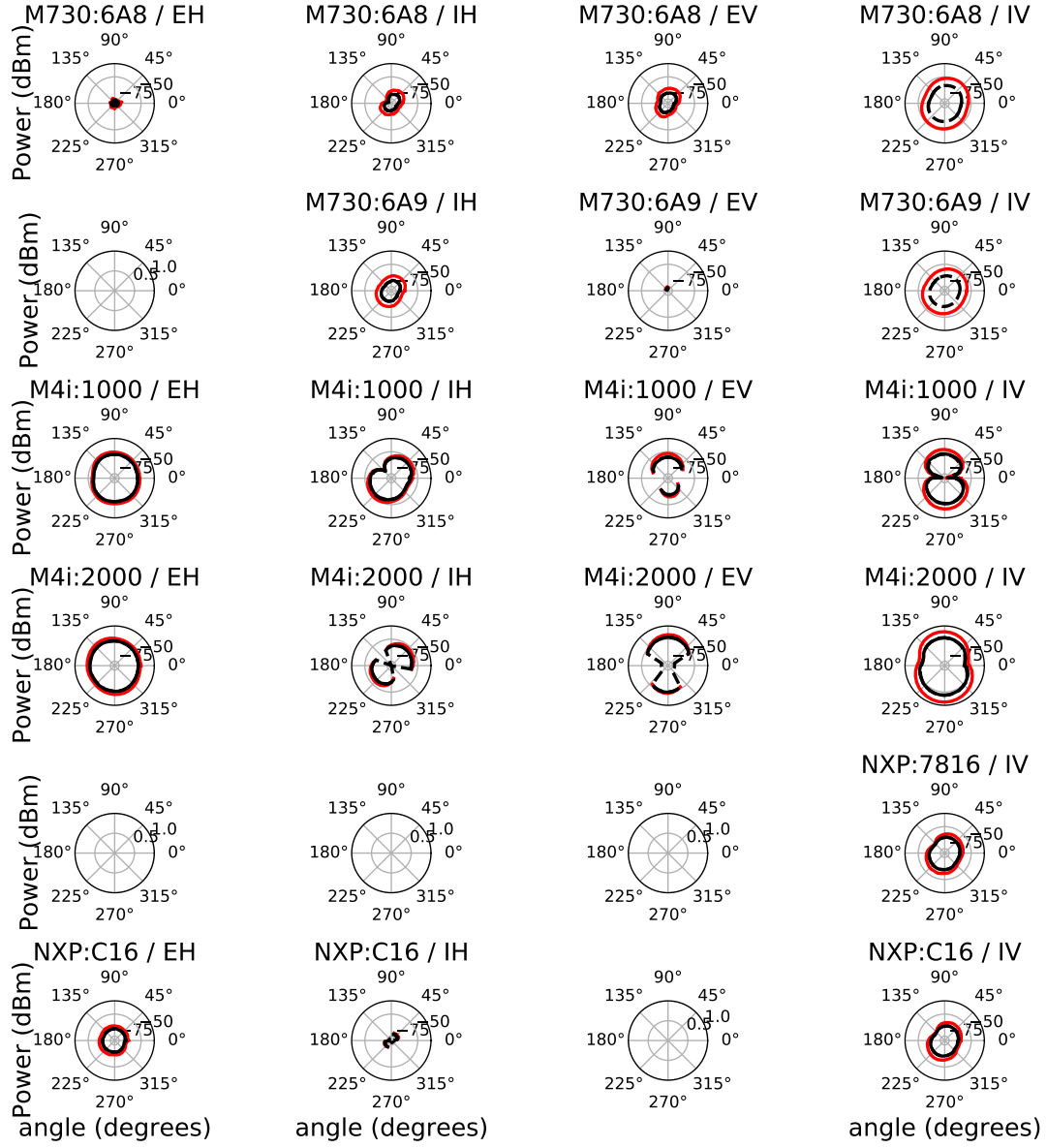


Figure C.1 – Tag top angular pattern (Antenna 0 top) for  $P_r^{max}$  (red) and  $P_r^{th}$  (black)

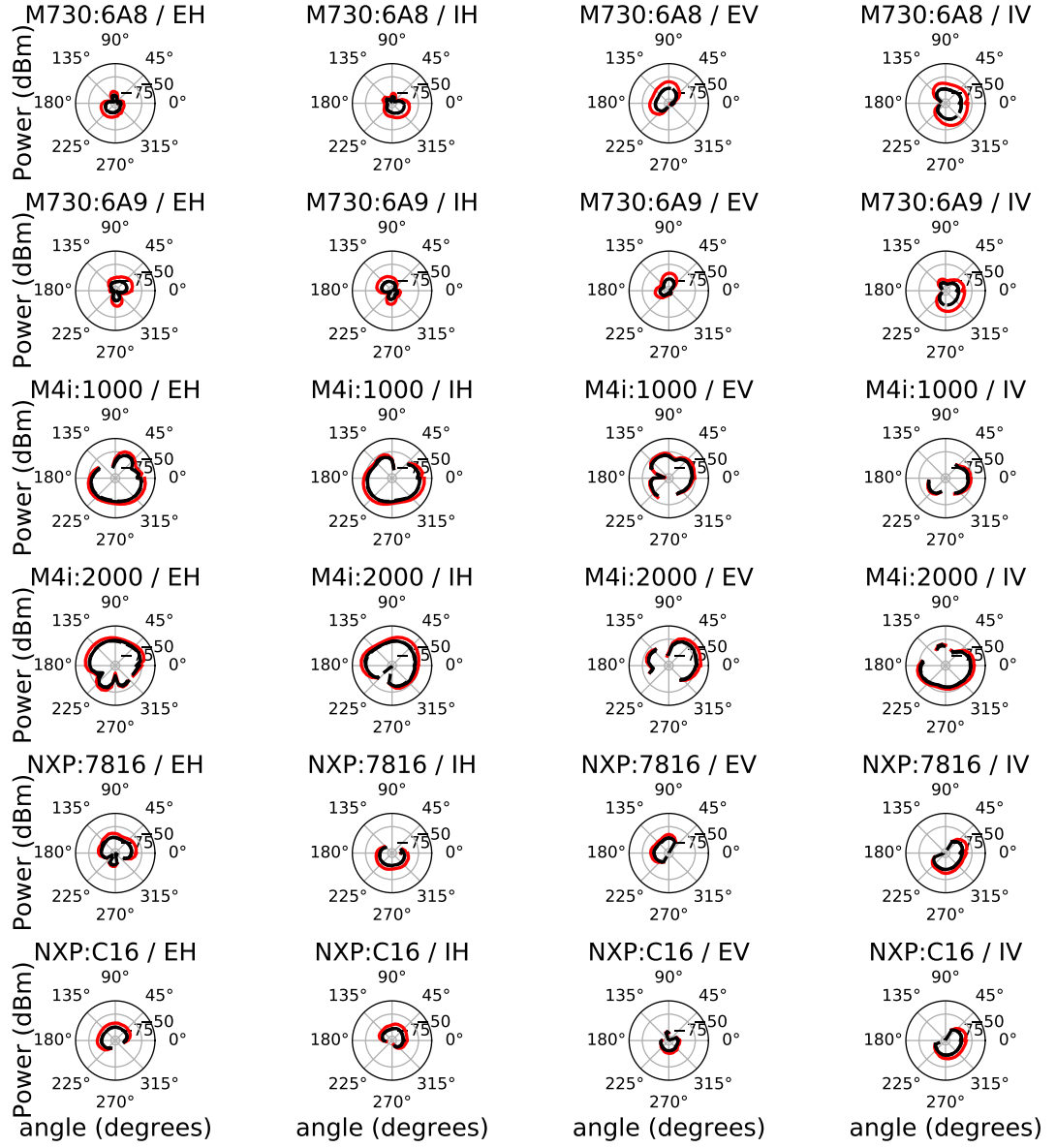


Figure C.2 – Tag angular pattern (Antenna 1 right) for  $P_r^{max}$  (red) and  $P_r^{th}$  (black)



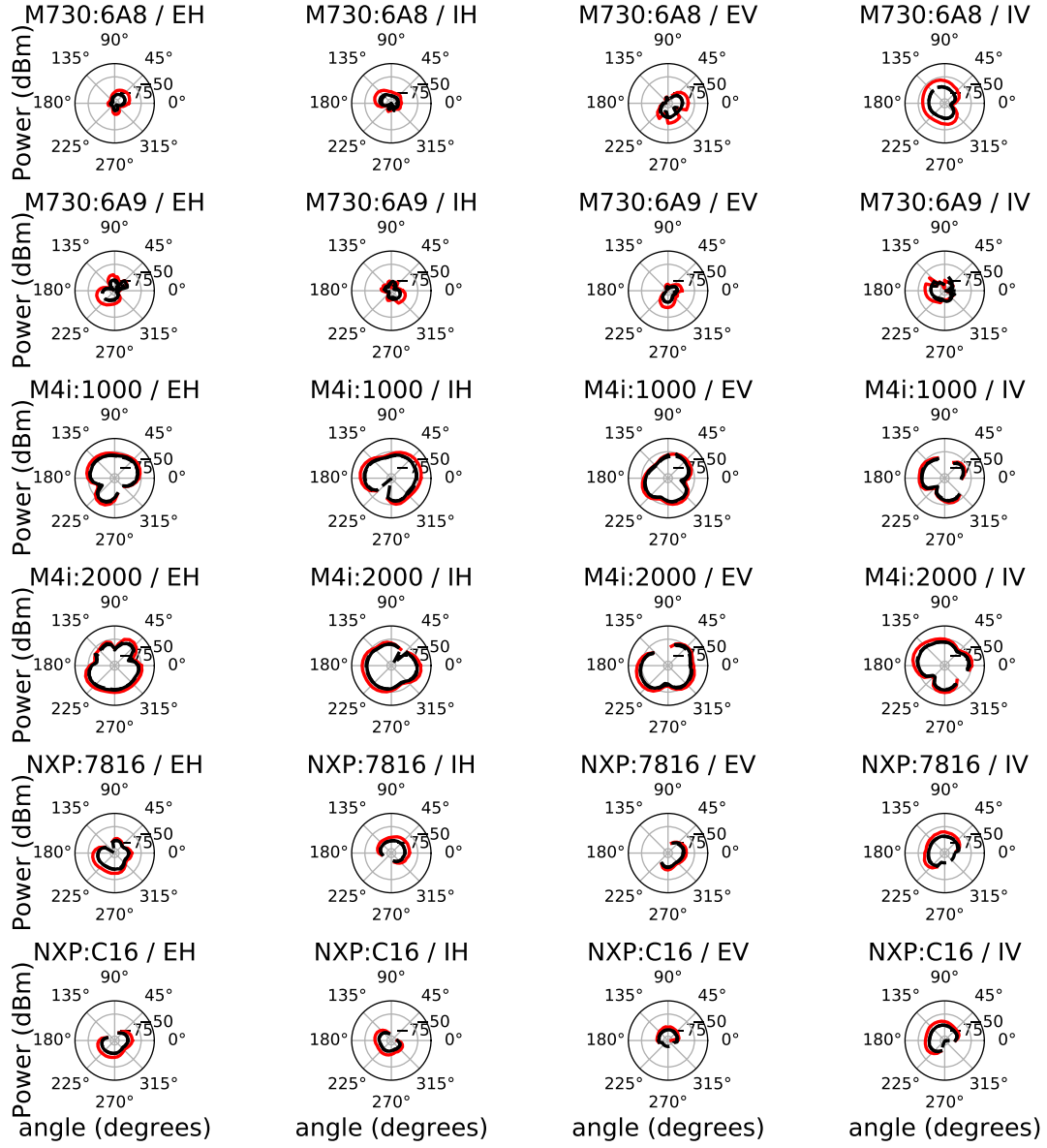


Figure C.3 – Tag angular pattern (Antenna 2 left) for  $P_r^{max}$  (red) and  $P_r^{th}$  (black)

# ANNEX D

We represent in this annex the mosaic of configuration 2, 3, 4 and 5. In addition, we represent the power profiles acquisition, using the impinj reader, of the group of tags placed in all configurations.

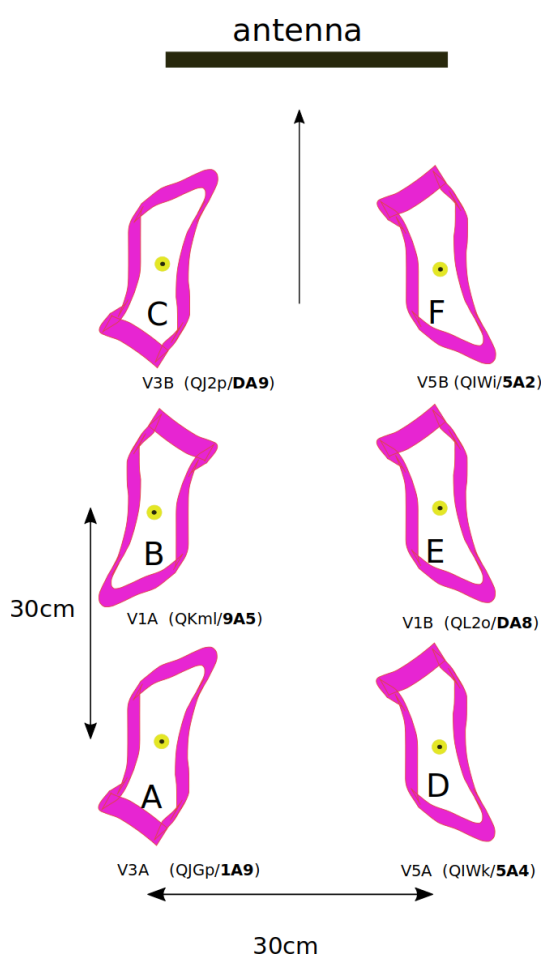


Figure D.1 – Mosaic of Configuration 2

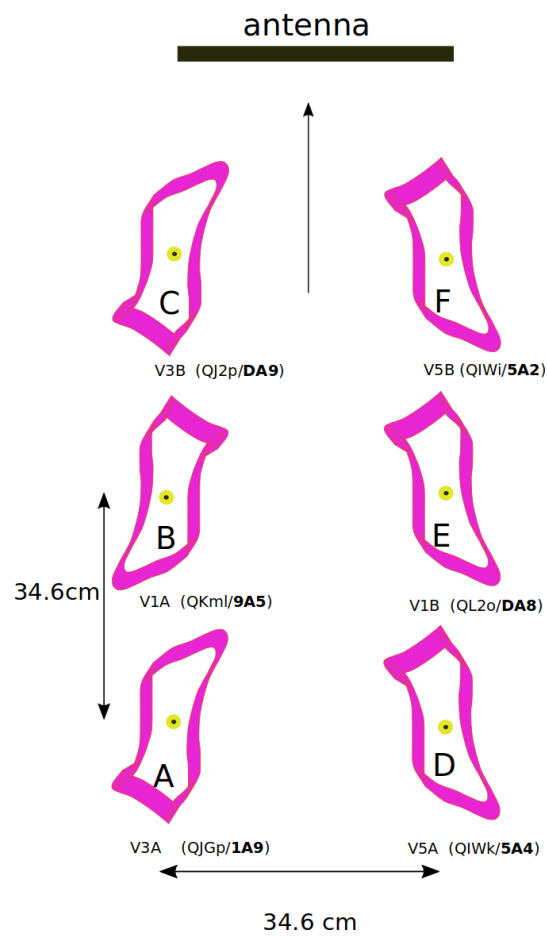


Figure D.2 – Mosaic of Configuration 3

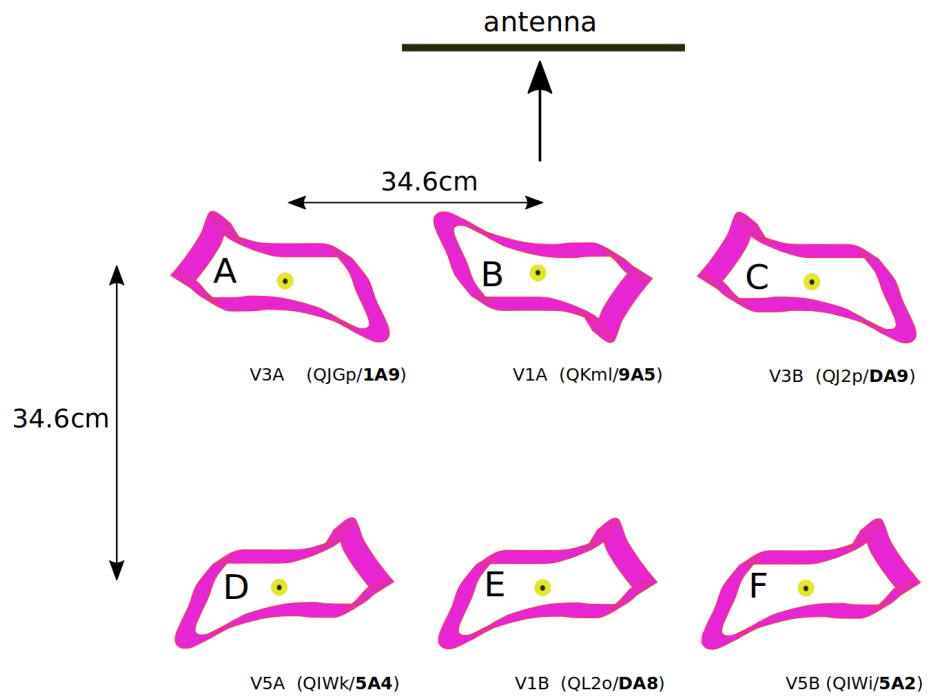


Figure D.3 – Mosaic of Configuration 4

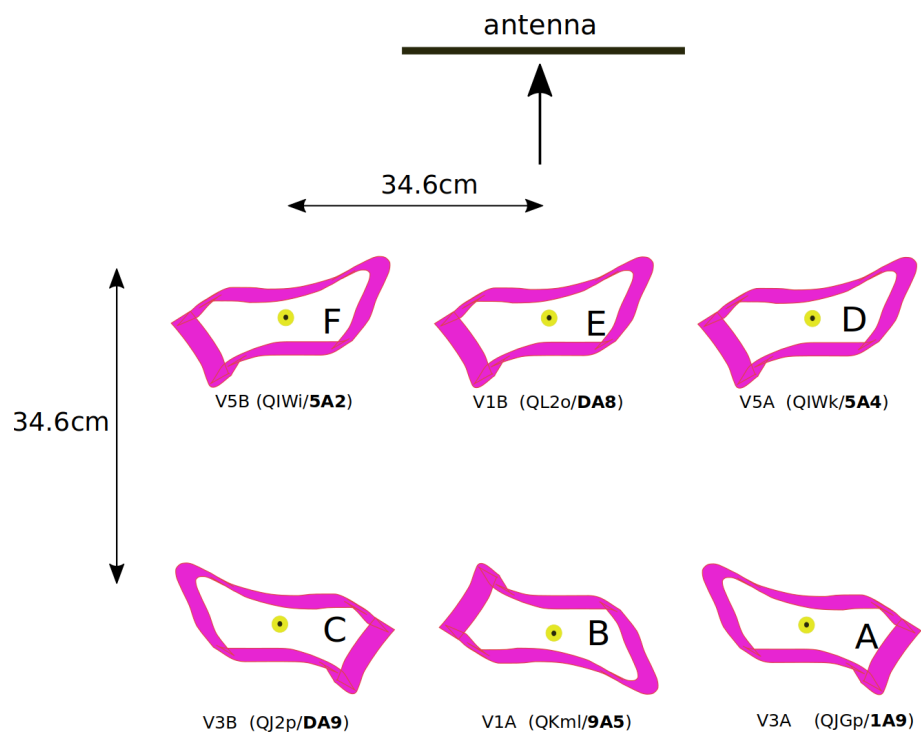


Figure D.4 – Mosaic of Configuration 5

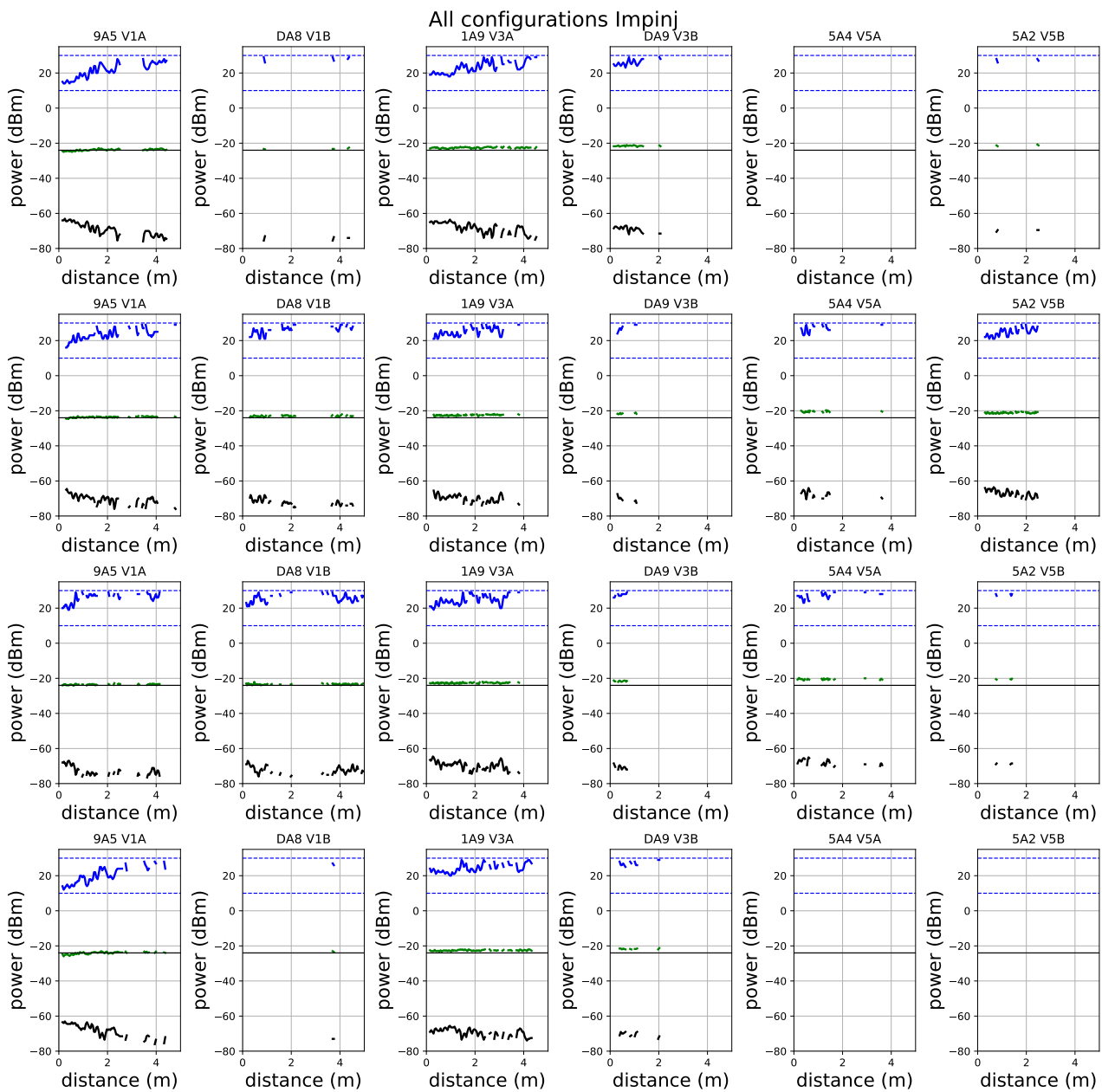


Figure D.5 – Measured profiles for configurations 1, 2, 3 and 4 with Impinj reader

# LIST OF PUBLICATIONS

---

## Journal papers

1. **Hadi El Hajj Chehade**, B. Uguen and S. Collardey, "UHF-RFID Read Range Characterization Method Using Power Activation Profiles," in IEEE Journal of Radio Frequency Identification, vol. 7, pp. 134-144, 2023, doi: 10.1109/JRFID.2023.3277313.

## International Conference Papers

1. **Hadi El Hajj Chehade**, B. Uguen and S. Collardey, "UHF-RFID Power Distance Profiles for Analysis of Propagation Absorbing Effect," 2021 IEEE International Conference on RFID Technology and Applications (RFID-TA), Delhi, India, 2021, pp. 157-160, doi: 10.1109/RFID-TA53372.2021.9617321.
2. **Hadi El Hajj Chehade**, B. Uguen and S. Collardey, "Transmission and Receiving Power Profiles for RFID Tags Performances Evaluation," 2022 7th International Conference on Smart and Sustainable Technologies (SpliTech), Split / Bol, Croatia, 2022, pp. 01-05, doi: 10.23919/SpliTech55088.2022.9854308.
3. **Hadi El Hajj Chehade**, B. Uguen and S. Collardey, "Environment Propagation Scanning using Identical UHF RFID tags configuration," 2023 IEEE International Conference on RFID Technology and Applications (RFID-TA), Aveiro, Portugal



# BIBLIOGRAPHY

---

- [1] J. Landt, « The history of RFID », in: *IEEE Potentials* 24.4 (2005), pp. 8–11, DOI: 10.1109/MP.2005.1549751.
- [2] A.R. Koelle, S.W. Depp, and R.W. Freyman, « Short-range radio-telemetry for electronic identification, using modulated RF backscatter », in: *Proceedings of the IEEE* 63.8 (1975), pp. 1260–1261, DOI: 10.1109/PROC.1975.9928.
- [3] R. Want, « An introduction to RFID technology », in: *IEEE Pervasive Computing* 5.1 (2006), pp. 25–33, DOI: 10.1109/MPRV.2006.2.
- [4] Kirti Chawla et al., « Real-time RFID localization using RSS », en, in: *2013 International Conference on Localization and GNSS (ICL-GNSS)*, TURIN, Italy: IEEE, June 2013, pp. 1–6, ISBN: 978-1-4799-0486-0 978-1-4799-0484-6, DOI: 10.1109/ICL-GNSS.2013.6577259, URL: <http://ieeexplore.ieee.org/document/6577259/> (visited on 04/16/2021).
- [5] Dean Brennan and Jan Kolaja, « Real time location system using passive UHF RFID », in: *Proceedings of the 2014 15th International Carpathian Control Conference (ICCC)*, 2014, pp. 58–62, DOI: 10.1109/CarpathianCC.2014.6843569.
- [6] R. Krigslund et al., « A Novel Technology for Motion Capture Using Passive UHF RFID Tags », in: *IEEE Transactions on Biomedical Engineering* 60.5 (2013), pp. 1453–1457, DOI: 10.1109/TBME.2012.2209649.
- [7] Lukas Görtschacher, Wolfgang Bösch, and Jasmin Grosinger, « UHF RFID Sensor Tag Antenna Concept for Stable and Distance Independent Remote Monitoring », in: *2018 IEEE International Microwave Biomedical Conference (IMBioC)*, 2018, pp. 16–18, DOI: 10.1109/IMBIOC.2018.8428853.
- [8] *Impinj Monza I*, [Online], 2005, URL: <https://orangetags.com/wp-content/downloads/datasheet/Impinj/MonzalaDatasheet.pdf>.



- 
- [9] *Impinj Monza M700*, [Online], 2020, URL: <http://www.orangetags.com/wp-content/downloads/datasheet/Impinj/ImpinjM700Datasheet.pdf>.
- [10] *AD Dogbone M750 Datasheet*, Product Datasheet, Avery Dennison Smartrac, 2023, URL: <https://rfid.averydennison.com/content/dam/rfid/en/products/rfid-products/data-sheets/datasheet-Dogbone-M750.pdf>.
- [11] *RFID Range*, skyRFID, 2022, URL: [https://skyrfid.com/RFID\\_Range.php](https://skyrfid.com/RFID_Range.php).
- [12] Raymond E. Floyd, « RFID in Animal-Tracking Applications », in: *IEEE Potentials* 34.5 (2015), pp. 32–33, DOI: 10.1109/MPOT.2015.2410308.
- [13] Lyngsoe Systems Kristine P. Koldkjær, *RFID for Baggage Handling and Tracking*, Lyngsoe Systems, 2017, URL: [https://rainrfid.org/wp-content/uploads/2017/11/RFID\\_for\\_Baggage\\_Handling\\_and\\_Tracking-UK.pdf](https://rainrfid.org/wp-content/uploads/2017/11/RFID_for_Baggage_Handling_and_Tracking-UK.pdf).
- [14] Alice Buffi et al., « A Phase-based Method for UHF RFID Gate Access Control », in: *2019 IEEE International Conference on RFID Technology and Applications (RFID-TA)*, 2019, pp. 131–135, DOI: 10.1109/RFID-TA.2019.8892120.
- [15] Xuan Wang et al., « RF-Access: Barrier-Free Access Control Systems with UHF RFID », in: *Applied Sciences* 12.22 (2022), ISSN: 2076-3417, DOI: 10.3390/app122211592, URL: <https://www.mdpi.com/2076-3417/12/22/11592>.
- [16] R. Glidden et al., « Design of ultra-low-cost UHF RFID tags for supply chain applications », in: *IEEE Communications Magazine* 42.8 (2004), pp. 140–151, DOI: 10.1109/MCOM.2004.1321406.
- [17] Khalid Mahmud, « Analysis of bit error rate performance of active and passive RFID communication systems with diversity », in: 2015.
- [18] D. Dobkin, *The RF in RFID: Passive UHF RFID in Practice*, Newline, 2008.
- [19] Cristian Herrojo et al., « Chipless-RFID: A Review and Recent Developments », in: *Sensors* 19.15 (2019), ISSN: 1424-8220, DOI: 10.3390/s19153385, URL: <https://www.mdpi.com/1424-8220/19/15/3385>.

- 
- [20] Felix Adrion et al., « Novel approach to determine the influence of pig and cattle ears on the performance of passive UHF-RFID ear tags », in: *Computers and Electronics in Agriculture* 140 (2017), pp. 168–179, ISSN: 0168-1699, DOI: <https://doi.org/10.1016/j.compag.2017.06.004>, URL: <https://www.sciencedirect.com/science/article/pii/S0168169917300145>.
- [21] Karsten Fyhn et al., « Fast Capture—Recapture Approach for Mitigating the Problem of Missing RFID Tags », in: *IEEE Transactions on Mobile Computing* 11.3 (2012), pp. 518–528, DOI: 10.1109/TMC.2011.62.
- [22] Jia Liu et al., « RF-scanner: Shelf scanning with robot-assisted RFID systems », in: *IEEE INFOCOM 2017 - IEEE Conference on Computer Communications*, 2017, pp. 1–9, DOI: 10.1109/INFOCOM.2017.8056985.
- [23] Chao Yu Jiang et al., « A Wireless Motion Capture System for Shoulder Rehabilitation based on RFID Passive Tag Antenna Array », in: *2021 IEEE International Conference on RFID Technology and Applications (RFID-TA)*, 2021, pp. 16–19, DOI: 10.1109/RFID-TA53372.2021.9617358.
- [24] *Overview of UHF frequency allocations (860 to 960 MHz) for RAIN RFID*, GS1 2022-2023, 2022, URL: [https://www.gs1.org/docs/epc/uhf\\_regulations.pdf](https://www.gs1.org/docs/epc/uhf_regulations.pdf).
- [25] EPCglobal, in: *EPC radio frequency identity protocols classe-1 generation-2 UHF RFID Protocol for communications at 860 MHz 960 MHz*, version 1.2.0, 2008.
- [26] E. Perret, *Radio Frequency Identification and Sensors*, ISTE Ltd and John Wiley & Sons, Inc., 2014.
- [27] J. D. Griffin and G. D. Durgin, « Complete Link Budgets for Backscatter-Radio and RFID Systems », in: *IEEE Antennas and Propagation Magazine* 51.2 (Apr. 2009), Conference Name: IEEE Antennas and Propagation Magazine, pp. 11–25, ISSN: 1558-4143, DOI: 10.1109/MAP.2009.5162013.
- [28] K.V.S. Rao, P.V. Nikitin, and S.F. Lam, « Antenna design for UHF RFID tags: a review and a practical application », in: *IEEE Transactions on Antennas and Propagation* 53.12 (2005), pp. 3870–3876, DOI: 10.1109/TAP.2005.859919.

- 
- [29] Jean Charles Bolomey et al., « Electromagnetic Modeling of RFID-Modulated Scattering Mechanism. Application to Tag Performance Evaluation », en, in: *Proceedings of the IEEE* 98.9 (Sept. 2010), pp. 1555–1569, ISSN: 0018-9219, 1558-2256, DOI: 10.1109/JPROC.2010.2053332, URL: <http://ieeexplore.ieee.org/document/5508334/> (visited on 05/07/2021).
- [30] Pavel V. Nikitin et al., « Sensitivity and Impedance Measurements of UHF RFID Chips », in: *IEEE Transactions on Microwave Theory and Techniques* 57.5 (2009), pp. 1297–1302, DOI: 10.1109/TMTT.2009.2017297.
- [31] Hongbin Ge et al., « Binary RFID chip impedance measurement for UHF tag antenna design », in: *2014 IEEE Antennas and Propagation Society International Symposium (APSURSI)*, 2014, pp. 1682–1683, DOI: 10.1109/APS.2014.6905167.
- [32] Zhuo Su, Shing-Chi Cheung, and Koon-Ting Chu, « Investigation of radio link budget for UHF RFID systems », in: (June 2010), DOI: 10.1109/RFID-TA.2010.5529938.
- [33] Pavel V. Nikitin and K. V. S. Rao, « Antennas and Propagation in UHF RFID Systems », in: *2008 IEEE International Conference on RFID*, 2008, pp. 277–288, DOI: 10.1109/RFID.2008.4519368.
- [34] K. Kurokawa, « Power Waves and the Scattering Matrix », in: *IEEE Transactions on Microwave Theory and Techniques* 13.2 (1965), pp. 194–202, DOI: 10.1109/TMTT.1965.1125964.
- [35] Pavel V. Nikitin, Kvs Rao, and Sander Lam Intermec, « UHF RFID TAG CHARACTERIZATION : OVERVIEW AND STATE-OF-THE-ART », in: 2012.
- [36] Márcio Félix et al., « Using labview to automate RFID tag tests: comparison between implemented system and voyantic test system », in: *2015 IEEE Brasil RFID*, 2015, pp. 1–5, DOI: 10.1109/BrasilRFID.2015.7523832.
- [37] Pavel Nikitin, K.V.s Rao, and R.D. Martinez, « Differential RCS of RFID tag », in: *Electronics Letters* 43 (Feb. 2007), pp. 431–432, DOI: 10.1049/el:20070253.
- [38] Nicolas Barbot, Olivier Rance, and Etienne Perret, « Differential RCS of Modulated Tag », in: *IEEE Transactions on Antennas and Propagation* (2021), pp. 1–1, DOI: 10.1109/TAP.2021.3060943.

- 
- [39] Nicolas Barbot, Olivier Rance, and Etienne Perret, « Classical RFID Versus Chipless RFID Read Range: Is Linearity a Friend or a Foe? », in: *IEEE Transactions on Microwave Theory and Techniques* 69.9 (2021), pp. 4199–4208, DOI: 10.1109/TMTT.2021.3077019.
- [40] Jong-wook Lee, Hongil Kwon, and Bomson Lee, « Design Consideration of UHF RFID Tag for Increased Reading Range », in: *2006 IEEE MTT-S International Microwave Symposium Digest*, 2006, pp. 1588–1591, DOI: 10.1109/MWSYM.2006.249638.
- [41] Nicolas Barbot and Ionela Prodan, « Optimal Impedance Matching for UHF RFID Chip », in: *2023 IEEE International Conference on RFID (RFID)*, 2023, pp. 96–101, DOI: 10.1109/RFID58307.2023.10178515.
- [42] Lukas Mayer, « Antenna design for future multi-standard and multi-frequency RFID systems », PhD thesis, Technische Universität Wien, 2009.
- [43] Florian Muralter et al., « UHF RFID chip impedance and sensitivity measurement using a transmission line transformer », in: *2021 IEEE International Conference on RFID (RFID)*, 2021, pp. 1–4, DOI: 10.1109/RFID52461.2021.9444382.
- [44] Luca Catarinucci et al., « A Cost-Effective SDR Platform for Performance Characterization of RFID Tags », in: *IEEE Transactions on Instrumentation and Measurement* 61.4 (2012), pp. 903–911, DOI: 10.1109/TIM.2011.2174899.
- [45] Riccardo Colella et al., « Characterization system for radiation pattern and sensitivity estimation of UHF RFID tags », in: *2015 IEEE International Symposium on Antennas and Propagation & USNC/URSI National Radio Science Meeting*, 2015, pp. 1754–1755, DOI: 10.1109/APS.2015.7305266.
- [46] Riccardo Colella et al., « Cost-effective electromagnetic characterization system for radiation pattern and sensitivity estimation of UHF RFID tags », in: *2015 IEEE 15th Mediterranean Microwave Symposium (MMS)*, 2015, pp. 1–4, DOI: 10.1109/MMS.2015.7375388.
- [47] Riccardo Colella and Luca Catarinucci, « Reduction of Power-Discretization Effects in UHF RFID Tag Performance Estimation Systems based on Off-the-Shelf Programmable Readers », in: *2018 3rd International Conference on Smart and Sustainable Technologies (SpliTech)*, 2018, pp. 1–5.

- 
- [48] Riccardo Colella, Francesco P. Chietera, and Luca Catarinucci, « Considerations on Rigorous UHF RFID Tag Electromagnetic Performance Evaluation in Non-Anechoic Environments », in: *2020 International Workshop on Antenna Technology (iWAT)*, 2020, pp. 1–3, DOI: 10.1109/iWAT48004.2020.1570615275.
- [49] Pavel V. Nikitin et al., « Phase based spatial identification of UHF RFID tags », in: *2010 IEEE International Conference on RFID (IEEE RFID 2010)*, 2010, pp. 102–109, DOI: 10.1109/RFID.2010.5467253.
- [50] Andrea Motroni et al., « Indoor Multipath channel modeling effects on UHF-RFID Localization with Synthetic Arrays », in: *2023 17th European Conference on Antennas and Propagation (EuCAP)*, 2023, pp. 1–5, DOI: 10.23919/EuCAP57121.2023.10133138.
- [51] Alien Technology, in: *Alien ALR-9900+ enables users to deploy best-in-class EPC Gen 2 RFID solutions for supply chain, manufacturing and asset management applications*. 2013.
- [52] Fagui Liu, Dexiang Zhong, and Songchao Luo, « A three-dimensional localization algorithm for passive radio-frequency identification device tag », en, in: *International Journal of Distributed Sensor Networks* 13.10 (Oct. 2017), Publisher: SAGE Publications, p. 1550147717736176, ISSN: 1550-1477, DOI: 10.1177/1550147717736176, URL: <https://doi.org/10.1177/1550147717736176> (visited on 06/28/2021).
- [53] D. Brennan and J. Kolaja, « Real time location system using passive UHF RFID », in: *Proceedings of the 2014 15th International Carpathian Control Conference (ICCC)*, May 2014, pp. 58–62, DOI: 10.1109/CarpathianCC.2014.6843569.
- [54] Pavel Nikitin, John Kim, and KVS Rao, « RFID Tag Analysis Using an Equivalent Circuit », in: *2021 IEEE International Symposium on Antennas and Propagation and USNC-URSI Radio Science Meeting (APS/URSI)*, 2021, pp. 167–168, DOI: 10.1109/APS/URSI47566.2021.9704608.
- [55] *Dogbone Monza4D Datasheet*, Product Datasheet, Avery Dennison Smartrac, 2021, URL: <https://rfid.averydennison.com/content/dam/rfid/en/products/rfid-products/data-sheets/datasheet-Dogbone-Monza-4D.pdf>.

- 
- [56] *Impinj Monza 4 Series Datasheet*, Tag Chip Datasheet, Impinj, 2022, URL: [https://support.impinj.com/hc/article\\_attachments/6619788904851/Impinj\\_Monza\\_4\\_Series\\_Tag\\_Chip\\_Datasheet\\_20220315.pdf](https://support.impinj.com/hc/article_attachments/6619788904851/Impinj_Monza_4_Series_Tag_Chip_Datasheet_20220315.pdf).
- [57] *Impinj Monza R6 Series Datasheet*, Tag Chip Datasheet, Impinj, 2021, URL: [https://support.impinj.com/hc/article\\_attachments/1500019253582/Impinj\\_Monza\\_R6\\_Tag\\_Chip\\_Datasheet\\_V7\\_20210521.pdf](https://support.impinj.com/hc/article_attachments/1500019253582/Impinj_Monza_R6_Tag_Chip_Datasheet_V7_20210521.pdf).
- [58] Product data sheet COMPANY PUBLIC, *UCODE 8/8m Datasheet*, [https://www.nxp.com/docs/en/data-sheet/SL3S1205\\_15.pdf](https://www.nxp.com/docs/en/data-sheet/SL3S1205_15.pdf), 2021.
- [59] *Impinj Monza 5 Series Datasheet*, Tag Chip Datasheet, Impinj, 2016, URL: [https://support.impinj.com/hc/article\\_attachments/203268870/Monza%205%20Tag%20Chip%20Datasheet%20R3%2020160823.pdf](https://support.impinj.com/hc/article_attachments/203268870/Monza%205%20Tag%20Chip%20Datasheet%20R3%2020160823.pdf).
- [60] *Higgs 3 Datasheet*, EPC Class 1 Gen 2 RFID Tag IC, Alien, 2020, URL: <file:///home/hadi/ALC-360%20Higgs-3%202020-02-21.pdf>.
- [61] Product data sheet COMPANY PUBLIC, *UCODE 7 Datasheet*, <https://www.nxp.com/docs/en/data-sheet/SL3S1204.pdf>, 2019.
- [62] A.C. de Souza et al., « Normalized power calculation to UHF RFID passive tags characterization », in: *2014 IEEE Brasil RFID*, 2014, pp. 54–56, DOI: 10.1109/BrasilRFID.2014.7128965.
- [63] *AD-806u7 Datasheet*, Product Datasheet, Avery Dennison Smartrac, 2021, URL: <https://rfid.averydennison.com/content/dam/rfid/en/products/rfid-products/data-sheets/datasheet-AD-806u7.pdf>.
- [64] Spyros Megalou et al., « Power and Phase Variation of Backscattered RFID Signal with Respect to the Incident Power at the Tag », in: *IEEE International Conference on RFID Technology and Applications (RFID-TA)*, 2021.
- [65] K. Finkenzeller, *RFID Handbook*, Second Edition, West Sussex, England: Wiley Publishing, 2003.
- [66] Lukas W. Mayer, Martin Wrulich, and Sebastian Caban, « Measurements and channel modeling for short range indoor UHF applications », in: *2006 First European Conference on Antennas and Propagation*, 2006, pp. 1–5, DOI: 10.1109/EUCAP.2006.4584782.

- 
- [67] Tutku Karacolak et al., « Dielectric Properties of Porcine Skin Tissue and In Vivo Testing of Implantable Antennas Using Pigs as Model Animals », *in: IEEE Antennas and Wireless Propagation Letters* 11 (2012), pp. 1686–1689, DOI: 10.1109/LAWP.2013.2241722.
- [68] Felix Adrion et al., « Development, function and test of a static test bench for UHF-RFID ear tags », *in: Landtechnik* (May 2015).
- [69] *Dielectric measurement system*, SPEAG, URL: <https://speag.swiss/products/dak/dak-probes/>.
- [70] *Impinj M700 Series Datasheet*, Tag Chip Datasheet, Impinj, 2023, URL: [https://support.impinj.com/hc/article\\_attachments/18082064482963/Impinj\\_M700\\_Series\\_Tag\\_IC\\_Datasheet\\_20230626\\_v6.4.pdf](https://support.impinj.com/hc/article_attachments/18082064482963/Impinj_M700_Series_Tag_IC_Datasheet_20230626_v6.4.pdf).
- [71] Imad Adjali, « Approche statistique pour la quantification des performances d’antennes fortement couplées : application à la RFID dans le contexte d’une densité élevée de tags », PhD thesis, Université Paris-Est, 2020.





---

**Titre :** Contribution à la caractérisation over-the-air des transpondeurs RFID UHF

**Mot clés :** RFID UHF, Tags, Caractérisation, Canal de propagation, Expérimentation

**Résumé :** La technologie RFID UHF permet de récupérer à distance et par ondes radio des données stockées sur une étiquette constituée d'une antenne et d'une puce. Le transpondeur élément clé d'un système RFID a fait l'objet de nombreuses recherches et d'améliorations au cours des dernières années. Dans ce contexte, cette thèse contribue à l'évaluation des performances des transpondeurs RFID en environnement réel par le développement d'une méthode de caractérisation originale. Cette approche expérimentale permet d'accéder aux paramètres intrinsèques d'un tag RFID en tenant compte de la réciprocité du canal de propagation entre les liaisons montante et descendante.

A partir de profils d'activation en fonction de la distance et de la puissance, ce travail permet d'introduire de nouveaux critères d'évaluation et de comparaisons des tags comme le facteur  $Q$  et l'efficacité  $\gamma$  liés au coefficient de transmission de puissance moyen  $\tau$  et au facteur de modulation  $M$ . En exploitant ces profils de puissance, un nouveau graphique  $(\sqrt{M}, \tau)$  ou  $(Q, \gamma)$  a été proposé permettant d'illustrer la comparaison des tags et de définir une zone de fonctionnement optimal pour la puce RFID. Les outils de caractérisation en RFID UHF proposés dans ce travail ont été mis efficacement à contribution dans le cadre du développement de tags pour les animaux d'élevage.

---

**Title:** Contribution to Over-the-air Characterization of UHF RFID tags

**Keywords:** UHF RFID, Tags, Characterisation, Propagation channel, Experimentation

**Abstract:** The aim of UHF RFID technology is to remotely retrieve data stored on a tag consisting of an antenna and a chip, using radio waves. The transponder, a key element of an RFID system, has been the subject of much research and improvement in recent years. In this context, this thesis contributes to the evaluation of RFID transponder performance in a real environment through the development of an original characterisation method. This experimental approach provides access to the intrinsic parameters of an RFID tag by taking account of the reciprocity of the propagation channel between the forward and the

backward links. Using activation profiles as a function of distance and power, this work introduces new tag evaluation and comparison criteria such as the  $Q$  factor and the  $\gamma$  efficiency, linked to the mean power transmission coefficient  $\tau$  and the modulation factor  $M$ . By exploiting these power profiles, a new graph  $(\sqrt{M}, \tau)$  or  $(Q, \gamma)$  was proposed to illustrate the comparison of tags and to define an optimal operating zone for the RFID chip. The UHF RFID characterisation tools proposed in this work have been put to effective use in the development of RFID tags for livestock.